



© Sven Lachmann (Seaq68 on Pixabay)



GADEST 20/24



TUBAF
Die Ressourcenuniversität.
Seit 1765.

Program and abstract booklet

20th meeting
Gettering and Defect Engineering
in Semiconductor Technology

Bad Schandau (Saxony, Germany)
September 8 - 13, 2024



© Hotel Elbresidenz / Bernhard Strauss

GADEST 20/24 Sponsors



Fraunhofer

IISB

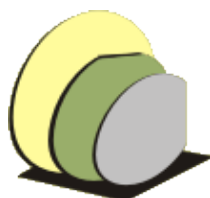


SENTECH

Erfolg durch Leistung



BRUKER



EL-CAT Inc.



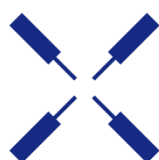
Freiberg Instruments



soitec



Quantum Design
EUROPE



Zurich
Instruments





TUBAF
Die Ressourcenuniversität.
Seit 1765.

Preface

A very warm welcome to the 20th International Conference on Gettering and Defect Engineering in Semiconductor Technology GADEST 20/24, held at Bad Schandau (Saxony, Germany) from September 8 to 13, 2024.

The GADEST conference series was established in 1985 by Hans Richter of the Institute for Physics of Semiconductors of the Academy of Science of the former German Democratic Republic. From its beginning, it was intended as an international forum for experts in the fields of semiconductor technology, semiconductor device physics, and defect physics with participants from academia and industry. Since 1985, GADEST has been organized biennially at typically remote sites to encourage discussions among the participants.

The GADEST 20/24 conference covers a broad range of semiconductor science and technology topics. Topics ranging from fundamental aspects to engineering solutions were included in a forum and serve as a ground for fruitful interaction between scientists and engineers in semiconductor defect physics, materials science, and all the way to quantum technology. Defects in materials and devices, physics, and technology of devices used in nano-, micro-electronics, power electronics, and photovoltaics are traditionally at the heart of the conference.

We sincerely thank the members of the conference committees for their suggestions, evaluation of submitted abstracts, and strong support during the conference preparation process. We gratefully acknowledge financial support from our sponsors. The local Organizing Committee members did all best possible to get the conference running and to be successful.

Conference chairs: Johannes Heitmann, Franziska Bayer, and Daniel Hiller

Editorial group: Teimuraz Mtchedlidze and Matthias Müller

GADEST 20/24 Committees

Executive Committee:

Simona Binetti, Università degli Studi di Milano-Bicocca, Italy
Moritz Brehm, Johannes Kepler University, Linz, Austria
Marisa Di Sabatino, NTNU, Trondheim, Norway
Robert Falster, University of Manchester, United Kingdom
Hermann Grimmeiss, University of Lund, Sweden
Johannes Heitmann, TU Bergakademie Freiberg, Germany
Martin Kittler, IHP, Frankfurt (Oder), Germany
Dawid Kot, IHP, Frankfurt (Oder), Germany
Teimuraz Mtchedlidze, TU Bergakademie Freiberg, Germany
Felipe Murphy Armando, University College Cork, Ireland
John Murphy, University of Warwick, United Kingdom
Peter Pichler, Fraunhofer IISB, Erlangen, Germany
Hans Richter, GFWW, Frankfurt (Oder), Germany
Heike Riel, IBM Zurich, Switzerland
Hele Savin, Aalto University, Espoo, Finland
Gunther Springholz, Johannes Kepler University, Linz, Austria

GADEST 20/24 Committees

International Program Committee:

Gabriel Aeppli, ETH Zurich / EPFL Lausanne / PSI Villingen, Switzerland
Michel Bockstedte, Johannes Kepler University, Linz, Austria
Hartmut Bracht, University of Münster, Germany
Nicholas Grant, University of Warwick, United Kingdom
Pavel Hazdra, Czech Technical University in Prague, Czech Republic
Brett Johnson, University of Melbourne, Australia
Oleg Kononchuk, SOITEC, Bernin, France
Antonino La Magna, Italian National Research Council, Italy
Huiyun Liu, University College London, United Kingdom
Jan Meijer, University of Leipzig, Germany
Francesco Montalenti, Università degli Studi di Milano-Bicocca, Italy
Tim Niewelt, University of Warwick, United Kingdom
Tony Peaker, University of Manchester, United Kingdom
Sławomir Prucnal, HZDR Dresden-Rossendorf, Germany
Stefan Schmult, NaMLab gGmbH Dresden / TU Dresden, Germany
Jonatan Slotte, Aalto University, Espoo, Finland
Koji Sueoka, Okayama Prefectural University, Japan
R. Radhakrishnan Sumathi, IKZ, Berlin, Germany
Alexei Tchelnokov, CEA Leti, Grenoble, France
Walter Weber, TU Vienna, Austria
Deren Yang, Zhejiang University, China

GADEST 20/24 Committees

Local Committee (Institute for Applied Physics, TU Bergakademie Freiberg, and Fraunhofer Technology Center of High-Performance Materials, Freiberg, Germany)

Behm, Thomas
Beyer, Jan
Keller, Kerstin
Kern, Jonas
Mtchedlidze, Teimuraz
Müller, Matthias

Ratschinski, Ingmar
Röder, Christian
Schmid, Alexander
Schneider, Aline
Schneider, Sophia
Seidel, Sarah



Initiative group at the start of preparation (2022, left to right):

Dr. Jan Beyer, Thomas Behm, Aline Schneider, Dr. Christian Röder,
Dr. Franziska Beyer, Prof. Dr. Daniel Hiller, Dr. Teimuraz Mtchedlidze,
Prof. Dr. Johannes Heitmann

20th meeting

Gettering and Defect Engineering in Semiconductor Technology

GADEST 20/24

PROGRAM

Starts: 08 September, 2024, Monday

Finishes: 13 September, 2024, Friday

Sunday, 08 September, 2024				Page
13:30-15:30			Registration	
15:30-15:40	Opening: Johannes Heitmann		Welcome address from the Rector of the Bergakademie Freiberg, Professor Dr. Klaus-Dieter Barbknecht	
15:40-17:00			Plenary session. Session chair: Johannes Heitmann	
15:40-16:15	Hans Richter		40 years of GADEST	10
16:15-17:00	Stefan Eichler		Investigation of dislocations in III-V Semiconductors	12
17:00-18:20			SuA Session: Novel approaches. Session chair: Johannes Heitmann	
17:00-17:40	I01	Joachim Knoch	Cryogenic Electronics and Novel Semiconductor Doping Approaches	14
17:40-18:20	I02	Michael Trupke	Quantum sensing and quantum photonics with spin centres in crystals	16
19:00-22:00			Get together & Vernissage Walter Padao: „hopefully something goes wrong - defects in art“/ artist talk	248

Monday, 09 September, 2024				Page
08:30-10:10 MoM1 Session: Material processing. Session chair: Daniel Hiller				
08:30-09:10	I03	Enrico Napolitani	Laser-assisted crystallisation and hyperdoping	20
09:10-09:30	O01	Tim Niewelt	Recombination-active Defects in Crystalline Silicon after Muon Implantation	20
09:30-09:50	O02	Damiano Ricciarelli	Realistic Simulation and Physical Understanding of Laser Melting in Silicon-Germanium Substrates	22
09:50-10:10	O03	Hui Jia	Effects of phosphorous and antimony doping on Ge layers grown on Si	24
Coffee break				
10:40-12:20 MoM2 Session: Defects and Devices. Session chair: Franziska Beyer				
10:40-11:20	I04	Marianne E. Bathen	Radiation Induced Defects in SiC Material and Devices	26
11:20-11:40	O04	Vladimir Markevich	Electron-irradiation-induced EE1 trap in GaN: unusual electronic properties of a defect linked to the nitrogen vacancy	28
11:40-12:00	O05	Aravind Subramanian	Dislocation analyses in the boron-doped germanium crystals grown under near-equilibrium conditions	30
12:00-12:20	O06	Martin Perrosé	Defect engineering for enhanced silicon RF substrates	32
Lunch break				
13:30-15:30 MoA1 Session: Group IV alloys. Session chair: Enrico Napolitani				
13:30-14:10	I05	Jörg Schulze	Growth of Silicon-based Germanium Tin Alloys	34
14:10-14:30	O07	Kevin Sewell	Disorder and Strain in Limiting the n-type Mobility of GeSn Alloys: Calculations from First Principles.	36
14:30-14:50	O08	Christoph Zechner	TCAD Model for SiGe Oxidation and Ge Diffusion along Oxide/SiGe Interfaces	38
14:50-15:10	O09	Christoph Wilflingseder	Ge nanosheets on Si substrates enabled by ultra-low temperature epitaxy	40
15:10-15:30	O10	Felipe Murphy Armando	First principles calculation of G-Centre Photoluminescence in SiGe and comparison to Experiments	42
Coffee break				
16:00-17:40 MoA2 Session: Nano materials and structures. Session chair: John Murphy				
16:00-16:40	I06	Jonathan Veinot	Are silicon nanoparticles “crystalline to the core” and does it make a difference in post-synthesis doping?	44
16:40-17:00	O11	Laurie Dentz	From nanosphere lithography to localised heteroepitaxy of GaAs on Si	46
17:00-17:20	O12	Raphael Behrle	Comparative Study of Charge Carrier Transport in Al-Si and Al-Ge Nanowire Heterostructure Transistors	48
17:20-17:40	O13	Moritz Brehm	Direct band transitions and light emission from ion-implanted SiGe Quantum Dots grown on Si-on-Insulator Substrates	50
17:40-18:20	Industrial session. Session chair: Johannes Heitmann			
19:00-22:00	MOP poster session. Session chair: Franziska Beyer			

MOP poster session 19:00-22:00			Page
MP01	Lyudmila Khirunenko	Temperature-induced transformation of the BO ₂ atomic configuration in boron-doped Si	52
MP02	Pejk Amoroso	Point defects in Ga- and B-doped Ge	54
MP03	Ulrich Bläß	Basal dislocations in HVPE grown GaN – characterisation and importance for stress relaxation during growth.	56
MP04	Oleg Olikh	The peculiarities of the ultrasound influence on the FeB pair association in silicon structures	58
MP05	Oleg Olikh	Defect content characterization in solar cells with the assistance of machine learning	60
MP06	Ingmar Ratschinski	Modulation Acceptor Doping of Silicon using Gallium-Doped SiO ₂	62
MP07	Martin Herms	Residual Stress and Defects in a Single-crystalline (0001)AlN Wafer Investigated by Scanning Infrared Depolarization and White Beam X-ray Topography	64
MP08	Hitesh Jayaprakash	Suppression of Stacking Fault Expansion with Energy-Filtered Ion Implantation in 4H-SiC Epitaxial Material	66
MP09	Merve Karaman	Self-assembly of W centers and their optical properties in microdisk resonators	68
MP10	Kevin Lauer	Investigation of Ti-doped silicon by low temperature photoluminescence during LID treatments	70
MP11	Ezekiel Omotoso	DLTS characterisation of 107 MeV krypton ion-irradiated nitrogen-doped 4H-silicon carbide	72
MP12	Faiza Al-Hamed	Point defect calculations with finite-size supercells in monolayer MoS ₂	74
MP13	Aaron Flöttotto	Theoretical investigation of single Boron defects in silicon	76
MP14	Antonino Scandurra	Effects of Hydrogen Bonding in Silicon Nitride/Polyimide Passivation Stack for SiC Power Devices	78
MP15	Jérémie Crozelon	Progress of characterization methodology for oxygen-related defects in silicon substrates for advanced technologies	80
MP16	Christian Röder	operando analysis of self-heating effects on AlN-based HEMTs on SiC by confocal micro-Raman spectroscopy	82
MP17	Sergey Pavlov	Violation of selection rules for parity-forbidden optical intracenter transitions in crystalline silicon: substitutional versus interstitial defects	84
MP18	Andrey Sarikov	Thermodynamic study of phase composition of Si oxynitrides obtained at different temperatures	86
MP19	John Murphy	Spectral engineering of photoluminescence from monolayer MoS ₂	88
MP20	Diego Haya Enriquez	Design analysis of group IV light emitters containing SiGe dot-based active medium	90
MP21	Lorenzo Calcaterra	Optoelectronic, Microstructural and Chemical Characterization of 2D PEA ₂ PbBr ₄ Perovskite Thin Films	92
MP22	Enrique Prado Navarrete	(Si)Ge nanosheets on SOI, grown by Molecular Beam Epitaxy at Ultra Low Temperatures, as a planar platform for RFET devices.	94
MP23	Eskil Einmo	Morphology and refractive index dependence on laser parameters in subsurface ultrashort pulsed laser processing of ZnS	96
MP24	Rustam Ashurov	Ion flux distribution in ion beam assisted silicon molecular beam epitaxy	98
MP25	Nikolay Arutyunov	Centers of bismuth and phosphorus in silicon for devices of quantum communications in space: open volume point defects	100
LA MP26	Christopher Dawe	DLTS analysis of (010) β-Ga ₂ O ₃ epilayers grown by metal organic chemical vapour deposition on native Sn-doped substrates	240

Tuesday, 10 September, 2024				Page
08:30-10:10 TuM1 Session: Defects in solar cells. Session chair: Tim Niewelt				
08:30-09:10	I07	José Coutinho	Theory of hydrogen reactions in solar silicon and connections with LeTID	102
09:10-09:30	O14	Vladimir Voronkov	Properties of hydrogen species in n-type silicon deduced from in-diffusion profiles	104
09:30-09:50	O15	Teimuraz Mchedlidze	On-stage solar cell degradation process: DLTS and LT-PL-EL study	106
09:50-10:10	O16	Clara Rittmann	Recombination Activity of Crystal Defects in Epitaxially Grown Silicon Wafers for Highly-Efficient Solar Cells	108
Coffee break				
10:40-12:20 TuM2 Session: Passivation methods. Session chair: Hele Savin				
10:40-11:20	I08	Bart Macco	Recent Advances and Trends in Atomic Layer Deposited Surface Passivation Schemes for Silicon, Germanium and III-V Semiconductors	110
11:20-11:40	O17	Nicholas Grant John Murphy	Separating surface and bulk recombination mechanisms during the activation of Al ₂ O ₃ passivation	112
11:40-12:00	O18	John Murphy	Hafnium oxide surface passivation of silicon	114
12:00-12:20	O19	Konstantinos Efstathios Falidas	In-situ mixed and cycle-to-cycle Atomic Layer Deposition for Al-doped ZrO ₂ based Metal-Insulator-Metal decoupling capacitors placed in BEoL	116
Lunch break				
13:30-15:30 TuA1 Session: Group IV: defects. Session chair: Moritz Brehm				
13:30-14:10	I09	Laetitia Vincent	Growth-related I3 defects in hexagonal Ge-2H and their thermal evolution	118
14:10-14:30	O20	Eddy Simoen	DLTS assessment of grown-in defects in hetero-epitaxial gate stacks for stacked silicon nanosheet channels	120
14:30-14:50	O21	Alexandra Abbadie	Study of gettering in Silicon and SOI	122
14:50-15:10	O22	Felix Kipke	The Diffusion Behavior of Sulfur in Silicon – A New Perspective	124
15:10-15:30	O23	Dawid Kot	Comparison of experimental and simulated results on the formation of N-related complexes in silicon	126
Coffee break				
16:00-18:00 TuA2 Session: WBG-devices. Session chair: Jörg Schulze				
16:00-16:40	I10	Martin Kuball	Next Generation of Electronics Devices: Heterogenous Integration with Diamond	128
16:40-17:00	O24	Antonino Scandurra	Defect formation mechanisms and 2-DEG isolation induced by low-energy Ar, C, Fe ion implantation of Al _{0.2} Ga _{0.8} N/GaN heterostructure	130
17:00-17:20	O25	Lijie Sun	Optical and electrical characteristics of the FeGa defect in dilute Al _x Ga _{1-x} N alloys	132
17:20-17:40	O26	Alexander Kinstler	Direct investigation of localized leakage currents in GaN on sapphire pin diodes with respect to structural defects and conduction mechanisms	134
17:40-18:00	O27	Stefan Schmult	A novel deep acceptor in GaN	136
19:00-22:00 TUP poster session. Session chair: Daniel Hiller				

TuP poster session 19:00-22:00			Page
TP01	Diana Ryzhak	Investigation of dislocations introduced in Si wafers during flash lamp annealing by means of photoluminescence (PL) and μ -PL spectroscopy	138
TP02	Oleg Olikh	Influence of illumination spectrum on dissociation kinetic of iron-boron pairs in silicon	140
TP03	Paul U. Feiler	Point defect characterisation of proton irradiated n-type GaAs	142
TP04	Katell Blanco	In-situ observation of pressurized micro cracks in GaN	144
TP05	Sirine Houam	Experimental investigation of the interaction between structural defects and impurities in silicon for photovoltaic applications	146
TP06	Mette Schouten	I3 defects in hexagonal silicon germanium	148
TP07	Ingmar Ratschinski , Daniel Hiller	ALD-HfO ₂ and ALD-SiO ₂ as a Charge-lean Capping Layer Materials for Modulation Acceptor Doping of Silicon	150
TP08	Vladimir Kolkovsky	Shallow hydrogen-related donors after a dc H plasma treatment in Si	152
TP09	Vladimir Kolkovsky	Surface photovoltage spectroscopy for evaluation of oxidation processes in the microelectronics industry	154
TP10	Umutcan Bektas	Spatially-Resolved Ion Beam Induced Phase Transition and Defect Analysis in Gallium Oxide	156
TP11	Mykola Kras'ko	Kinetics of carrier lifetime degradation in high-temperature 1 MeV electron-irradiated Cz n-Si associated with the formation of divacancy-oxygen defects	158
TP12	Mariia Terletskaia	Efficient surface passivation of germanium by porous Ge layer	160
TP13	Teimuraz Mchedlidze	Pros for using MFIA in deep level transient spectroscopy studies	162
TP14	Tamás Szarvas	Edge inspection of Si wafers for Bulk Microdefects	164
TP15	Steffen Fengler	Detection of defect transitions in ultra-wide bandgap semiconductors by dc and ac surface photovoltage spectroscopy	166
TP16	Kevin Sewell	First-Principles Calculation of Electron Absorption and Recombination in Strained GeSn	168
TP18	Dirk König	The Nanoscopic Electronic Structure Shift Induced by Anions at Surfaces (NESSIAS) to replace doping in nano-Si for VLSI	170
TP19	Andreas Salomon	Advanced device designs for group IV double-heterostructure light-emitting diodes operating at room temperature	172
TP20	Amy Albrecht	Optical characterization of colour centres in AlN	174
TP21	Franziska C. Beyer	Process Mode Engineering of Atomic Layer Etching of Wide-Bandgap Materials	176
TP22	Stephan Wege	Falp® (Fast Atomic Layer Processing) a Chamber for Combined PEALD and ALE Processes at low temperatures	178
TP23	Vitor Jose Torres	Exceptional phonon point versus free phonon coupling in CdZnTe semiconductor mixed crystals under pressure	180
TP24	Christoph Zechner	Process Model for SiC Oxidation for a Large Range of Conditions	182
TP25	Enrico Napolitani	Synthesis of MoS ₂ layers by sputter deposition and pulsed laser annealing	184
LA TP26	Koeun Lee	Investigation of Cu Corrosion Defects Induced by Humidity Imbalance in the Cu Damascene Process of Semiconductors	242

Wednesday, 11 September, 2024				Page
08:30-10:10 WeM1 Session: Si-based Quantum devices. Session chair: Walther Weber				
08:30-09:10	I11	Shao Qi Lim	Towards a silicon semiconductor vacuum: donor spin decoherence in isotopically engineered 28-silicon	186
09:10-09:30	O28	Alexander Malwin Jakob	Engineered Donor-Qubit Arrays for Silicon Quantum Computing	188
09:30-09:50	O29	Kevin Lauer	Exploring ASi-Sii-defects as qubits	190
09:50-10:10	O30	Johannes Aberl	Fabrication and vertical position control of silicon colour centres via ultra-low temperature molecular beam epitaxy	192
10:10-19:00 Excursion				
19:00-22:00 Conference dinner				

GADEST 20/24 Sponsors (part I)

Fraunhofer Institute for Integrated Systems and Device Technology IISB



 **Fraunhofer**
IISB

SENTECH Instruments




SENTECH
Erfolg durch Leistung

Semiconductor Shop Online



 **EL-CAT Inc.**

Bruker Technologies




BRUKER

Freiberg Instruments



 Freiberg Instruments

PLASWAY - Technologies GmbH




plasway
ways to efficiency

Semilab




SEMILAB

Thursday, 12 September, 2024				Page
08:30-10:10 ThM1 Session: Material growth & characterization. Session chair: Deren Yang				
08:30-09:10	I12	Kaspars Dadzis	Multiphysical modelling of bulk crystal growth: from furnace design to defect engineering	194
09:10-09:30	O31	Shuai Yuan	Growth stability and defect generation of grain boundaries during directional solidification	196
09:30-09:50	O32	Jie Huang Shuai Yuan	Phosphorus gettering effect on iron-related defects around dislocations with different densities in N-type cast-mono silicon	198
09:50-10:10	O33	Katja Mustonen	Characterization of electrically active defects in semiconductor-grade Cz-Si by photoluminescence imaging	200
Coffee break				
10:40-12:20 ThM2 Session: Solar Cell Degradation. Session chair: Matthias Müller				
10:40-11:20	I13	Mariana Bertoni	Hydrogen-induced degradation dynamics in silicon heterojunction solar cells via machine learning	202
11:20-11:40	O34	Katharina Peh	Relationship between the P-line in indium-doped silicon spectra and the recent ASi-Sii defect model.	204
11:40-12:00	O35	Zhenyi Ni	Resolving the defects in polycrystalline metal halide perovskite by photoluminescence technique	206
12:00-12:20	O36	Daniela Cavalcoli	The role of Electron Trapping and Ion Drift on Photo-Induced Current Transient Spectroscopy of Metal Halide Perovskites	208
Lunch break				
13:30-15:30 ThA1 Session: Defect characterization I. Session chair: Hartmut Bracht				
13:30-14:10	I14	Koji Yokoyama	Muon probes of charge carrier kinetics in semiconductors	210
14:10-14:30	O37	Martin Herms	Photo-elastic Characterization of Twin Structures and Growth Striations in InP and GaAs Crystals	212
14:30-14:50	O38	Tim Böckendorf	Characterization of electrically active defects in elemental and compound semiconductors by means of Scanning Spreading Resistance Microscopy	214
14:50-15:10	O39	Vladimir Kolkovsky	Positively charged defects in Ta ₂ O ₅ and Nb ₂ O ₅ : are they correlated with sodium ions?	216
15:10-15:30	O40	Samira Khelifi	Secondary phases detection in CuInS ₂ single crystal	218
Coffee break				
16:00-17:40 ThA2 Session: Defect characterization II. Session chair: Jonathan Slotte				
16:00-16:20	O41	Roland Weingärtner	Threading dislocation line mapping in aluminum nitride wafers using X-ray topography in reflection geometry	220
16:20-16:40	O42	Viktoriaa Nikonova	Investigating the surface quality of wide bandgap materials using surface photovoltaic spectroscopy	222
16:40-17:00	O43	Houwei Pang	Enhanced emission in erbium and ytterbium doped gallium oxide devices based on the sensitization of oxygen vacancies	224
17:00-17:20	O44	Nishant Saini	Defect Noise & Multi-Defect Leakage Paths in Amorphous PECVD SiCN	226
17:20-17:40	O45	Kuei-Shen Hsu	Investigation of striations in single-crystalline silicon wafers by THz-TDS and other characterization methods	228
Dinner				

Friday, 13 September, 2024				Page
08:30-10:30 FrM1 Session: Doping. Session chair: Stefan Schmult				
08:30-09:10	I15	Michele Perego	Nanoscale Periodic Modulation of Doping over Large Areas by Means of Block Copolymer Lithography and Ion Implantation	230
09:10-09:50	I16	Dirk König	Direct Acceptor Modulation Doping for nano-Si: Foundations, Material Systems, Applications	232
09:50-10:10	O46	Soundarya Nagarajan	The Effect of Aluminium-Modulation-Doped SiO ₂ on the Transport Properties of Silicon	234
10:10-10:30	O47	Andrea Pulici	Ex-situ doping of ultra-thin silicon nanofilms: phosphorus deactivation and mobility enhancement	236
10:30-11:00 Coffee break				
11:00-12:00 Closing session				
11:00-11:20 Announcements				
11:20-11:40 Young Scientist Awards				
11:40-12:00 Closing: Johannes Heitmann, Daniel Hiller, Franziska Beyer				
12:20-13:30 Lunch and departure				

GADEST 20/24 Sponsors (part II)

Siltronic AG



SOITEC



Quantum Design Europe



Zurich Instruments



Physica Status Solidi A (Wiley-VCH GmbH)



Freiberger Compaund Materials GmbH





TUBAF
Die Ressourcenuniversität.
Seit 1765.

20th meeting
Gettering and Defect Engineering
in Semiconductor Technology

GADEST 20/24

Abstracts

Arrangement and editing of abstracts: Teimuraz Mtchedlidze

Printed by: Media Center Bergakademie Freiberg, Prüferstr. 1, 09599, Freiberg Germany

Plenary session: The 20th GADEST Conference – 40 Years of Research on Defects in Semiconductors

Forty Years of GADEST

Hans Richter

Society for the Promotion of Science and Economy -GFWW- e. V., In the Technology Park 1
Frankfurt (Oder), Germany

Email: richter@gfww.ge

The GADEST was constituted in the first half of the 80s of the last millennium as a result of discussions between scientists from different countries. It was the phase in which the semiconductor technology completed the transition from 2 inch diameter to 3 inch diameter of silicon single crystals. This transition was combined with the suppression of the formation of *as grown* dislocations (originally 10^3 - 10^4 dislocation per cm^2). In CZ-Si the dominant impurity was oxygen partially above the solubility limit. Another challenge was the entry into size-dimensions in the sub-micrometer range for electrical structures combined with discussions about possible physical limits that had to be exceeded. These challenges required on the one hand an increased international cooperation and on the other hand a close interdisciplinary research cooperation between industry and academic institutions.

Mechanical, electrical and optical effects of defects had to be understood [1, 2]. It was necessary to investigate to what extent they could be prevented or to what extent they could enhance new properties for functional elements or the production yield. A typical example for the application of defects was intrinsic gettering associated with the newly emerging term of defect engineering [3]. In addition, with the transition from large-scale integration (LSI) to very large integration (VLSI), the costs for the new technology was compensated by the opening up of new application fields, e.g. the “white goods”.

The first conference took place in October 1985 in the Resort Garzau near Berlin. Further conferences followed every two years in the State of Brandenburg until 1995 and in 1997 the conference was held in Spa/Belgium and from then on in changing European countries outside large urban areas. Among others, the main topic was the introduction of new technologies for the generations of 4 inch-, 6 inch-, 8 inch-, and 12 inch silicon-based microelectronics associated with a growing adoption of new materials in the process flow, up to hetero-integration [4]. Focal points were also topics in the area of photovoltaics applications such as the control of carbon and oxygen. “*Let the PV community discover the studies of oxygen and carbon carried on in the past (much done by the GADEST community) to push farther the efficiency of silicon solar cells*” [5].

From the roots of the GADEST to its role in the future: First, with new Back End Technologies as Advanced Packaging/system integration it is now possible to split the chip into a number of functional blocks (Chiplets). The communication of these Chiplets will base on photonics technologies ensuring unprecedented rates for the data transfer. To realize this vision a direct integration of photonics and nanoelectronics will be necessary. Second, in the 80s of the last century, basic researchers began to create man-made quantum effects in III-V semiconductor structures with structural sizes in the submicron range. Well known examples include the quantization of the conductivity in point contacts and single electron tunneling in transport through quantum dots at low temperatures. With today's industrial technology one is able to realize much smaller, customary tailored systems with sizes down to the Angstrom level on silicon thus suitable for mass production. It is evident that for the description of these new structures the

traditional drift-diffusion model including its refinements is insufficient. Advanced semiconductor devices require quantum transport theory such as the Landauer-Büttiker formalism. The access to the quantum world for industrial electronics opens a vast range of unprecedented new possibilities for new devices and new Chip technology. An example for such a new quantum transistor architecture which works at room temperature is given in Ref. [6].

We want the GADEST family to play a pioneering role in the thrilling forthcoming Angstrom era.

References:

- [1] C. L. Clays and J. Vanhellemont, Proc. of the GADEST 1985. ed. H. Richter. p. 100-119.
- [2] K. Sumino, Proc. of the GADEST 1985, ed. H. Richter. p. 41-55.
- [3] J. Chikawa, K. Sumino, and K. Wada in 'Defects and properties of semiconductors: Defect engineering'. KTK Scientific Publications 1987.
- [4] H. R. Hull and R. K. Goodall, GADEST'95 in Solid State Phenomena, Volume 47-48.
- [5] S. Benetti. Proc. of the GADEST 2022 in Solid State Physics.
- [6] Patentschrift „Doppelgate-Vierpol-Halbleiterbauelement mit finförmigen Kanalgebiet“ DE 10 2021 107 880 B3 2022.07.28, U. Wulf and H. Richter.



The GADEST Family, Erice/Sicily/2007

Plenary session: The 20th GADEST Conference – 40 Years of Research on Defects in Semiconductors

Investigation of dislocations in III-V Semiconductors

S. Eichler

Freiberger Compound Materials GmbH, Am Junger Löwe Schacht 5, D-09599

Email: stefan.eichler@freiberger.com

Formation mechanism and local distribution of dislocations in melt grown III-V semiconductors as well as in III-nitrides are discussed since decades [1,2]. There are various methods to investigate dislocations. The relatively high density of the dislocations (10^3 - 10^6 cm $^{-2}$) complicates the experimental investigation of the dynamics of single dislocations. Recent developments of crystal growth technologies resulted in very low dislocation densities in the order of 10 to several 100 cm $^{-2}$ for highly n-type or semi-insulating GaAs and InP. We have used different characterization methods to investigate the type of the dislocations as well as their local arrangements. Some of the dislocation structures can be explained by theoretical modelling of dislocation dynamics at characteristic stress conditions during crystal growth.

References:

- [1] Rudolph P. Defect formation during crystal growth from the melt. In: Dhanaraj G., Byrappa K., Prasad V., Dudley M., editors. Springer Handbook of Crystal Growth. Heidelberg: Springer Verlag, 2010. p. 159.
- [2] Bickermann M., Paskova T., Vapor Transport Growth of Wide Bandgap In: Rudolph P. editor. Handbook of Crystal Growth. Elsevier, 2015, p. 1621-669.

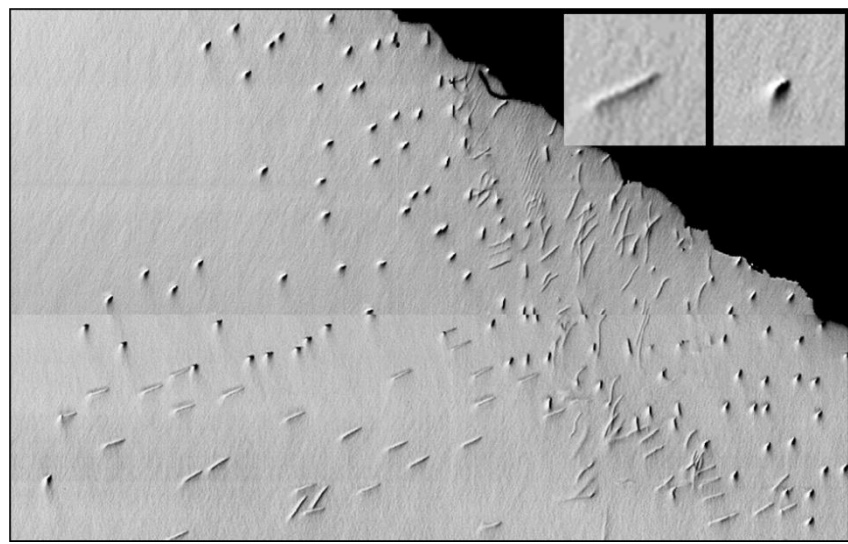


Figure: IR-transmission image of dislocations in 15°off (100) GaAs:Si

Cryogenic Electronics and Novel Semiconductor Doping Approaches

Joachim Knoch¹

¹ Institute of Semiconductor Electronics, RWTH Aachen University, Sommerfeldstr. 18, 52074, Aachen,
 Germany

Email: knoch@iht.rwth-aachen.de

Cryogenic electronics has recently attracted an increasing attention, in particular as control electronics of semiconductor spin qubits whose implementation, tuning and coupling relies on a multitude of gate electrodes. Furthermore, in order to realize a large number of logic qubits including error correction schemes, a rather large number of physical qubits is required. Thus, to control all these devices a classical electronics needs to be located in immediate vicinity to the chip hosting the qubits. Since the cooling power of fridges is very limited at typical qubit operating temperatures, the classical control electronics needs to be operable at cryogenic temperatures with extremely low power consumption, i.e. at operating voltages in the few tens of mV range. While textbook MOSFET theory predicts a switching behaviour linearly dependent on temperature, enabling in principle very steep inverse subthreshold swings (SS), temperature-dependent measurements of real devices show a saturation of SS below a certain temperature [1]. Moreover, the switching behaviour is further degraded in the transition region around threshold which is called inflection phenomena [2]. The subthreshold swing saturation is due to disorder of the MOS-interface giving rise (on average) to a density of mobile states that exponentially decays into the band gap, called band-tailing. Inflection, on the other hand, is due to a density of localized defect states around the band gap deteriorating the gate control of the transistor. Finally, impurity doping of MOSFETs at cryogenic temperatures becomes increasingly problematic, due to random dopants effects leading to an additional source for disorder, Coulomb oscillation or freeze-out effects due to a possible deactivation of dopants. As a result, suppressing the impact of defects/impurities or even avoid them altogether is instrumental to achieving performance improvements of cryogenic field-effect transistors. Here, we will discuss a number of approaches including interface engineering, improved screening as well as the use of 2D materials to reduce band tailing and inflection [3-5,8]. Moreover, two approaches to removing dopants from the source/drain contacts will be discussed [5-8].

References:

- [1] H. Bohuslavskyi, A.G.M. Jansen, S. Barraud, V. Barral, M. Casse, L. Le Guevel, X. Jehl, L. Hutin, B. Bertrand, G. Billiot, G. Pillonnet, F. Arnaud, P. Galy, S. De Franceschi, M. Vinet, and M. Sanquer, *IEEE Electron Dev. Lett.*, **2019**, 40, 784.
- [2] A. Beckers, F. Jazaeri, and C. Enz, *IEEE Trans. Electron Dev.*, **2020**, 67, 1357.
- [3] B. Richstein, Y. Han, Q.T. Zhao, L. Hellmich, J. Klos, S. Scholz, L.R. Schreiber, J. Knoch, *IEEE Electron Dev. Lett.*, **2022**, 42, 2149.
- [4] J. Knoch, B. Richstein, Y. Han, C. Jungemann, E. Icking, L.R. Schreiber, R. Xue, J.-S. Tu, T. Gökcöl, J. Neugebauer, C. Stampfer, Q.T. Zhao, *2023 IEEE Nanotechnol. Mater. Dev. Conf.*, **2023**, 440.
- [5] Y. Han, J. Sun, B. Richstein, F. Allibert, I. Radu, J.-H. Bae, D. Grütmacher, J. Knoch, Q.-T. Zhao, *IEEE Electron Dev. Lett.*, **2022**, 43, 1187.
- [6] D. König, M. Frentzen, D. Hiller, N. Wilck, G. Di Santo, L. Petaccia, I. Pís, F. Bondino, E. Magnano, J. Mayer, J. Knoch, S.C. Smith, *Adv. Phys. Res.*, **2023**, 2, 2200065.
- [7] D. König, M. Frentzen, N. Wilck, B. Berghoff, I. Pis, S. Nappini, F. Bondino, M. Müller, S. Gonzalez, G. Di Santo, L. Petaccia, J. Mayer, S.C. Smith, J. Knoch, *ACS Appl. Mater. & Interf.*, **2021**, 13, 20479.
- [8] J. Knoch, B. Richstein, Y. Han, C. Jungemann, E. Icking, L.R. Schreiber, R. Xue, J.-S. Tu, T. Gökcöl, J. Neugebauer, C. Stampfer and Q.T. Zhao, *2023 IEEE Nanomater. Dev. Conf. (NMDC)*, 440-445 (2023).

For your remarks

Quantum sensing and quantum photonics with spin centres in crystals

Michael Trupke

Austrian Academy of Sciences, IQOQI-Vienna, Boltzmanngasse 3, 1090 Vienna, Austria

Email: michael.trupke@oeaw.ac.at

Spin centres in crystals, particularly in diamond and silicon carbide (SiC), have emerged as a key platform for the development of quantum technology. Following a brief overview of the field, two defect systems will be discussed which are being researched at IQOQI-Vienna.

The nitrogen-vacancy (NV) centre in diamond has spearheaded the development of spin centres for quantum technology, chiefly towards devices for quantum sensing. Their sensitivity is in part limited by the spin contrast and by the collection of photoluminescence. I will present a method to improve the spin contrast by tailoring the optical initialization to the NV's ionization cycle¹. I will also describe progress on electrical readout, which allows to circumvent optical collection, with a view to enhanced state readout². Finally, I will discuss a method to control and read out scalable arrays of sensors based on NV centres.

For quantum photonics, other systems are being explored in search of better optical properties. In many cases, their performance is significantly reduced by wavelength conversion from the telecom range to the optical transition frequency of the atoms or defects³. Vanadium in SiC has emerged as a strong candidate for these applications⁴⁻⁹: It has a strong optical transition at 1.3 μm, compatible with optical fiber networks, a long-lived electron spin, and is hosted in a material that is available with high quality at an industrial scale. Our investigations have resulted in significant advances in our understanding of this remarkable system, the control of its electron spin, and the development of photonic interfaces for quantum networks¹⁰.

Spin-dependent optical transitions, which are crucial for quantum communication and computation applications, have now been demonstrated (see Fig. 2 d)⁹. Together with its long spin lifetime of over 20 s at cryogenic temperatures, this defect holds promise for a spin-based quantum technology platform with photon-mediated entanglement operations^{7,11}. Furthermore, we have shown that vanadium can be used as an extremely sensitive probe for the crystalline structure and electronic properties of the silicon carbide host: Its charge state stability depends strongly on the electronic environment in the SiC crystal, and its zero-phonon line resonance frequency is dependent on the isotope composition of the neighbouring lattice sites⁹.

References:

- [1] D. Wirtitsch et al., Phys. Rev. Research 5 1, 013014 (**2023**); DOI: 10.1103/PhysRevResearch.5.013014.
- [2] M. Gulkka et al., Nat Commun 12 1, 4421 (**2021**); DOI: 10.1038/s41467-021-24494-x.
- [3] S. Wei et al., Laser & Photonics Reviews 16 3, 2100219 (**2022**); DOI: 10.1002/lpor.202100219.
- [4] L. Spindlberger et al., Phys. Rev. Applied 12 1, 014015 (**2019**); DOI: 10.1103/PhysRevApplied.12.014015.
- [5] C. M. Gilardoni et al., New J. Phys. 23 8, 083010 (**2021**); DOI: 10.1088/1367-2630/ac1641.
- [6] B. Tissot et al., Phys. Rev. Research 4 3, 033107 (**2022**); DOI: 10.1103/PhysRevResearch.4.033107
- [7] T. Astner et al., arXiv (**2022**); DOI: 10.48550/ARXIV.2206.06240.
- [8] J. Hendriks et al., arXiv (**2022**); DOI: 10.48550/ARXIV.2210.09942.
- [9] P. Cilibrizzi et al., Nature Communications 14 1, 8448 (**2023**); DOI: 10.1038/s41467-023-43923-7.
- [10] J. Fait et al., Appl. Phys. Lett. 119 22, 221112 (**2021**); DOI: 10.1063/5.0066620.
- [11] K. Nemoto et al., Physical Review X 4 3 (**2014**); DOI: 10.1103/PhysRevX.4.031022.

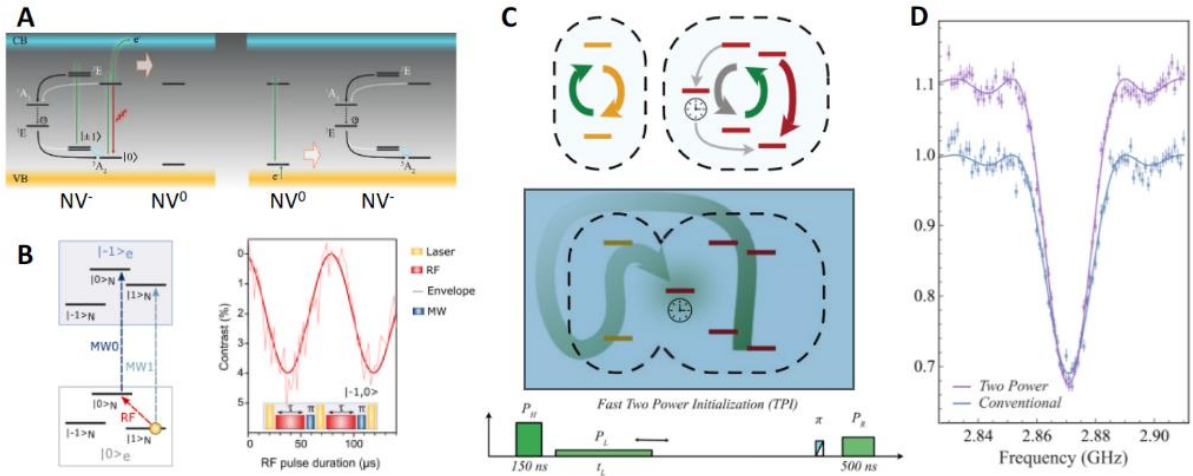


Fig. 1 **a)** Ionization cycle of the NV centre, leading to spin-dependent photocurrent. **b)** Transition diagram and measurement for the detection of coherent rotations of a single nuclear spin. **c)** Concept of contrast enhancement by two-power initialization. **d)** Measurement of pulsed optically detected magnetic resonance for conventional initialization and readout compared with the two-power initialization.

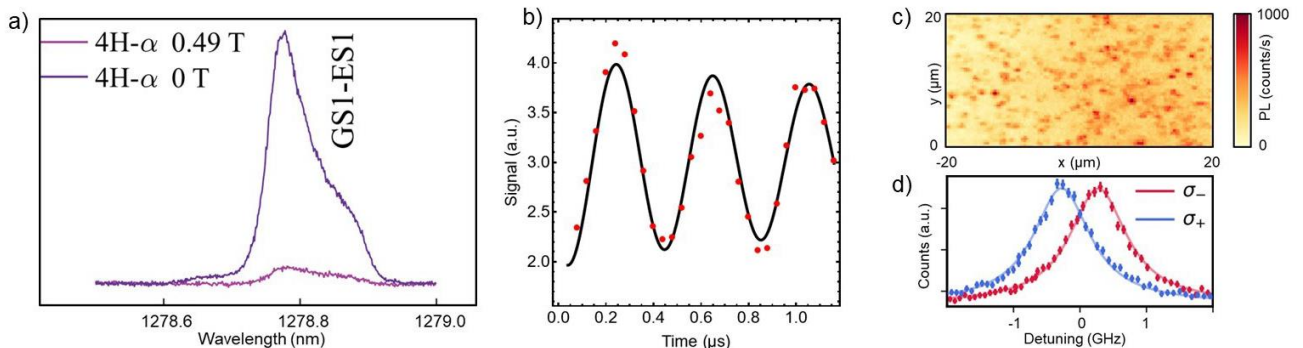


Fig. 2 **a)** Spectrum of an ensemble of neutral vanadium (V_{4+}) α in 4H SiC at 100 mK. **b)** Ensemble Rabi oscillations at 0.4 K (unpublished). **c)** Photoluminescence map of V_{4+} α defects in 4H SiC. **d)** Spin-dependent optical excitation of a single V_{4+} spin centre.

Laser-assisted crystallisation and hyperdoping

Enrico Napolitani¹

¹Dipartimento di Fisica e Astronomia, Università di Padova and CNR-IMM and LNL-INFN, Via Marzolo 8,
 I-35131 Padova, Italy

Email: enrico.napolitani@unipd.it

Doping of group-IV semiconductors at concentrations well above equilibrium solubilities, so called ‘hyperdoping’, is crucial for advanced applications in several fields, such as nanoelectronics, photonics, plasmonics, photovoltaics, quantum computing (solid state qubits), etc.

This talk will review recent results obtained with the Pulsed Laser Melting (PLM) technique which, thanks to the ultra-fast solidification of laser-induced liquid layers, enables record solubilities in most systems. The focus will be on the structural, electrical and optical properties of Ge hyperdoped, both n-type and p-type, on Ge alloyed with Sn, and on Si hyperdoped.

We’ll show that, during PLM, several complex phenomena take place which must be investigated and properly controlled for material development, such as dopant clustering (both in the liquid and in the solid phase), dopant segregation, in-diffusion of contaminants, evolution of extended defects and strain, surface morphology, etc.[1-6] The stability of the metastable layers upon post-PLM thermal processes need also to be addressed.[7]

Beyond record solubilities and the possibility to tailor extended defects and strain, PLM provides also excellent spatial and temperature confinement, with sample heating limited to the uppermost layers and with extremely sharp junctions, which makes PLM extremely interesting for future device development.

References:

- [1] R. Duffy, E. Napolitani, F. Cristiano, Materials science issues related to the fabrication of highly doped junctions by laser annealing of Group IV semiconductors, in: Laser Annealing Process. Semicond. Technol., Elsevier, 2021: pp. 175–250. <https://doi.org/10.1016/B978-0-12-820255-5.00007-6..>
- [2] E. Di Russo, F. Sgarbossa, P. Ranieri, G. Maggioni, S. Ndiaye, S. Duguay, F. Vurpillot, L. Rigutti, J.-L. Rouvière, V. Morandi, D. De Salvador, E. Napolitani, Synthesis of relaxed Ge0.9Sn0.1/Ge by nanosecond pulsed laser melting, Appl. Surf. Sci. 612 (2023) 155817. <https://doi.org/10.1016/j.apsusc.2022.155817>.
- [3] K. Chen, E. Napolitani, M. De Tullio, C. Jiang, H. Guthrey, F. Sgarbossa, S. Theingi, W. Nemeth, M. Page, P. Stradins, S. Agarwal, D.L. Young, Pulsed Laser Annealed Ga Hyperdoped Poly-Si/SiO_x Passivating Contacts for High - Efficiency Monocrystalline Si Solar Cells, Energy Environ. Mater. 6 (2023) 1–12. <https://doi.org/10.1002/eem2.12542>.
- [4] D. Fontana, F. Sgarbossa, R. Milazzo, E. Di Russo, E. Galluccio, D. De Salvador, R. Duffy, E. Napolitani, Ex-situ n-type heavy doping of Ge1-xSnx epilayers by surface Sb deposition and pulsed laser melting, Appl. Surf. Sci. 600 (2022) 154112. <https://doi.org/10.1016/j.apsusc.2022.154112.F>.
- [5] C. Carraro, R. Milazzo, F. Sgarbossa, D. Fontana, G. Maggioni, W. Raniero, D. Scarpa, L. Baldassarre, M. Ortolani, A. Andriguetto, D.R. Napoli, D. De Salvador, E. Napolitani, N-type heavy doping with ultralow resistivity in Ge by Sb deposition and pulsed laser melting, Appl. Surf. Sci. 509 (2020) 145229. <https://doi.org/10.1016/j.apsusc.2019.145229>.
- [6] S.F. Lombardo, S. Boninelli, F. Cristiano, I. Deretzs, M.G. Grimaldi, K. Huet, E. Napolitani, A. La Magna, Phase field model of the nanoscale evolution during the explosive crystallization phenomenon, J. Appl. Phys. 123

(2018) 105105. <https://doi.org/10.1063/1.5008362>.

[7] R. Milazzo, G. Impellizzeri, D. Piccinotti, D. De Salvador, A. Portavoce, A. La Magna, G. Fortunato, D. Mangelinck, V. Privitera, A. Carnera, E. Napolitani, Low temperature deactivation of Ge heavily n-type doped by ion implantation and laser thermal annealing, *Appl. Phys. Lett.* 110 (2017) 011905. <https://doi.org/10.1063/1.4973461>.

Recombination-active Defects in Crystalline Silicon after Muon Implantation

Tim Niewelt^{1,2,3}, Anup Yadav¹, Sophie L. Pain¹, Koji Yokoyama⁴, Vladimir P. Markevich⁵, James Lord⁴, Nicholas E. Grant¹ and John D. Murphy¹

¹ School of Engineering, University of Warwick, Coventry CV4 7AL, United Kingdom

² Institute for Sustainable Systems Engineering, University of Freiburg, Emmy-Noether-Straße 2,
 79110 Freiburg, Germany

³ Fraunhofer Institute for Solar Energy Systems ISE, Heidenhofstraße 2, 79110 Freiburg, Germany

⁴ ISIS, STFC Rutherford Appleton Laboratory, Didcot OX11 0QX, United Kingdom

⁵ Department of Electrical and Electronic Engineering, University of Manchester, Manchester M13 9PL,
 United Kingdom

Email: tim.niewelt@ise.fraunhofer.de

Muons are a main contributing factor to cosmic radiation. Given their often large kinetic energy in the GeV range they can penetrate through shielding and are the main species of charged cosmic particles that semiconductor devices encounter. For example they have a major impact on the dark current of cooled and lead-lined single-photon avalanche diodes (SPADs) [1]. Muons of lower energy in the MeV range created in accelerator facilities can be used for material characterisation, e.g. in the form of photoexcited μ SR [2]. In such an experiment we recently demonstrated that the implantation of muons in silicon damages the crystal [3]. In this contribution we report on further characterisation of this damage.

Si samples were exposed to high doses of 150-1500 million antimuon implantation events at the Rutherford Appleton Laboratory ISIS Neutron and Muon source, roughly corresponding the lifetime dose of 20-40 years of cosmic muon exposure of terrestrial device open sky application (e.g. for outdoor devices such as solar cells or telescopes). The muons featured a kinetic energy of 3.8 MeV and hence interacted significantly more strongly with the Si lattice than can be expected for cosmic muons. In addition, we used metal degrader foils to alter the muon energy and hence implantation depth and dissipated energy in our samples. Furthermore, we investigated p-type and n-type substrates and investigated the impact of muon transmission versus implantation. Fig.1 illustrates the performed muon implantations. The impact of muon exposure on the Si lattice was investigated via photoluminescence imaging and charge carrier lifetime measurements. We observe significant reduction in carrier lifetime, hence confirming the formation of recombination active defects (see Fig.2). Stronger degradation is observed in n-type Si compared to p-type and energy deposition during muon transmission gives rise to defect formation. We have observed that the caused damage scales superlinear for slowed or stopping muons. This may indicate that very slow muons or the positrons emitted upon their decay create additional or different defects. We hope to clarify this with upcoming DLTS measurements. We will have another session of beamline experiments prior to the conference and thus may be able to clarify some of the points further.

References:

- [1] A. R. Smith, R. J. McDonald, D. C. Hurley, S. E. Holland, D. E. Groom, W. E. Brown *et al.*, presented at Sensors and Camera Systems for Scientific, Industrial, and Digital Photography Applications III, San Jose, USA, 2002, doi: 10.1117/12.463423.
- [2] K. Yokoyama, J. S. Lord, J. Miao, P. Murahari, and A. J. Drew, *Phys Rev Lett*, **2017**, vol. 119, p. 226601, doi: 10.1103/PhysRevLett.119.226601.
- [3] J. D. Murphy, N. E. Grant, S. L. Pain, T. Niewelt, A. Wratten, E. Khorani *et al.*, *Journal of Applied Physics*, **2022**, vol. 132, p. 065704, doi: 10.1063/5.0099492

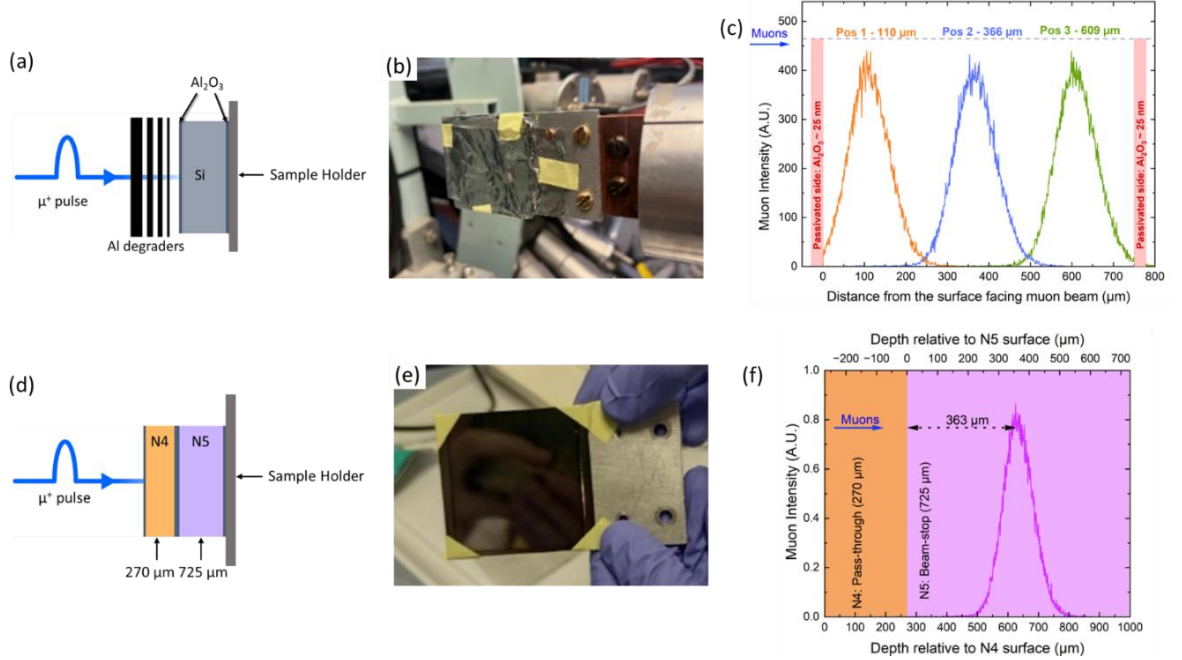


Fig. 1. (a) Experiment schematic. (b) Photograph of mounted sample with Al degraders. (c)&(f) Simulated muon deposition depth profile for the used degrader configurations. (d) Schematic representation of transmission vs. implantation experiment. (e) Photograph of stacked sample mounting.

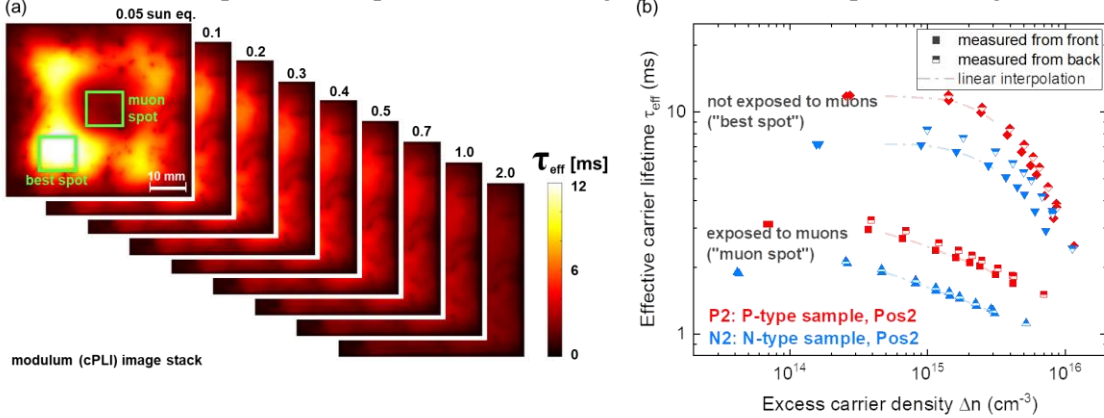


Fig. 2. (left) lifetime-calibrated photoluminescence image stack illustrating the comparison of pristine and muon exposed areas on the Si sample. (right) extracted effective carrier lifetimes for a p-type and an n-type sample.

Realistic Simulation and Physical Understanding of Laser Melting in Silicon-Germanium Substrates

Damiano Ricciarelli,¹ Jonas Müller,² Guilhem Larrieu,² Ioannis Deretzs,¹ Gaetano Calogero,¹ Enrico Martello,¹ Giuseppe Fisicaro,¹ Jean-Michel Hartmann,³ Sébastien Kerdilès,³ Mathieu Opprecht,³ Antonio Massimiliano Mio,¹ Richard Daubriac,² Fuccio Cristiano,² Antonino La Magna¹

¹ National Research Council of Italy, Institute for Microelectronics and Microsystems (IMM-CNR), VIII Strada 5, 95121, Catania, Italy

² The French National Center for Scientific Research, Laboratory for Analysis and Architecture of Systems (LAAS-CNRS) and University of Toulouse, 7 Av. du Col. Roche, 31400, Toulouse, France

³ Université Grenoble Alpes, CEA-LETI, Minatec Campus, 17 rue des martyrs, F-38054, Grenoble Cedex 9, France

Email: damiano.ricciarelli@imm.cnr.it

Si-Ge alloys are increasingly used in microelectronics due to their compatibility with silicon, allowing engineering in strain, carrier mobility, and optical band gaps, because of germanium's higher hole mobility, smaller band gap and larger lattice parameters [1]. Ultraviolet nanosecond laser annealing (UV-NLA) has emerged as a promising technique in micro- and nano-electronics for activating dopants and thermally treating specific regions without damaging adjacent device components, showing higher potential than traditional rapid thermal annealing [2]. Effective UV-NLA implementation demands optimal control and reliable simulations to fine-tune parameters and minimize experimental trials amidst growing device complexity. Challenges for continuum simulations of laser annealing include using accurate description of solid and liquid Si_{1-x}Ge_x reflectivity governing the source-to- specimen heat transfer, affecting melt depths (Fig. 1a), Ge segregation and dopant redistribution profiles. We addressed these issues with numerical simulations using a phase field approach within a Technology Computed-Aided Design (TCAD) software [3]. We firstly calibrated dielectric functions and reflectivity (R) of liquid and solid Si_{1-x}Ge_x alloys, shown in Fig. 1b-c, from experiment, unraveling a non-linear behaviour of liquid Si_{1-x}Ge_x R as a function of the Ge content, near the melting point [4]. We explain this unconventional behaviour with ab-initio molecular dynamics, reproducing the trend as shown in Fig. 1d and further highlighting a direct correlation between liquid R Si-Ge and the local coordination of Si and Ge atoms in the liquid structure [5]. The calibrated and physically understood TCAD tool has been further applied to more complex laser annealed structures, consisting of SiO₂ stripes atop Si_{1-x}Ge_x patterned structures, shown in Fig. 2a, achieving an optimal agreement between simulated and experimental results (Fig. 2b), further stressing the predictive capabilities of the calibrated software. Last but not least, capping Si_{1-x}Ge_x with SiO₂ stripes turned out to be a promising technique to foster a higher morphological control of the liquid regrowth during the UV-NLA melting process.

References:

- [1] Ong, Pey, Lee, *Sci. Engineer. B*, **2004**, 114-115,25-28.
- [2] Manku, McGregor, Nathan, *IEEE Trans. Electron Devices*, **1993**, 11, 1990-1996.

- [3] Lombardo, Fisicaro, Deretzs, *Appl. Surf. Sci.*, **2019**, 467-468, 666-672.
- [4] Ricciarelli, Mannino, Deretzs, *Mater. Sci. Semicond. Proc.*, **2023**, 165, 107635.
- [5] Ricciarelli, Deretzs, Calogero, *J. Phys. Chem. C*, **2024**, 128, 3019-3025

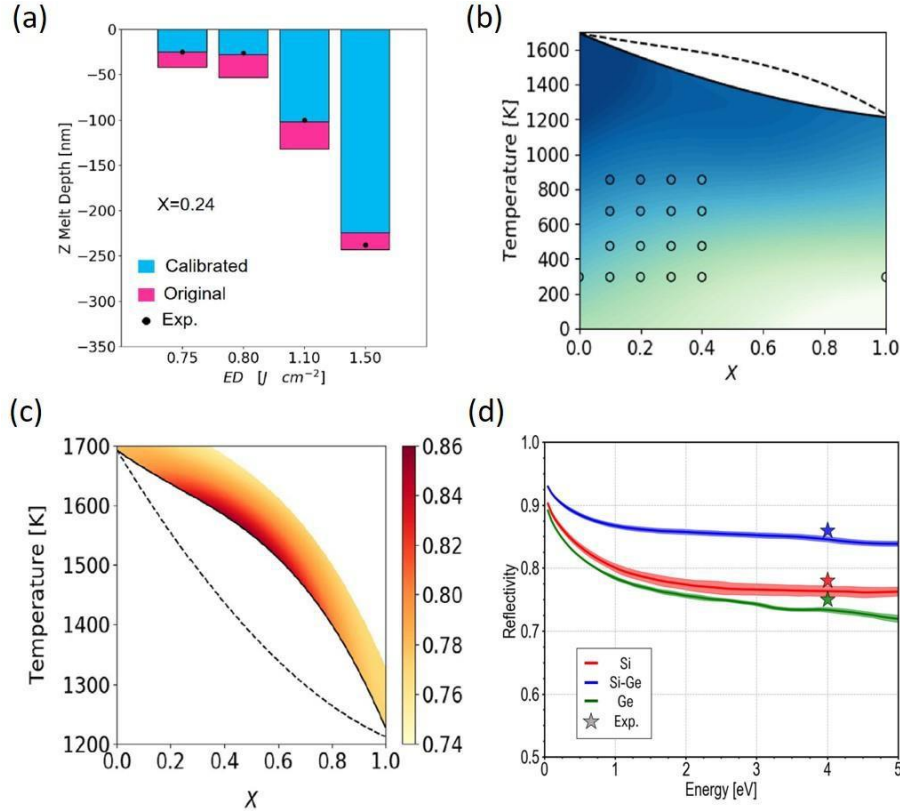


Fig. 1. (a) Melt depths obtained from calibrated and non-calibrated models for relaxed $\text{Si}_{0.8}\text{Ge}_{0.2}$, reflectivity of (b) crystal and (c) liquid $\text{Si}_{1-X}\text{Ge}_X$ as a function of Ge content (X) and temperature, (d) reflectivity of Si, $\text{Si}_{0.5}\text{Ge}_{0.5}$ and Ge computed from ab-initio molecular dynamics at the melting points.

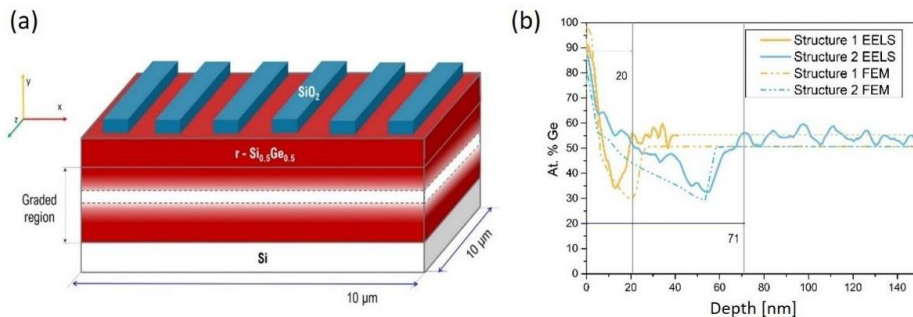


Fig. 2. (a) Simplified scheme of relaxed $\text{Si}_{0.5}\text{Ge}_{0.5}$ samples capped with SiO_2 stripes and (b) comparison of Ge segregation profiles for selected structures between experiment (EELS) and calculations (FEM).

Effects of phosphorous and antimony doping on Ge layers grown on Si

Hui Jia^{1,*} Xueying Yu¹ Junjie Yang,¹ Mateus G Masteghin,² Harvey Beere,³ Makhayeni Mtunzi,¹ Huiwen Deng,¹ Suguo Huo⁴ Chong Chen,³ Siming Chen,¹ Mingchu Tang,¹ Stephen J Sweeney,⁵ David Ritchie,³ Alwyn Seeds¹ and Huiyun Liu¹

1 Department of Electronic and Electrical Engineering, University College London, Torrington Place, WC1E 7JE London, United Kingdom

2 Advanced Technology Institute, University of Surrey, Guildford, Surrey, GU2 7XH, United Kingdom

3 Cavendish Laboratory, University of Cambridge, Cambridge CB3 0HE, United Kingdom

4 London Centre for Nanotechnology, 17-19 Gordon Street, London WC1H 0AH, United Kingdom

5 James Watt School of Engineering, University of Glasgow, G12 8LT, United Kingdom

Email: hui.jia@ucl.ac.uk

The suppression of threading dislocations (TDs) in thin germanium (Ge) layers grown on silicon (Si) substrates has been critical for realizing high-performance Si-based optoelectronic and electronic devices. In this work, we investigate the impact of P dopants in 500-nm thin Ge layers, with doping concentrations from 1 to $50 \times 10^{18} \text{ cm}^{-3}$ grown by molecular beam epitaxy. The introduction of P dopants has efficiently reduced the TD density, whose potential mechanism has been explored and compared to the well-established Sb-doped Ge-on-Si system. It was found that thanks to the enhanced Ge/Si interdiffusion brought by P doping in the initial Ge nucleation layer on Si, a graded GeSi layer formed at the interface. It may play the role of bending the TDs towards the edge of the wafer due to the difference in propagation speed of TDs [1-4] in the graded GeSi. Sb dopants reveal different defect-suppression mechanisms in Ge-on-Si samples. Apart from the surfactant effect that reduces islanding thus results in less defect generation, the large Sb atoms may also alter the local strain field and redirect the TDs. In addition, it has been reported that the co-doping of Sb and P can compensate the dopant-related stress and increase the substitutional solubility of both dopants and free electron concentration [5]. This change will react on the number of double negatively charged dopant-vacancy pair and thus the dopants diffusion and TD dynamics. Inspired by this, a novel co-doping technique by exploiting the advantages of both dopants has been demonstrated that further reduces the surface TDD of the Ge buffer on Si to the order of 10^7 cm^{-2} within a thin thickness of only 500 nm as revealed by electron channeling contrast imaging. This growth technique can provide a feasible and high-quality platform for high-performance Si-based semiconductor devices.

References:

- [1] S. Strite, M. et al., Appl. Phys. lett. 1990, vol. 56, no. 17, pp. 1673-1675, 1990.
- [2] Y. Takagi, et al., Jap. J. Appl. Phys. 1994, vol. 33, no. 6R, p. 3368, 1994.
- [3] J. Ayers, Journal of applied physics 1995, vol. 78, no. 6, pp. 3724-3726.
- [4] M. Yamaguchi, et.al., Applied physics letters 1998, vol. 53, no. 23, pp. 2293-2295.
- [5] J. Vanhellemont and E. Simoen, Materials Science in Semiconductor Processing 2012, vol. 15, no. 6, pp. 642-655.

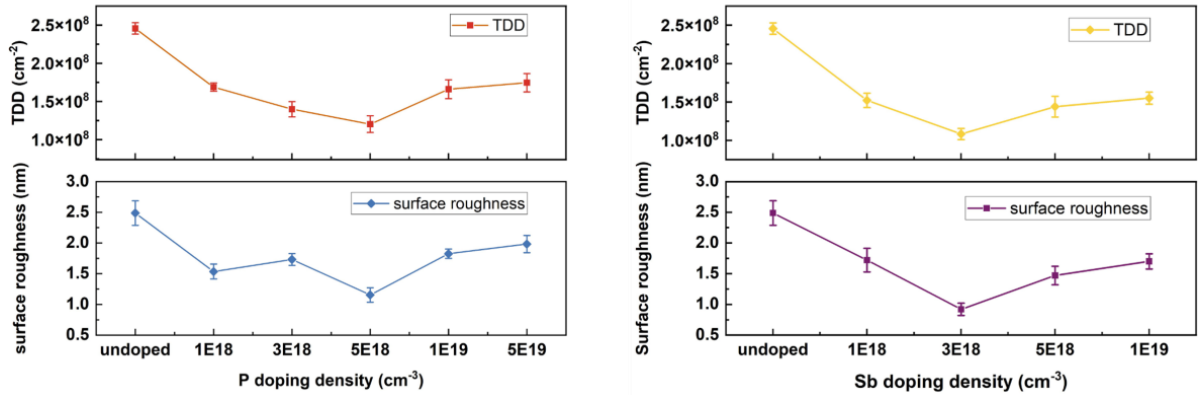


Fig. 1. Summarized plots of TDD and RMS roughness of samples with (a) P doping density of 0, 1, 3, 5, 10, and $50 \times 10^{18} \text{ cm}^{-3}$, indicating the lowest TDD occurs at P concentration of $5 \times 10^{18} \text{ cm}^{-3}$ and (b) Sb doping density of 0, 1, 3, 5 and $7 \times 10^{18} \text{ cm}^{-3}$, indicating the lowest TDD occurs at Sb concentration of $3 \times 10^{18} \text{ cm}^{-3}$.

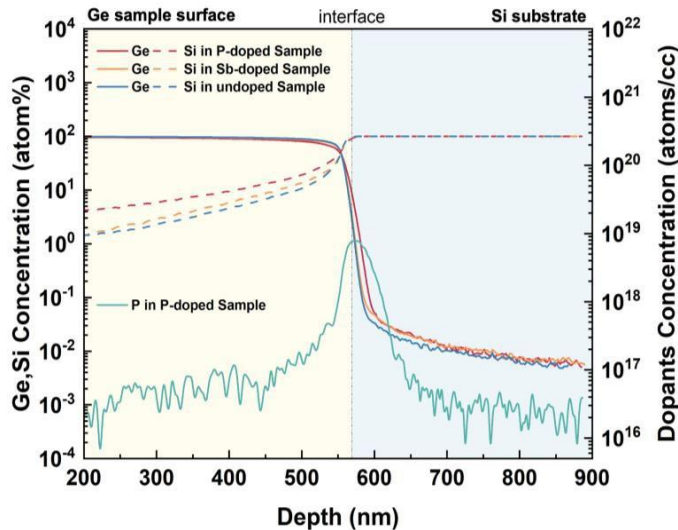


Fig. 2. SIMS results describe the varied concentration of compositions in the $5 \times 10^{19} \text{ cm}^{-3}$ P-doped, the $3 \times 10^{18} \text{ cm}^{-3}$ Sb-doped, and the undoped samples, respectively.

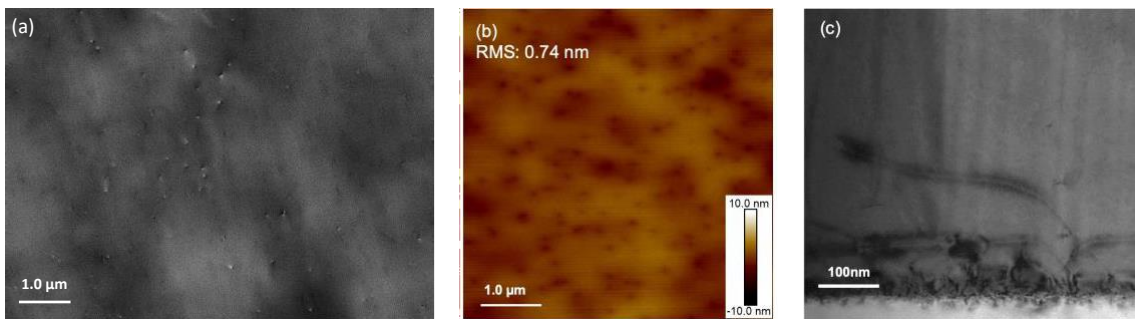


Fig. 3. (a) ECCI scan describing the surface TDD; (b) $5 \mu\text{m} \times 5 \mu\text{m}$ AFM image showing the surface morphology of the sample with co-doping of $1 \times 10^{18} \text{ cm}^{-3}$ P and $3 \times 10^{18} \text{ cm}^{-3}$ Sb and (c) Cross-sectional TEM image presenting the TDs at the Ge/Si interface of the co-doped sample.

Radiation Induced Defects in SiC Material and Devices

Marianne E. Bathen,^{1,2} Corinna Martinella² and Ulrike Grossner²

¹ Department of Physics/Centre for Materials Science and Nanotechnology, University of Oslo, 0316, Oslo, Norway

² Advanced Power Semiconductor Laboratory, ETH Zürich, 8092, Zürich, Switzerland

Email: m.e.bathen@fys.uio.no

Silicon carbide is an intriguing material for applications ranging from power devices for extreme environments to quantum technologies (QT) [1]. While defects are a key building block for SiC based QT [2], they pose a major obstacle for the utilization of SiC material in power electronics applications [1], especially in radiation-prone environments such as space. Indeed, particle impacts can introduce electrically active defects in SiC material that can, e.g., reduce device efficiency [3] or lead to single event effects (SEEs) [4], effectively diminishing the reliability of SiC power devices. In this contribution, we discuss the characterization of SiC material, defect and device properties following exposure to particle radiation (protons, neutrons and heavy-ions) using electrical and optical techniques. The resulting defect types range from point to extended defects depending on impinging particle and energy.

Fig. 1 illustrates the difference in defect formation and stability after exposing SiC wafers to (a) high (200 MeV) and (b) low (1.8 MeV) energy protons as measured using deep level transient spectroscopy (DLTS). Point defects are predominantly generated in these cases [5]. In Fig. 2, the impact of the low-energy protons on a SiC Schottky diode is demonstrated, where the edge transient current technique (edge-TCT) is used to monitor the defect formation caused by the protons [3]. In this case, a highly defective region causes a reversal of space charge polarity inside the device. Considering more advanced devices, like SiC power MOSFETs, defects can have a significant and debilitating impact. For example, Xe broad-beam can cause SEEs and induce bright-spot anomalies that are detected using cathodoluminescence (CL) spectroscopy and attributed to defects in the SiC epitaxial layers [6], see Fig. 3. The large spatial extension indicates extended defects.

The contribution at GADEST2024 will discuss the formation of point- and extended defects under different radiation conditions, and link the different defect types to SiC device performance.

References:

- [1] T. Kimoto and J. A. Cooper, Fundamentals of Silicon Carbide Technology: Growth, Characterization, Devices and Applications (Wiley, 2014).
- [2] J. R. Weber, et al., PNAS 107, 8513-8518 (2010).
- [3] C. Dorfer, M. E. Bathen, et al., APL 122, 183503 (2023).
- [4] C. Martinella, et al., Microelectron. Reliab. 128, 114423 (2022).
- [5] P. Kumar, M. E. Bathen, et al., Materials Science Forum 1092, 187-192 (2023).
- [6] C. Martinella, M. E. Bathen, et al., Materials Science Forum 1090, 179-184 (2023).

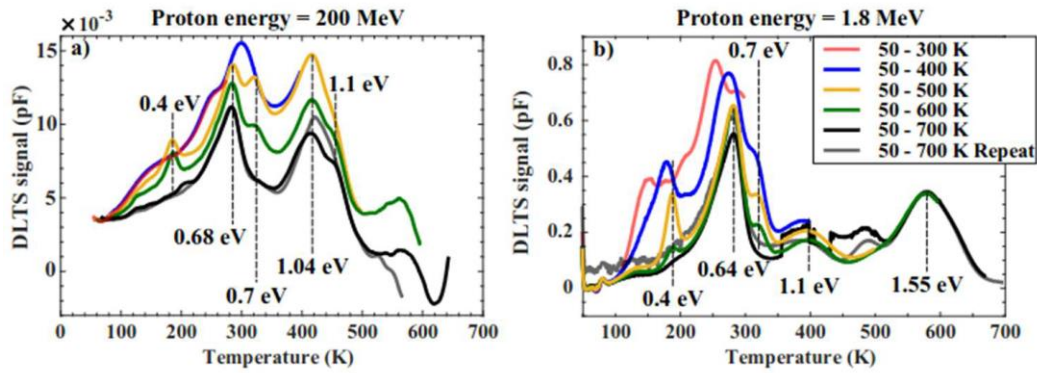


Fig. 1. DLTS spectra showing point defects induced in SiC material by a) 200 MeV and b) 1.8 MeV proton irradiation. After Ref. [5].

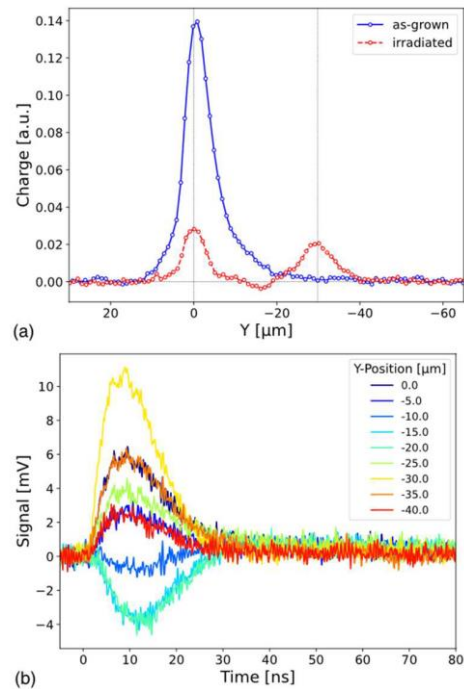


Fig. 2. (a) Charge collection profiles obtained using the edge-TCT showing increased charge collection in the irradiation peak of 1.8 MeV protons, and (b) signal polarity showing negative signal in the irradiated sample due to reversed electric field in the bulk of the device. After Ref. [3].

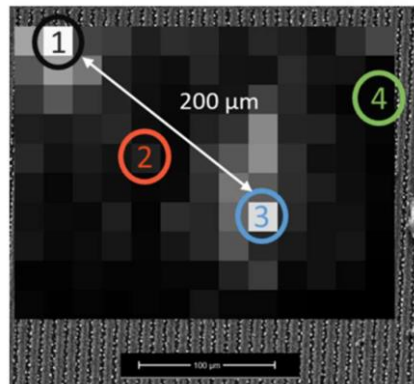


Fig. 3. CL analysis after exposure to Xe broad-beam showing bright spots indicating formation of extended defects. After Ref. [6].

Electron-irradiation-induced EE1 trap in GaN: unusual electronic properties of a defect linked to the nitrogen vacancy

V.P. Markevich,¹ C.A. Dawe,¹ M.P. Halsall,¹ I.D. Hawkins,¹ P. Kruszewski²,
 J. Plesiewicz², P. Prystawko², and A.R. Peaker¹

¹ Photon Science Institute and Department of Electrical and Electronic Engineering,
 The University of Manchester, Manchester M13 9PL, United Kingdom

² Institute of High Pressure Physics, Polish Academy of Sciences, 01-142 Warsaw, Poland

Email: v.markevich@manchester.ac.uk

Experimental information on the properties of simple native defects, vacancies and self-interstitial atoms, in GaN is very limited. Recently, solid arguments have been presented by Horita et al. [1] that the EE1 trap, which is frequently detected by deep level transient spectroscopy (DLTS) in GaN samples subjected to irradiation with high energy particles, is related to an energy level of the nitrogen vacancy (V_N). However, this identification is not fully consistent with the results of previous DLTS studies on irradiated GaN crystals, in which multiple components with some unusual properties have been reported for the EE1 trap [2,3].

In this work, results of a DLTS study of radiation-induced electron traps in Si-doped GaN layers grown by MOVPE on conductive n-type ammono-GaN substrates are reported. The samples have been irradiated with different doses of electrons with energies in the range from 370 keV to 9 MeV. It is found that irradiation with electron energies within the above-mentioned range has resulted in effective introduction of the EE1 trap. Consistent with previous studies [3,4], strong changes in the EE1 DLTS peak shape and magnitude have been observed upon changes in the filling pulse length used for recording the DLTS spectra (Fig. 1). Such filling- pulse-length dependencies are very unusual for point like defects and resemble those observed for extended defects in semiconductors [4]. Further, it is found that there is a strong electric field enhancement of electron emission rates for all components of the EE1 emission signal.

It is argued that the EE1 trap in electron-irradiated GaN consists of contributions from V_N and N-related Frenkel pairs. The N-related Frenkel pairs cannot be treated as simple point defects in the DLTS spectra and more sophisticated analysis, as for extended defects [4], is needed. Some properties of the complex have been elucidated.

Polish authors would like to thank the National Science Centre, Poland, for financial support through Project No. 2020/37/B/ST5/02593.

References:

- [1] M. Horita, T. Narita, T. Kachi, and J. Suda, *Appl. Phys. Lett.* **2021**, *118*, 012106.
- [2] L. Polenta, Z-Q. Fang, and D.C. Look, *Appl. Phys. Lett.* **2000**, *76*, 2086.
- [3] G.A. Umana-Membreno et al., *Appl. Phys. Lett.* **2002**, *80*, 4354.
- [4] W. Schröter, J. Kronewitz, U. Gnauert, F. Riedel, and M. Seibt, *Phys. Rev. B* **1995**, *52*, 13726.

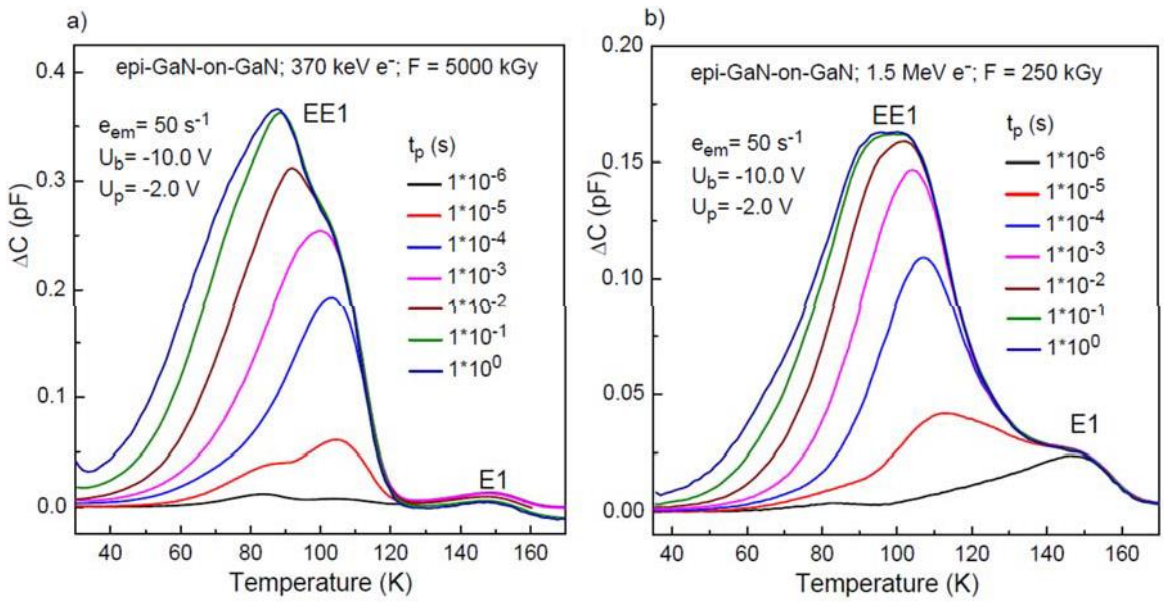


Fig. 1. DLTS spectra recorded with different filling pulse length (t_p) on Schottky barrier diodes on epi GaN:Si samples, which were irradiated with either a) 370 keV electrons or b) 1.5 MeV electrons. The doses of irradiation and measurements conditions are given in the graphs.

Dislocation analyses in the boron-doped germanium crystals grown near-equilibrium conditions

Aravind Subramanian^{1*}, Merve Kabukcuoglu², Carsten Richter¹, Uta Juda¹, Nikolay Abrosimov¹ and Sumathi Radhakrishnan¹

¹ Leibniz-Institut für Kristallzüchtung (IKZ), Max-Born-Straße 2, 12489 Berlin, Germany

² Institut für Photonenforschung und Synchrotronstrahlung (IPS), Karlsruhe Institute of Technology, Hermann-von-Helmholtz-Platz 1, 76344 Eggenstein-Leopoldshafen, Germany

Email: aravind.subaramanian@ikz-berlin.de

In the realm of germanium (Ge)-based technologies, there is a critical need for a thorough comprehension of dopant behaviour within Ge [1]. Among all the conventional semiconductors, Ge displays the highest hole mobilities. The conventionally used p-type dopant in Ge, i.e. gallium (Ga) suffers diffusion losses following the heat treatment, and a potential remedy for this is to replace Ga with boron (B) due to its lower diffusion coefficient in Ge [2, 3]. Currently produced Ge:B substrates, prepared via implantation technique, possess quite a large number of defects consequently leading to device failure. In this study, we present our recent investigations on the structural quality of B-doped [100] oriented Ge crystals grown in our lab from the melt using the Czochralski method. B concentrations of up to $7 \times 10^{17} \text{ cm}^{-3}$ were obtained in the crystals, almost close to the B solubility limit of 10^{18} cm^{-3} in Ge (in equilibrium). Various X-ray imaging techniques, including X-ray rocking curve imaging (RCI) analysis and white beam X-ray topography (WB-XRT) were utilised in this study. X-ray topography full wafer mappings were obtained from a (110) surface using the 0-22, 2-24, 3-13, 400, -2-24, and -3-13 reflections. A Burger's vector analysis was carried out on some of the dislocations/features marked in Figure 1a. The results from the analysis facilitate further understanding of the edge and screw characteristics of the dislocations. The introduced dislocations are largely influenced by the concentration of B in the lattice. From Figure 1a, one can observe that the dislocations are clustered at growth striations, mainly due to the high segregation coefficient of B in Ge [4, 5]. It causes a “mismatch” of lattice in the crystallization front. This is also suggested by the RCI map measured on the similar (110) surface obtained along the longitudinal direction of the crystal. A strain in the lattice is observed within the top region mainly due to the higher B concentration (see Figure 1b). A detailed investigation of the prominent dislocation types along with their Burgers' vector analyses will be presented. Furthermore, the implications of the current results in improving the crystal growth process will be discussed.

References:

- [1] R. Pillarisetty, Nature 479, 324 (2011).
- [2] A. Satta, et al., Appl Phys Lett 87, (2005).
- [3] C. Porret et al., Physica Status Solidi (a) 217, (2020).
- [4] T. Taishi, et al., J Cryst Growth 311, 59 (2008).
- [5] A. Subramanian et al., J Electron Mater 52, 5178 (2023).

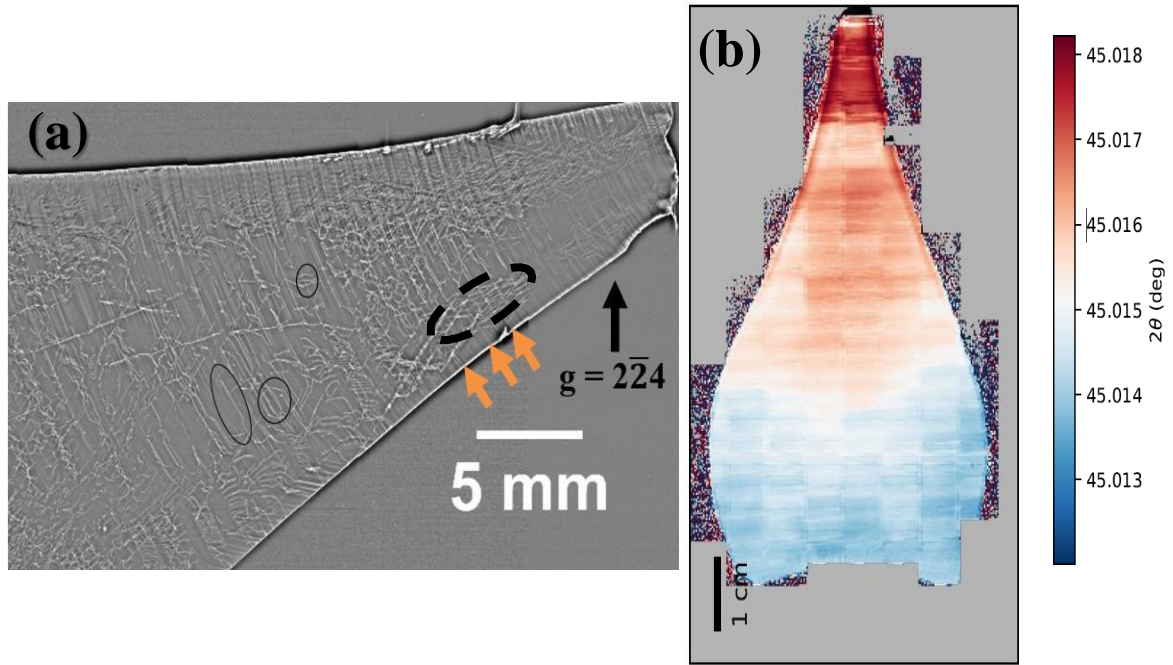


Fig. 1. (a) WB-XRT image of the surface along the longitudinal direction of the Ge crystal (surface orientation (110)) measured using the symmetric reflection 2-24. The features marked in black circles represent some of the dislocations whose Burgers vector analysis was carried out. Furthermore, the orange arrows indicate dislocations introduced at growth striations mainly due to higher B incorporation in the top part of the crystal along with the dislocation clusters present at the growth striations (b) X-ray RCI of the sample shown in (a), the top region close to the seed displays a higher strain as compared to the bottom region. The behaviour of strain along the crystal correlates well with the B-segregation (6-12) in Ge.

Defect engineering for enhanced silicon RF substrates

M. Perrosé¹, Y. Baron¹, B. Lefaucher², P. Acosta Alba² and J.-P. Raskin³

¹ CEA-Leti, Univ. Grenoble Alpes, 17 rue des Martyrs, F38000 Grenoble, France

² CEA-IRIG, Univ. Grenoble Alpes, 17 rue des Martyrs, F38000 Grenoble, France ³

ICTEAM, Univ. catholique de Louvain, Louvain-la-Neuve, Belgium

Email: martin.perrose@cea.fr

Nowadays, radiofrequency (RF) signals are widely used for telecommunications. In the RF domain, substrate losses highly affect devices performance. In the microelectronics industry, Silicon-on-Insulator (SOI) substrates are used for advanced CMOS nodes applications [1]. However, SOI substrates suffered from positive fixed charges at the SiO₂/Si interface, creating a so-called Parasitic Surface Conduction (PSC) layer. This PSC layer makes SOI substrate not compatible with RF applications. In this context, the introduction of a trap-rich layer beneath the BOX is proposed to avoid the formation of the PSC and thus conserve the high resistivity properties of the SOI substrate which guarantee low losses and high linearity to the RF integrated functionalities [1]. In this work, we propose to implant ions below the BOX to generate crystalline defects and thus create an efficient trap-rich layer. Particularly, we studied He⁺ implantation in High-Resistivity (HR) Silicon substrate [2]. For the first time, we assessed the Photo-Luminescence (PL) signature of crystalline defects leading to high RF performances, giving insights for defect engineering for RF applications.

First, using PL spectra (**Fig. 1**), we show that defects morphology evolves with the post-implantation annealing temperature [2]. This is confirmed by Scanning Transmission Electron Microscopy (STEM) observations in **Fig. 2**. Actually at 600°C, {311} defects are observed while at 800°C, they evolve into DLs.

Second, we have measured RF performances through the extraction of the effective resistivity as described in [3]. As shown in **Fig. 3**, the 600°C 2-hour annealed sample shows excellent RF performances. Combining morphological observations with RF measurements, we can argue that {311} are extremely efficient for charge carriers trapping in the RF domain.

For the first time, experimental results link defects morphology in Si substrates analyzed by PL and their RF performances, enabling the development of defects engineering strategies for enhanced RF semiconductor substrates.

References:

- [1] M. Rack and J.-P. Raskin, ECS Trans. 92 79, 2019
- [2] Lingxi OuYang *et al*, Micro & Nano Letters, 2016
- [3] M. Perrosé *et al*, IEEE MTT-S International Microwave Symposium, 2024 (To be published)

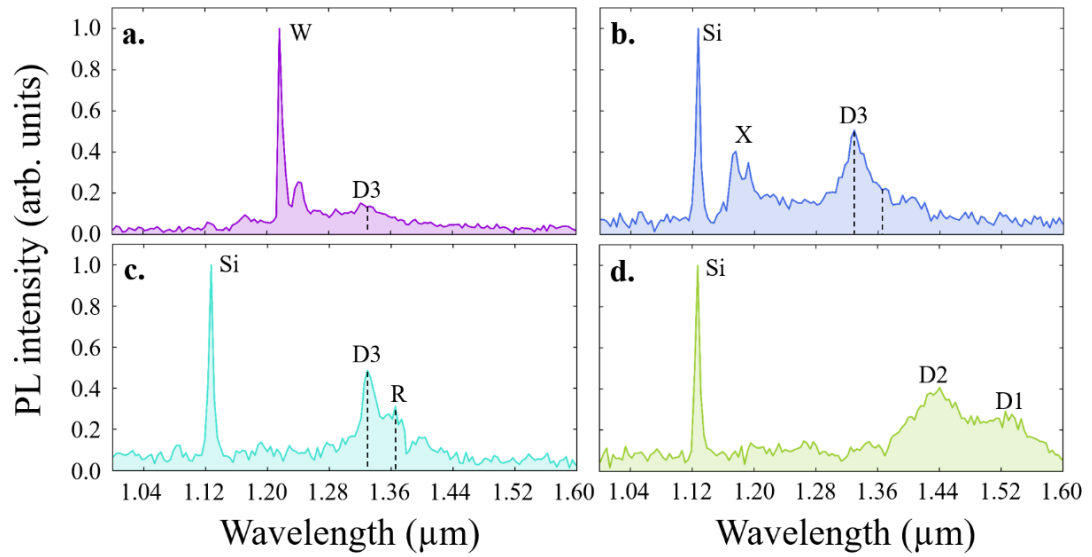


Fig. 1. Photoluminescence spectra measured at 10K with a 488 nm laser for He⁺ implanted Si samples with (a) no anneal, or annealed during 2 hours at (b) 400°C, (c) 600°C, (d) 800°C.

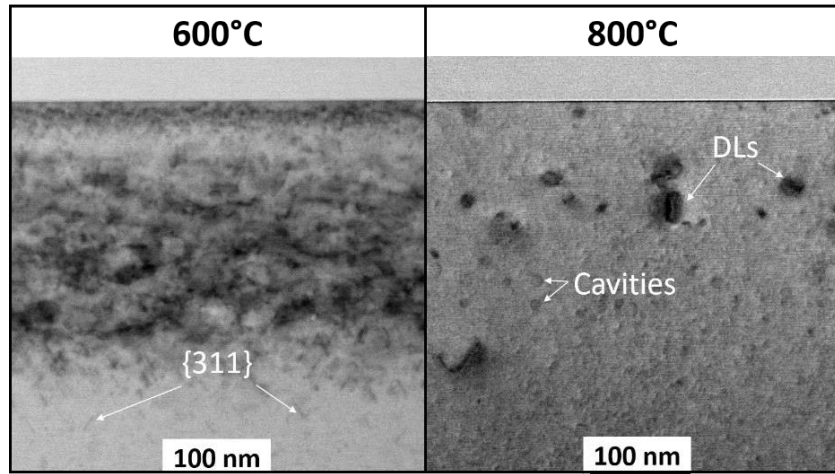


Fig. 2. STEM-BF of He⁺ implanted Si samples annealed during 2 hours at 600°C and 800°C, respectively.

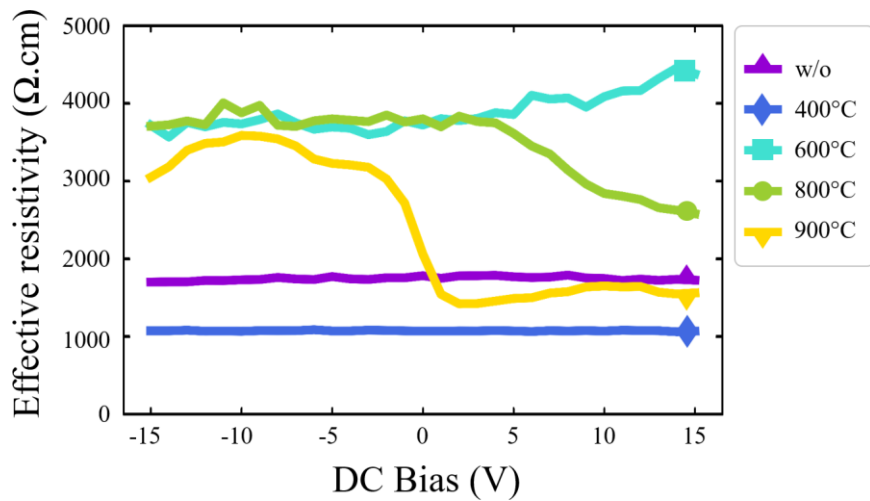


Fig. 3. Effective resistivity (extracted at 6 GHz) vs. bias applied to CPW for all samples.

Growth of Silicon-based Germanium Tin Alloys

Jörg Schulze

Friedrich-Alexander-Universität Erlangen-Nürnberg, Lehrstuhl für Elektronische Bauelemente (LEB),
 Cauerstr. 6, 91058 Erlangen

&

Fraunhofer-Institut für Integrierte Systeme und Bauelementetechnologie IISB,
 Schottkystr. 10, 91058 Erlangen

E-Mail: joerg.schulze@fau.de

Ternary alloy $\text{Si}_{1-x-y}\text{Ge}_x\text{Sn}_y$ has become the subject of intense experimental efforts [1-4]. The growth of relaxed bulk $\text{Ge}_{1-y}\text{Sn}_y$ alloys which become direct for high Sn contents is difficult because of the low equilibrium solubility of Sn in Ge (~ 1 %) [5] and the large lattice mismatch of 14.7 %.

The fabrication of relaxed graded buffer substrates or low-dimensional structures such as Sn rich quantum wells formed by the overgrowth of a few monolayers of pure Sn with Ge [6, 7] could be a way to realize $\text{Ge}_{1-y}\text{Sn}_y$ structures with a high Sn content to obtain a direct bandgap material.

In this contribution the status of work for the growth of Sn-rich $\text{Ge}_{1-y}\text{Sn}_y$ alloys using these proposed techniques will be discussed in detail. The structural information on the grown layers were obtained by X-Ray Diffraction measurements. Low-temperature photoluminescence measurements were used to obtain transition energies in the finally grown $\text{Ge}_{1-y}\text{Sn}_y$ alloys. Furthermore, the influence of defects decorated by Sn on the growth of $\text{Ge}_{1-y}\text{Sn}_y$ alloys will be discussed.

As an outlook the use of $\text{Ge}_{1-y}\text{Sn}_y$ alloys in opto-electron devices will be highlighted.

References:

- [1] Kouvetsakis J and Menendez J, TIN-BASED GROUP IV SEMICONDUCTORS: New Platforms for Opto- and Microelectronics on Silicon, Annu. Rev. Mater. Res. **36**(1), 497-554 (2006).
- [2] Zhang Z P et al, Structural properties of GeSn thin films grown by molecular beam epitaxy, AIP Adv. (2017).
- [3] Oehme M, Kostecki K, Schmid M, Oliveira F, Kasper E and Schulze J, Epitaxial growth of strains and unstrains GeSn alloys up to 25% Sn, Thin Solid Films, **557**, 169-172 (2014).
- [4] Wirths S et al, Lasing in direct-bandgap GeSn alloy grown on Si, Nat. Photonics, **9**, no.2, 88-92 (2015).
- [5] Thurmond C D, Trumbore F A and Kowalchik M, germanium Solidus Curves, J. Chem. Phys, **25**, 799-800 (1956).
- [6] F. Oliveira, I. A. Fischer et al., Appl. Phys. Lett. **107** (26), 262102 (2015).
- [7] F. Oliveira, I. A. Fischer et al., Journal of Applied Physics **117** (12), 125706 (2015).

For your remarks

Disorder and Strain in Limiting the n-type Mobility of GeSn Alloys: Calculations by First-Principles

Kevin Sewell¹ and Felipe Murphy-Armando¹

¹ Tyndall National Institute, University College Cork, Lee Maltings Complex Dyle Parade, T12R5CP,
Cork, Ireland.

Email: kevin.sewell@tyndall.ie
philip.murphy@tyndall.ie

We calculate from first principles the mobility of n-type GeSn as a function of Sn composition, biaxial tensile strain and temperature, using the Boltzmann transport equation in the relaxation time approximation. We determine the intra- and inter-valley electronic alloy scattering parameters [1,2] from the energy splitting of nearly degenerate Bloch states, which arise when one host atom in a supercell is replaced by a Ge or Sn atom. We calculate the alloy scattering parameters for all relevant L, Γ , $\frac{1}{2}X$ and X intra- valley and inter-valley transitions. The electron-phonon contribution is calculated using the deformation potentials of Refs [3-5].

We find that, without introducing strain, a Sn concentration of at least 12.5% is needed to achieve an electron mobility greater than that of Ge. Our results show that the mobility of Ge can be increased 10x by adding Sn beyond 12%. Applying biaxial tensile strain to GeSn achieves increases in the mobility at lower Sn content than in unstrained GeSn (Figure 1).

References:

- [1] F. Murphy-Armando and S. Fahy, Phys. Rev. Lett. **97** 096606 (2006).
- [2] J. D Sau and M. L. Cohen, Phys. Rev. B. **75** 045208 (2007).
- [3] F. Murphy-Armando and S. Fahy, Phys. Rev. B. **78** 035202 (2008).
- [4] M. Fischetti and S. Laux, J. Appl. Phys. **80**, 2234 (1996).
- [5] C. Jacoboni and L. Reggiani, Reviews of Modern Physics, Vol. 55, No. 3 (1983).

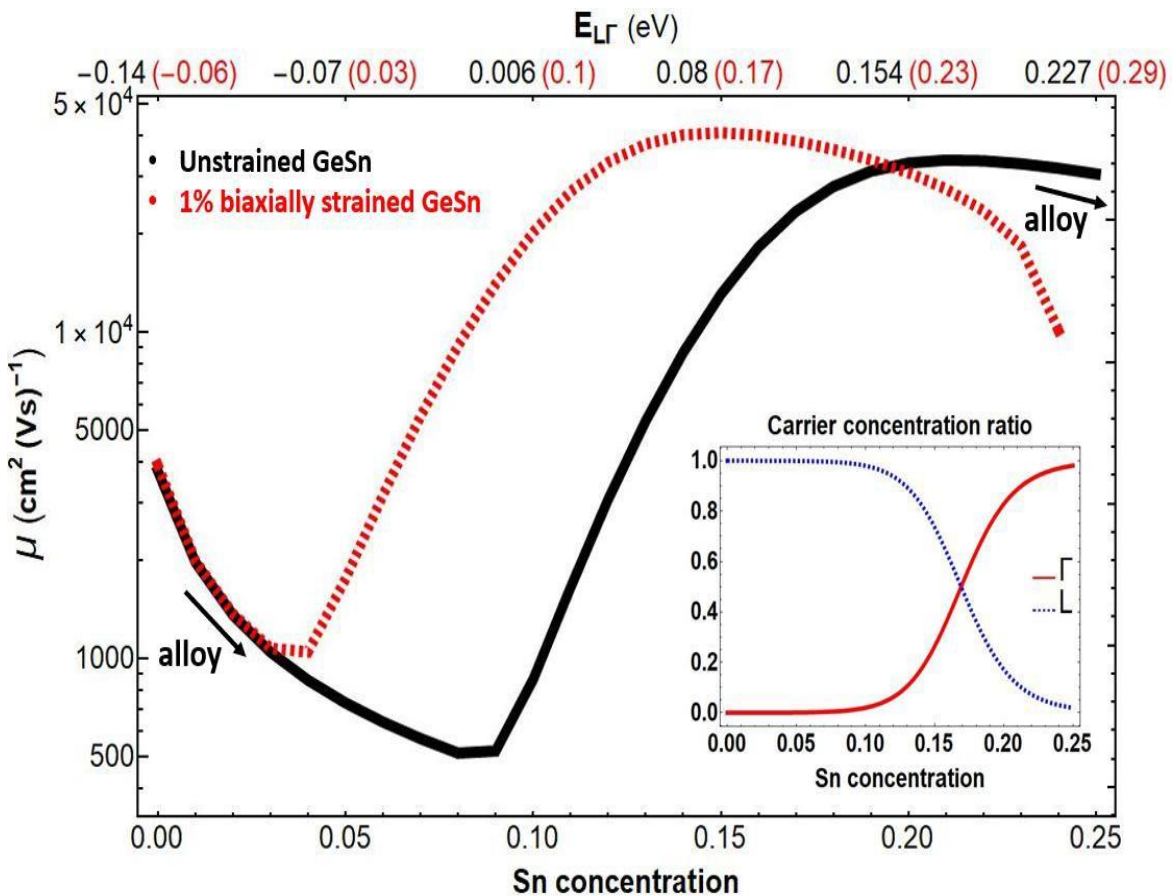


Figure 1: Room-temperature intrinsic n-type electron mobility of unstrained GeSn and GeSn under 1% biaxial tensile strain as a function of Sn concentration and difference (in eV) in bandgaps: $E_{L\Gamma} = E_L - E_\Gamma$

TCAD Model for SiGe Oxidation and Ge Diffusion along Oxide/SiGe Interfaces

Christoph Zechner¹ and Nikolas Zographos²

¹ Synopsys GmbH, Karl-Hammerschmidt-Str. 34, 85609 Aschheim/Dornach, Germany

² Synopsys Switzerland LLC, Thurgauerstrasse 40, 8050 Zurich, Switzerland

Email: zechner@synopsys.com

During the oxidation of SiGe regions, Si is preferably incorporated into the oxide, whilst Ge atoms accumulate at the SiGe side of the interface [1,2,3]. The Ge concentration has its peak at the SiGe side of the oxide/SiGe interface. This peak broadens due to Ge/Si interdiffusion inside SiGe [2,3]. Brewer [4] and Thornton [5] described the oxidation of fin structures of Si/SiGe superlattices (see figs. 1, 2). During oxidation Ge atoms diffuse along the oxide/SiGe interface [4]. This may lead to the formation of Si nanowires surrounded by SiGe and can be exploited for the manufacturing of gate all around transistors. Apparently, Ge atoms can be trapped inside an atomically thin interface layer, diffuse along the interface with a higher diffusivity, and be re-emitted from the interface into the SiGe bulk.

In this work a new, calibrated TCAD process simulation model is presented which describes SiGe oxidation and the diffusion of Ge atoms along the interface. The model is compatible with Synopsys' standard models [6] for process simulation and reproduces the Ge profiles observed by [4], [5].

A three-phase segregation model [7] is used to describe the capturing and release of Ge atoms at the oxide/SiGe interface. Ge diffusion inside the two-dimensional interface layer is modelled by Fickian diffusion and depends on the surface orientation (it is faster on <110> surfaces than on <100> surfaces) and on the oxidation rate of the interface (it is zero for inert anneals). Ge/Si interdiffusion in SiGe is described with the model calibrated by Zechner[8]. The oxidation rate of SiGe depends on the Ge mole-fraction at the SiGe side of the oxide/SiGe interface and has been calibrated with published data [4,5,9,10]. The rate of interstitial injection into SiGe due to oxidation depends on the local Ge mole fraction and has been calibrated against data on B marker layer diffusion during oxidation [11]. The concentration of vacancies is reduced at oxidizing surfaces. This reduction depends on the oxidation rate and on the Ge mole fraction and has been calibrated against the measured broadening of the Ge profile peak during SiGe oxidation [2,3], predominantly mediated by vacancy diffusion [8].

References:

- [1] D. Fathy, et al., Appl. Phys. Lett. 51, 17 (1987).
- [2] T. David et al., Journal of Physical Chemistry C, 2015, 119. (43), pp.24606 - 24613
- [3] V. Boureau, priv. communication; V. Boureau et al., Mat. Sci. in Semicond. Proc. 42 (2016) 251–254 [4]
- W. M. Brewer et al., Nano Lett. 2017, 17, 2159–2164
- [5] C. S. Thornton et al., ACS Appl. Mater. Interfaces 2022, 14, 29422–29430
- [6] Synopsys, Inc, Advanced Calibration for Sentaurus™ Process User Guide, Mountain View, CA, USA, 2023
- [7] Y.-S. Oh and D. E. Ward, IEDM Technical Digest, San Francisco, CA, USE p. 509, December 1998
- [8] C. Zechner and N. Zographos, Mater. Sci. in Semicond. Proc. 42 (2016) 230–234
- [9] M. Spadafora et al., Appl. Phys. Lett 83, 18, p.3713 (2003)
- [10] O. Gourhant et al., 2014 ECS Trans. 64 469
- [11] E. Napolitani et al., J. Appl. Phys. 97, 036106, 2005.

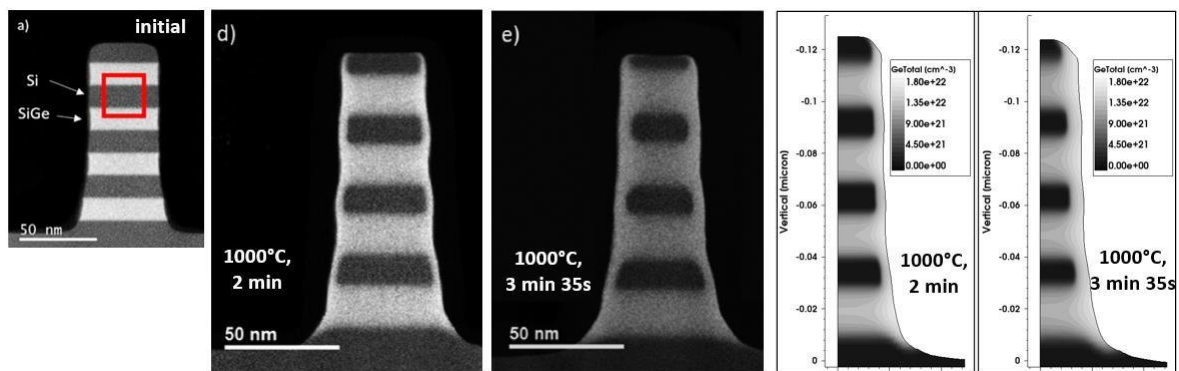


Fig. 1: Ge profiles measured by high angular dark field scanning transmission electron spectroscopy (left, adapted with permission from W. M. Brewer et al., Nano Lett. 2017, 17, 2159-2164. Copyright 2017 American Chemical Society), compared to process simulation results (right).

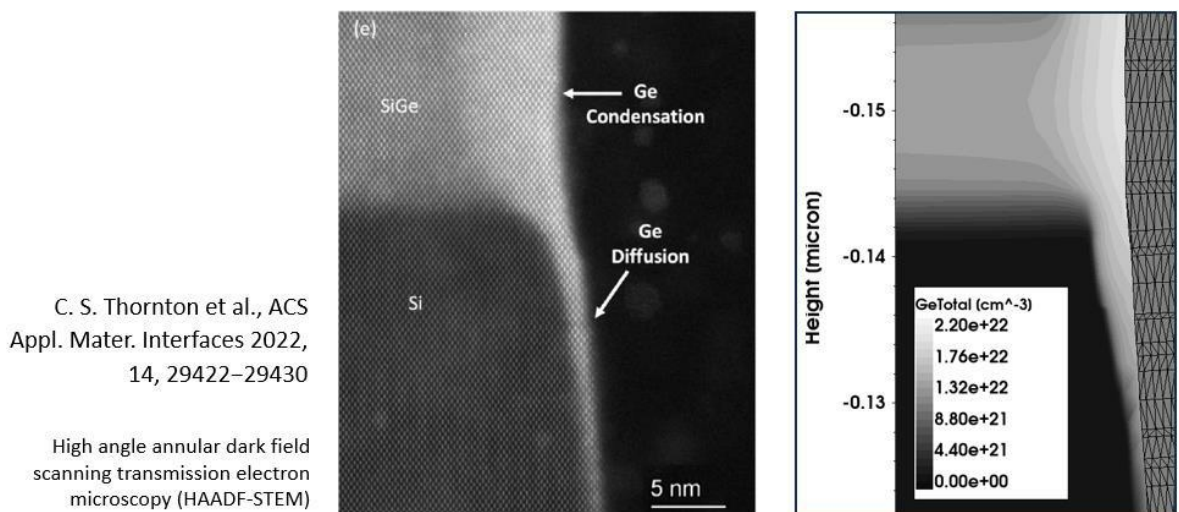


Fig. 2: Ge profiles after 20 min dry oxidation at 900°C of SiGe/Si layer stacks. High resolution STEM image (reprinted with permission from C. S. Thornton et al., ACS Appl. Mater. Interfaces 2022, 14, 29422–29430. Copyright 2022 American Chemical Society), compared to simulation results (right).

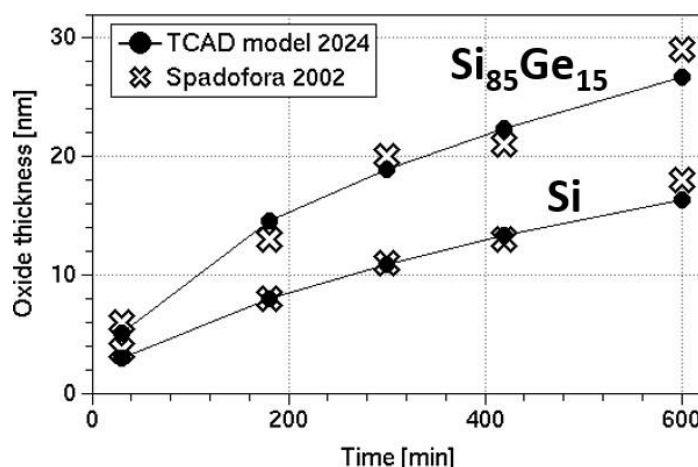


Fig. 3: Oxide thickness after dry oxidation of Si (lower curves) and SiGe (upper curves), at 1000°C for various times. Data measured by Spadafora (crosses, adapted from M. Spadafora et al., Appl. Phys. Lett 83, 18, p.3713 (2003), <https://doi.org/10.1063/1.1622439>, with the permission of AIP Publishing) are compared to TCAD process simulation results with the new model.

Ge nanosheets on Si substrates enabled by ultra-low temperature epitaxy

C. Wilflingseder¹, J. Aberl¹, E. Prado-Navarrete¹, G. Hesser², H. Groiss², C. Corley-Wiciak³, M. H. Zoellner⁴, G. Capellini^{4,5}, T. Fromherz¹ and M. Brehm¹

¹ Institute of Semiconductor and Solid State Physics, Johannes Kepler University, Altenberger Straße 69, 4040, Linz, Austria

² Christian Doppler Laboratory for Nanoscale Phase Transformations, Center for Surface and Nanoanalytics (ZONA), Johannes Kepler University, Altenberger Straße 69, 4040, Linz, Austria

³ ESRF – European Synchrotron Radiation Facility, 71, Avenue des Martyrs, CS 40220, 38043 Grenoble Cedex 9, Franc

⁴ IHP – Leibniz-Institut für innovative Mikroelektronik, Im Technologiepark 25, D-15236, Frankfurt(Oder), Germany

⁵ Dipartimento di Scienze, Università Roma Tre, Viale G. Marconi 446, 00146, Roma, Italy

Email: christoph.wilflingseder@jku.at

Next-generation electronics relies on implementing additional materials to enhance device performance. Recently, it was shown that SiGe heterostructures grown on SOI can be, e.g., the cornerstone for excellent reconfigurable transistors [1,2]. However, the lattice mismatch between Ge and Si (~4%) inherently limits the layer thickness (Θ_{Ge}) to only a few monolayers of Ge on Si [3] before elastic and plastic strain-relaxation sets in via nanodots and dislocation formation, respectively. While Θ_{Ge} is growth-temperature (T_G)-dependent under conventional growth conditions [4], the layers remain far too thin for nanoelectronics. Thus, until now, vapor-liquid-solid-grown Ge nanowires had been used for nanoelectronic demonstrators, even though this approach inevitably leads to scalability issues. Top-down patterning of Ge nanowires from nanosheets would benefit scalability, device integration, and added functionality.

Here, we departed from typical (Si)Ge epitaxy T_{GS} of $\geq 500^\circ\text{C}$ to significantly increase the Ge layer supersaturation to achieve a Θ_{Ge} usable for nanoelectronics device applications [1]. We used molecular beam epitaxy growth of Ge on Si at ultra-low temperatures (ULT), i.e., $100^\circ\text{C} \leq T_G \leq 300^\circ\text{C}$. Thereby, *growth pressures* around 10^{-10} mbar are essential, as ULT hinders efficient desorption of residual gas molecules from the substrate. Besides T_G , we systematically varied Θ_{Ge} from 1 nm to 16 nm, i.e., far beyond conventional critical thicknesses. Atomic force microscopy measurements of the samples indicates the absence of elastic relaxation. From X-ray diffraction (XRD) and high-resolution transmission electron microscopy (HRTEM) experiments, we found that even at $T_G = 100^\circ\text{C}$, local high quality epitaxial growth is possible. After the onset of plastic relaxation, the XRD and HRTEM analyses revealed alternating regions of pseudomorphic, highly crystalline growth and distorted growth down to $T_G = 100^\circ\text{C}$ and an overall degree of relaxation, which increases with T_G and Θ_{Ge} . The samples formed typical 60° dislocations, which are immobile due to the presence of ULTs and tend to pair. Our current investigation is focused on the potential presence of 90° Lomer dislocations. Since a certain thermal budget is required, we expect that they will be comparatively rare [5].

References:

- [1] A. Fuchsberger, et al., *IEEE Journal of the Electron Devices Society* **2024**, 12, 83-87.
- [2] A. Fuchsberger, et al., *Advanced Electronic Materials* **2023**, 9(6), 2201259.
- [3] M. Brehm, et al., *Physical Review B* **2009**, 80(20), 205321.
- [4] R. Bergamaschini, et al., *Nanotechnology* **2011**, 22(28), 285704.
- [5] A. Marzegalli, et al., *Physical Review B* **2013**, 88(16), 165418.

Reviewer remark: It may be of interest to have an indication of whether the crystal quality improves (or not) after such processing.

Author's response: I can comment on the already fabricated RFET with the SiGe heterostructures grown on SOI. These crystals didn't show any relevant degradation after processing. The group of Weber/Sistani heated up samples with SiGe and Ge quantum wells grown at ultra-low temperatures to 1174 K (900°C) for 3 min to produce a SiO₂ gate dielectric [1,2].

First principles calculation of G-Centre Photoluminescence in SiGe and comparison to Experiments

F. Murphy-Armando¹, J. Aberl², M. Brehm²

¹Tyndall National Institute, University College Cork, Cork T12R5CP, Ireland

²Institute of Semiconductor and Solid State Physics Johannes Kepler University Linz Altenberger Strasse 69, A-4040 Linz, Austria

Email: philip.murphy@tyndall.ie

Many quantum photonic applications are based on single-photon emitters for quantum state generation. A versatile source of single photons is the G-centre in Si, a Si-C-C defect complex, that emits at wavelengths of 1278 nm. Ideally, emission at longer wavelengths is desirable to take advantage of the present world-wide fiber-optic infrastructure.

In this work, we study the effects of alloying Si and Ge on the emission wavelength of the G-centres to achieve a wavelength shift. We use first principles calculations based on Density Functional Theory[1] to obtain several alloy configurations and determine their electronic band-structure. Figure 1 shows the zero-phonon recombination gap of G-centres in $\text{Si}_{0.9}\text{Ge}_{0.1}$ as a function of the average distance of Ge atoms from the G-centre complex. We compare the different configurations with the gap obtained using an average alloy, using the virtual crystal approximation (VCA). We observe that several recombination energies are possible, which would result in a broadening of the light emission peak in an alloy.

From these results, we expect the emission in SiGe to be broader than in Si, as observed in our experimental measurements, due to the different possible atomic configurations. We expect that shifting the emission of G-centres to higher wavelength is possible, but requires substantial alloying with Ge. In our presentation we will show our calculations of the photo-luminescence for higher alloy contents and compare to experiment.

Reference:

- [1] F. Murphy-Armando, et al., Phys. Rev. B 103, 085310 (2021)

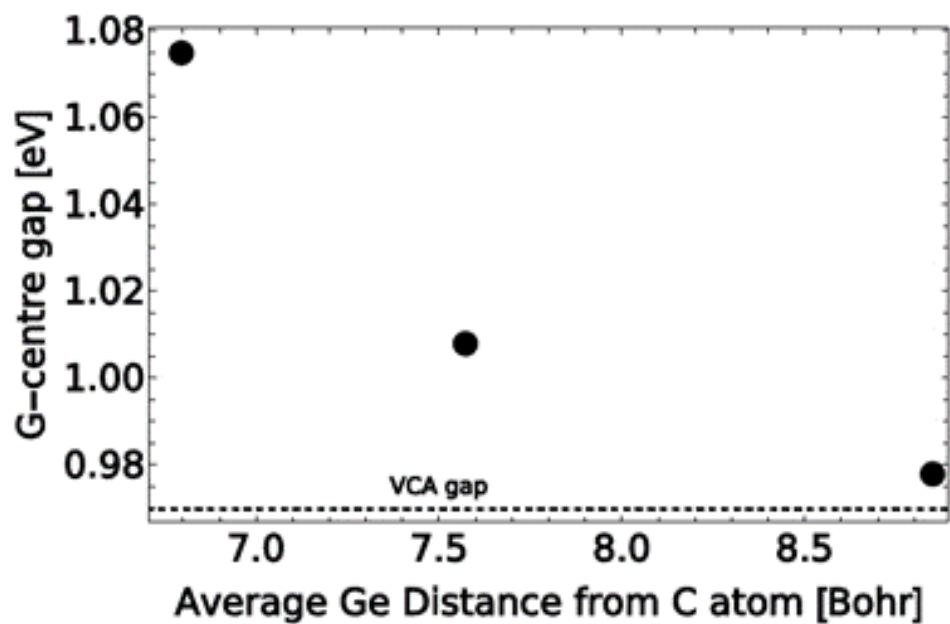


Figure 1: Zero-phonon emission energy of the G-center defect vs average distance of Ge atoms from C atoms in $\text{Si}_{0.9}\text{Ge}_{0.1}$

Are silicon nanoparticles “crystalline to the core” and does it make a difference in post-synthesis doping?

Jonathan G.C. Veinot

Department of Chemistry, University of Alberta, 11227 Saskatchewan Drive, T6G 2G2, Edmonton, Alberta, Canada

Email: jveinot@ualberta.ca

Silicon quantum dots (SiQDs) exhibit attractive optoelectronic properties and biocompatibility that make them desirable for biological imaging, sensing, and display applications. Unfortunately, their optical response is also plagued by low quantum yields and broad bandwidth that could limit their eventual use in the “real world”. It is well-established that nanomaterial structure influences optical, chemical and material properties. As such, it is essential that we establish a fundamental understanding of the structure of SiQDs if their properties are to be optimized for target uses. We have employed a combination of complementary methods including, ^{29}Si solid state NMR, FTIR, XPS, XRD and transmission electron microscopy to interrogate the structure of SiQDs obtained from thermal reduction of hydrogen silsesquioxane (HSQ). We discovered hydrogen-terminated SiQDs obtained using this well-established procedure consist of a size dependent layered structure made up of surface, sub-surface and core silicon species [1].

With this knowledge in hand, we investigated whether this unique layered structure impacted the uptake of boron atoms from during thermal diffusion-based post-synthesis doping. The structural disorder within the parent SiQDs, as well as the “drive-in” conditions strongly influence the resulting dopant concentration in the of B-doped particles [2, 3]. This presentation will discuss the size dependent structure of silicon nanoparticles derived from HSQ as well as the insight we have gained throughout our doping studies. If time permits discussion will extend to our preparation of metal silicide nanomaterials and the particle size dependence of these reactions.

References:

- [1] A. N. Thiessen, M. Ha, R. W. Hooper, H. Yu, A. O. Oliynyk, J. G. C. Veinot, and V. K. Michaelis, *Chemistry of Materials*, **2019**, 31, 678–688.
- [2] S. Milliken, K. Cui, B.A. Klein, I.T. Cheong, H. Yu, V.K. Michaelis, and J.G.C. Veinot, *Nanoscale*, **2021**, DOI:10.1039/D1NR05255AF.
- [3] S. Milliken, I.T. Cheong, K. Cui, and J.G.C. Veinot, *ACS Applied Nano Materials*, **2022**, 5, 15785–15796.

For your remarks

From nanosphere lithography to localised heteroepitaxy of GaAs on Si

L. Dentz¹, F. Hamouda¹, G. Hallais¹, L. Vincent¹, E. Herth¹, T. Baptiste¹, L. Leroy¹,
 L. Largeau¹, D. Bouchier¹, A. Jaffré², J. P. Connolly², D. Mencaraglia², C. Renard¹

¹ C2N, Centre de Nanosciences et de Nanotechnologies, CNRS, Université Paris-Saclay, Palaiseau, France

² GeePs, Génie Electrique et Electronique de Paris, Gif-sur-Yvette, France

Email: laurie.dentz@c2n.upsaclay.fr

The scientific community has long pursued the integration of GaAs on Si, especially for optoelectronic applications, particularly in the fields of photovoltaics and photonics. The main challenge to GaAs integration on Si is related to their significant lattice mismatch (4.1%) which leads to the formation of dislocations. The anti-phase domains creation remains also a problem. To address these issues, we have developed the ELTON method (Fig. 1.): Epitaxial Lateral overgrowth on Tunnel Oxide from nano-seed. This involves epitaxially growing GaAs microcrystals from nano-openings ($< \phi 90$ nm) thermally formed in the ultra-thin silicon oxide layer (< 2 nm) (Fig. 2.). This process has demonstrated perfectly epitaxial GaAs microcrystals on silicon without structural defects, with good optoelectronic integration across their entire surface (GaAs/Si and GaAs/SiO₂/Si stacking by tunnel effect) [1].

Our current objective is to cover as much silica surface as possible with GaAs to achieve a quasi-layer. For this purpose, we are developing a quick, reproducible, and cost-effective lithography method based on nanosphere lithography to localize the growth of μ -crystals in a hexagonal array (Fig. 3.). This lithography method have the advantage to maintain a very thin silica layer and create nano-openings to preserve defect-free and electrically connected crystal growth.

The other essential part of the project focuses on controlling the doping of GaAs micro-crystals. The crystals had previously exhibited significant unintentional P-type doping due to high carbon incorporation resulting from improper dissociation of the precursor gas used for Gallium (TMGa) [2]. TEGa can also be used as the Gallium precursor gas to enhance doping control. We will present and compare the results with those previously obtained with TMGa (Fig. 4.).

References:

- [1] C. Renard et al, Sci. Rep, 2016, 6, 25328. doi:10.1038/srep25328.
- [2] T. Mollière et al, Journal of applied physics, 2017, 121(3):035704

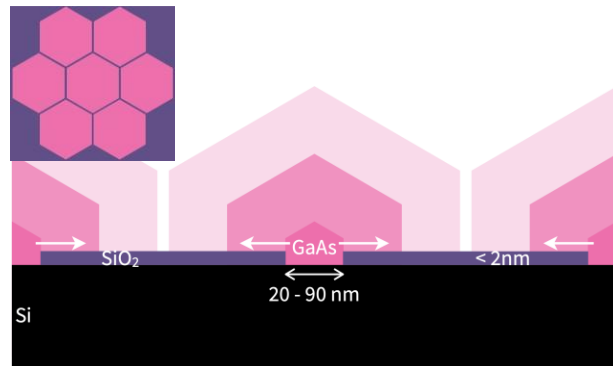


Fig. 1. Targeted architecture: GaAs μ -crystal growth on Si by ELTOOn method.

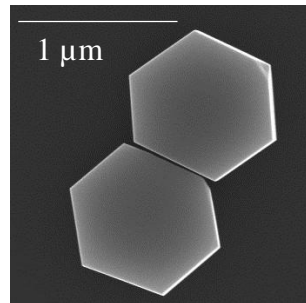


Fig. 2. GaAs μ -crystal on Si.

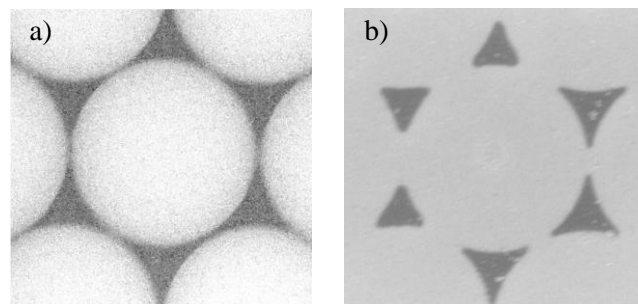


Fig. 3. a) Polystyrene nanosphere of 1 μ m diameter on Si; b) Metallic deposition in the gaps between the nanospheres.

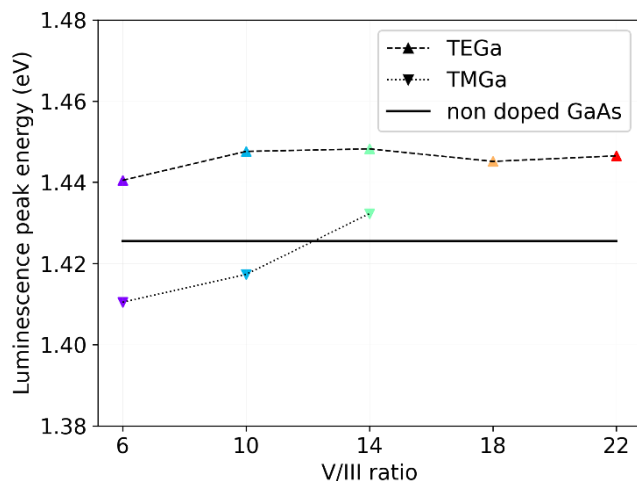


Fig. 4. Photoluminescence peak position of the GaAs crystals resulting from growth at different V/III ratios of the precursor gases (TEGa and TMGa) compared with the photoluminescence peak of an undoped GaAs (110) substrat.

Comparative Study of Charge Carrier Transport in Al-Si and Al-Ge Nanowire Heterostructure Transistors

Raphael Behrle,¹ Corban G. E. Murphey,² James F. Cahoon,² Sven Barth,³
 Martien I. den Hertog,⁴ Walter M. Weber,¹ and Masiar Sistani¹

¹ Institute of Solid State Electronics, TU Wien, Gußhausstraße 25, 1040, Vienna, Austria

² Department of Chemistry, Univ. of North Carolina at Chapel Hill, Caudill 019, NC 27599, Chapel Hill, US

³ Physics Institute, Goethe Univ. Frankfurt, Max-von-Laue-Straße 1, 60438, Frankfurt am Main, Germany

⁴ Institut Néel, CNRS, 25 rue des Martyrs BP 166, 38042, Grenoble, France

Email: raphael.behrle@tuwien.ac.at

Overcoming the difficulty in deterministically defining the metal phase of metal-semiconductor heterojunctions is among the key prerequisites for next-generation nano- and quantum-electronics. Thereto, a comprehensive understanding of the charge carrier injection and the electronic conduction mechanisms is necessary.

Here, we provide an in-depth discussion of the transport mechanisms in Si and Ge nanowires (NWs) integrated in Schottky barrier (SB) FETs. Key for the fabrication of these devices is the selective transformation of the Si/Ge NWs into Al, enabling oxide-free metal-Si/Ge junctions. TEM and EDX confirmed both the composition and single-crystal nature of the presented heterostructures, with no evidence of intermetallic phases being formed during the exchange process. Having physically and electrically equal Al leads to both Si and Ge provides an unique opportunity for comparisons of the electronic transport that is relevant for diverse Beyond-CMOS applications. Detailed and systematic electrical characterizations were carried out by temperature dependent multi-parameter measurements denoted bias spectroscopy to visualize a detailed image of the electronic transport and operation regimes.[1] Thereof, activation energy maps have been extracted to evaluate the effective SB height for electrons and holes in both material systems. The Al-Si material system revealed highly symmetric effective SBs for electrons and holes, necessary for the realization of reconfigurable electronics that require equal electron and hole currents.[2] In stark contrast, the Al-Ge material system revealed a highly transparent contact for holes due to Fermi level pinning close the valence band and charge carrier injection saturation by a thinned Schottky barrier, while electrons experience a distinct SB.[3] In this regime, negative differential resistance (NDR) followed by a sudden current increase indicating the onset of impact ionization is observed. Importantly, using multi-gate Al-Ge SBFETs allow to shift the NDR- peak by electrostatic gating, delivering runtime circuit tunability, e.g. in oscillators and multi- level logic.[4]

Reference:

- [1] R. Behrle, C. G. E. Murphey, J. F. Cahoon, S. Barth, M. I. den Hertog, W. M. Weber and M. Sistani, *ACS Applied Materials & Interfaces* **2024**, (in review).
- [2] R. Böckle, M. Sistani, M. Bažíková, L. Wind, Z. Sadre-Momtaz, M. I. den Hertog, C. G. E. Murphey, J. F. Cahoon and W. M. Weber, *Advanced Electronic Materials* **2022**, 9, 2200567.
- [3] R. Behrle, M. Bažíková, S. Barth, W. M. Weber and M. Sistani, *IEEE NMDC* **2023**, pp. 889-894.
- [4] R. Behrle, M. I. den Hertog, A. Lugstein, W. M. Weber and M. Sistani, *ESSDERC* **2023**, pp. 37-40.

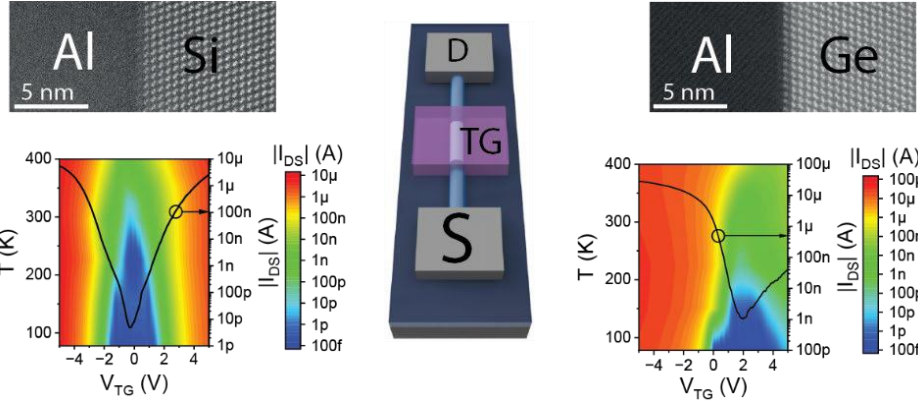


Fig. 1. TEM images showing the abrupt and flat Al-Si and Al-Ge NW interfaces. Temperature dependent transfer characteristic maps of the material specific transport mechanisms allowing to deduce the junction properties.

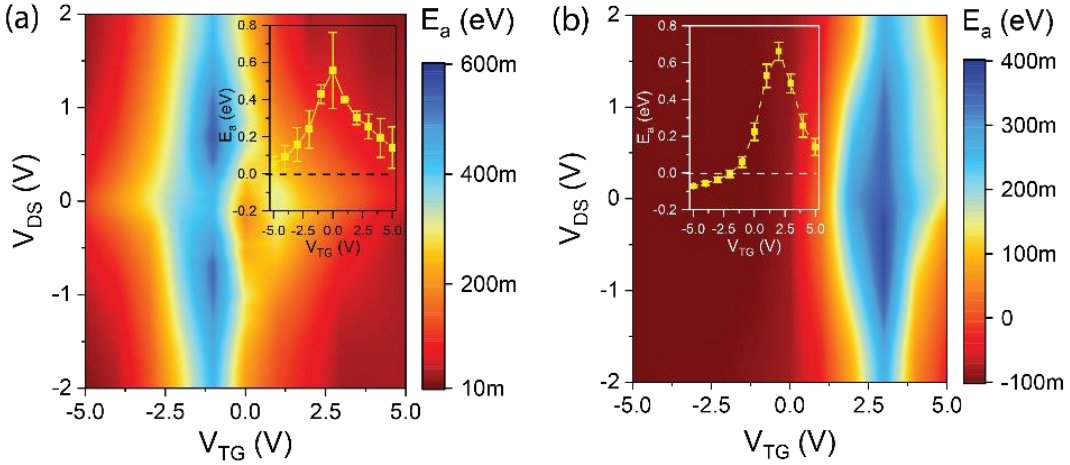


Fig. 2. Activation energy maps extracted from output I/V data over temperature of the (a) Al-Si and the (b) Al-Ge SBFET. The insets show the intrinsic activation energy in dependence of V_{TG} . The error bars represent the standard deviation of three similar SBFETs for both material systems.

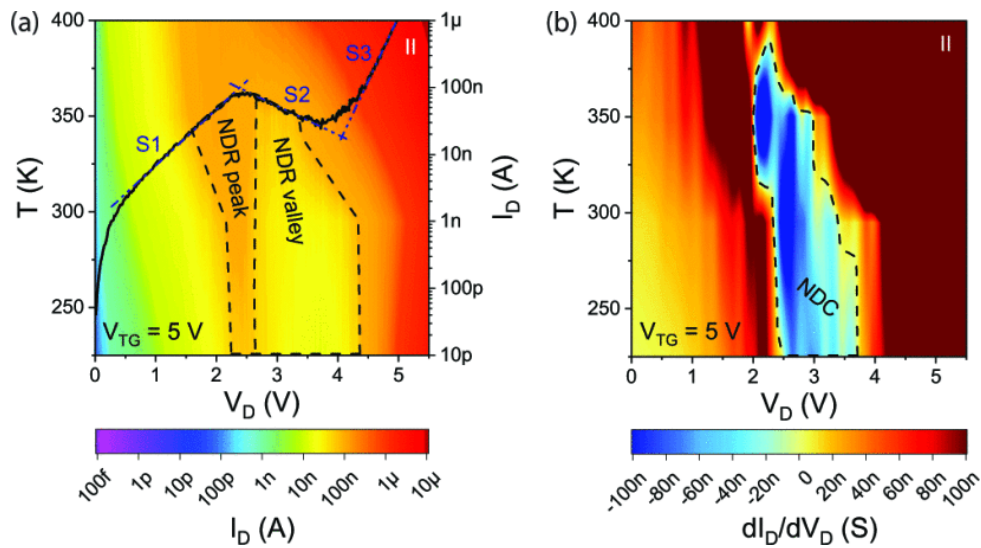


Fig. 3. (a) Bias spectroscopy of the NDR characteristic over temperature of a Ge SBFET. For reference, the right y-axis shows the $\log_{10}I/V$ at $T = 225$ K. (b) Thereof calculated NDC temperature dependent colormap.

Direct band transitions and light emission from ion-implanted SiGe Quantum Dots grown on Si-on-Insulator Substrates

L. Spindlberger¹, J. Aberl¹, L. Vukušić¹, T. Fromherz¹, J.-M. Hartmann², F. Fournel², S. Prucnal³, F. Murphy-Armando⁴, M. Brehm¹

¹ Institute of Semiconductor and Solid State Physics Johannes Kepler University Linz Altenberger Strasse 69, A-4040 Linz, Austria

² University Grenoble Alpes, CEA, LETI, Grenoble, France

³ Institute of Ion Beam Physics and Materials Research, Helmholtz-Zentrum Dresden-Rossendorf Bautzner Landstraße 400, Dresden 01328, Germany

⁴ Tyndall National Institute, University College Cork, Cork T12R5CP, Ireland

Email: moritz.brehm@jku.at

Photonics can bring a lot of versatility to our digital world, for example, by combining Si-based electronics with photonics, where applications related to short and medium-range data transfer and sensing on chips are envisioned. Integrated digital technology is dominated by Si, which is an excellent optical material due to its high refractive index and high-quality Si/SiO₂ interface. However, the integration of appropriate light sources for interlacing on-chip electronics and optics is challenging. Integrating Ge, another group-IV material, can help to add versatility to the Si photonics platform [1].

Recently, it was shown that the QD's light emission can be enhanced by interlacing them with point defects introduced through *in-situ* low-energy ion implantation [2,3,4].

Here, we report on electroluminescence spectroscopy experiments demonstrating room-temperature light emission from heavily alloyed SiGe quantum dots, for which the light emission properties are enhanced due to incorporated split-[110] self-interstitials [5]. The quantum dots are formed during molecular beam epitaxy deposition of Si_{0.6}Ge_{0.4} alloys on n-doped silicon-on-insulator substrates. To create the split-[110] self-interstitials the quantum dots were co-implanted *in-situ* using Si and Ge ions. The emitters were further embedded into the intrinsic region of a p-i-n diode structure to enable electrical pumping [5]. In contrast to previous theoretical results on unstrained Ge-based quantum dots containing these defects, radiative direct transitions at the Brillouin zone center are impossible in these SiGe light emitters [2]. Nevertheless, first-principles calculations indicate that the presence of the Ge split-[110] self-interstitial defect in SiGe can lead to optically direct transitions in momentum space in the X-direction of the Brillouin zone [5].

Reference:

- [1] I. A. Fischer et al. APL Photonics 7, 050901 (2022)
- [2] F. Murphy-Armando, et al., Phys. Rev. B 103, 085310 (2021)
- [3] M. Grydlik, et al., Nano Lett. 16, 6802 (2016)
- [4] P. Rauter, et al., ASC Photonics 5, 431 (2018)
- [5] L. Spindlberger, et al. (under review)

For your remarks

Temperature-induced transformation of the BO₂ atomic configuration in boron-doped Si

L.I. Khirunenko,¹ M.G. Sosnin,¹ A.V. Duvanskii¹, N.V. Abrosimov²

¹*Institute of Physics, National Academy of Sciences of Ukraine, Prospekt Nauky 46, 03028 Kyiv, Ukraine*

²*Leibniz-Institut für Kristallzüchtung, Department of Classical Semiconductors, Max-Born Str. 2, 12489 Berlin, Germany*

Email: lukh@iop.kiev.ua

To date, silicon remains an active area of research due to its widespread use in the conventional industry, power electronics, in the production of solar cells, as well as in quantum technologies. In modern micro-industry based on p-Si, the most widely used impurity is boron.

In this work we present new information about a recently identified B_sO_{2i}* defect in Si [1], which differ from the B_sO_{2i} associated with the light-induced degradation of solar cells by local atomic configuration. The investigations were performed by study of boron intracenter transitions, which are known to be highly sensitive to the perturbations from the local environment, and vibrational spectroscopy.

When studying the thermal stability of the B_sO_{2i}* defect in Si:B, the appearance of a new intracenter transition was detected in the absorption spectrum of boron. It was found that an increase in the intensity of the revealed absorption component is accompanied by the synchronous disappearance of the intracenter transition associated with the B_sO_{2i}* complex. Such a correlation may indicate the transformation of the B_sO_{2i}* defect into a defect associated with the detected line. Studies showed the quadratic dependence of the line intensity on the oxygen content in the samples and its linear dependence on the boron concentration. This suggests that the defect responsible for the revealed line can also be identified as B_sO_{2i}. It is assumed that there is a temperature-induced change in the atomic configuration of the B_sO_{2i}* defect. The detected transformation of the B_sO_{2i}* configuration occurs with the activation energy of 2.59 eV.

In the absorption spectra of Si:B samples, two local vibrational modes were detected, which have a strong correlation of the temperature changes in intensity with the observed electronic transitions for the B_sO_{2i}* defect. The bands are identified as local vibrations modes associated with B_sO_{2i}* in two configurations.

Reference:

- [1] L. I. Khirunenko, M. G. Sosnin, A. V. Duvanskii, N. V. Abrosimov, and H. Riemann, *J. Appl. Phys.* **2022**, 132, 135703.

For your remarks

Point defects in Ga- and B-doped Ge

P. Amoroso¹, W. Särs¹, J. Slotte^{1,2}, F. Tuomisto¹, A. Subramanian³, R.R. Sumathi³, and K. Mizohata¹

¹Department of Physics, University of Helsinki, P.O. Box 43, FI-00014 Helsinki, Finland

²Department of Applied Physics, Aalto University, P.O. Box 15100, FI-00076 Espoo, Finland

³Leibniz-Institut für Kristallzüchtung (IKZ), Max-Born-Str. 2, 12489 Berlin, Germany

Email: pejk.amoroso@helsinki.fi

Point defects play an important role for the electronic properties of semiconductor materials. Positron Annihilation Spectroscopy is a unique method for characterizing and quantifying neutrally and negatively charged vacancy-type defects. However, p-type Ge has been researched very little using Positron Annihilation Spectroscopy due to the low sensitivity of the method to positively charged defects.

Here, we studied both highly Ga-doped and B-doped bulk Ge, with doping concentrations of 10^{18} - 10^{20} and $5\text{-}8 \times 10^{17} \text{ cm}^{-3}$, respectively. Comparing gallium and boron is particularly interesting as both are p-type dopants, while differing in both size and electron structure. The bulk crystals were grown by the Czochralski method. The samples were irradiated with 6 MeV protons at room temperature with a fluence of $1 \times 10^{14} \text{ cm}^{-2}$ and upwards, thus introducing vacancy defects into the lattice. The vacancy defect distribution was studied using Positron Annihilation Lifetime Spectroscopy. The lifetime setup consisted of two collinear detectors with BaF₂-scintillators and quartz-windowed photomultiplier tubes, with a resolution of 282 ps. A conventional ²²Na positron source was used.

Analysis of the positron lifetime spectra reveals vacancies in the samples after irradiation. Since monovacancies in pure Ge are not stable at room temperature [1], these are vacancy-dopant complexes. The average lifetime results indicate that the highest-doped samples have either significantly less vacancies or weaker positron traps, or both. A lifetime component analysis seems to suggest less open volume in the trapping vacancies in the highest-doped samples, compared to the samples with lower dopant concentration. These results and their implications will be discussed in the poster.

Reference:

- [1] J. Slotte, S. Kilpeläinen, F. Tuomisto, J. Räisänen and A. Nylandsted Larsen, *Physical Review B* **2011**, 83, 235212.

For your remarks

Basal dislocations in HVPE grown GaN – characterisation and importance for stress relaxation during growth

Bläß U. W.¹, Lukin G.¹, Röder C.¹, Bastin D.², Hofmann P.², Doradziński R.², Meissner E.¹, Besendörfer S.¹, Beyer F. C.¹ and Friedrich J.¹

¹ Fraunhofer Institute for Integrated Systems and Device Technology IISB, Schottkystraße 10, 91058 Erlangen, Germany

² Freiberger Compound Materials GmbH, Am Junger-Löwe-Schacht 5, 09599 Freiberg, Germany

Email: Ulrich.Blaess@iisb.fraunhofer.de

High-quality GaN bulk crystals are essential as substrates for epitaxy of ultra-wide band gap semiconductor devices and are typically grown by hydride vapour phase epitaxy (HVPE) due to the possibility of realising high growth rates ($>100 \mu\text{m/h}$). Unfortunately, high dislocation densities usually result from applying foreign substrates like e.g. sapphire [1] for hetero- epitaxial HVPE growth and deteriorates the outstanding physical properties of this material. In order to achieve good crystal quality, the general challenge appears to minimise dislocation densities, associated lattice bow [2] and remaining internal strain.

In this study, we investigate the types and distribution of dislocations occurring in a GaN crystal of several millimetre thickness grown by HVPE. The threading dislocation (TD) density was determined by etch pit counting after wet etching, whereas the axial and radial distribution and propagation of dislocations inside the crystal were characterised by cathodo- luminescence (CL). In addition, dislocation densities and types were characterised by transmission electron microscopy techniques.

The residual stress of the crystal was ascertained by confocal micro-Raman spectroscopy at room temperature. It is shown that tensile strain along the crystal surface is consistent with the evolution of the dislocation density.

As a major result of this study, we demonstrate that for this test crystal the strain evolution during crystal growth is not only controlled by TD inclination [3], but also to a large extent by the formation of basal plane dislocations (BPD). The dislocation densities increase from crystal centre to the edge as well as with increasing crystal thickness, indicating that beside local annihilation new dislocations form during growth. Especially the role of BPDs will be discussed in the context of their formation, the resulting lattice bow and local strain reduction.

References:

- [1] Editors: D. Ehrentraut, E. Meissner, M. Bockowski, "Technology of GaN Crystal growth" (Springer Verlag, Heidelberg, 2010)
- [2] G. Lukin, E. Meissner, J. Friedrich, F. Habel, G. Leibiger, *J. Cryst. Growth* **2020**, 550, 125887
- [3] A. Romanov and J. Speck, *Appl. Phys. Lett.* **2003**, 83, 2569

For your remarks

The peculiarities of the ultrasound influence on the FeB pair association in silicon structures

Oleg Olikh¹ and Nikolay Arutyunov^{2,3}

¹ Taras Shevchenko National University of Kyiv, 64/13, Volodymyrska Street, 01601, Kyiv, Ukraine

² Department of Physics, Martin Luther University Halle, 06120, Halle, Germany

³ Leibniz-Institut für Kristallzüchtung (IKZ), Max-Born-St.-2, D-12489, Berlin, Germany

Email: olegolikh@knu.ua

It is well known that ultrasound (US) can be effective tool for defects engineering [1-2]. The wide-ranging US capabilities are closely associated with the ability to adjust the frequency and the type of acoustic waves. Such versatility enables the selection of an ultrasound loading regime tailored to the specific type of targeted defects. Recent research [1] has indicated that US loading conditions can accelerate the association of FeB pairs in silicon solar cells. This effect is believed to result from a reduced energy barrier for iron ion migration: $E_m \xrightarrow{\text{US}} E_{m,0} - \Delta E_{\text{US}}$ (where ΔE_{US} is the acoustically induced (AI) change).

Further investigations using Cz-silicon n^+ - p - p^+ structures revealed a paradoxical divergence in the frequency dependency of ΔE_{US} when using longitudinal and transverse waves. Specifically, under transverse acoustic wave loading, the AI energy change increased with rising of US frequency. In contrast, the frequency rising of longitudinal waves resulted in a decrease in ΔE_{US} value. The observed qualitatively different response of FeB center is a reliable and intriguing evidence of anisotropic deformation field tied to this center in the crystal lattice of silicon.

The oversized core of Fe atom reveals itself in emitting the gamma-quanta of the element-specific electron-positron distribution, just as it has been observed for the point defects in diamond-like semiconductors [3,4]. This emission obeys both the dynamics and kinetics of the rate of positron localization and, as estimated, follows the qualitatively different response to US loading caused by longitudinal and transverse acoustic waves. The value of the positron trapping rate (Fig. 2) provides for reliable measurements of both the positron annihilation lifetime and coincidence Doppler broadening. We believe that FeB complex is effective positron trap and the experiments on verifying predictions for center microstructure based on the phenomenon of the electron-positron annihilation in the field of the ultrasound loading will be considered.

References:

- [1] O. Olikh *et al.*, *J. Mater Sci: Mater Electron* **2022**, 33, 13133.
- [2] M. Virot *et al.*, *J. Phys. Chem. C* **2012**, 116, 15493.
- [3] N. Arutyunov and R. Krauserehberg, *Sol. State. Phenom.* **2004**, 95-96, 507.
- [4] N. Arutyunov, V. Emtsev, A. Mikhailin and C. Humphreys, *Physica B* **2003**, 340–342, 412.
- [5] B. Paudyal, K. McIntosh and D. Macdonald, “Proceedings of the 34th IEEE Photovoltaic Specialists Conference (PVSC, 2009), p. 001588.
- A. Istratov, H. Hieslmair and E. Weber, *Appl. Phys. A: Mater. Sci. Process.* **1999**, 69, 13

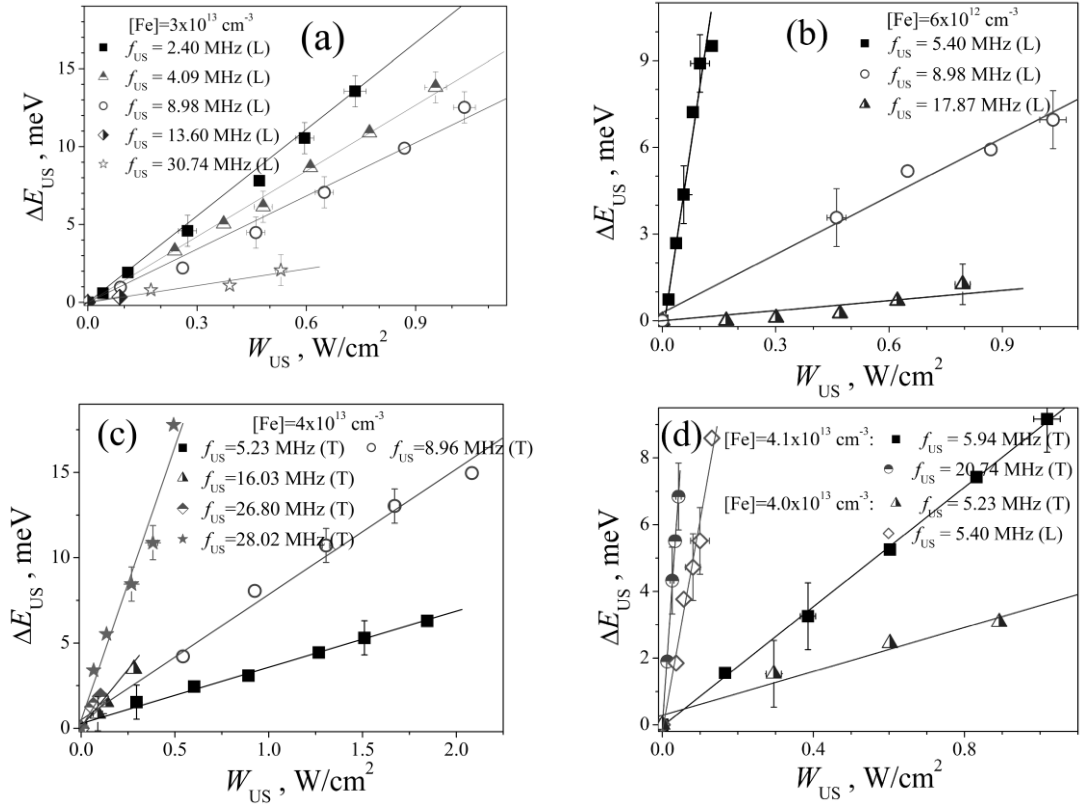


Fig. 1. Dependencies of acoustically induced changes in iron ion migration energy on ultrasound intensity using longitudinal (L) and transverse (T) waves of different frequencies. Points represent experimental data, and the lines are the linear fitted curves.

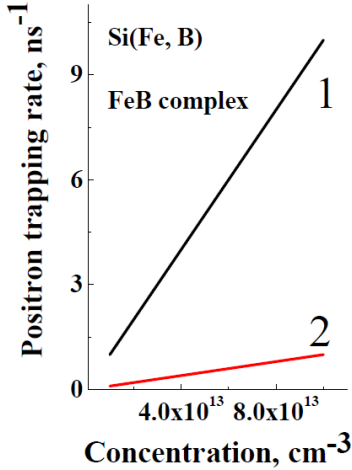


Fig. 2. The positron trapping rate (k) estimated for FeB complex with the positron trapping cross-section 10^{-11} cm² (curve 1) and 10^{-12} cm² at room temperature versus concentration (n_d) of Fe impurity atoms in Si. It is noteworthy that yet much larger values of cross-sections 3.32×10^{-11} cm² and 10^{-10} cm² related to excitonic Auger capture of holes and multiphonon emission capture, respectively, have been reported for the FeB complex [5,6]. The oversized ion core of the Fe impurity atom dominates in the emission of the elementally specific electron-positron annihilation radiation thus giving an identifying distinctive feature of the FeB complex in its energetically anisotropic reaction to US loading depending on wave type. As a result, the $k(n_d)$ dependency is a function of US loading.

Defect content characterization in solar cells with the assistance of machine learning

Oleg Olikh, and Oleksii Zavhorodnii

Taras Shevchenko National University of Kyiv, 64/13, Volodymyrska Street, 01601, Kyiv, Ukraine

Email: olegolikh@knu.ua

Integrating artificial intelligence into sustainable clean energy research, particularly using machine learning (ML) for defect characterization, is increasingly compelling. A prevalent strategy is to identify extended defects from electroluminescence images. Recently, however, there has been a notable shift in focus towards point defects [1,2]. Our research aims to create an efficient, low-cost machine learning-based methodology for evaluating recombination defects in solar cells (SCs) using current-voltage (IV) measurement data, eliminating the need for extra equipment.

To demonstrate our methodology, we focused on identifying iron-related defect concentrations in silicon SC. Fig. 1(a) presents the workflow. Using SCAPS-1D software, the performance of back surface field SCs under both standard AM1.5 and monochromatic (940 nm) illumination were modeled. Simulated IV curves captured the behaviour of iron- acceptor pairs and scenarios with only interstitial iron. Then the relative changes in short- circuit current εI_{sc} , open-circuit voltage εV_{oc} , efficiency $\varepsilon \eta$, and fill factor εFF were extracted. ML techniques – deep neural networks (DNN), random forest (RF), and gradient boosting (GB) – were employed to estimate iron concentrations. The accuracy of predictions from various models was compared using data obtained under different lighting conditions and with varying numbers (ranging from 4 to 7) of descriptors. In the simplest case, the descriptors included the SC's base depth and doping level, temperature, and εI_{sc} . For cases involving 5, 6, and 7 descriptors, the $\varepsilon \eta$, εV_{oc} , and εFF , were added respectively. The results are shown in Tables 1 and 2 and Fig. 1(b).

References:

- [1] O. Olikh, O. Lozitsky and O. Zavhorodnii, *Prog Photovolt Res Appl.* **2022**, *30*, 648.
- [2] Y. Buratti, J. Dick, Q.L. Gia and Z. Hameiri, *ACS Appl. Mater. Interfaces* **2022**, *14*, 48647.

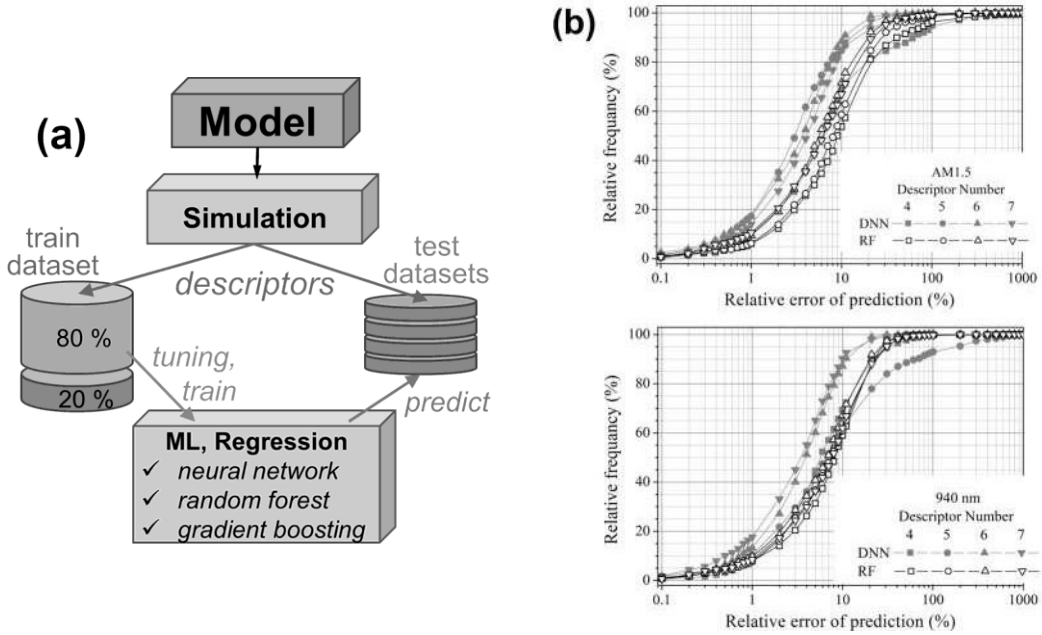


Fig. 1. (a) Workflow. (b) Fraction of samples for which the error does not exceed the threshold versus the threshold value for neural networks and random forest models. Top and down panels correspond to standard and monochromatic illumination, respectively.

Table 1. Results of 5-fold cross-validation for train dataset

Model	Illumination	Mean squared error (10^{-3})			
		4	5	6	7
DNN	AM1.5	42±5	9±3	4±2	2±1
	940 nm	10±5	6.1±0.4	6±2	1.5±0.7
RF	AM1.5	33±2	11±3	5±2	4±1
	940 nm	6±1	4.6±0.2	3.0±0.5	3.0±0.8
GB	AM1.5	34±2	9±2	5±2	4±1
	940 nm	4.2±0.6	3.5±0.2	2.3±0.6	2.1±0.5

Table 2. Prediction accuracy for test dataset

Model	Number of descriptors	Mean squared error (10^{-3})						Mean relative error (%)	R^2
		Illumination							
DNN	4	58	6	53	10	0.905	0.977		
	5	4	33	7	36	0.988	0.881		
	6	0.9	0.6	5	5	0.992	0.993		
	7	5	0.8	11	5	0.990	0.988		
RF	4	41	3	142	11	0.930	0.968		
	5	10	3	15	10	0.959	0.967		
	6	4	3	10	9	0.972	0.956		
	7	5	3	11	10	0.958	0.963		
GB	4	33	3	43	8	0.947	0.965		
	5	9	2	13	8	0.955	0.980		
	6	5	2	10	7	0.969	0.967		
	7	5	2	10	8	0.960	0.961		

Modulation Acceptor Doping of Silicon using Gallium-Doped SiO₂

Ingmar Ratschinski,¹ Shail Shah,¹ Somayeh Shams,¹ Selina Schneider,¹ Marie Venzke,²
 Philipp Hönicke^{2,3} and Daniel Hiller¹

¹ Institute of Applied Physics, Technical University Bergakademie Freiberg, Leipziger Straße 23, 09599, Freiberg, Germany

² Physikalisch-Technische Bundesanstalt (PTB), Abbestraße 2-12, 10587, Berlin, Germany

³ Helmholtz-Zentrum Berlin, Hahn-Meitner Platz 1, 14109, Berlin, Germany

Email: Ingmar.Ratschinski@physik.tu-freiberg.de

Modulation doping of silicon using specific metal impurities in SiO₂ is a novel doping concept that overcomes the limitations of conventional impurity doping, especially for nanostructures (diffusion, dielectric and quantum confinement, statistics of small numbers, etc.). An impurity doped SiO₂ layer or shell interacts with the silicon volume via a charge transfer process, that charges the unoccupied acceptor state induced by the impurity and leaves a hole behind in the silicon as free charge carrier. Hence, by this method the free carrier is separated from its parent dopant atom, which is embedded in the SiO₂ but located only a few nanometers from the silicon to allow direct tunneling.

Based on this concept, extensive experimental evidence of the doping mechanism was gathered for Al-doped SiO₂ [1-4]. Most recently, we demonstrated that modulation-doped silicon nanowires (Si NWs) with Al-doped SiO₂-shells have several orders of magnitude lower electrical resistances than Si NWs with undoped SiO₂-shells [5,6]. Density functional theory (DFT) calculations predict that gallium is another promising element for modulation acceptor doping [7].

In this presentation, recent results of atomic layer deposition (ALD) of Ga₂O₃ are shown, including the crystallization behavior and the quantification of the deposited Ga for the first ALD cycles and the associated (sub-)monolayers of gallium oxide by using synchrotron- based reference-free grazing incidence X-ray fluorescence spectrometry (GIXRF). The modulation doping effect is studied by using SiO₂:Ga MOS capacitors.

References:

- [1] D. König et al., *Sci. Rep.* **2017**, *7*, 46703.
- [2] D. Hiller et al., *ACS Appl. Mater. Interfaces* **2018**, *10*, 30495.
- [3] D. Hiller et al., *J. Appl. Phys.* **2019**, *125*, 015301.
- [4] D. Hiller et al., *J. Phys. D Appl. Phys.* **2021**, *54*, 275304.
- [5] I. Ratschinski et al., *Phys. Status Solidi A* **2023**, *220*, 2300068.
- [6] S. Nagarajan et al., *Adv. Mater. Interfaces* **2024**, *11*, 2300600.
- [7] D. König et al., *Phys. Rev. Appl.* **2018**, *10*, 054034.
- [8] P. Hönicke et al., *J. Vac. Sci. Technol. A* **2019**, *37*, 041502.

For your remarks

Residual Stress and Defects in a Single-crystalline (0001)AlN Wafer Investigated by Scanning Infrared Depolarization and White Beam X-ray Topography

Martin Herms¹⁾, Laura Narvaez¹⁾
 Carsten Hartmann²⁾, Carsten Richter²⁾, Thomas Straubinger²⁾
 Merve Kabukcuoglu³⁾, Daniel Hänschke³⁾, Elias Hamann³⁾

¹⁾ PVA Metrology & Plasma Solutions GmbH, Im Westpark 10-12, D-35435 Wettenberg, Germany

²⁾ Leibniz-Institut für Kristallzüchtung (IKZ), Max-Born-Str. 2, D-12489 Berlin, Germany

³⁾ Institute for Photon Science and Synchrotron Radiation (IPS), Karlsruhe Institute of Technology (KIT), Eggenstein-Leopoldshafen, D-76344, Germany

Email: martin.herms@pvatepla.com

The residual shear stress and the defect distribution in a single-crystalline c-plane AlN wafer grown by PVT (Physical Vapour Transport) [1] are visualized using SIRD (Scanning Infrared Depolarization) [2] and compared to WB-XRT (White Beam X-ray Topography) utilizing synchrotron radiation [3]. The SIRD images qualitatively depict the same defect distribution as the XRT images, which naturally exhibit higher resolution and can differentiate between individual dislocations. However, SIRD is a laboratory system qualified for industrial in-line applications. Moreover, the multi-polarization analysis (MPA) allows for creating quantitative maps of the maximum value and principal direction of stress-induced birefringence, which can be converted into shear stress maps [4].

For a wafer grown under high-temperature gradients, the global maximum shear stress is determined to be approximately 6 MPa. Both SIRD and WB-XRT reveal a Star of David pattern formed by a-type dislocations (density approximately 10^4 cm^{-2}) with dislocation lines parallel to the c-plane and three m-glide-planes [5]. A wafer grown under lower temperature gradients does not exhibit a Star of David pattern.

References:

- [1] C. Hartmann, M. P. Kabukcuoglu, C. Richter, A. Klump, D. Schulz, U. Juda, M. Bickermann, D. Hänschke, T. Schröder, and T. Straubinger, *Applied Physics Express* 16, 075502 (2023), DOI: 10.35848/1882-0786/ace60e.
- [2] M. Herms, M. Wagner, A. Molchanov, P. Lin, I. De Wolf, and M. Zhao, *Phys. Status Solidi C* 12 (2015), No. 8, 1085–1089, DOI: 10.1002/pssc.201400356.
- [3] A. N. Danilewsky, *Cryst. Res. Technol.* 55, 9 (2020), pp. 1–14, DOI: 10.1002/crat.202000012.
- [4] M. Herms, G. Irmer, G. Kupka, N. Kirchner, and M. Wagner, *Journ. Electronic Mater.* (2020), DOI: 10.1007/s11664-020-08141-7.
- [5] S. Hu, H. Fang, Y. Liu, H. Peng, Q. Cheng, Z. Chen, R. Dalmau, J. Britt, R. Schlessner, B. Raghothamachar, and M. Dudley, *J. Cryst. Growth* 584, 126548 (2022), DOI: 10.1016/j.jcrysgro.2022.126548.

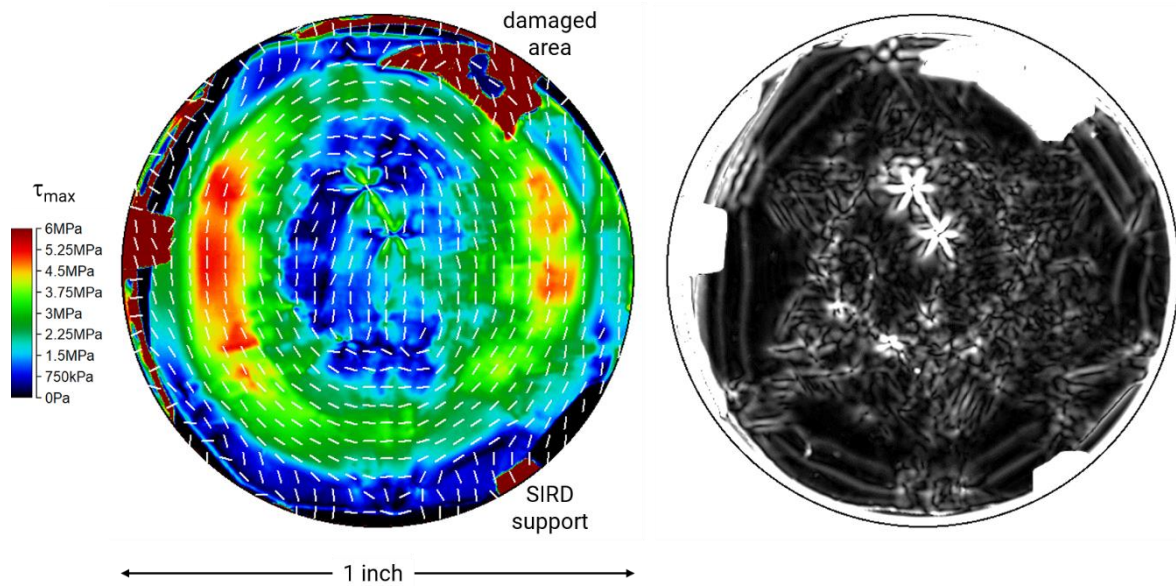


Fig. 1. Map of shear stress maximum of a (0001) AlN wafer, complemented by isostatic lines representing the fast principal axis of stress-induced birefringence (left side). On the right side, the corresponding map is shown, generated using the MPA based on high-pass filtered data.

Suppression of Stacking Fault Expansion with Energy-Filtered Ion Implantation in 4H-SiC Epitaxial Material

Hitesh Jayaprakash,^{1,2} Constantin Csato,¹ Florian Krippendorf,¹ Michael Rüb,^{1,2} and Jörg Schulze^{3,4}

¹ mi2-factory GmbH, Jena, Germany

² SciTec, Ernst-Abbe-Hochschule, Jena, Germany

³ Chair on Electron Devices (LEB), Friedrich-Alexander Universität, Erlangen, Germany

⁴ Fraunhofer Institute for Integrated Systems and Device Technology (IISB), Erlangen, Germany.

Email: hitesh.jayaprakash@eah-jena.de

Conventional 4H-SiC epitaxial materials for power devices face reliability concerns due to defects leading to device failure. Despite efforts, including the use of recombination- enhanced buffer layer¹ and monoenergetic proton implantation (2D) at the drift-substrate interface to suppress stacking fault expansion², issues persist with converted Basal Plane Dislocations (BPD) acting as nucleation sites for Stacking Fault (SF) expansion in the drift zone, causing device degradation. To overcome these reliability challenges, 19MeV Energy Filtered Ion Implantation³ (EFII) which is a blanket implant (3D) of nitrogen was employed to suppress BPD/SF expansion, reducing sensitivity to bipolar degradation. The reduction in expanded Single Shockley Stacking Fault (1SSF) density was observed by optically studying the Recombination Enhanced Dislocation Glide (REDG) mechanism using UV illumination (UVL)^{1,2}. The impact of EFII on suppressing stacking fault expansion was investigated based on effective implant concentration. Using photoluminescence (PL), quantification of 1SSF density before and after the process was conducted.

6-inch commercially available 4H-SiC epitaxial wafers (Table. 1) were used for experiments. Nominally undoped wafer A was EFII-implanted with nitrogen concentration in each quadrant ranging from 1E15cm⁻³ to 1E16cm⁻³ and annealed*, retaining one quadrant without ion implantation for reference. This wafer underwent UVL at each region with 72 Wcm⁻². PL measurements did not reveal any 1SSF expanded. Hence, the UV intensity was increased to 142 Wcm⁻² to activate the nucleation sites and >10x 1SSF expanded. Fig. 1 shows 1SSF density in as grown epitaxial material compared to EFII implanted regions. Wafer B was identically doped to confirm the results. This wafer was subjected to identical UVL conditions. There was no 1SSF detected on the EFII implanted regions, except negligible change around triangular defect showing in fig.2. Previously, MPS diodes fabricated with EFII, showed characteristics (BV_{DSS}, R_{on}, I_{DSS}) like that of conventional epitaxially doped devices³. Overall, it is evident that the REDG is significantly suppressed in EFII implanted, showing huge potential of enhancing the reliability of 4H-SiC power devices over traditional methods and achieving precise doping of the voltage sustaining in a single unit process step.

References:

- [1] K. Takano, Y. Igarashi, Mater. Sci. For., vol. 1062, pp. 273–277, 2022. [2] M. Kato, et al., Sci. Rep., vol. 12, no. 1, p. 18790, 2022.
- [3] R. Rupp, et al., Mater. Sci. For., vol. 858, pp. 531–534, 2016.

*Activation annealing step: 1700°C for 30 minutes with carbon capping layer

Table 1. Commercially available 4H-SiC wafer description used in the experiment.

Wafer ID	Epitaxy thickness [μm]	Buffer thickness [μm]	In-situ doping concentration [cm-3]	After EFII, doping concentration [cm-3]	BPD Density [#] [cm-2]
Wafer A	5	0.5	<5E14	1E15, 5E15 and 1E16	68
Wafer B	5	0.5	<5E14	1E15, 5E15 and 1E16	3

[#]claimed by the wafer vendor

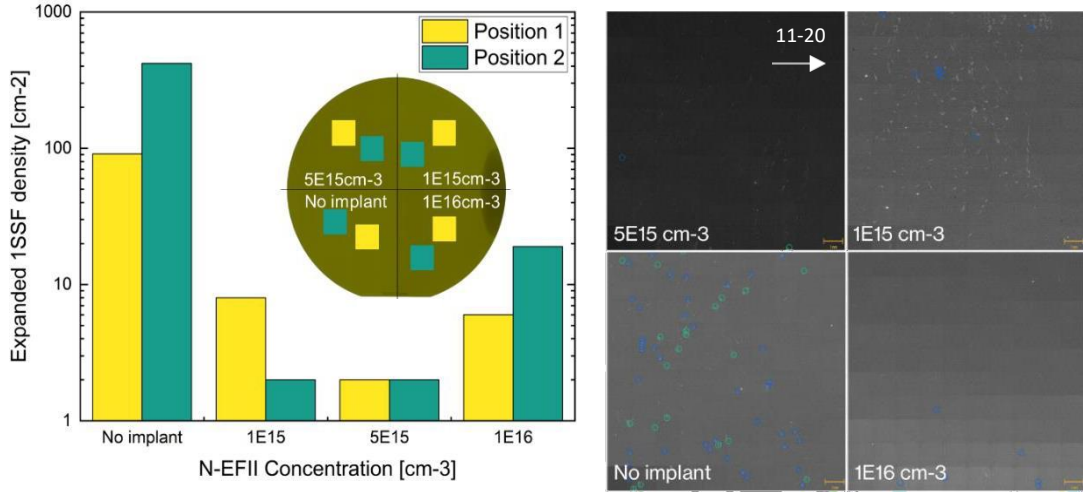


Fig. 1 On wafer A, after 142 Wcm-2 UV illumination for 60 min, plot on left PL reveals very low - similar 1SSF density within each of the three quadrants implanted with EFII (inset) The no implant region shows significantly higher expanded 1SSF (circled blue, green) density on corresponding PL images right, using 420nm filter at position 1. with area 10x10 mm in each quadrant. for statistics, two positions were measured on each quadrant as illustrated.

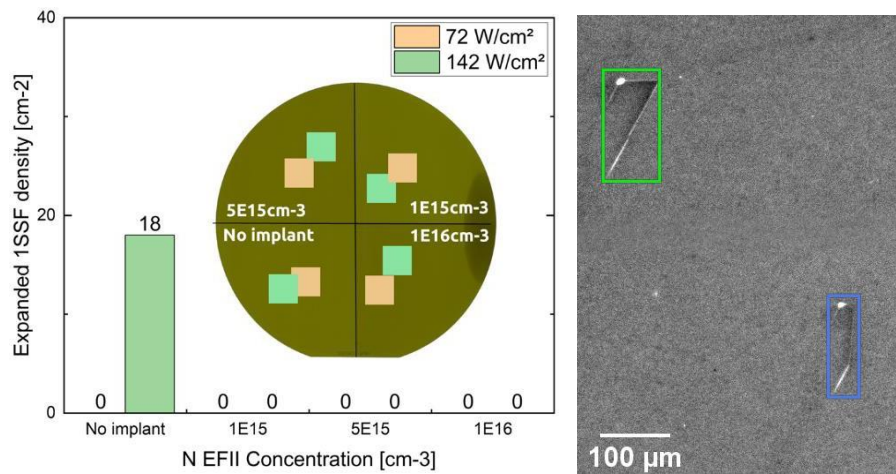


Fig. 2 On left Wafer B, there was no expanded 1SSF detected after implant with 72 Wcm-2 UVL stress but even with higher intensity of 142 Wcm-2, it is evident that EFII implanted regions have no signature of 1SSF in comparison to a reference region with 18 cm-2 1SSF detected. right shows the PL image (> 700nm) of partially expanded 1SSF and fully expanded 1SSF encircled blue and green respectively in the not implanted region nucleated from the partial dislocation (bright spot).

Self-assembly of W centers and their optical properties in microdisk resonators

M. Karaman¹, J.Aberl¹, D. Haya Enriquez¹, E.Prado-Navarette¹, T.Fromherz¹, M. Brehm¹

¹Institute of Semiconductor Physics, Johannes Kepler University Linz, Altenbergerstr. 69, A-4040 Linz, Austria

Email: merve.karaman@jku.at

Silicon, the most important semiconductor material, is essential for microelectronics and integrated photonics and is a promising candidate for expanding large-scale quantum technologies. However, the indirect nature of the band gap in silicon is a significant disadvantage for optoelectronics applications. Despite the promise of silicon-based photonic devices, the fundamental problem of light emission remains a challenge [1].

Lately, a wide range of single-photon emitters has been made possible by the use of Si color centers (SiCCs), which were previously mainly known as radiation damage centers that are induced by ion implantation and other processes [2]. Some of them are related to carbon-Si point defects, carbon-hydrogen-Si, oxygen-Si complexes, or Si self-interstitials. The W center is a color center composed of interstitial silicon atoms that are characterized by a Zero- Phonon Line (ZPL) emission at 1218 nm [3]. Recently, the W-centers noticed an increased interest in Si-based photonics [4,5], in particular Si-based quantum photonics, for which the emission properties are boosted by embedding the emitters into photonic resonators [5].

However, there is a significant challenge in achieving deterministic high-yield photonic integration of SiCCs. The major bottleneck is the dependence on ion implantation, which results in broad ion distribution profiles [4,6]. In this study, we introduce a new method to create color centers in Silicon (Si) without the need for traditional ion implantation techniques, which is based on the self-assembly of SiCC during epitaxial growth using molecular beam epitaxy (MBE) at low temperatures (ULT-growth <300°C). This approach offers significant advantages similar to quantum dot emitters by limiting the vertical emitter location within the epilayer to the nanoscale. Photoluminescence measurements showed a pronounced ZPL emission at 1218 nm. These W-center color centers can be overgrown with higher quality Si, allowing for placement of the emitters where, e.g., photonics modes have a maximum. Furthermore, microdisks were created using e-beam lithography with varying diameters of the microdisks, leading to a significant increase in the light emission intensity of the self-assembled color centers of W-type.

References:

- [1] Redjem W, A. Durand., et al. "Single artificial atoms in silicon emitting at telecom wavelengths." *Nature Electronics* 3.12 **2020** 738-743.
- [2] Khouri, Mario, and Marco Abbarchi. "A bright future for silicon in quantum technologies." *Journal of Applied Physics* **2022** 131.20.
- [3] Davies, Gordon. "The optical properties of luminescence centers in silicon." *Physics reports* **1989** 176.3-4: 83-188.
- [4] Baron, Y., Durand, A., Udvarhelyi, P., Herzig, T., Khouri, M., Pezzagna, S., ... & Dréau, A. Detection of single W-centers in silicon. *ACS Photonics*, **2022** 9(7), 2337-2345.
- [5] Lefaucher, Baptiste, et al. "Purcell enhancement of silicon W centers in circular Bragg grating cavities." *ACS photonics* **2023** 11.1: 24-32.
- [6] M. Hollenbach, Y. Berencén, U. Kentsch, M. Helm, G. V. Astakhov, Engineering telecom single photon emitters in silicon for scalable quantum photonics, *Optics Express* **2020** 28, 2611.

For your remarks

Investigation of TI-doped silicon by low temperature photoluminescence during LID treatments

Kevin Lauer,^{1,2} Robin Müller,² Katharina Peh,² Dirk Schulze,² Stefan Krischok,² Stephanie Reiß,¹ Andreas Frank¹ and Thomas Ortlepp¹

¹ CiS Forschungsinstitut für Mikrosensorik GmbH, Konrad-Zuse-Str. 14, 99099 Erfurt, Germany

² Technische Universität Ilmenau, Institut für Physik, Weimarer Str. 32, 98693 Ilmenau, Germany

Email: klauer@cismst.de

Light-induced degradation (LID) in silicon is well known for the acceptor boron [1] as well as for the acceptor indium. [2] In indium-doped silicon a mode of the underlying defect, which was proposed to be an $\text{In}_{\text{Si}}\text{-Si}_i$ -defect, shows photoluminescence activity. This photoluminescence activity, the so-called P-line, was found to change under LID cycles. Speculations [3] were made early, that similar PL features in thallium-doped silicon [4] may be caused by a $\text{Tl}_{\text{Si}}\text{-Si}_i$ -defect. This implies that the PL features in thallium-doped silicon may also follow LID treatments.

In this contribution low temperature photoluminescence measurements on thallium-implanted silicon samples are reported during LID treatments. Changes in the intensity of the A- and P-line in these samples during LID treatments are found to be similar to the earlier observed changes in the P-line in indium-doped silicon. These experimental results support the identification of the underlying defect for the A- as well as the P-line in thallium-doped silicon as different modes of a $\text{Tl}_{\text{Si}}\text{-Si}_i$ -defect.

References:

- [1] K. Bothe and J. Schmidt, *Electronically Activated Boron-Oxygen-Related Recombination Centers in Crystalline Silicon*, J Appl Phys **99**, 013701 (2006).
- [2] K. Lauer, K. Peh, D. Schulze, T. Ortlepp, E. Runge, and S. Krischok, *The ASi-Sii Defect Model of Light-Induced Degradation (LID) in Silicon: A Discussion and Review*, Phys. Status Solidi A **219**, 2200099 (2022).
- [3] K. Lauer, C. Möller, D. Schulze, and C. Ahrens, *Identification of Photoluminescence P Line in Indium Doped Silicon as InSi-Sii Defect*, AIP Adv. **5**, 017101 (2015).
- [4] H. Conzelmann, A. Hangleiter, and J. Weber, *Thallium-Related Isoelectronic Bound Excitons in Silicon. A Bistable Defect at Low Temperatures*, Phys. Status Solidi B **133**, 655 (1986).

Tl implantation in FZ silicon, n-type, $10\text{k}\Omega\text{cm}$

natural oxide on surface

$E_{\text{Implantation}} = 200\text{keV}$

Dose = $1.5 \times 10^{12}\text{cm}^{-2}$

RTP: 10s, 1000°C

glowing in flame
water quenching

$T_{\text{measure}} = 4.2\text{K}$

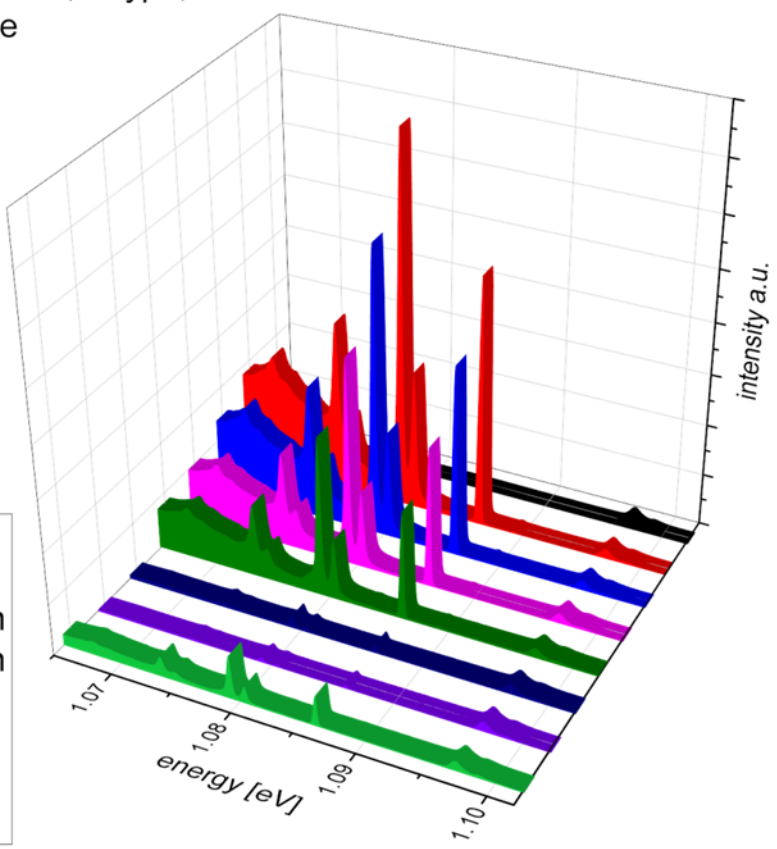
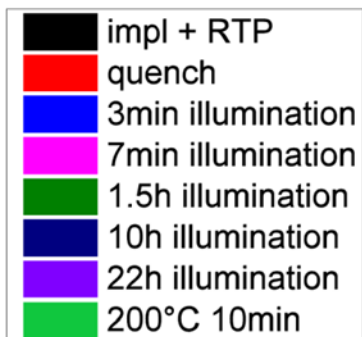


Fig. 1. Low temperature photoluminescence spectra of thallium-implanted and annealed silicon during a typical LID cycle. PL intensities are normalized to the free exciton peak.

DLTS characterisation of 107 MeV krypton ion-irradiated nitrogen-doped 4H-silicon carbide

Ezekiel Omotoso^{1,2}, Emmanuel Igumbor² and Walter E. Meyer²

¹*Department of Physics and Engineering Physics, Obafemi Awolowo University, Ile-Ife, 220005, Nigeria*

²*Department of Physics, University of Pretoria, Pretoria, 0083, South Africa*

Email: omotoeze@gmail.com; eomotoso@oauife.edu.ng

Swift heavy ions, such as krypton ions, play an important role in the development and improvement of various devices. In the study, the influence of Kr²⁺ on nitrogen-doped 4H-silicon carbide has been investigated by deep level transient spectroscopy (DLTS). Kr²⁺ with energy of 107 MeV was used to irradiate the Au/Ni/4H-SiC Schottky contacts at a fluence of $1 \times 10^{10} \text{ cm}^{-2}$ at room temperature (300 K). Before the irradiation of the samples, the electrical measurements revealed good rectifying behaviour. Rectification properties of the Au/Ni/4H-SiC Schottky barrier diodes (SBDs) was completely lost after irradiation at fluence of $1 \times 10^{10} \text{ cm}^{-2}$. After annealing at 300 °C in flowing argon, the current-voltage (I-V) and capacitance-voltage (C-V) revealed partial rectification. DLTS of the as-grown devices showed the presence of four deep level defects as shown in Fig. 1. After the annealing, the DLTS spectra of the partially rectifying devices showed a reduction in the intensity of the E_{0.10} and the disappearance of the E_{0.12} as well as the E_{0.16} defects as shown in Fig. 2. Also, in Fig. 2, two defects with energy 280 and 410 meV showed inverted peaks, as would have been expected from minority carriers trap instead of majority carriers which led to confusion as the peaks were inverted. It was concluded that the peculiar characteristics of DLTS measurements on SBDs may be due to the extremely high value of the series resistance as well as the low capacitance. The results will provide insight into the behaviour of SBDs under irradiation and can be used to improve the radiation tolerance of electronic devices made from SiC.

Reference:

- [1] E. Omotoso, W.E. Meyer, F.D. Auret, A.T. Paradzah, M. Diale, S.M.M. Coelho, P.J. Janse van Rensburg, The influence of high energy electron irradiation on the Schottky barrier height and the Richardson constant of Ni/4H-SiC Schottky diodes, Materials Science in Semiconductor Processing 39(0) (2015) 112-118.

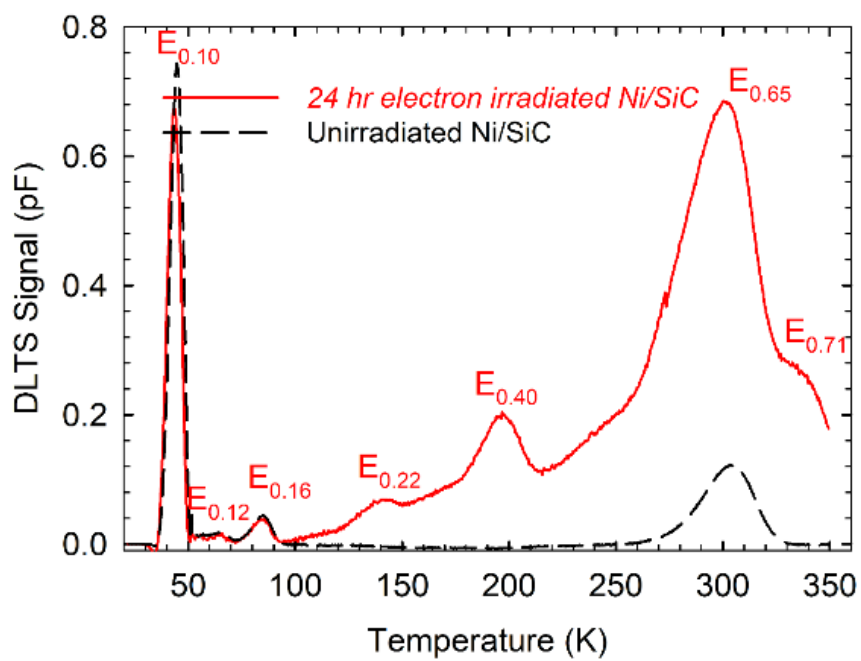


Fig. 1: DLTS spectra of unirradiated and high-energy electron irradiated Ni/4H-SiC diode reported by Omotoso *et al* [1].

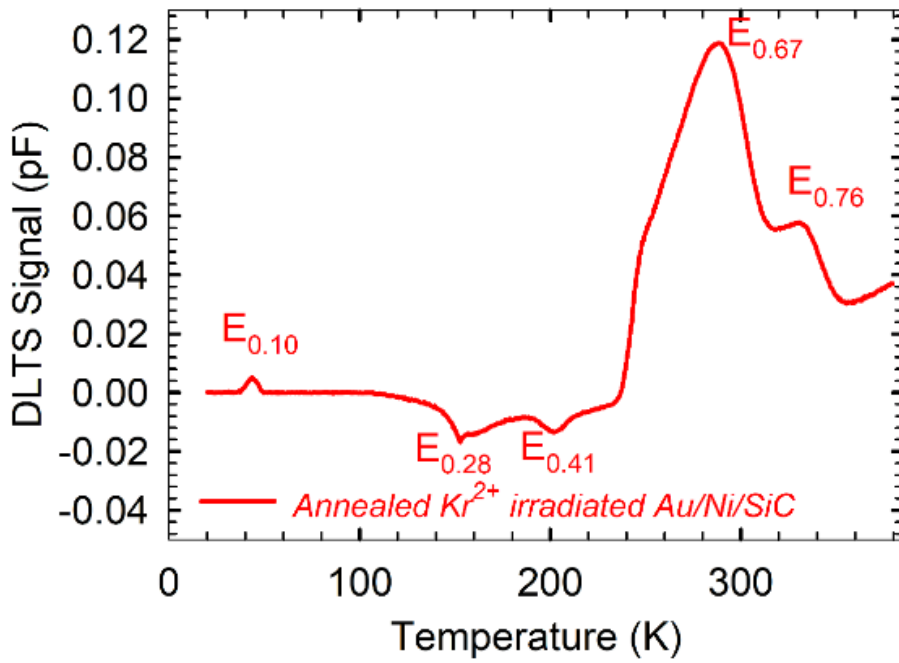


Fig. 2: DLTS spectrum obtained after annealing the 107 MeV Kr²⁺ irradiated Au/Ni/4H-SiC Schottky barrier diode at 300 °C.

Point defect calculations with finite-size supercells in monolayer MoS₂

Faiza H Alhamed^{1,2}, Jonathan P Goss¹, Patrick R Briddon¹, Mark J Rayson¹ and Aleksey Kozikov¹

¹ School of Mathematics, Statistics and Physics, Newcastle University, Newcastle upon Tyne, NE1 7RU, UK

² College of Science and Arts, Physics, Najran University, Najran, Saudi Arabia

Email: F.Al-Hamed2@newcastle.ac.uk

Mono- and few-layer two-dimensional transition metal dichalcogenides, such as MoS₂, are suited for applications in quantum technology, photovoltaics and catalysis [1-3]. Their properties are affected by point defects, particularly defects that introduce donor and acceptor levels to the bandgap, such as efficiency limiting effects from carrier traps for a photovoltaic device [4]. It is therefore of great importance to understand the electrical properties of defects and how they impact upon the materials properties, but experimental determination of carrier trap positions relative to the band-edges can be challenging for single-layer 2D materials. As a result, there is a desire to use quantum-chemical modelling approaches to quantitatively predict the trap positions of point defects such as vacancies and impurities, but periodic boundary conditions render modelling charged system problematic [5,6]. Extrapolation strategies include varying the effective concentration and the periodic boundary conditions. We performed density functional calculations with various cell sizes for the formation energy of vacancies in MoS₂, varying boundary conditions. The standard formation energies form

$$E^f(X, q) = E_{\text{total}}(X, q) - E_{\text{pure}} + \Delta\mu_x + q\mu_e + \chi(X, q),$$

where $E_{\text{total}}(X, q)$ is the total energy of system X in charge state q , E_{pure} is the total energy of the comparable defect-free system, $\Delta\mu_x$ account for the difference in composition, μ_e is the electron chemical potential relative to the valence band maximum and χ corrects for the periodic boundary condition artifacts.

Interactions between periodic images are a combination of electrostatic and quantum-overlap in origin, and χ is not formally known. However, the formation energies vary approximately systematically with cell size. By considering a wide range of supercell sizes and calculating the formation (and therefore the ionisation) energies with varying boundary conditions, we find that the extrapolations for the infinitely dilute solution of acceptor and donor levels are 0.90 ± 0.04 eV and 0.07 ± 0.03 eV above the valence band, respectively (Fig. 1). The ranges provided arise from the variation of the boundary condition in the vacuum-direction, with the distance between MoS₂ layers either being fixed for all cell sizes or begin scaled proportionally with the in-plane lattice constant. Our estimates are in broad quantitative agreement with the literature [7,8]. More generally, we find that the choice of boundary condition does not seem to affect the calculated donor or acceptor level, and the extrapolation does not differ significantly between states with different levels of delocalisation. We demonstrated that fixed or variable vacuum thicknesses can provide a relatively consistent estimate of trap sites.

References:

- [1] Zong, X., et al., *Am. Chem. Soc.*, **2008**, 130(23), p.7176-7177.
- [2] Mak, K.F., et al., *Phys. Rev. Lett.*, **2010**, 105(13), p.136805.
- [3] Paul, J. T., et al., *J. Phys. Condens. Matter*, **2020**, 32(15), p.1.
- [4] Al-Ghiffari, A.D., et al., *Materials Today Communications*, **2022**, 32, p.104078.
- [5] Komsa, H.-P., et al., *Phys. Rev. B*, **2012**, 86(4), p.045112.
- [6] We use the AIMPRO DFT package as described, for example, in *Phys. Rev. Materials*, **2023**, 7(9), p.094003.

[7] Tan, A.M.Z., Freysoldt, C. and Hennig, R.G., Phys. Rev. Materials, **2020**, 4(6), p.064004.

[8] Noh, J.-Y., et al., Phys. Rev. B, **2014**, 89(20), p.205417.

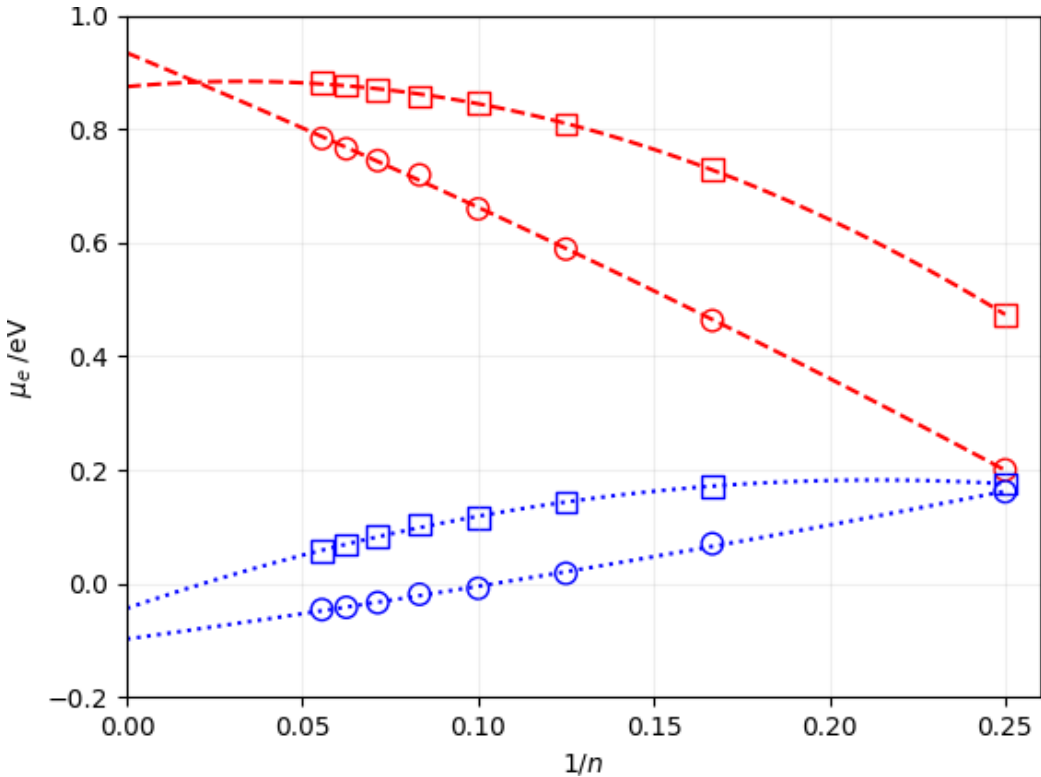


Fig. 1. The calculated trap levels for vacancies in MoS₂, V_{Mo} (dashed lines) and V_s (dotted lines). The trap levels relative to the valence band top are plotted as an inverse function of the supercell size, where the supercells are made up from $n \times n$ primitive cells. The dashed and dotted lines show quadratic fits to these data. Data shown as circles are for where the out-of-plane spacing is fixed at 12.3 Å, and squares where the spacing is approximately 3.2n Å. The extrapolation to the intercept on at $1/n = 0$ provides the estimates of the donor and acceptor level locations for the dilute solution.

Theoretical investigation of single Boron defects in silicon

Aaron Flötotto,¹ Wichard J. D. Beenken¹, Kevin Lauer^{1,2} and Erich Runge¹

¹ Technische Universität Ilmenau, Institut für Physik, Weimarer Straße 25, 98693 Ilmenau, Germany

² CiS Forschungsinstitut für Mikrosensorik GmbH, Konrad-Zuse-Straße 14, 99099 Erfurt, Germany

Email: aaron.floetotto@tu-ilmenau.de

Boron is an important dopant for silicon. However, it has some shortcomings. Together with silicon interstitials, it can form the so-called $B_{Si}Si_i$ defect. This defect has been suggested as a source of light-induced degradation (LiD) in solar cells made of boron-doped Czochralski- grown silicon [1]. Using first-principles methods, we investigate the potential energy landscape in the vicinity of the $B_{Si}Si_i$ defect. Besides the original $B_{Si}Si_i$ defect, our analysis includes configurations consisting of a single interstitial B atom as well as B-Si pairs sharing a lattice vacancy. The meta-stable defect configurations are identified and their formation energies are determined. We use the charge and configuration dependent electronic density of states (DOS) to locate deep defects which may serve as recombination centers. Using the Nudged Elastic Band method, we calculate the minimum energy paths between these meta- stable configurations and thus reveal the potential energy landscape. A comparative analysis with previous models for boron diffusion and LiD highlights the relevance of our results.

Reference:

- [1] K. Lauer, K. Peh, D. Schulze, T. Ortlepp, E. Runge, and S. Krischok, Phys. Status Solidi A, 2022, 219, 2200099.

For your remarks

Effects of Hydrogen Bonding in Silicon Nitride/Polyimide Passivation Stack for SiC Power Devices

Antonino Scandurra^{1,2}, Gabriele Bellocchi³, Giuseppe Arena³, Simone Rascunà³, Michele Calabretta³, Massimo Boscaglia³, Mario Saggio³, Giacometta Mineo^{1,2}, Valentina Iacono^{1,2}, Stefano Boscarino^{1,2}, Salvatore Mirabella^{1,2}, Francesco Ruffino^{1,2}, Maria Grazia Grimaldi^{1,2}

¹Department of Physics and Astronomy “Ettore Majorana”, University of Catania, via Santa Sofia 64, 95123 Catania, Italy;

²Institute for Microelectronics and Microsystems of National Research Council of Italy (CNR- IMM, Catania University Unit), via Santa Sofia 64, 95123 Catania, Italy

³STMicroelectronics, Stradale Primosole 50, 95121 Catania, Italy;

Email: antonino.scandurra@dfa.unict.it

The passivation layer of SiC power devices represents one of the most critical issues of reliability. Its function is to preserve the surfaces of active regions and metals of the device against moisture, corrosion and ionic contamination. Its function is also to insulate the device against electric and magnetic fields. The passivation layer can be of inorganic type e.g. silicon nitride (SixNy), silicon oxide (SiO_2) or silicon oxynitride (SiON); organic, such as polyimide, or both. Silicon nitride shows a good compromise between resistance to humidity and dielectric behavior. The moisture resistance of silicon nitride, however, depends heavily on its stoichiometry, on the hydrogen content, thus, the concentration of SiH_x and NH_x residual groups and the type of residual mechanical stress. All these properties are influenced by the deposition technique and the corresponding parameters.

In this work we have investigated the composition and morphology of stack formed by silicon nitride, obtained by plasma-enhanced chemical vapor deposition (PECVD) starting from silane and ammonia, and polyimide layers, obtained by spin coating of the polyamic acid precursor (SiN/PI). The stack is used as an efficient passivation layer against moisture in power microelectronics devices assembled in plastic packages or multichip module. Two types of silicon nitrides, having different chemical and physical properties, were obtained by changing the process parameters. Samples with different Si/N atomic ratios and hydrogen content were obtained. Rutherford Backscattering Spectrometry (RBS) analyses showed that the Si/N ratio of the two samples varies from 0.8 to 0.6, respectively. Elastic Recoil Detection Analysis (ERDA) characterization show that the sample with higher nitrogen content also has a higher bound hydrogen content than the other sample by about 10 %. Hydrogen in SiN is bonded both as SiH_x and NH_x groups. The obtained results are in agreement with the literature which indicates that residual hydrogen, depending on the parameters of the deposition process, remains preferentially bound to nitrogen. Nitride films with high concentration of NH_x groups show higher reactivity and permeability to water, making it less effective as a passivation layer [1]. Atomic Force Microscopy (AFM) measurements of the two nitride samples show that both have a granular morphology with a rms of 1.1 nm (Si/N 0.6) and 2 nm (Si/N 0.8), respectively. AFM analyses of the polyimide layer on the SiN film (SiN/PI stack) show a similar roughness by the two samples, indicating the presence of an effect of surface roughness planarization which could give a contribution to increase SiN/PI adhesion. These results may be useful to reduce the water diffusion through the grain boundaries in the SiN layer and, then, its reliability and at the same time improve the passivation stack for high-power applications.

Reference:

- [1] C. Cazako, K. Inal, A. Burr, F. Georgi, R. Cauro, *Metall. Res. Technol.*, **2018**, *115*, 406
10.1051/metal/2018072.hal-02968666

Progress of characterization methodology for oxygen-related defects in silicon substrates for advanced technologies

J. Crozelon^{1,2}, J. M. Bluet², G. Bremond², A. Abbadie¹

¹ STMicroelectronics, 850 rue Jean Monnet, 38920, Crolles, France

² INSA Lyon, Ecole Centrale de Lyon, CNRS, Université Claude Bernard Lyon 1, CPE Lyon,
 INL, UMR5270, 69621, Villeurbanne, France

Email: jeremi.crozelon@st.com; jeremi.crozelon@insa-lyon.fr

Oxygen-related defects are of great interest in the semiconductor industry, especially Bulk microdefects (BMD), as they can improve the mechanical robustness of p-type Czochralski (CZ) silicon substrates [1,2]. Their formation is challenging on high resistivity (HR) silicon used for radio frequency applications, being characterized by low or intermediate interstitial oxygen (O_i) concentrations [3,4]. Furthermore, the characterization and quantification of these defects is challenging due to the lack of relevant and sensitive techniques [5].

In this work, we aimed to develop a robust methodology for the characterization of oxide precipitates generated by thermal processes (rapid thermal annealing followed by 2-stage precipitation annealing with a nucleation plateau at 800°C and a growth plateau at 1050°C). We studied different CZ silicon substrates with different ranges of (O_i) and p-type doping (boron) content, as summarized in Table 1. Using light scattering tomography (LST), we estimated a BMD density approximately $5 \times 10^9 \text{ cm}^{-3}$ with a size of about 70 nm (Figure 1). This promising result for BMD formation in HR silicon was correlated with spectroscopic signatures using low-temperature (77 K) infrared spectroscopy, low-temperature photoluminescence (LTPL) spectroscopy (10 K), and deep-level transient spectroscopy (DLTS). For example, Figure 2 compares the LTPL spectra of annealed and unannealed HR substrate #B. After annealing, two peaks appear in the spectrum: the broad D1 band due to dislocations, which is associated with oxygen precipitation [6,7], and the sharp P line at 1618 nm due to the C_i-O_2 complex [8]. We suggest that the sharp peak located at 1529 nm in spectra is an associated oxygen-related center [6]. Combined with DLTS, these results pointing out the signature of the oxygen precipitation process in HR silicon materials will be discussed in detail.

In this study, we developed a combination of techniques to control and monitor oxygen- related defects in HR silicon substrates.

References:

- [1] C. Claeys, E. Simoen, J. Vanhellemont, *J. Phys. III* **1997**, 7, 1469-1486.
- [2] A. Borghesi, “Oxygen precipitation in silicon” (*J. Appl. Phys.*, 1995), 4169.
- [3] K. Kajiwara, K. Harada, K. Torigoe, *Phys. Status Solidi* **2019**, 216, 1900272.
- [4] I. Bertrand, P. Flatresse, G. Besnard, *ECS Transactions* **2022**, 2022-01, 1273-1273.
- [5] G. Kissinger, T. Müller, A. Sattler, *Mat. Sci. Semiconductor Proc.* **2006**, 9, 236-240.
- [6] S. Binetti, S. Pizzini, E. Leoni, *Solid State Phenomena* **2002**, 82-84, 75-80.
- [7] M. Tajima, M. Tokita, M. Warashina, *Mat. Sci. Forum* **1995**, 196-201, 1749-1754.
- [8] T. Mehl, I. Burud, E. Letty, *Energy Procedia* **2017**, 124, 107-12.

Table 1. Characteristics of the silicon substrate samples studied.

Czochralski silicon substrate type	(O_i) $10^{17} \text{ at.cm}^{-3}$	Incoming resistivity range $\Omega.\text{cm}$	Notes
#A	4-9	1-50	High (O_i) Standard resistivity
#B	3-5	400-1300	Medium (O_i) High resistivity
#C	1-2.5	2000	Low (O_i) High resistivity

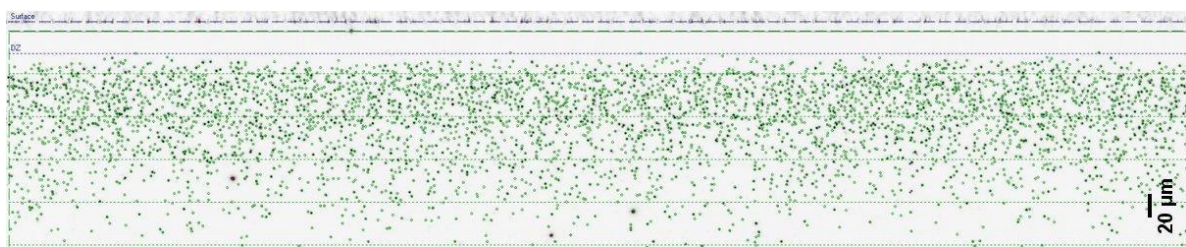


Figure. 1. LST image of the BMD generated in substrate bulk #B after rapid thermal annealing followed by 2-step precipitation annealing (labelled OXP). The defect free Denuded zone (DZ) is located approximately 20 μm below the substrate surface.

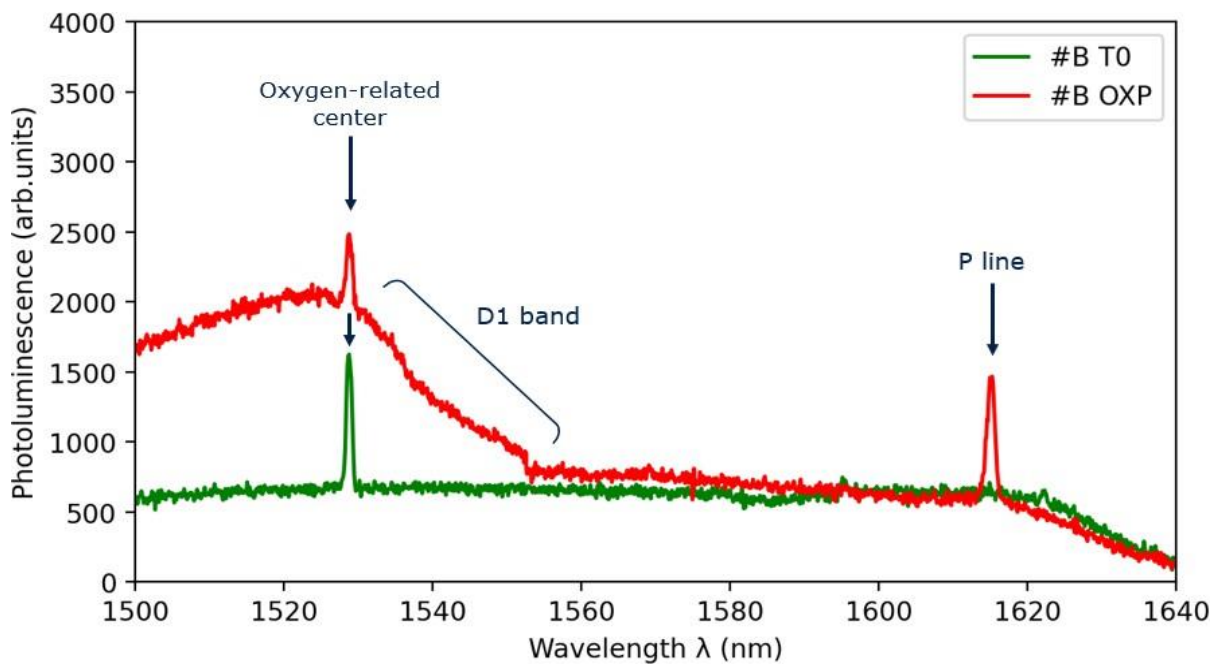


Figure. 2. PL spectra (10 K) of unannealed (T0) and annealed/precipitated (OXP) #B samples. Precipitated sample (OXP) has been passivated with SiN.

operando analysis of self-heating effects on AlN-based HEMTs on SiC by confocal micro-Raman spectroscopy

Christian Röder¹, Jennifer Schwarz², Alexander Schmid², Oliver Hilt³, Franziska C. Beyer¹, and Johannes Heitmann^{1,2}

¹ *Fraunhofer Institute for Integrated Systems and Device Technology (IISB), Schottkystr. 10, 91058 Erlangen,
 Germany*

² *TU Bergakademie Freiberg, Institute of Applied Physics, Leipziger Str. 23, 09599 Freiberg, Germany*

³ *Ferdinand-Braun-Institut (FBH), Gustav-Kirchhoff-Str. 4, 12489 Berlin, Germany*

Email: christian.roeder@iisb.fraunhofer.de

High Electron Mobility Transistors (HEMTs) based on semiconductors materials with wurtzite-type crystal structure such as Gallium nitride (GaN) or Aluminium nitride (AlN) are of great interest in high-power technologies due to high breakdown fields and large carrier mobilities. The device performance can suffer from self-heating effects due to prevailing (leakage) currents and inadequate heat dissipation which trigger and accelerate degradation processes. [1-3]

Micro-Raman spectroscopy is a versatile method in order to determine temperatures from characteristic phonon frequency shifts and providing a high spatial resolution. However, the phonon frequency change is also affected by additional external impacts such as stress and electric field which have to be taken into account for the data analysis as well as the theoretical description and the interpretation of the observed wavenumber shifts.

In this study, self-heating effects of AlN-based HEMTs on 4H-SiC were investigated at different device operation modes. Since AlN and SiC are transparent with respect to the applied excitation wavelength, the confocal technique was used to set the focus in the backside region of the electrodes (gate, drain, source) while entering the sample from the substrate.

We present room-temperature Raman investigations in order to assess the residual stress and its distribution without electric field. The spectral position of the non-polar E₂(high) Raman mode is discussed in terms of residual stress.

operando micro-Raman measurements were performed varying the drain-source voltage in the off- and on-state condition. The wavenumber shifts of the Raman modes were determined with respect to the phonon frequency of the unbiased state and will be discussed in detail.

The spectroscopic characterization is complemented by electrical measurements, i.e. the output characteristics of the investigated transistors.

This work is financially supported by the Federal Ministry of Education and Research (BMBF) within the grant ForMikro LeitBAN (grant no. 16ES1114).

References:

- [1] M. Meneghini, C. D. Santi, I. Abid, M. Buffolo, M. Cioni, R. A. Khadar, L. Nela, N. Zagni, A. Chini, F. Medjdoub, G. Meneghesso, G. Verzellesi, E. Zhanoni, E. Matioli, *Journal of Applied Physics* **2021**, *120*, 181101.
- [2] K. R. Bagnall, C. E. Dreyer, D. Vanderbilt, E. N. Wang, *Journal of Applied Physics* **2016**, *120*, 155104.
- [3] K. R. Bagnall, E. A. Moore, S. C. Badescu, L. Zhang, E. N. Wang, *Review of Scientific Instruments* **2017**, *88*, 113111.

For your remarks

Violation of selection rules for parity-forbidden optical intracenter transitions in crystalline silicon: substitutional versus interstitial defects

Sergey G. Pavlov,¹ Nikolay V. Abrosimov²

¹ Institute of Optical Sensor Systems, German Aerospace Center (DLR), Rutherfordstr. 2, 12489 Berlin,
 Germany

² Leibniz-Institut für Kristallzüchtung (IKZ), Max-Born-Str. 2, 12489 Berlin, Germany

Email: sergeij.pavlov@dlr.de

Binding energy of excited even-parity states of hydrogen-like impurities in silicon (Si) are of critical importance for understanding of the state coherency and the rates of electronic nonradiative decay. Infrared absorption spectroscopy, the main analytical technique for determination of impurity content in doped semiconductors, returns data on binding energy of odd-parity excited impurity states (p-, f-, h- types) due to dipole-allowed intracenter transitions of electrons bound to the 1s ground state, conventionally observed at low lattice temperatures, while optical transitions into the even-parity excited states (s-, d-, g- types) (Fig. 1) have vanishing strengths due parity selection rules.

Different defects in crystals cause lattice distortion that may violate selection rules and affect the probability of particular intracenter optical transitions of conventional substitutional donors. Perturbations due to large concentration of donors enhance, in principle, all parity- forbidden atomic transitions, which becomes significant, however, only at the densities approaching the Mott transition value, and by this - exhibits too large line' broadening which prohibits spectral resolution of optical transitions at close photon energies.

Substitutional residual carbon in silicon at similar concentrations induces weaker broadening of donor lines at moderate densities and enables resolution of several parity-forbidden intracenter transitions, namely into 1s (Fig. 1), 2s, 3s, 3d₀, 3d_± states using conventional, low- temperature infrared absorption spectroscopy of bulk Si crystals doped by substitutional, hydrogen-like group-V and also by interstitial group-Ia donor centers. The results show unambiguous correlation of the enhancement of detected parity-forbidden transitions with substitutional carbon. In contrast, no such enhancement has been observed due to interstitial oxygen, up to $7 \times 10^{17} \text{ cm}^{-3}$. The best trade-off concentrations of defects providing the largest transition' intensity contrast together with the necessary spectral resolution of impurity lines is $(3-7) \times 10^{15} \text{ cm}^{-3}$ for a dominant donor and $(1-3) \times 10^{16} \text{ cm}^{-3}$ for carbon [1, 2].

The experimental binding energy of excited s-, d- states made corrections to the most of known energies of even-parity excited states, which were derived by other analytical techniques (photoluminescence, Raman spectroscopy) or from absorption spectroscopy of heavily-doped *n*-Si [3]. Several excited even-parity states were resolved for the first time. The derived values for 1s, 2s, 3d₀ states fit well to theoretical predictions on a base of the effective-mass approximation [4] while those for 3d_± states are in a close vicinity to the theory with prolate ellipsoid conduction band valleys [5].

Other lattice defects, such as in polycrystalline Cz-Si and in neutron transmutation doped FZ- Si, also exhibit enhancement of intracenter transitions into the excited s-states, but it is less useful for determination of their binding energies because of inherent, strong line broadening.

References:

- [1] S. G. Pavlov and N. V. Abrosimov, *Materials Science in Semiconductor Processing* **2024**, 172, 108076.
- [2] S. G. Pavlov, N. V. Abrosimov and H.-W. Hübers, *Physical Review B* **2023**, 107, 115205.

- [3] B. Pajot, “Optical absorption of impurities and defects in semiconducting crystals: Hydrogen-like centers” (Springer Series in Solid-State Sciences, volume 158, NY, 2010).
 [4] Yia-Chung Chang, T. C. McGill, and D. L. Smith, *Physical Review B* **1981**, *23*, 4169.
 [5] J. Broeckx, P. Clauws and J. Vennik, *Journal of Physics C: Solid State Physics* **1986**, *19*, 511.

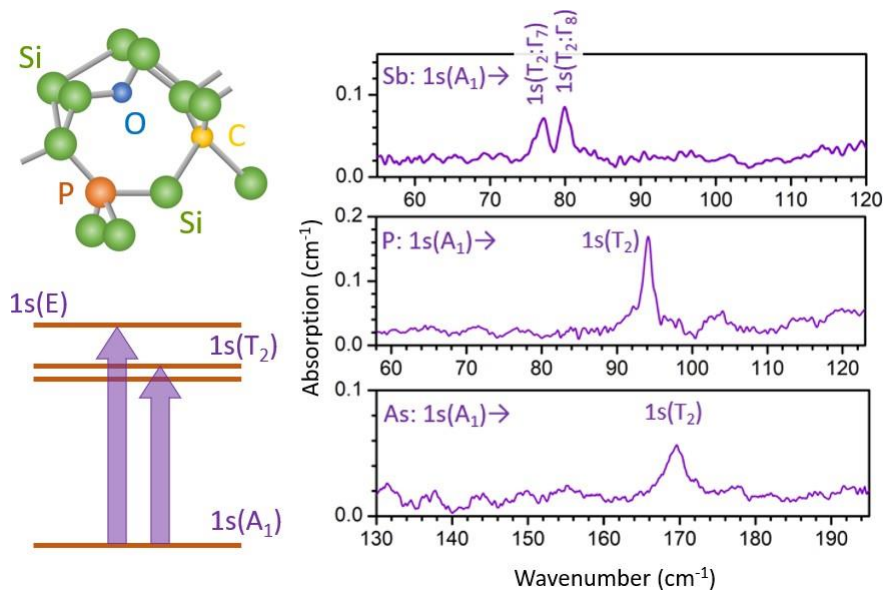


Fig. 1. Parity-forbidden $1s \rightarrow 1s$ intracenter optical transitions (e.g. as schematically shown on the left panel) becomes detectable in the low-temperature infrared absorption spectra (right panel) of moderately doped n -Si with concentrations of substitutional carbon about 10^{16} cm^{-3} .

Thermodynamic study of phase composition of Si oxynitrides obtained at different temperatures

Andrey Sarikov,^{1,2} Mariia Babiichuk,² Maria Voitovych¹ and Vasyl Voitovych³

¹ V. Lashkaryov Institute of Semiconductor Physics, National Academy of Sciences of Ukraine, 41 Nauky Avenue, 03028 Kyiv, Ukraine

² Educational Scientific Institute of High Technologies, Taras Shevchenko National University of Kyiv, 4-g Hlushkova Avenue, 03022 Kyiv, Ukraine

³ Institute of Physics, National Academy of Sciences of Ukraine, 46 Nauky Avenue, 03028 Kyiv, Ukraine

Email: sarikov@isp.kiev.ua

Si rich silicon oxynitride (SiO_xN_y , $0 \leq x \leq 2$, $0 \leq y \leq 4/3$) films are perspective to use in new-generation microelectronic and optoelectronic devices such as for gate oxides with extended scalability in CMOS technology devices, optical waveguide cores, and antireflection and passivation solar cell coatings. Moreover, multilayer $\text{SiO}_2/\text{SiO}_x\text{N}_y$ structures with Si nanocrystals embedded in a dielectric matrix are considered to raise the solar cell efficiency as well as for light emitting device applications. Hence, a detailed understanding of the structure of SiO_xN_y films obtained at different conditions is essential for improving the performance of optical and microelectronic devices based on this material and/or creating new types of such devices with promising characteristics.

This work is devoted to a detailed thermodynamic study of the dependence of phase composition of non-stoichiometric Si oxynitride films on the temperature and SiO_xN_y stoichiometry. A thermodynamic model relating the SiO_xN_y Gibbs free energy to its phase composition and temperature is developed based on the thermodynamic theory of formation of equilibrium states in Si/Si oxide systems proposed by us earlier [1]. Random bonding and random mixture models of the SiO_xN_y film structure were analyzed. In the latter case, coexistence of pure (generally, non-stoichiometric) Si oxide and Si nitride phases or Si oxynitride phases with different stoichiometries were considered. The equilibrium distribution of phases within the SiO_xN_y films corresponded to the minimum values of the film Gibbs free energy. The modeling results were compared to the infrared (IR) spectroscopy data [2], providing the information about the Si oxynitride film structure based on deconvoluting the measured IR spectra into elementary Gaussian profiles corresponding to the Si oxynitride structural units.

It was demonstrated that at low stoichiometry values and temperatures, the Gibbs free energy of Si oxynitride consisting of separated Si oxide and Si nitride phases is lower as compared to that of homogeneous SiO_xN_y phase. Hence, Si oxynitrides tend to form two-phase compositions consistent with the random mixture model description in this case. Increase of the values of the stoichiometry indices and/or the temperature led to the inverse relation between the mentioned Gibbs free energy values meaning the energy favor for the formation of homogeneous films described by the random bonding model. The temperature dependences of the critical stoichiometry indices x and y for the transition between one- and two-phase SiO_xN_y composition were determined.

References:

- [1] A. Sarikov and M. Zacharias, *J. Phys.: Cond. Matter* **2012**, 24, 385403.
- [2] I. P. Lisovskyy, M. V. Voitovych, A. V. Sarikov, S. O. Zlobin, A. N. Lukianov, O. S. Oberemok and O. V. Dubikovsky, *J. Non-Cryst. Solids* **2023**, 617, 122502.

For your remarks

Spectral engineering of photoluminescence from monolayer MoS₂

Brendan F.M. Healy,¹ Sophie L. Pain,¹ James Lloyd-Hughes,² Nicholas E. Grant,¹ and
John D. Murphy¹

¹ School of Engineering, University of Warwick, Coventry, CV4 7AL, UK

² Department of Physics, University of Warwick, Coventry, CV4 7AL, UK

Email: john.d.murphy@warwick.ac.uk

Transition metal dichalcogenides (TMDCs) are an exciting class of two-dimensional (2D) materials that exhibit exceptional physical and chemical behaviour at the monolayer limit. Molybdenum disulfide (MoS₂), a prototypical TMDC, is a leading candidate for inclusion in numerous optoelectronic technologies, owing to its novel optical properties. Monolayer MoS₂ comprises a hexagonal plane of Mo atoms sandwiched between two hexagonally arranged planes of S atoms to yield a S-Mo-S structure with a thickness of ~0.7 nm. With a direct bandgap in the visible spectral range, monolayer MoS₂ emits a relatively strong photoluminescence (PL) signal. The ability to engineer the PL character of MoS₂ is necessary for full realisation of its optoelectronic potential.

We demonstrate systematic control of the intensity, energy, and spectral width of the PL emission from monolayer MoS₂ via simple external treatments. Treating MoS₂ with solutions formed from the superacid bis-(trifluoromethanesulfonyl)amide (TFSA) [1] enhances, blueshifts and sharpens the PL spectrum of monolayer MoS₂ (Fig. 1). Treatments with solutions from structurally analogous chemicals which lack sulphur in the case of bis(trifluoroacetamide) (BTFA) and lack fluorine in the case of methanesulfonamide (MSA) show the same trend, suggesting a two-component mechanism involving the presence of electronegative species and sulphur vacancy passivation. We achieve up to ~100× enhancement of the MoS₂ PL intensity with the peak blueshifted by ~30 meV and the spectral linewidth narrowed by half. On the other hand, direct thermal atomic layer deposition (ALD) of an aluminium oxide (Al₂O₃) or hafnium oxide (HfO₂) film is found to suppress the monolayer MoS₂ PL signal by up to a factor of ~3, redshift by up to ~70 meV, and broadened by ~3×.

We combine single-spot and mapping Raman/PL techniques in a robust characterisation process [2] to link changes in the PL character to charge doping effects. We demonstrate the optical behaviour of atomically thin MoS₂ can be conveniently tuned (Fig. 2) by variation of the electron density via chemical treatment or ALD of a dielectric material.

References:

- [1] S.L. Pain, N.E. Grant, J.D. Murphy, *ACS Nano*, **2022** *16* 1260, doi: 10.1021/acsnano.1c09085.
- [2] B.F.M. Healy, S.L. Pain, J. Lloyd-Hughes, N.E. Grant, J.D. Murphy, *Materials Research Express*, **2024** *11* 015002, doi: 10.1088/2053-1591/ad18ef.

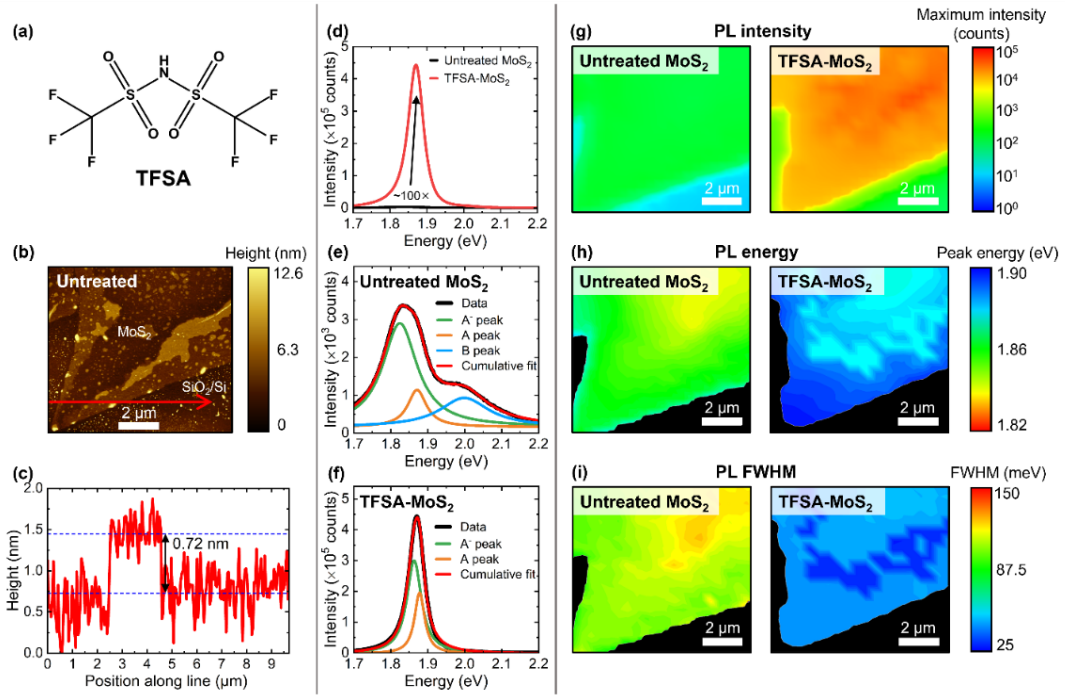


Fig. 1. (a) Schematic chemical structure of TFSA. (b) Topographic AFM image of MoS₂ triangular structure from which PL characterisation was performed. (c) Height profile measured along the red arrow in (b). (d) Raw single-spot PL spectra measured from monolayer MoS₂ before and after submersion in a TFSA-DCM solution for 10 minutes. Multipeak deconvolution of the PL spectrum obtained from monolayer MoS₂ (e) before and (f) after TFSA treatment. The cumulative fit, and contributions of the A', A and B peaks are given in red, green, orange, and blue, respectively. Maps of the (g) maximum absolute PL intensity, (h) energy position of the peak PL intensity, and (i) FWHM of the PL signal emitted from MoS₂ before and after TFSA treatment.

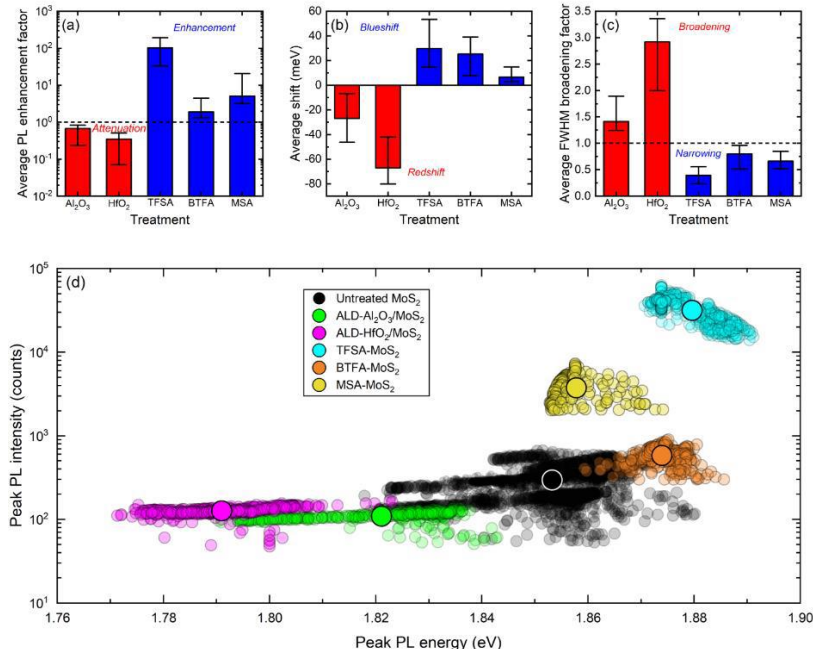


Fig. 2. (a) Comparison of average (a) PL enhancement factors, (b) shifts in energy position and (c) FWHM broadening factors. (d) Peak PL intensity as a function of the corresponding peak PL energy for each applied treatment. The small translucent markers arise from every pixel extracted from each relevant PL map, with the larger solid circles indicating each calculated mean average. The logarithmic scale to account for the large increase in PL intensity following TFSA treatment should be noted in (a) and (d).

Design analysis of group IV light emitters containing SiGe dot-based active medium

Diego Haya Enriquez¹, Moritz Brehm¹, Thomas Fromherz¹

¹ Institute of Semiconductor and Solid State Physics, Altenberger Straße 69, 4040, Linz, Austria

Email: diego.haya_enriquez@jku.at

Microprocessors (MPs) permeate every electronic system and are an integral part of our daily lives. This remarkable technology owes much to the relentless miniaturization of transistors over the years, made feasible by the ubiquitous complementary metal oxide semiconductor (CMOS) technology. However, as lithography approaches atomic scales, Gordon Moore's prophecy appears to reach its limits [1].

Hence, a "More than Moore" approach becomes imperative to enable MPs to operate with minimal delay and low power consumption. One particularly promising route involves hybridizing photonics with microelectronics, offering applications in telecommunication, and data transmission but also optical and quantum computing [2,3]. Nonetheless, challenges persist in achieving a light source that meets all the demands for a photonic integrated circuit. Currently, III-V semiconductor lasers are utilized through heterogeneous and monolithic integration approaches [4]. While these lasers exhibit decent performance, the integration process remains complex. To address these challenges, silicon-based group-IV materials are being considered, and ongoing efforts focus on overcoming hurdles like indirect bandgaps and improving performance [5]. Particularly, quantum dots-based lasers offer advantages over bulk and quantum well lasers [6]. Considering these factors, an active medium based on self-assembled SiGe quantum dot heterostructures, enabled by ultra-low temperature epitaxy [7] emerges as an ideal candidate for integration into Silicon-based lasers [8].

In this paper, we propose a novel distributed feedback laser design using a SiGe dot-based active material, a few nm in width, for which optical gain in the order of 30 cm^{-1} appears to be feasible based on model calculations. Using finite-difference-time-domain and finite elements tools, we provide an overall scheme to optimize the laser characteristics with respect to cavity and grating parameters. We compare our results with the standard coupled-wave theory and conduct theoretical analyses to identify the most significant relations between device characteristics and parameters. Finally, we discuss the potential of our device for use in photonic integrated circuits.

References:

- [1] M.R. Betker, J.S. Fernando and S.P. Whalen, *Bell Labs Technical Journal* **1997**, 2, 29; J. Shaft, *Phil. Trans .R Soc. A.*, **2020**, 378, 20190061
- [2] D. Woods and T.J. Naughton, *Nature Physics*, **2016**, 8, 144
- [3] X. Qiang, X. Zhou and J. Wang et al., *Nature Photonics*, **2018**, 12, 534
- [4] C. Cornet, “*Integrated Lasers on Silicon*” (ISTE press, London, 2016), p. 47.
- [5] X. Wang and J. Liu, *IEEE Journal of semiconductors*, **2018**, 39, 1
- [6] Y. Wan, J. Norman and S. Liu et al., *IEEE Nanotechnology Magazine*, **2021**, 15, 8
- [7] A. Salomon et al., *physica status solidi (a)* **2022**, 219, 2200154
- [8] M. Brehm, “Light-Emission from Ion-Implanted Group-IV Nanostructures” (Springer International Publishing, Cham, 2021), p. 67.

For your remarks

Optoelectronic, Microstructural and Chemical Characterization of 2D PEA₂PbBr₄ Perovskite Thin Films

Lorenzo Calcaterra¹, Andrea Ciavatti¹, Marisa Di Sabatino² and Daniela Cavalcoli¹

¹ Department of Physics and Astronomy, University of Bologna, Viale Berti Pichat 6/2, 40127 Bologna, Italy

² Department of Materials Science and Engineering, Norwegian University of Science and Technology,
 Sem Sælands vei 14, 7491 Trondheim, Norway

Email: lorenzo.calcaterra@studio.unibo.it, daniela.cavalcoli@unibo.it

The remarkable potential of metal halide perovskite semiconductors makes them promising candidates for various applications such as solar cells, LEDs and photo-detectors [1]. However, one critical challenge hindering their widespread commercialization is their limited long-term stability and optoelectronic quality, arising from ion migration, structural defects and degradation upon external stimuli. This work presents a comprehensive investigation into the optical, electrical and structural properties of two-dimensional (2D) PEA₂PbBr₄ perovskite micro-crystalline thin films, which has already demonstrated high stability and sensitivity for photo detectors applications [2].

Starting from the fabrication process, pixelated Cr/Au interdigitated electrode pattern was fabricated on glass substrates using photolithography, followed by evaporation of the metals. The perovskite precursor solutions were deposited by spin-coating in nitrogen-environment glovebox. By changing the spin-coater parameters, as well as the composition of the solutions, we obtained samples with different grain size (Fig. 1), leading to different electrical and structural properties. The measured I-V characteristics indicate that the films with larger grains generate higher photocurrent than the ones with smaller grains, with grain size varying from 5 μm up to 40 μm. From photocurrent spectroscopy, we were also able to extract the exciton binding energy and the energy gap of our samples.

Regarding the microstructural and chemical characterization, we employed two main techniques: Glow Discharge – Optical Emission Spectroscopy (GD-OES) and Scanning Electron Microscopy (SEM). The results of GD-OES analysis indicate that the film was chemically uniform, avoiding compositional mismatch between the surface and the bulk, leading to unwanted and detrimental effects.

SEM investigation gave us detailed information about grain size and grain boundaries, as well as film thickness and morphology.

These findings contribute to unravel the material's electronic properties, its correlation with microstructural and chemical characteristics, and its potential for efficient light conversion. The results obtained pave the way for further advancements in the design and fabrication of perovskite-based devices with improved efficiency and stability, ultimately advancing the field of optoelectronics and renewable energy.

References:

- [1] Zhang, L., Mei, L., Wang, K. et al. Advances in the Application of Perovskite Materials. *Nano-Micro Lett.*, **2023**, 15, 177
- [2] F. Lédée, A. Ciavatti, M. Verdi, L. Basiricò, B. Fraboni, Ultra-Stable and Robust Response to X-Rays in 2D Layered Perovskite Micro-Crystalline Films Directly Deposited on Flexible Substrate. *Adv. Optical Mater.* **2022**, 10, 2101145

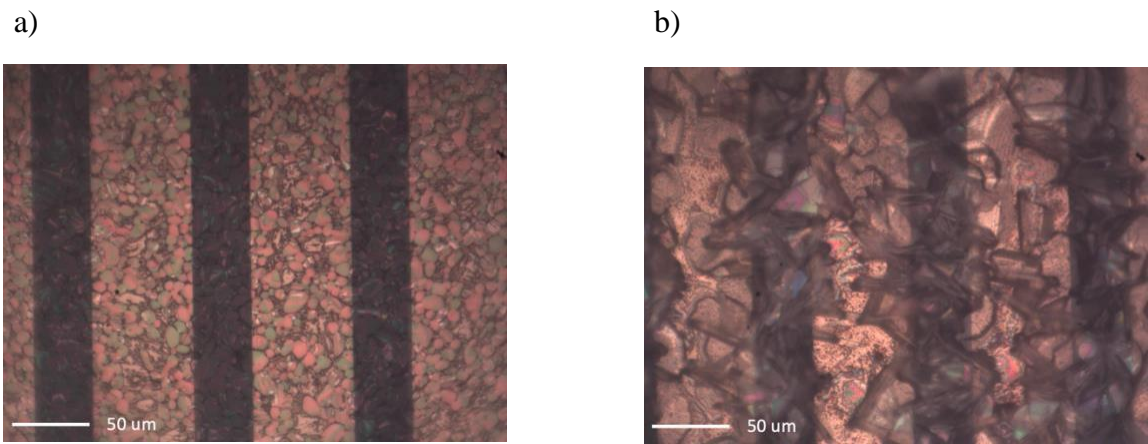


Fig. 1 Optical micrographs of film with different perovskite precursor solution and fabrication parameters, leading

(Si)Ge nanosheets on SOI, grown by Molecular Beam Epitaxy at Ultra Low Temperatures, as a planar platform for RFET devices

E. Prado-Navarrete¹, J. Aberl¹, A. Fuchsberger², L. Wind², D. Nazzari², M. Sistani², Walter M. Weber², L. Vogl³, P. Schweizer³, X. Maeder³, M. Brehm¹

¹ Institute of Semiconductor and Solid-State Physics, Johannes Kepler University, Altenberger Straße 69, 4040, Linz, Austria

² Institute of Solid-State Electronics, Technische Universität Wien, Gußhausstraße 25-25a, Vienna 1040, Austria

³ Swiss Federal Laboratories for Materials Science and Technology, Laboratory for Mechanics of Materials and Nanostructures, Feuerwerkstrasse 39, Thun 3602, Switzerland

Email: moritz.brehm@jku.at

In recent decades, heteroepitaxial layers comprising crystalline stacks of Group-IV alloys, predominantly SiGe, have been employed to enhance the operational efficiency of Si-based devices [1]. However, achieving defect-free pseudomorphic (Si)Ge layers on Si(001) substrates with high Ge compositions ($x \gtrsim 50\%$) poses significant challenges due to strain- induced relaxation beyond a layer thickness of a few monolayers [2].

This study explores molecular beam epitaxy (MBE) growth at ultra-low temperatures (ULT), ranging from 100°C to 350°C, departing from conventional epitaxy temperatures (>500°C). Reduced surface kinetics in ULT conditions leads to notable layer supersaturation, allowing for the growth of thicker pseudomorphic layers than previously achieved [3]. We show that maintaining pristine growth pressures at the lower end of the ultra-high-vacuum range ($\sim 10^{-11}$ mbar) is crucial to minimizing impurities and preserving superior electrical and optical properties of grown heterostructures. This is particularly true during ULT growth, where a limited thermal budget hampers efficient gas desorption from substrates.

Here, we demonstrate that the combination of ULT and excellent growth pressures enables the fabrication of high-quality thin films, exemplified by fully strained, defect-free (Si)Ge epitaxial layers directly grown on Si and silicon-on-insulator (SOI) substrates. These layers exhibit remarkable structural qualities, as confirmed by Atomic Force Microscopy (AFM), X-ray diffraction (XRD) and transmission electron microscopy (TEM) experiments [3]. Furthermore, we show that these nanosheets serve as a scalable platform for advanced SiGe and Ge-based reconfigurable field-effect transistors, capable of dynamic run-time switching between n- and p-type operation, exhibiting outstanding performance [4], [5]. For these devices, high-resolution TEM reveals sharp and reproducible interfaces with single-element crystalline Al contacts formed through a thermally induced Al-Si_{1-x}Ge_x exchange reaction [6]. The precisely chosen (Si)Ge channel stoichiometry and abrupt interfaces contribute to exceptional symmetric I-V operability in RFET devices, as observed in their transfer characteristics [4], [5].

References:

- [1] I. A. Fischer *et al.*, *APL Photonics*, **2022**, vol. 7, no. 5, p. 050901.
- [2] M. Brehm and M. Grydlik, *Nanotechnology*, **2017**, vol. 28, no. 39, p. 392001.
- [3] A. Salomon *et al.*, *Phys. status solidi*, **2022**, vol. 219, no. 17, p. 2200154.
- [4] A. Fuchsberger *et al.*, *Adv. Electron. Mater.*, **2023**, vol. 9, no. 6, p. 2201259.
- [5] A. Fuchsberger *et al.*, *IEEE J. Electron Devices Soc.*, **2024**, vol. 18, no. 9, pp. 83–87.
- [6] L. Wind *et al.*, *Small*, **2022**, vol. 18, no. 44, p. 2204178.

For your remarks

Morphology and refractive index dependence on laser parameters in subsurface ultrashort pulsed laser processing of ZnS

E. Einmo¹, N. Tolstik^{2,3}, C. Grivas², M. Demesh², P. Kontis¹, I. T. Sorokina^{2,3} and M. Di Sabatino¹

¹Department of Materials Science and Engineering, Norwegian University of Science and Technology (NTNU), Sem Sælands vei 12, 7034, Trondheim, Norway

²Department of Physics, NTNU, Høgskoleringen 5, 7034, Trondheim, Norway

³ATLA lasers AS, Richard Birkelands vei 2B, 7034, Trondheim, Norway

Email: eskil.j.n.eimmo@ntnu.no

Subsurface ultrashort pulsed laser processing of dielectrics and semiconductors is a promising technique in various materials, including materials for energy applications, laser technology, photonics, optical sensing, in-chip micro structuring, microfluidics and optical storage [1]. Precise confinement of highly intense pulses allows fine 3D-micro-modification of materials, changing their molecular structure and optical properties in a controllable fashion. Earlier works have primarily been concentrated on amorphous materials and few on crystalline materials such as ZnS [2] and Cr:ZnS [3, 4], which belong to the class of semiconductors. This study presents a laser parameter control investigation for tailoring the refractive index to achieve reproducible 3D waveguide structures in the bulk of ZnS crystals with the highest induced refractive index change $|\Delta n|$ up to $(3.88 \pm 0.18) \cdot 10^{-2}$. The study also provides an insight into the morphology of such localized 3D structures.

Subsurface modifications were induced using a $2.09\text{ }\mu\text{m}$ laser, with picosecond pulse duration, by scanning the sample perpendicular to the beam. With a repetition rate of 20 kHz and writing speeds ranging from 4 to 20 mm/s , dotted lines were written in the bulk of the crystal with a spatial pulse separation, Δ , between 0.2 and $1.0\text{ }\mu\text{m}$ (Fig. 1). To determine the optimal depth range, all writing parameters were studied at four different processing depths, ranging between ~ 935 and $1020\text{ }\mu\text{m}$, using five different average laser powers P .

The dependences of the cross-sectional axial length on Δ , P , and depth are shown in Fig. 2. At shallow depths, the evolution of the structure length in the axial direction is persistent for average powers between 10 and 50 mW . However, at greater depths, the focal volume exhibits severe elongation for smaller Δ , suggesting spatial overlapping of pulses. The distorted length at greater depths observed in Fig. 2b originates from a decreased energy density deposited in the focal volume as the beam propagates through the crystal. Correlative refractive index contrasts $|\Delta n|$ of $\sim 10^{-2}$ were measured with Quantitative Phase Microscopy (QPM) and are shown in Fig. 3. At larger spatial pulse separations Δ , $|\Delta n|$ starts to saturate to a peak value at P above 30 mW . However, at smaller Δ , where the degree of overlap between successive pulses is smaller, the peak in $|\Delta n|$ appears at lower P . Unlike the morphology, the depth does not seem to affect the behaviour of $|\Delta n|$ as it remains consistent. The analysis shows no clear correlation between the refractive index contrast and the axial morphology of the cross-section, although both are affected by the laser writing speed.

In conclusion, we observe that the defect morphology is significantly affected by the writing speed and depth. However, only the writing speed severely limits $|\Delta n|$ and is adaptable for inducing maximum change at lower average power. Optimizing the two paves the way for morphology control, enhanced localization and larger $|\Delta n|$ values.

References:

- [1] A. Tien, et al., *Physical Review Letters* **1999**, 82.19, 3883-3886.
- [2] Q. An, Y. Ren, Y. Jia, J.R.V. Aldana, F. Chen, *Optical Materials Express* **2013**, 3.4, 466-471.
- [3] E. Sorokin, et al., *Optical Materials Express* **2022**, 12.2, 414-420.
- [4] J.R. Macdonald, et al., *Optics Express* **2014**, 22.6, 7052-7057.

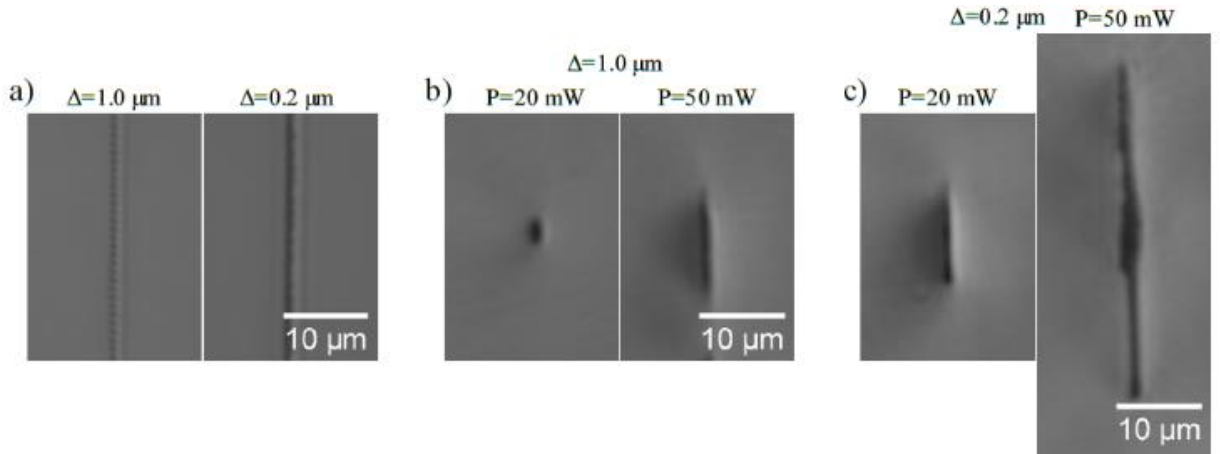


Fig. 1. Optical micrographs of laser modified regions in the crystal. Visualizing top view of pulse separation $\Delta=1.0\text{ }\mu\text{m}$ and $\Delta=0.2\text{ }\mu\text{m}$ induced with average power 20 mW at 995 μm depth a). Cross-sectional view of structures written with average powers of 20 mW and 50 mW at 1020 μm depth shown in b) and c) with $\Delta=1.0\text{ }\mu\text{m}$ and $\Delta=0.2\text{ }\mu\text{m}$, respectively.

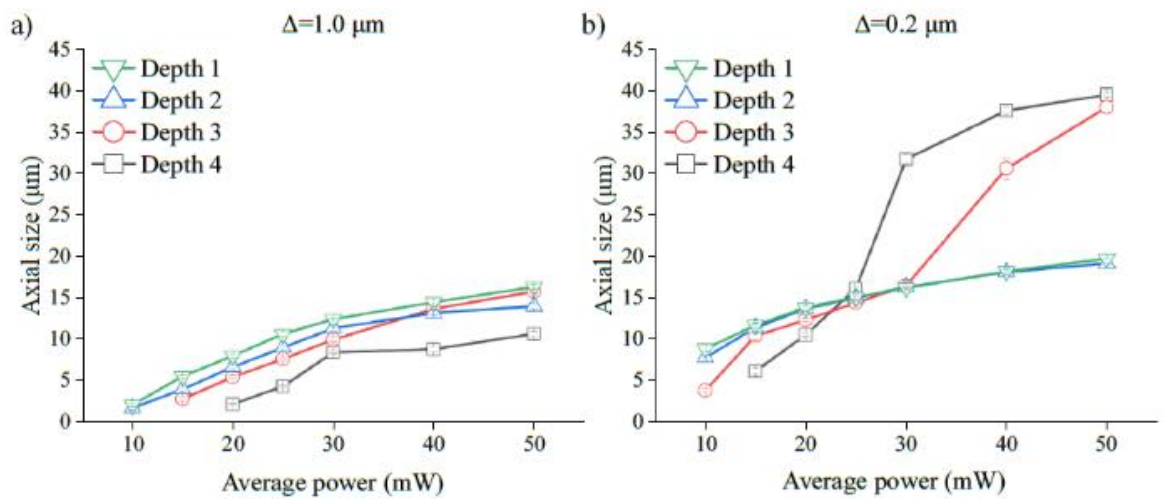


Fig. 2. Cross-sectional measurements of axial size as a function of average writing power in four different depths 1, 2, 3 and 4 as 935, 968, 995 and 1020 μm , respectively. Evolutions are presented for separation of successive pulses of $\Delta=1.0\text{ }\mu\text{m}$ a), and $\Delta=0.2\text{ }\mu\text{m}$ b).

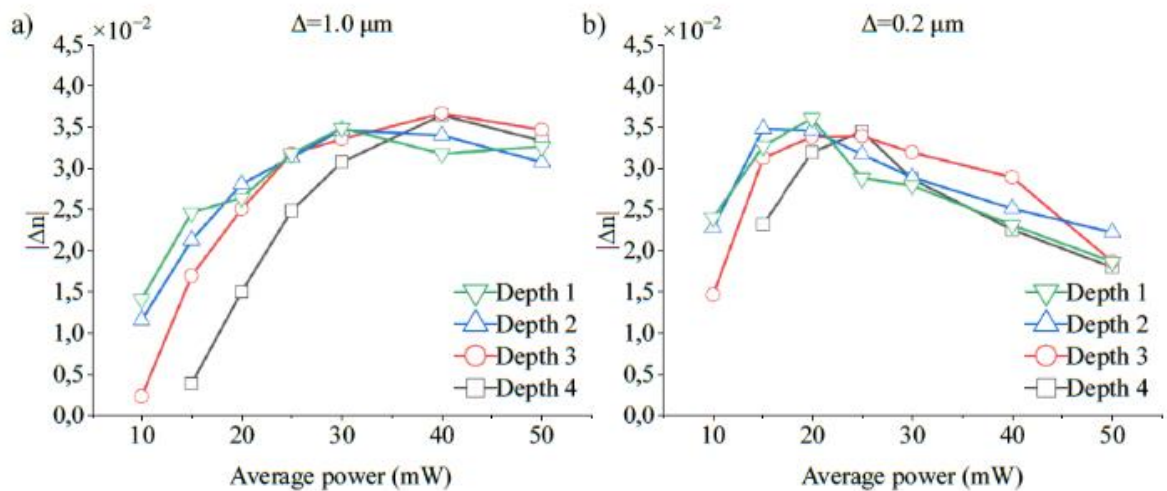


Fig. 3. Refractive index change $|\Delta n|$ measured by QPM presented for direct comparison with Fig. 2.

Ion flux distribution in ion beam assisted silicon molecular beam epitaxy

R. Ashurov,¹ T. Turdaliev¹, M. Oehme², K. Lyutovich², Kh. Ashurov¹ and E. Kasper²

¹ Institute of Ion Plasma and Laser Technologies, Do'rmon yo'li 33, 100125, Tashkent, Uzbekistan

² University of Stuttgart, Institute of Semiconductor Engineering, Pfaffenwaldring 47, 70569 Stuttgart, Germany

Email: ashurov@iplt.uz

This study explores the influence of ion-induced antimony (Sb) incorporation during the epitaxial growth of silicon (Si) layers using a molecular beam epitaxy (MBE) system. While MBE traditionally employs an electron gun evaporator as a source of Si beams [1], we demonstrate its capability to also generate Si ions. Ions can play a significant role in surface related growth effects [2], like dopant segregation, point defect generation [3], dislocation annihilation, self-ordering and surface corrugation. A Si-molecular beam (MBE) equipment was slightly modified in order to allow for ion beam assisted MBE(IBAMBE) (fig.1). The system features an off-axis electron gun evaporator and a movable measuring head for quantifying the ion flux. The key finding is that applying a negative substrate voltage during growth considerably concentrates the Si ion flux onto the wafer surface, resulting in a substantial increase in Sb incorporation. This simple modification allows the manipulation of generated ions, enabling their interaction with the growing film.

The paper also addresses the complexities associated with non-uniform thickness and doping observed on non-rotated substrates. To address this challenge, we proposed a method for two-dimensional mapping of the sheet resistance employing a four-point probe technique. The 2D distribution at the substrate surface is electrically measured by the n- doping from a Sb pre built up. This method delivers relative values with the incorporation cross section as scaling factor. The second method monitors ion currents directly by a linearly moving ion probe. Both methods confirm an inhomogeneous current distribution with peak current densities of 350nA/cm² due to the off-axis electron gun position. Typical measurements of ion current density across the substrate are given in Fig.2.

The results demonstrate a clear correlation between the distribution of the ion flux and the electrical properties of the grown layers. This finding strongly suggests the effectiveness of this method for achieving controlled n-type doping of silicon.

Furthermore, the paper delves into the limitations of the employed method. We acknowledge the presence of a "noisy area" (fig.3) in the specific conductivity measurements, limiting the accuracy for specific conductivities below a certain threshold. Additionally, the simple equation used to relate sheet resistance and thickness is acknowledged to be valid only under specific conditions, namely when the depletion layer at the epi/substrate interface does not significantly influence the n-carriers. The paper concludes by suggesting further investigation into these limitations for a more comprehensive understanding of the method's applicability.

References:

- [1] K. Lyutovich, et al., Mat. Sci. Eng. B71 (2000)14–19
- [2] E. Wendler, et al., Phys. Status Solidi B 253 209 (2016)9–2109
- [3] M. Oehme and E. Kasper, MBE Growth Techniques, In: Silicon Heterostructure Handbook: Materials, Fabrication, Devices, Circuits, and Applications of SiGe and Si Strained-Layer Epitaxy (ed. J. D. Cressler) CRC Press, USA (2006) 85-94

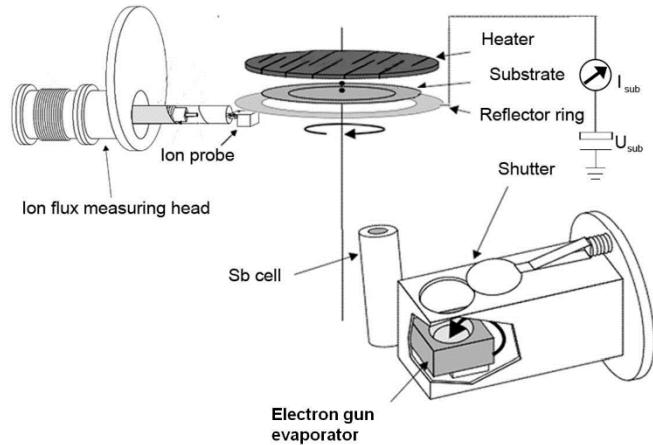


Fig. 1. MBE arrangement with insulated substrate holder and movable ion flux monitor.

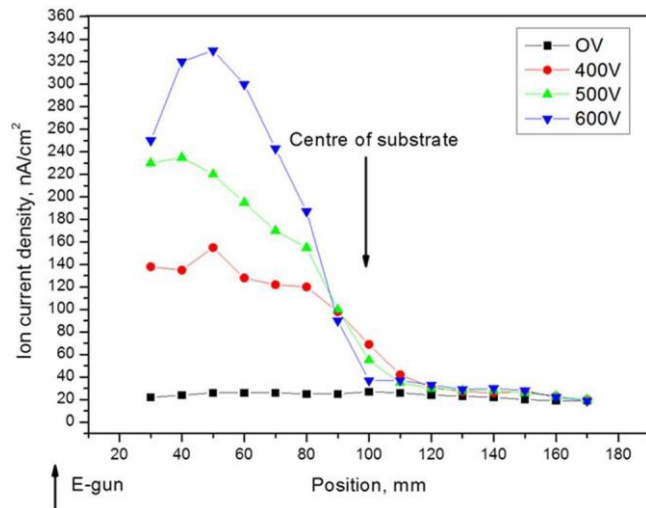


Fig. 2. Ion current density across the substrate

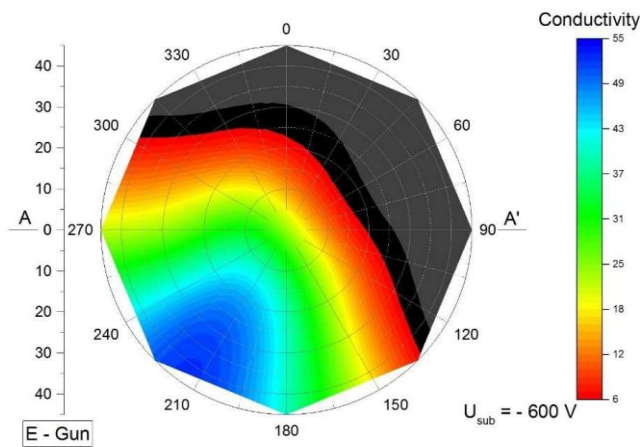


Fig. 3. Specific conductivity map of the epitaxy layer grown with 600 substrate voltage. Area with low specific conductivity (low ion flux density) is marked as noisy

Centers of bismuth and phosphorus in silicon for devices of quantum communications in space: open volume point defects

Nikolay Arutyunov^{1, 2}, Nikolay Abrosimov², Reinhard Krause-Rehberg¹ and Mohamed Elsayed¹

¹Department of Physics, Martin Luther University Halle, 06120, Halle, Germany

²Leibniz-Institut für Kristallzüchtung (IKZ), Max-Born-St.-2, D-12489, Berlin, Germany

Email: n_arutyunov@yahoo.com

Demanding approaches for bringing into correlation the parameters of radiation tolerance of devices on the orbital silicon platforms with data of accumulation of the open volume defects will be touched upon. The positron annihilation lifetime spectroscopy (PALS) applied to probe the open volume defects has revealed the least radiation tolerance of silicon among other commercial semiconductor components of devices [1]. Having acquired open volume as a result of interaction with the primary radiation defects, the atoms of dopant change or lose their electrical activity, thus causing irreversible decrease of high-fidelity general global quantum communications network [1,2]. Some components of devices fail before ~ 1 krad of accumulated dose, and the parameters of failure cannot be determined a priori [3]. We applied the low-temperature PALS in order to gain deeper insight into microstructure of open volume defects related to both the centers of bismuth, ^{209}Bi ($J = 9/2$), and phosphorus, ^{31}P ($J = 1/2$), in n-type float-zone (FZ) silicon.

We are to report for the first time that non-local interaction of ^{209}Bi ($J = 9/2$) and ^{29}Si ($J = 1/2$) nuclear spins *delays* essentially local event of emission of two annihilation gamma– quanta out of Bi center. Hyperfine and superhyperfine interaction of donor spin system with surrounding ^{29}Si nuclear spins *inhibit* two-quantum annihilation of positron in the $^{\text{nat}}\text{Si}:\text{Bi}$, in contrast to isotopically-enriched ^{28}Si material (so-called “semiconductor vacuum”) where Bi center and ^{29}Si atoms are separated by a long distance: see Fig.1 and Fig.2(a).

The configuration of open volume point defects involving Bi- and P-donor atoms (i.e. complexes [$V_{\text{op}} - \text{Bi}$] and [$V_{\text{op}} - \text{P}$]) are discussed in the light of their both radiation tolerance [1,3] and challenging issues of identification of Group-V–impurity–vacancy complexes in silicon subjected to proton irradiation [4,5,6]: see Fig. 2(b; c). Suggestive of being deep donors, the defects may exhibit properties of *negative-U* centers [7]. The [$V_{\text{op}} - \text{Bi}$] defect is decomposed during isochronal annealing in the temperature range $\Delta T_{\text{ann.}} \sim 370$ to 470 °C (the activation energy $E_a \approx 0.9 \pm 0.08$ eV); this range is ~ 300 to ~ 650 °C ($E_a \sim$

0.67 eV) for the [$V_{\text{op}} - \text{P}$] complex. These *thermally stable* open volume point defects appear to *dominate* in the Si:Bi and Si:P components of devices functioning on the low Earth orbit satellite, where the most damaging factor is the irradiation by protons [1,3].

This dominance is surprising as in the literature a major role in forming the open volume point radiation defects is usually attributed to deep acceptor centers, such as A–, E-center, di-vacancy, i. e. those that are *relatively thermally unstable* and are annealed in the temperature interval $\Delta T_{\text{ann.}} \sim 60$ to ~ 300 °C. Thus, information obtained for [$V_{\text{op}} - \text{Bi}$] and [$V_{\text{op}} - \text{P}$] complexes necessitates to reconsider a whole conception of formation of the open volume point defects that is generally accepted in the literature for the n-type FZ silicon.

References:

- [1] J. Logan, K. Woller, P. Webster, C. Morath and M. Short, *J. Appl. Phys.* **2023**, 134, 225701.
- [2] B. Wilson, A. Miloshevski, D. Hooper and N. Peters, *Phys. Rev. Appl.* **2021**, 16, 064049.
- [3] J. Logan, M. Short, P. Webster and C. Morath, *IEEE Transactions on Nuclear Science* **2020**, 67, 2382.
- [4] N. Arutyunov, et al., *J. Phys. Condens. Matter* **2021**, 33, 245702.
- [5] N. Arutyunov, M. Elsayed, R. Krause-Rehberg et. al., *J. Phys. Condens. Matter* **2013**, 25, 035801.
- [6] H. Höhler N. Atodiresei, K. Schroeder, R. Zeller and P. Dederichs, *Phys. Rev.* **2005**, B71, 035212.
- [7] J. Coutinho, V. Markevich and T. Peaker, *J. Phys. Condens. Matter* **2020**, 32, 323001.

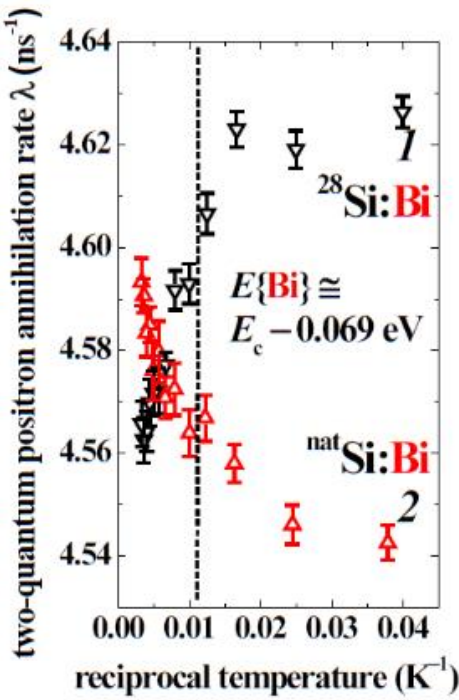


Fig.1. Observed for the first time the splitting of the positron annihilation rate λ (T) indicates hyperfine interaction of Bi impurity center electron spins with surrounding ^{29}Si ($J = 1/2$) nuclei in FZ silicon (cf. the temperature dependencies 1 and 2): 1 - isotopically enriched ^{28}Si ($J = 0$) single crystal doped with ^{29}Bi ($J = 9/2$) impurity atoms; 2 - $^{\text{nat}}\text{Si}$: Bi single crystal having natural isotope composition. The ^{28}Si : Bi material is characterized by *extremely low* concentration of magnetic isotope: $[^{29}\text{Si}]$ is equal to ≈ 50 ppm. The formation of triplet electron-positron states, whose two-quantum decay is forbidden, is argued to delay emitting two-quantum annihilation radiation out of Bi donor center in $^{\text{nat}}\text{Si}$: Bi material. The dashed line separates occupied ground donor states $E\{\text{Bi}\} \approx E_c - 0.69$ eV and excited states, D^* ($80 < T \leq 25$ K). The measured excited state radius of Bi^* equal to ~ 13 to 16 Å in Si: Bi (Li et al., Phys. Rev. B 2019, 90, 085423) is close to size ~ 9 Å of the structural fragment with Bi atom: see Fig.2 (a).

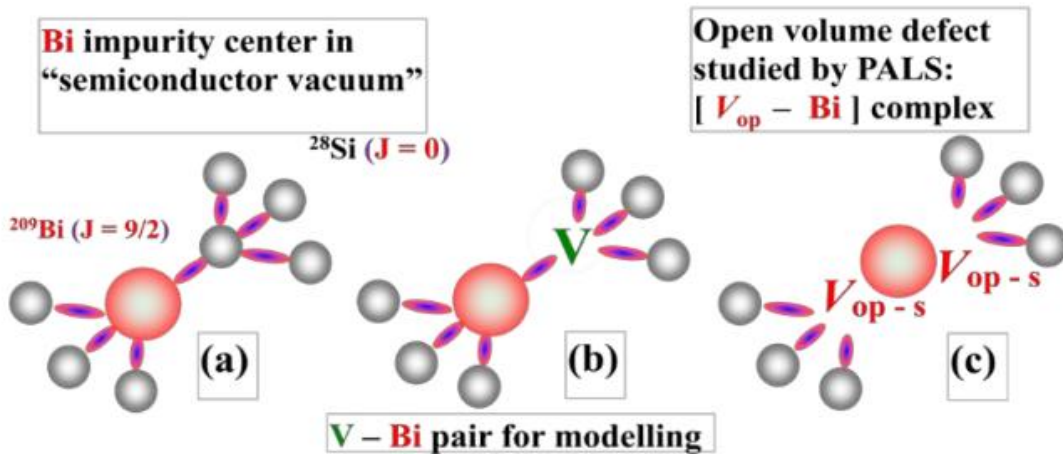


Fig.2. The configurations of Bi ($J = 9/2$) impurity center in the crystal lattice of “semiconductor vacuum”: the enrichment factor for ^{28}Si isotope is 0.99995.

The Si-Bi bonds are presented symbolically; the distortions are not shown.

(a) – Bi donor center in crystal lattice of ^{28}Si ($J = 0$) atoms. Concentration of [Bi] donor centers is equal to $\approx (0.7$ to $2) \times 10^{16}$ cm $^{-3}$; the hyperfine interaction of Bi and ^{29}Si nuclei is *drastically suppressed*. On the contrary, Bi ($J = 9/2$) center and ^{29}Si ($J=1/2$) atoms in Bi 1st and further coordination spheres are in hyperfine and superhyperfine interaction which results in a delay of emission of two-quantum annihilation radiation: cf. data (1) and (2) in Fig.1.

(b) – Oversized Bi atom is tied to a *simulated vacancy* (V); this *unstable modeled* {V – Bi} pair is used to find its stable configuration by *ab initio* calculations [6]. The *real* open volume V_{op} is detected by PALS in $[V_{\text{op}} - \text{P}]$ and $[V_{\text{op}} - \text{Bi}]$ complexes in $^{\text{nat}}\text{Si}$ [4,5]: it is argued that Bi atom shifts *inward towards* V_{op} , see below (c). It is these complexes that may dominate in the degradation of materials of devices of the silicon platform of Earth orbit satellites [1, 2, 3].

(c) – Bi atom *splits* the open volume V_{op} of *thermally stable* $[V_{\text{op}} - \text{Bi}]$ complex. Activation energy of its decomposition estimated by PALS data is $E_a \approx \sim 1 - 0.9$ eV; for $[V_{\text{op}} - \text{P}]$ defects E_a is 0.59 to 0.74 eV. These values are very close to the ones obtained by comprehensive cluster calculations [6]: the split-vacancy configuration was found to be preferable with both the energy gain of ~ 0.7 – 0.9 eV and *considerable relaxation* of the nearest neighbours of Bi impurity atom in {V – Bi} pair. This conclusion turns out to be less justifiable for P impurity atom under comparing the data of calculations with the results obtained by PALS for the $[V_{\text{op}} - \text{P}]$ complex.

Theory of hydrogen reactions in solar silicon and connections with LeTID

J. Coutinho,^{1,*} D. Gomes,¹ V. J. B. Torres,¹
 T. O. Abdul Fattah,² V. P. Markevich² and A. R. Peaker²

¹ i3N & Department of Physics, University of Aveiro, 3810-193 Aveiro, Portugal

² Photon Science Institute and Department of Electrical and Electronic Engineering, The University of Manchester, Manchester M13 9PL, United Kingdom

Email: jose.coutinho@ua.pt

We present a theoretical account of some of the most likely hydrogen-related reactions with impurities present in n-type and p-type solar-grade silicon. Reactions between H, dopants and carbon are addressed and analysed in the context of life-time degradation of silicon solar cells, most notably of light and elevated temperature degradation (LeTID) of lifetime. Among the problems investigated, we highlight a comparative study of acceptor-enhanced dissociation of hydrogen molecules in B- and Ga-doped material, their subsequent reaction steps toward formation of acceptor-hydrogen pairs, or the critical difference between the electronic activity of boron-dihydride (BH_2) and gallium-dihydride (GaH_2) complexes. We note that while the former complex has been linked to the root cause of LeTID in B-doped Si [1], the calculations show that GaH_2 is a shallow donor, and therefore unlikely to be involved in non-radiative recombination activity. Experimental evidence of this difference from junction spectroscopy techniques has also been found [2], and to some extent it may explain the apparently higher stability of Ga-based cells to long-term sunlight exposure.

Hydrogen interactions with impurities in n-type Si is currently of interest within the solar community. In part, this explains the current trend of the Si-PV industry in moving away from materials that are sensitive to boron-oxygen light induced degradation or LeTID. However, we are aware of several H-related and light-sensitive reactions in n-Si, and understanding them is crucial for tracking hydrogen relocation within the Si during cell operation. We investigated reactions involving H, P and C in Si, as well as effects from minority carrier capture by PH and CH pairs in n-type Si. Unlike previously thought, we find that light-/carrier-induced dissociation of PH pairs cannot be explained by a transformative model, where H switches between inequivalent sites next to P upon capture of minority and majority carriers. Instead, our results suggest a dissociative mechanism, driven by entropy, and triggered by a metastable hole trap accessible to the ground state via wagging vibrations of the Si-H unit of the PH pair. This result has a fundamental importance. It shows that static first-principles calculations predict that PH is electrically inert and unable to capture holes. On the other hand, hole capture can be explained when the picture includes electron-phonon coupling involving defect states resonant within the crystalline band edges [3]. We finally report on the mechanism behind the observed photo-/carrier-induced dissociation of CH pairs in n-type Si, reactions involving direct interactions between molecules with P and C, and the assignment of several electron and hole traps with respective atomistic and electronic models.

References:

- [1] J. Coutinho, D. Gomes, V. J. B. Torres, T. O. Abdul Fattah, V. P. Markevich, A. R. Peaker, *Physical Review B* **2023**, 108, 014111.
- [2] T. O. Abdul Fattah, V.. P. Markevich, D. Gomes, J. Coutinho, N. V. Abrosimov, I. D. Hawkins, M. P. Halsall, A. R. Peaker, *Solar Energy Materials & Solar Cells* **2023**, 259 112447.
- [3] J. Coutinho, D. Gomes, V. J. B. Torres, T. O. Abdul Fattah, V. P. Markevich, A. R. Peaker, *Solar RRL* **2024**, 8, 2300639.

Properties of hydrogen species in n-type silicon deduced from in-diffusion profiles

V. V. Voronkov¹ and R. Falster²

Global Wafers via Nazionale 59, 39012 Merano Italy Email:

Email: vvoronkov@gw-semi.com

Contrary to a complicated behaviour of hydrogen found in p-Si, the situation in n-Si appears to be simpler. The hydrogen (deuterium) depth profiles reported after an exposure to plasma (and also after subsequent annealing in a neutral ambient) of moderately doped samples are dominated by mobile hydrogen dimers (H_{2A}). The dimers are produced by two independent reactions of in-diffusing monoatomic hydrogen species:

- 1) bulk production presumably by a reaction $H^0 + H^- \rightarrow H_{2A} + e^-$ (emitting an electron),
- 2) near-surface production (in a sub-micron range) by still not specified reaction, probably related to the presence of a damaged near-surface layer.

By the depth profiles, one can deduce the dimeric diffusivity D_{2A} ; the temperature dependence is of a well pronounced Arrhenius type with the activation energy of 0.8 eV. By the rate of bulk production of H_{2A} , two important parameters of monoatomic species can be deduced: a) the diffusivity D^- of negative hydrogen ions, b) the characteristic electron concentration n^* marking the equal values of the diffusivity-concentration products for H^- and H^0 . The hydrogen transport is dominated by H^0 at $n \ll n^*$ and by H^- at $n \gg n^*$.

Representative values, at 150°C, are $D^- = 1.3 \times 10^{-11} \text{ cm}^2/\text{s}$ and $n^* = 10^{16} \text{ cm}^{-3}$.

For heavily doped samples, production of H_{2A} is negligible, and the depth profiles is due to the neutral hydrogen-donor pairs HD (passivated donors). The shape is controlled by the parameter $D^- K$ - the product of D^- and the equilibrium dissociation constant K of the HD pairs. The deduced $D^- K$ parameter is almost the same for the P and As dopants (about $1.5 \times 10^{15} \text{ cm}^{-1}\text{s}^{-1}$ at 150°C). Accordingly, the dissociation constant K for HD pairs is essentially larger than that for HB pair corresponding to a well smaller binding energy for the HD pairs.

For your remarks

On-stage solar cell degradation process: DLTS and LT-PL-EL study

Teimuraz Mchedlidze, Katharina Klose, August Weber, Matthias Müller,
 and Johannes Heitmann

Institute for Applied Physics, Technical University Bergakademie Freiberg, Freiberg 09599, Germany

Email: teimuraz.mtchedlidze@physik.tu-freiberg.de

The light and temperature-induced degradation (LeTID) of Si-based photovoltaic cells remains one of their common stability issues [1]. The degradation process and affecting factors are still widely discussed [2]. The reported influence of different impurities, dopants, and extended defects in combination with variation of degradation conditions complicates the study. Well-established methods like low temperature photoluminescence (LT-PL) [3] and deep-level transient spectroscopy (DLTS) [4] were used for the study among others. Comparison of the fabricated cells in initial (I), degraded (D) and regenerated (R) states by these methods is effective if used for the same location of the cell. Moreover, since the methods require a variation of measurement temperature only a small part of a cell (with an area \sim of 1-2 mm²) can be used. Thus, we studied mesa-diodes fabricated from the initial cells. The D and R processes can be done without moving the sample from the holder, inside the experimental setup using the current-induced degradation (CID) for generation of LeTID defects [5].

To explore the possibilities of the method we used initially M2-size PV cells fabricated in industrial-like PERC technology from B-doped Cz-Si crystal which showed a relatively strong LeTID effect. An image of the mounted mesa-diode samples is shown in Fig.1. The DLTS spectra detected from a mesa diode in I, D, and R stages are shown in Fig.2. The differences in the spectra detected from various locations of the single solar cell in the I stage indicated on the lateral variation of defect structure for the cell. Using possibilities of the DLTS setup based on the MFIA impedance analyzer [6] it was possible to detect DLTS signals from extended defects at $\Delta C/C = (0.2-1) \times 10^{-4}$ level with high signal/noise ratio. Changes of the DLTS spectra during CID at I, D, and R stages can be attributed to interaction of hydrogen with the extended defects. Significant changes were detected also for the LT-PL-EL spectra in the 1-1.15 eV photon energy range. The LT-EL spectra for the I, D, and R stages are presented in Fig.3.

We will present characteristic signatures of traps for the three stages (I, D, and R) obtained from the DLTS measurements, development of low temperature (10 K) PL and EL spectra for the photon energy range 1-1.15 eV for the I→D→R sequence. We will discuss the advantages and possibilities of the proposed method for the study of degradation processes in solar cells.

References:

- [1] For the latest review: Z.Y. Yeo, et.al., *Renewable and Sustainable Energy Reviews* **2022**, 159, 112223.
- [2] D. Chen, et al., *Progress in Photovoltaics* **2021**, 29, 1180.
- [3] T. Mehl, et al., *AIP Conf. Proc.* **2022**, 2487, 030007.
- [4] T.O. Abdul Fattah, et.al., *Solar En. Mat. Solar Cells* **2023**, 259, 112447.
- [5] S. Liu, et al., *AIP Conf. Proc.* **2018**, 1999, 130014.
- [6] T. Mchedlidze, *Pros for using MFIA in deep level transient spectroscopy studies*, **2024**, DOI: 10.13140/RG.2.2.19774.25920.

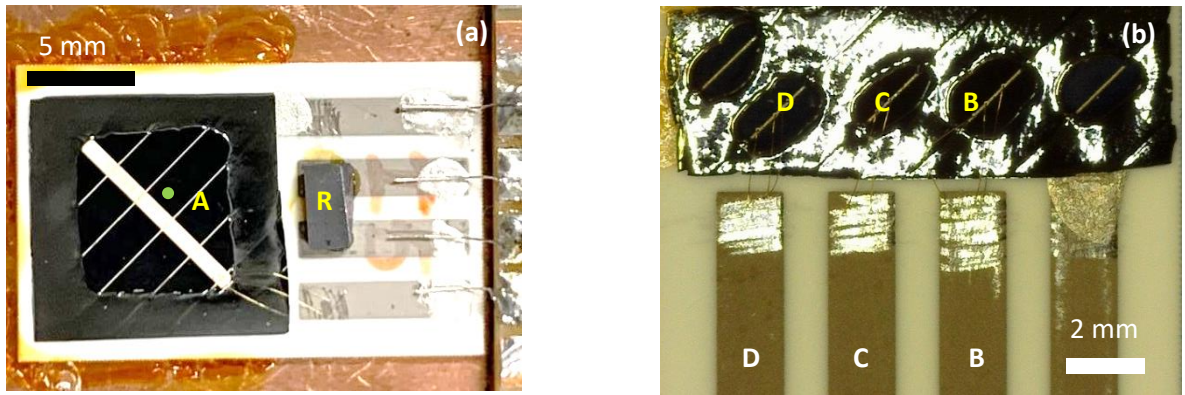


Fig. 1. Samples for on-stage LeTID studies using LT-EL-PL (a) and DLTS (b) methods. Mesa diode cathodes A(a) and B, C, D (b) are bonded to the electric contacts with thin Au wire, anode (back contact of the cell) is contacted using Ag-containing glue. Green spot in (a) indicates focus point of the PL-EL system. PL reference sample R (a) is low B-doped FZ-Si.

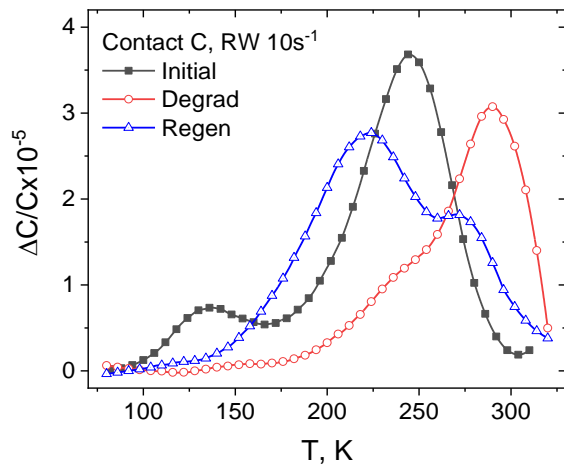


Fig. 2 DLTS spectra detected from the mesa diode C shown in Fig.1(b) in initial, degraded and regenerated stages. Rate window 10 Hz, $t_p = 1$ ms, SR= 54 kHz.

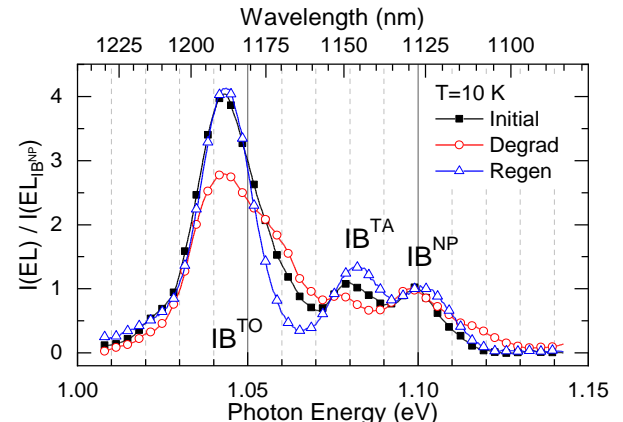


Fig. 3 EL spectra under forward bias of 0.9 V detected from the same location of the mesa-diode A, shown in Fig.1. Intensities of the spectra were normalized on the intensity of IB^{NP} peak.

Recombination Activity of Crystal Defects in Epitaxially Grown Silicon Wafers for Highly-Efficient Solar Cells

Clara Rittmann¹, Ella S. Supik¹, Marion Drießen¹, Friedemann D. Heinz^{1,2}, Florian Schindler¹, Charlotte Weiss¹, Martin C. Schubert¹ and Stefan Janz¹

¹ Fraunhofer Institute for Solar Energy Systems (ISE), Heidenhofstraße 2, 79110 Freiburg, Germany

² Department of Sustainable System Engineering (INATECH), University of Freiburg,
 Emmy-Noether-Straße 2, 79110 Freiburg, Germany

Email: clara.rittmann@ise.fraunhofer.de

Photovoltaic technologies based on silicon wafers (Si) produced by conventional ingot crystallization have mainly been optimized in terms of production cost and energy conversion efficiency until now [1, 2]. To additionally lower the carbon footprint of the wafers significantly, Si EpiWafers are grown epitaxially on reusable, highly-doped Si substrates with porous layers (PorSi) for detachment [3, 4]. We investigate the electrical and crystallographic properties of *p*-type Si EpiWafers and quantify quality limitations induced by the PorSi through a direct comparison to reference wafers EpiRef_p+ being epitaxially grown on polished, highly-doped Si substrates without PorSi [5-7]. Furthermore, we explore limitations induced by the high doping of the substrate by a comparison to EpiRef_p being grown on the same, but less doped substrate as EpiRef_p+. We assess the electrical material quality with spatially resolved, lifetime calibrated photoluminescence (PL) imaging as shown in Fig. 1, allowing for predictions of solar cell efficiencies [8-10].

Table 1 summarizes the mean minority carrier lifetimes of up to 1 ms and the predicted solar cell efficiencies of up to 24.8 % and demonstrates a correlation to the number of structural defects, namely stacking faults and dislocations. We further investigate the impact of isolated structural defects on the local electrical quality based on highly resolved μPL-mappings [11]. We figure that even isolated dislocations reduce the lifetime locally. Stacking faults are more recombination active when exhibiting a higher number of dislocations within, which depends in turn on the substrate type: Fig. 2 demonstrates that the high doping leads to topologically elevated stacking faults with more dislocations on EpiRef_p+ and that the PorSi leads to a higher density of stacking faults on EpiWafers.

With these observations, we demonstrate two major causes for losses in efficiency potential of EpiWafers, namely the high doping and the PorSi of the reusable substrates.

References:

- [1] C. Ballif, F. J. Haug et al., *Nat. Rev. Mater.*, **2022**, vol. 7, p. 597.
- [2] P. Verlinden, D. L. Young et al., *Device*, **2023**, vol. 1, p. 100013.
- [3] J. Gifford, *PV Magazin*, **2023**.
- [4] C. Weiss, W. Schreiber et al., *EU PVSEC*, **2020**, p. 444.
- [5] C. Rittmann, J. Dalke et al., *EU PVSEC*, **2021**, p. 198.
- [6] C. Rittmann, F. Schindler et al., *Solar RRL*, **2022**, vol 7, p. 2200698.
- [7] C. Rittmann, P. Messmer et al., *Solar RRL*, **2024**, online, p. 2300882.
- [8] J. A. Giesecke, M. C. Schubert et al., *Sol. Energy Mater. Sol. Cells*, **2011**, vol. 95, p. 1011.
- [9] B. Michl, M. Rüdiger et al., *Sol. Energy Mater. Sol. Cells*, **2012**, vo. 98, p. 441.
- [10] H. Höffler, F. Schindler et al., *EU PVSEC*, **2020**, p. 264.
- [11] F. D. Heinz, M. Oezkent et al., *Sol. Energy Mater. Sol. Cells*, **2023**, vol. 260, p. 112477.

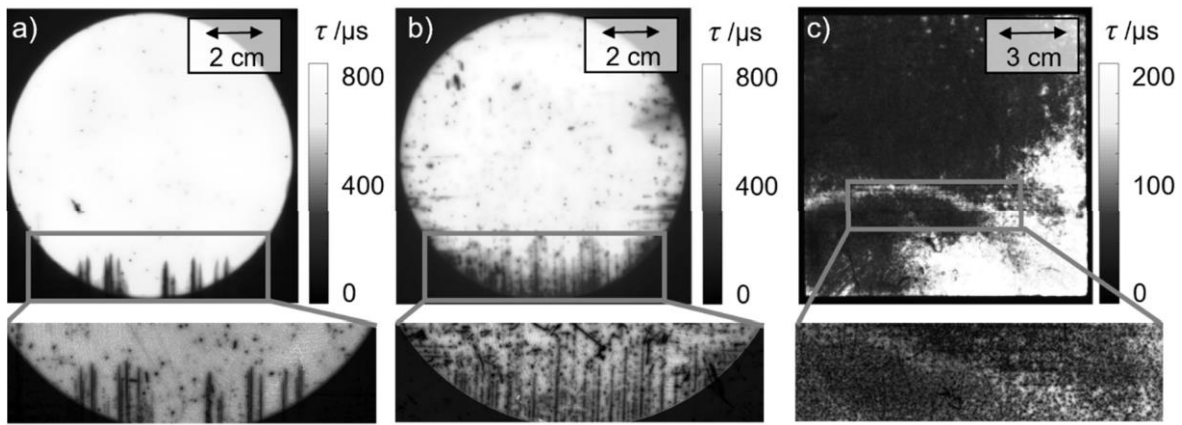


Fig. 1. Lifetime images detected at 1 sun eqs. (top row) and close-ups of μ PL-mappings (bottom row) of the three discussed samples: a) EpiRef_p epitaxially grown on polished, moderately-doped Si substrate without PorSi, b) EpiRef_p+ epitaxially grown on polished, highly-doped Si substrate without PorSi, and c) EpiWafer epitaxially grown on highly-doped, reusable Si substrate with PorSi.

Table 1. Overview of the electrical properties and number of structural defects of the discussed samples. The electrical quality is given by the square root harmonic mean of the minority carrier lifetime r_{mean} detected at 0.05 sun eqs (corresponding to a charge carrier density close to maximum power-point condition in a corresponding solar cell) and the predicted solar cell efficiency η_{mean} (high-efficiency solar cell design with a limit of 26.6 %). The crystal quality is given by the stacking fault density SFD and the etch pit density EPD representing dislocations.

	EpiRef_p	EpiRef_p+	EpiWafer
r_{mean} [μs]	1000	500	30
η_{mean} [%]	24.8	24.0	20.5
SFD [cm^{-2}]	0.7	4	> 200
EPD [cm^{-2}]	20	150	> 1000

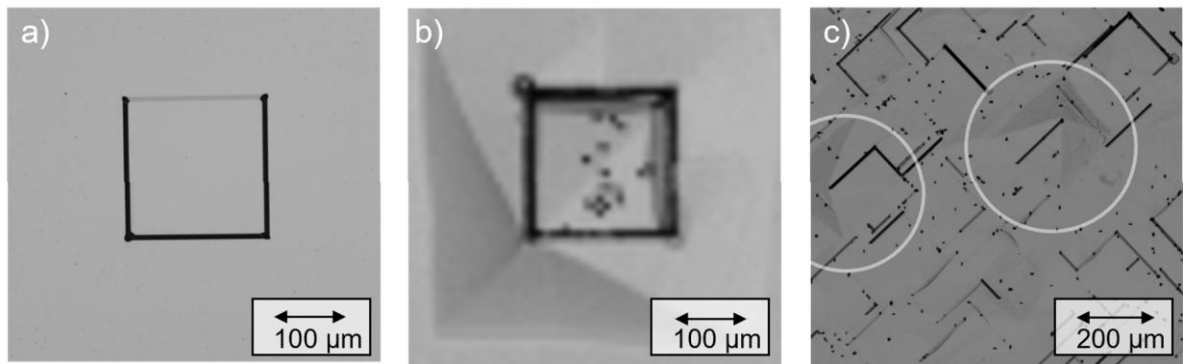


Fig. 2. Microscope images after defect selective etching of typical stacking faults (SF) at the discussed samples: a) Topologically planar SF at EpiRef_p, b) topologically elevated SF with dislocations within at EpiRef_p+, c) overlaying SF (topologically elevated marked with white circles) and etch pits on the EpiWafer.

Recent Advances and Trends in Atomic Layer Deposited Surface Passivation Schemes for Silicon, Germanium and III-V Semiconductors

Bart Macco,¹ Roel Theeuwes¹, Willem-Jan Berghuis¹, and Erwin Kessels¹

¹ Department of Applied Physics and Science Education, Eindhoven University of Technology, P.O. Box 513, 5600 MB, Eindhoven, The Netherlands

Email: b.macco@tue.nl

Over the last decade, our research group has pioneered many novel atomic layer deposition (ALD) materials and approaches for semiconductor surface passivation.[1] Our initial focus was on passivation of silicon within the context of photovoltaics, which in recent years expanded to germanium and III-V semiconductors. In this contribution, we put these developments and our main learnings in perspective. New materials and achieved performance (*defect density, fixed charge*) will be outlined, with a strong focus on mechanistic insights such as the role of hydrogen and annealing, surface preparation, interlayers and capping layers.

Of the new materials, special attention will be given to $\text{PO}_x/\text{Al}_2\text{O}_3$ stacks, for which we have demonstrated state-of-the-art passivation on silicon, germanium and InP nanowire surfaces.[2,3] These stacks provide a low interface defect density and are especially suited for the passivation of *n*-type surfaces owing to their exceptionally high positive fixed charge density. The unique working mechanism of these stacks will be outlined, relying on a combination of layer intermixing upon annealing, hydrogen release and subsequent passivation.

Expanding to germanium and III-V, interface management was found to be much more crucial. Whereas on Si defects can often be hydrogenated post-deposition, for Ge and III-V this is less the case and thus it is imperative to apply adequate native oxide removal and surface pretreatment, followed by ‘soft’ deposition. Interestingly, also the polarity of fixed charge in the passivation layer can depend on the semiconductor type, e.g. for SiN_x we found positive fixed charge on silicon and negative charge on germanium surfaces. The most successful approach on germanium that was developed from our learnings is the stack of *a*- Si:H/ Al_2O_3 . Here, we use *a*-Si:H as interlayer for its high chemical passivation while the Si- Al_2O_3 interface gives a strong negative fixed charge.[4]

References:

- [1] L.E. Black *et al.*, *Solar Energy Materials & Solar Cells* **2018**, 188, 182-189
- [2] R.J. Theeuwes *et al.*, *Solar Energy Materials & Solar Cells* **2022**, 246, 111911
- [3] R.J. Theeuwes *et al.*, *Applied Physics Letters* **2023**, 123, 091604
- [4] W.J.H. Berghuis *et al.*, *Journal of Applied Physics* **2021**, 130, 135303

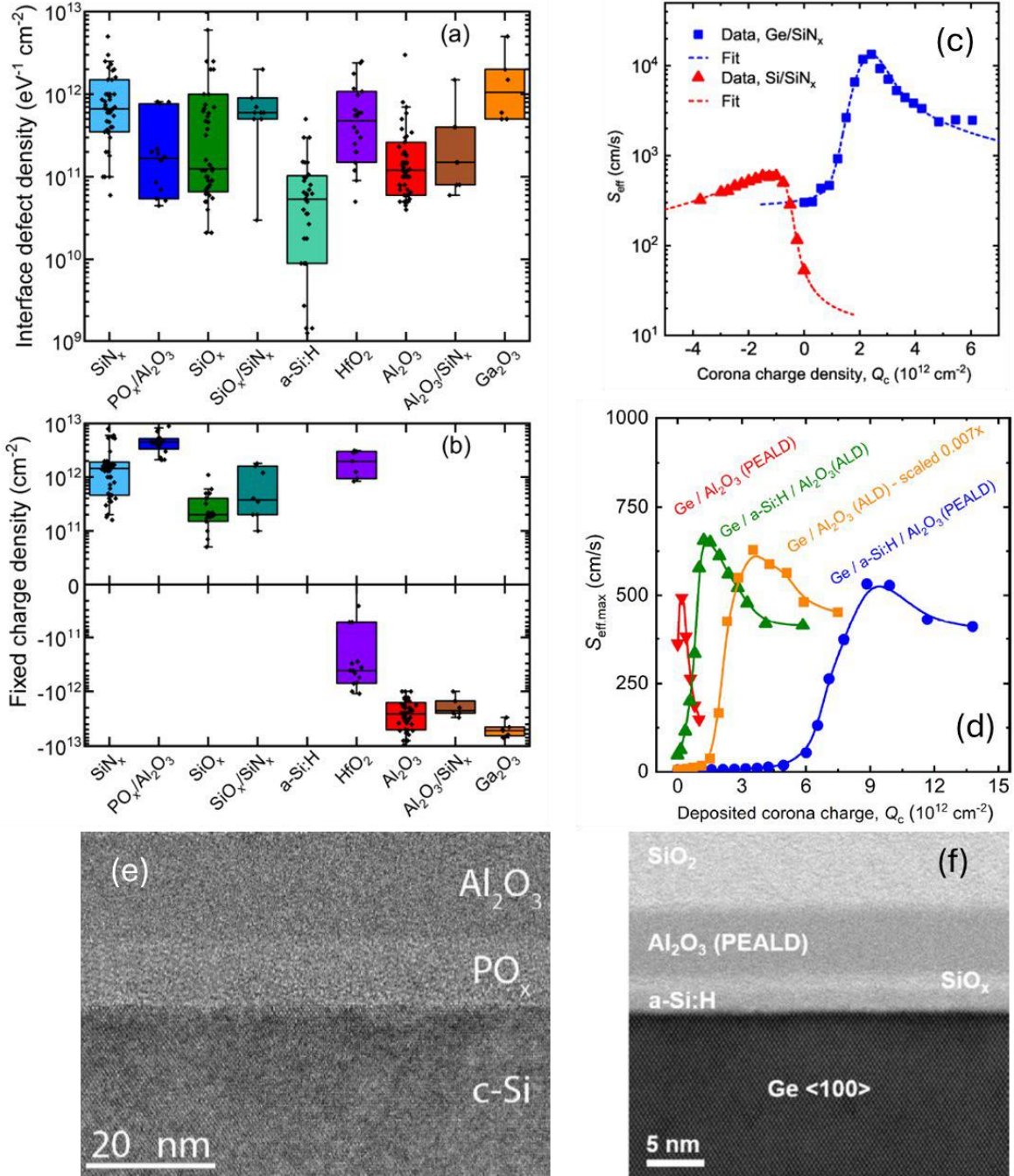


Fig. 1. Overview of interface properties of passivation schemes on c-Si, in terms of (a) interface defect density (D_{it}) and (b) fixed charge density (Q_f). (c) Comparison of corona charging experiments for SiN_x on silicon and germanium surfaces, showing a different polarity of fixed charge for both semiconductors. (d) Comparison of corona charging for various passivation stacks on germanium. The best performance in terms of good chemical passivation and high fixed charge is obtained by $a\text{-Si:H/PEALD Al}_2\text{O}_3$ stacks. TEM images of (e) the $\text{PO}_x/\text{Al}_2\text{O}_3$ stack on Si and (f) the $a\text{-Si:H/PEALD Al}_2\text{O}_3$ stack on Ge.

Separating surface and bulk recombination mechanisms during the activation of Al₂O₃ passivation

Nicholas E. Grant¹, Sophie L. Pain¹, Edris Khorani¹, Richard Jefferies¹, Ailish Wratten¹, Shona McNab², David Walker³, Yisong Han³, Richard Beanland³, Ruy S. Bonilla² and John D. Murphy¹

¹School of Engineering, University of Warwick, UK. ²Department of Materials, University of Oxford, UK.

³Department of Physics, University of Warwick, UK

Email: nicholas.e.grant@warwick.ac.uk

The re-emergence of aluminium oxide (Al₂O₃) in 2006 [1] has enabled high levels of surface passivation to be achieved for solar cells and electronic devices. Its success can be attributed to the high levels of negative charge and good chemical passivation properties achieved by this dielectric [2]. As such, Al₂O₃ is playing an ever-increasing role in mitigating surface recombination on either the front or rear surface of photovoltaic devices and test structures, thereby demonstrating its significance in the development of highly efficient solar cells [3]. However, as the efficiency continues to rise, front side surface passivation is becoming every more sensitive to recombination at the Si-Al₂O₃ interface, meaning efforts to understand this interface and thus develop solutions to mitigate interface defects could have a very large impact.

This work identifies the competing bulk and surface lifetime effects that occur during the activation of atomic layer deposited Al₂O₃, thereby enabling a more accurate assessment of the surface passivation mechanisms. We demonstrate that maximum passivation is achieved on *n*- and *p*-type silicon when the Al₂O₃ films are annealed at ~450 °C, irrespective of annealing ambient. Upon stripping the Al₂O₃ films and re-passivating the surfaces using a superacid-based technique, we find the bulk lifetime of float-zone and Czochralski silicon wafers degrade at annealing temperatures >450 °C, as demonstrated in Figure 1. By accounting for this bulk lifetime degradation, we demonstrate that the chemical passivation component associated with Al₂O₃ remains stable at activation temperatures of 450–500 °C, achieving an SRV of <1 cm/s on *n*- and *p*-type silicon. In contrast, the negative fixed charge density ($\sim 5 \times 10^{12}$ qcm⁻²) within the Al₂O₃ film remains stable over the full temperature range investigated (e.g. 300–600 °C). By examining the Si-Al₂O₃ interface by transmission electron microscopy and energy dispersive X-ray spectroscopy, we show that in the as-deposited state, a relatively thick SiO₂ layer of ~5nm is present between the Al₂O₃ film and silicon surface, however post annealing at temperatures $\geq 350^\circ\text{C}$, Al from the Al₂O₃ layer diffuses into the SiO₂ and forms an alloy, whereby the oxide layer reduces in thickness to

<2nm with a composition of Si_xAl_yO₂, as indicated by the EDX line scans and TEM images in Figure 2.

References:

- [1] B. Hoex *et al.*, *Applied Physics Letters*, **89**, p. 042112, 2006.
- [2] N. E. Grant *et al.*, *Applied Surface Science*, **645**, p. 158786, 2024.
- [3] International Technology Roadmap for Photovoltaic, 14th Edition, 2023.

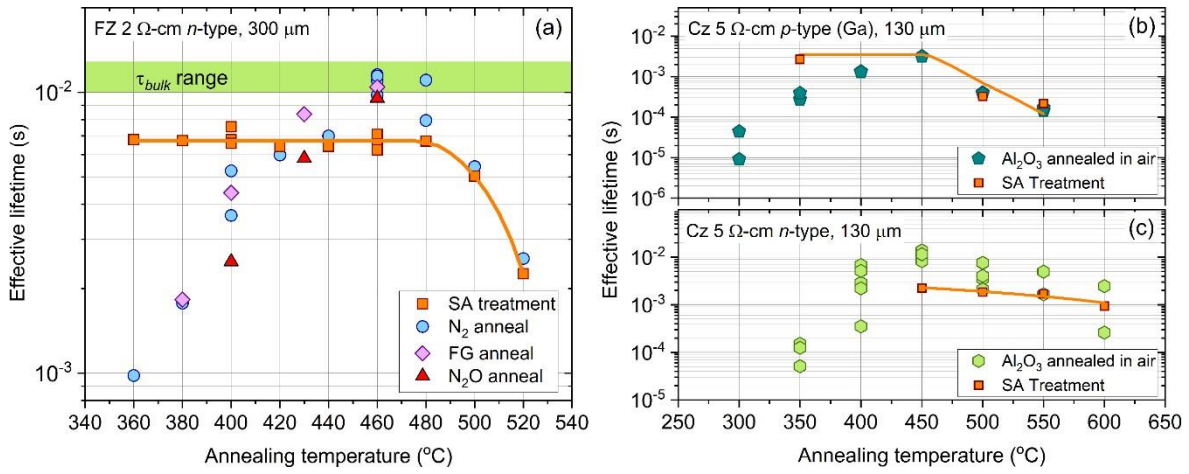


Figure 1: (a) Effective lifetime (at $\Delta n = 10^{15} \text{ cm}^{-3}$) of ALD Al₂O₃ passivated (~20 nm) FZ 2 Ω-cm *n*-type silicon samples. (b) and (c) effective lifetime at $\Delta n = 10^{15} \text{ cm}^{-3}$ of ALD Al₂O₃ passivated (~20 nm) Cz 5 Ω-cm *p*-type (gallium doped) and *n*-type silicon, respectively. All anneals were performed for 30 minutes.

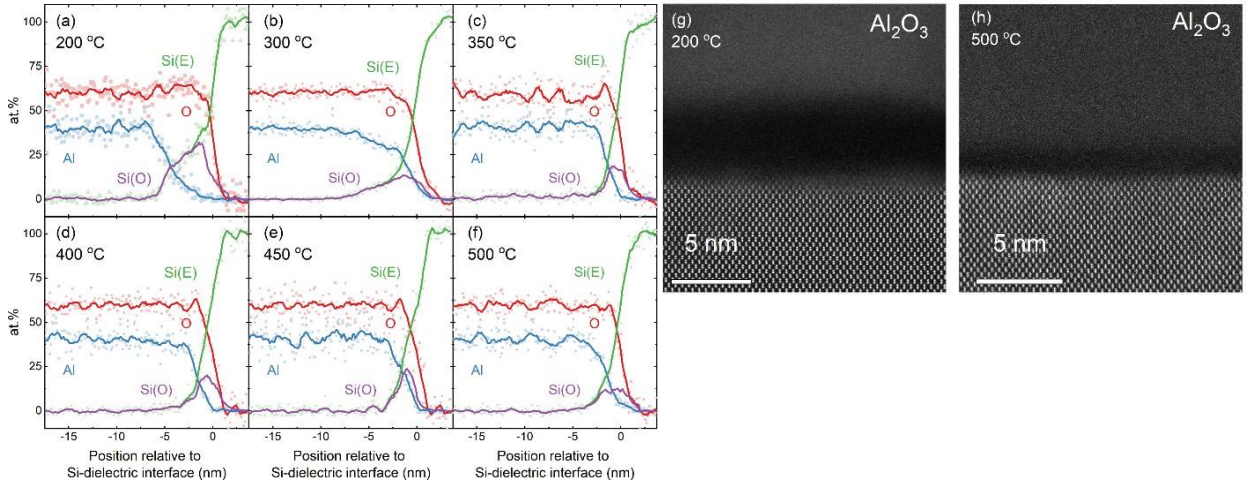


Figure 2: (a-f) EDX line scans for ~20 nm Al₂O₃ films annealed between 200–500°C. (g-h) TEM images of the Al₂O₃ films before and after annealing at 500°C.

Hafnium oxide surface passivation of silicon

Sophie L. Pain,¹ Ailish Wratten,¹ Anup Yadav,¹ Edris Khorani,¹ Tim Niewelt,^{1,2,3} Brendan F.M. Healy,¹ David Walker,⁴ Nicholas E. Grant,¹ and John D. Murphy¹

¹ School of Engineering, University of Warwick, Coventry, CV4 7AL, UK

² Fraunhofer Institute for Solar Energy Systems ISE, Heidenhofstraße 2, 79110 Freiburg, Germany

³ Chair for Photovoltaic Energy Conversion, Department of Sustainable Systems Engineering (INATECH), University of Freiburg, Emmy-Noether-Str. 2, 79110 Freiburg, Germany

⁴ Department of Physics, University of Warwick, Coventry, CV4 7AL, UK

Email: john.d.murphy@warwick.ac.uk

Surface passivation plays an essential role in mitigating charge carrier recombination in electronic devices, including in photovoltaic solar cells. Atomic layer deposition (ALD) is routinely used to produce nanometre-scale passivation layers. Annealed ALD-grown Al₂O₃ has excellent properties, including a surface recombination velocity < 1 cm/s for silicon [1], but other metal-oxide dielectrics have also demonstrated promise. One such example is HfO₂, which can give surface recombination velocities approaching those of Al₂O₃ [2], but has the added advantage of having chemical etch resistance (including in hydrofluoric acid) which can be tuned with annealing [3], hence providing flexibility in device fabrication. There are reports (summarised in [2]) claiming that HfO₂ layers can possess either negative or positive fixed charges, with the ALD precursor speculated to influence the charge polarity.

We have performed an extensive set of investigations into the surface passivation of silicon by ALD-grown HfO₂ films, exploring the effects of chemical precursor, co-reactant, thickness, and post-deposition annealing conditions (temperature and ambient). We determine the properties and effects of the films by using photoconductance charge carrier lifetime measurements (using superacid repassivation to isolate bulk and surface effects), Kelvin probe analysis, corona charging, and X-ray diffraction. We find the passivation level to be strongly dependent on the post-deposition annealing temperature, with the optimum passivation being achieved at 475 °C (Fig. 1 (a) and (b)). We also find the onset of good passivation to coincide with the crystallisation of the film (Fig. 1 (c)). The passivation level achieved is dependent on film thickness (Fig. 2), with HfO₂ found to passivate better than Al₂O₃ when at a thickness of order 1 nm, making it a possible candidate in a passivating contact structure.

We will present our latest results which show a direct comparison between films grown with tetrakis (dimethylamido) hafnium (TDMAH) and tetrakis (ethylmethylamido) hafnium (TEMAHf) precursors. From Kelvin probe measurements, we find that, irrespective of precursor, HfO₂ is negatively charged, contrary to claims in the literature. TEMAHf-HfO_x passivation quality is also influenced by annealing temperature, and passivates well, with surface recombination velocities ≤ 3 cm/s possible. Overall, HfO₂ provides excellent surface passivation, with options for tunability which are not available with more common schemes.

References:

- [1] N.E. Grant, et al., *Applied Surface Science*, **2024** 645 158786, doi: 10.1016/j.apsusc.2023.158786.
- [2] A. Wratten, et al., *Solar Energy Materials and Solar Cells*, **2023** 259 112457, doi: 10.1016/j.solmat.2023.112457.
- [3] A. Wratten, et al., *AIP Advances*, **2023** 13 065113, doi: 10.1063/5.0144639.
- [4] A. Wratten, et al., *IEEE Journal of Photovoltaics*, **2023** 13 40, doi: 10.1109/JPHOTOV.2022.3227624.

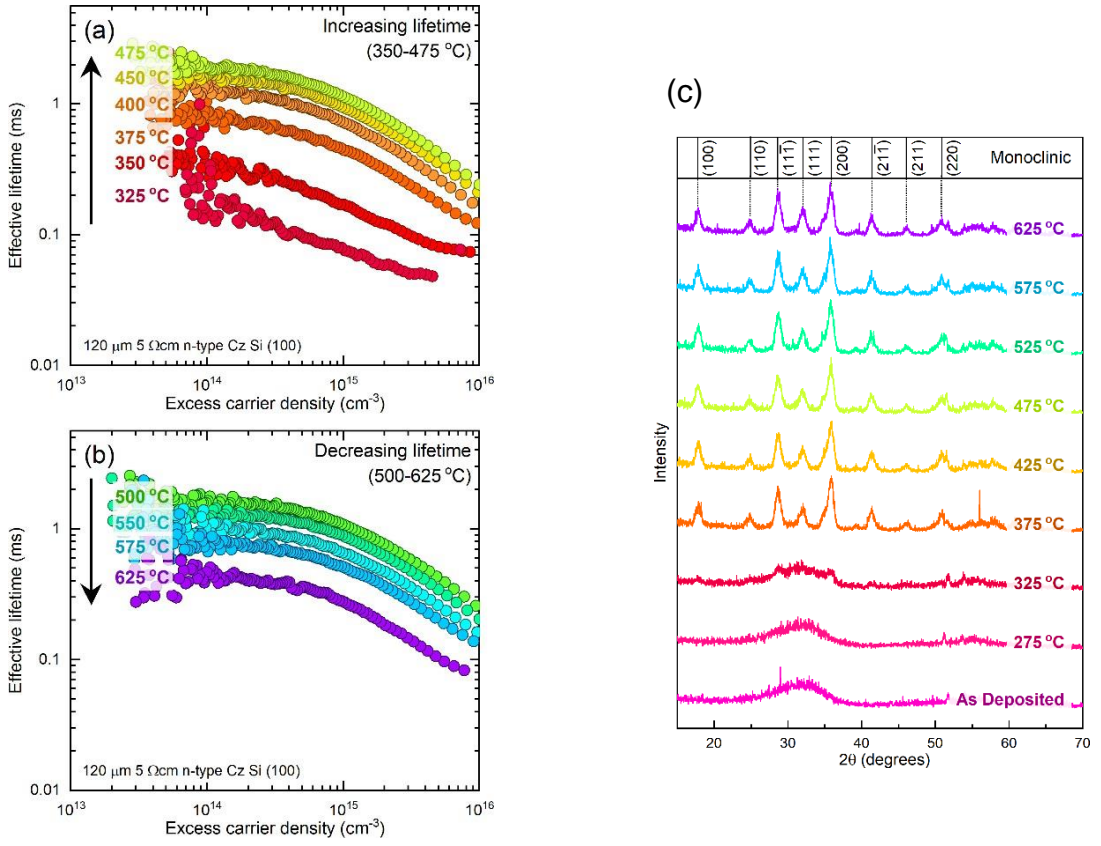


Fig. 1. (a) Lifetime curves for 12 nm (100 cycles) of ALD deposited HfO_2 films using a TDMAH precursor on 120 μm 5 Ωcm n-type Cz-Si wafers, annealed at various temperatures (300–475 °C) for 30 min. (b) Lifetime curves of the same type of samples annealed at higher temperatures (500–625 °C) for 30 min. (c) GI-XRD measurements, using $\text{Cu K}_{\alpha 1/2}$, taken from polished silicon wafers coated with 12 nm (100 cycles) of hafnium oxide grown by ALD using a TDMAH precursor annealed in air for 30 min at temperatures from as-deposited (200 °C) to 625 °C.

(Reproduced from [4] with copyright retained by authors under a CC-BY licence).

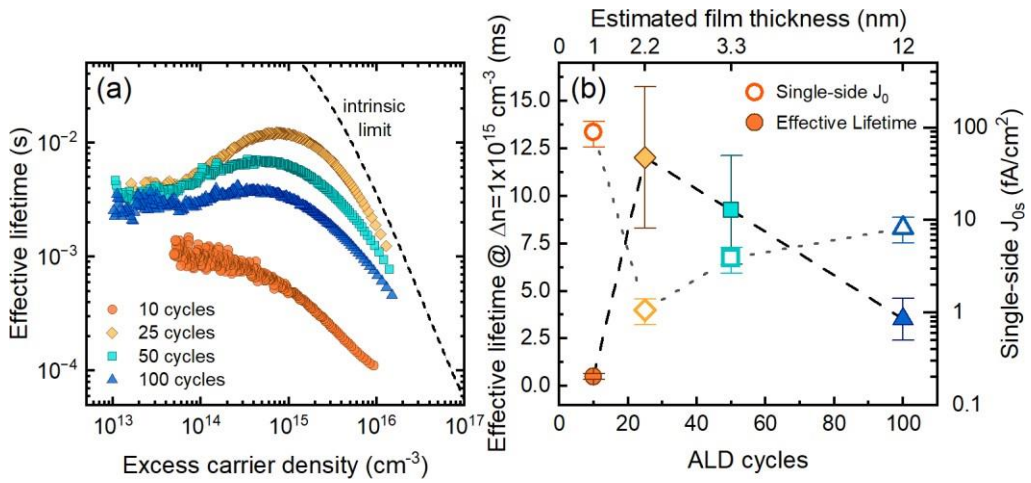


Fig. 2. (a) Effective lifetime curves for different HfO_2 films (10–100 cycles, corresponding to 1–12 nm estimated thickness), deposited via ALD using a TDMAH precursor on 150 μm 5 Ωcm n-type Cz-Si wafers, annealed in air at 475 °C for 30 min. (b) Effective lifetimes extracted at an excess carrier density of $1 \times 10^{15} \text{ cm}^{-3}$ and single-side J_{0s} values for each film thickness in (a). (Reproduced from [3] with copyright retained by authors under a CC-BY licence)

In-situ mixed and cycle-to-cycle Atomic Layer Deposition for Al-doped ZrO₂ based Metal-Insulator-Metal decoupling capacitors placed in BEoL

K. E. Falidas,¹ F. Schöne,¹ M. Czernohorsky,¹ and J. Heitmann²

¹ Fraunhofer Institute for Photonic Microsystems (IPMS), An der Bartlake 5, 01109, Dresden, Germany

² Institute for Applied Physics, TU Bergakademie Freiberg, Leipziger Str. 23, 09599, Freiberg, Germany

Email: konstantinos.efstathios.falidas@ipms.fraunhofer.de

CMOS technology in the nanometer regime faces challenges due to various noise sources, leading to supply voltage issues. The demand for electronic product miniaturization drives the need for integrated passive decoupling devices. On-chip Metal- Insulator-Metal (MIM) decoupling capacitors with high capacitance density are strategically placed in the back-end-of-line (BEoL) between metal interconnect layers. Aluminum oxide serves as a promising candidate to enhance reliability and control leakage currents during atomic layer deposition (ALD) of ZrO₂-based high- κ dielectrics [1]. Techniques, where compounds are deposited in a cycle-to-cycle manner, are used to alternate ZrO₂ and dopant deposition pulses, typically requiring less than 8 at.% concentration of Al dopant with a few ALD cycles [2]. However, achieving effective mixing between ZrO₂ and Al₂O₃ is challenging for thin dielectrics (<10 nm) when lowering the deposition temperature to meet the BEoL thermal budget (<400°C) while maintaining an amorphous state to minimize leakage current.

In this study, we propose a customized fabrication process incorporating in-situ mixing [3] of metal precursors during ALD to optimize the properties of Al-doped ZrO₂ films for MIM decoupling capacitors. Moreover, important ALD parameters such as deposition temperature (T_D) and stoichiometry between the 2 metals (Zr:Al) are varied. MIM capacitors were fabricated on 300 mm Si wafers in the BEoL using physical vapor deposition TiN electrodes. The ALD experiments utilized a cross-flow reaction chamber with ZrCl₄ and trimethylaluminum (TMA) as metal precursors for ZrO₂ and Al₂O₃ deposition, respectively.

The ALD processes were compared, with one involving in-situ precursor mixing and the other following cycle-to-cycle variation. Grazing incidence X-ray diffraction analysis confirmed the maintenance of amorphous structure in all samples. X-ray photoelectron spectroscopy revealed similar stoichiometric behavior between the two ALD processes. Capacitance-field characteristics were analyzed, demonstrating improved linearity by ~10% and capacitance stability over applied frequency and Al content for the in-situ mixing ALD process. Leakage current density and breakdown field were also evaluated at temperatures up to 200°C, indicating superior performance (<<1 μA/cm²) for in-situ mixed ALD with lower deposition temperatures and higher Al concentrations.

The study investigates Poole-Frenkel emission in Al₂O₃-ZrO₂ mixed and classic ALD capacitors, revealing similar defect energies for both field polarities and ALD processes, indicating a non-chemical impact of in-situ mixing ALD on high- κ films. Additionally, Time-Dependent Dielectric Breakdown (TDDB) analysis demonstrates that mixed ALD samples with higher Al concentration exhibit excellent reliability, achieving a 10-year lifetime even at 150°C, following a “ $\sqrt{E/T}$ ” PF-friendly extrapolation model [4].

References:

- [1] W. Weinreich et al., *J. Vac. Sci. Technol. B* **2013**, vol. 31, 01A109, [10.1116/1.4768791](https://doi.org/10.1116/1.4768791)
- [2] K. Falidas et al., *VLSI-TSA* **2023**, pp. 1-2, [10.1109/VLSI-TSA/VLSI-DAT57221.2023.10134346](https://doi.org/10.1109/VLSI-TSA/VLSI-DAT57221.2023.10134346)
- [3] C. Mart et al., *ACS Appl. Electron. Mater.* **2019**, vol. 1, pp. 2612-2618, [10.1021/acsaelm.9b00591](https://doi.org/10.1021/acsaelm.9b00591)
- [4] K. E. Falidas et al., *Microelectron. Reliab.* **2023**, vol. 150, 115191, [10.1016/j.microrel.2023.115191](https://doi.org/10.1016/j.microrel.2023.115191)

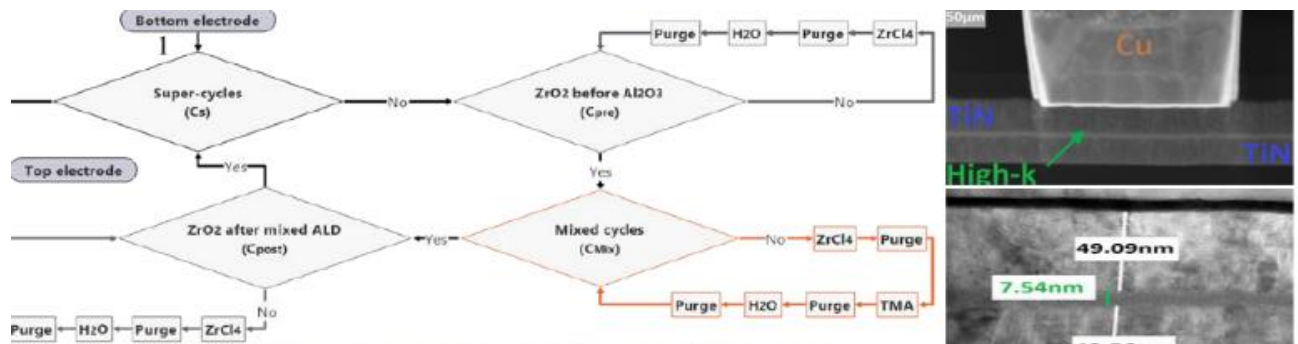


Fig. 1 Flow-chart of mixed ALD process for ZrAl_xO_y high-k dielectric layers.

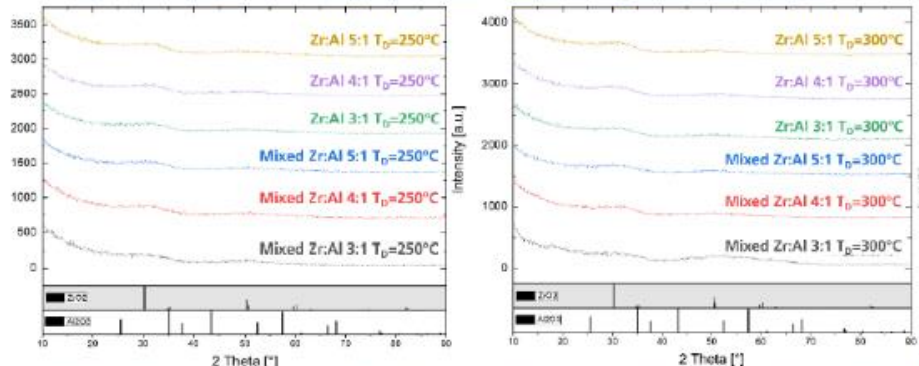


Fig. 3 XRD diffractograms of all Zr:Al ratios for both T_D and for both classic & mixed ALD.

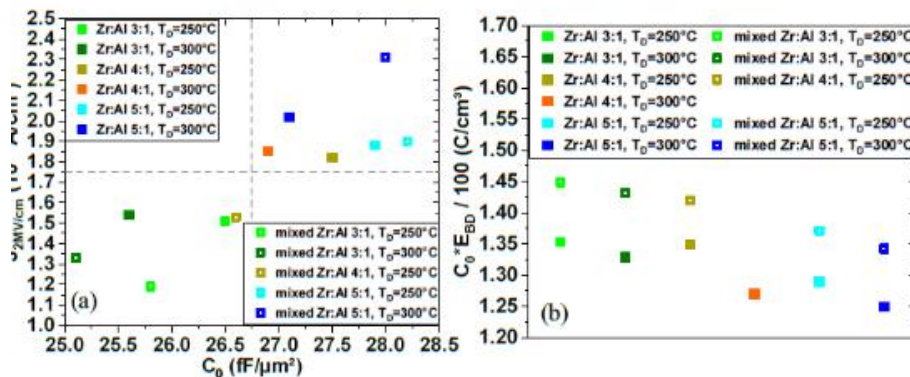


Fig. 4 Figure of Merit (FOM) plots for both classic and mixed ALD and all Zr:Al ratios (3-5:1)
(a) $J_{2\text{MV}/\text{cm}^2}$ and C_0 at 25°C and (b) C_0 and E_{BD} at 125°C.

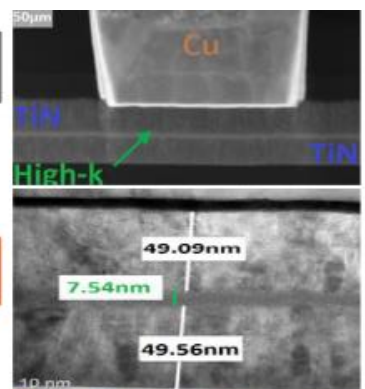


Fig. 2 TEM-micrographs of mixed ALD Zr:Al 4:1 $T_D=300^\circ\text{C}$.

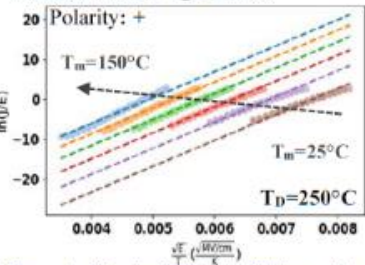


Fig. 5 Poole-Frenkel fitting for positive polarity of mixed ALD Zr:Al 3:1 & $T_D=250^\circ\text{C}$ at 25-150°C.

Table 1. TDDB for classic ALD

Zr:Al	T_D ($^\circ\text{C}$)	γ ((MV/cm) $^{1/2}$ K)
3:1	250	-9.35
3:1	300	-7.59
4:1	250	-9.33
4:1	300	-8.38
5:1	250	-9.40
5:1	300	-8.36

Table 2. TDDB for mixed ALD

Zr:Al	T_D ($^\circ\text{C}$)	γ ((MV/cm) $^{1/2}$ K)
3:1	250	-11.72
3:1	300	-10.10
4:1	250	-8.66
4:1	300	-8.33
5:1	250	-8.93
5:1	300	-7.90

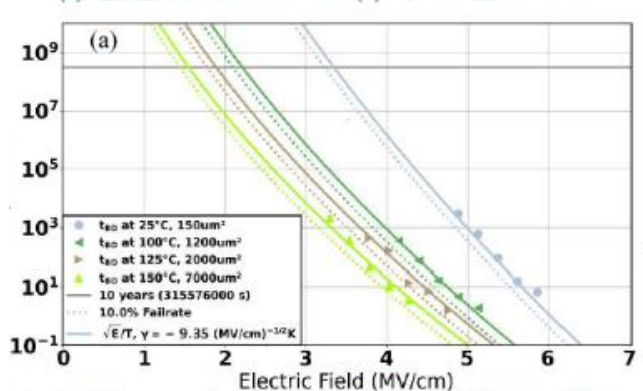
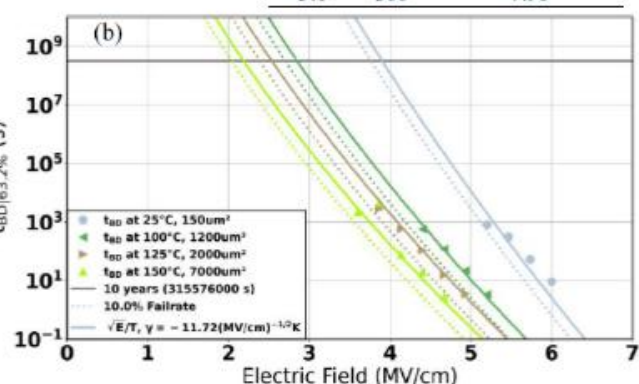


Fig. 6 TDDB extrapolation using “ $\sqrt{E/T}$ ” - model for Zr:Al 3:1 at $T_D=250^\circ\text{C}$ for (a) classic ALD vs. (b) mixed ALD.



Growth-related I3 defects in hexagonal Ge-2H and their thermal evolution

Laetitia Vincent¹, Marcel Verheijen², Elham Fadaly², Wouter Peters², Laurent Travers¹, Charles Renard¹, Erik Bakkers²

¹ Centre de Nanosciences et Nanotechnologies, UMR 9001, CNRS-Université Paris-Saclay, 10 Boulevard Thomas Gobert, 91120 Palaiseau France

² Department of Applied Physics, Eindhoven University of Technology, P.O. Box 513, 5600 MB Eindhoven The Netherlands

Email: Laetitia.vincent@c2n.upsaclay.fr

Silicon and Germanium crystallize in the cubic diamond structure 3C with which they dominate definitely the electronics. Playing on crystal phases in semiconductors occurs to be a valuable mean of electronic band engineering. Remarkably, the hexagonal 2H phase of turns to get a direct band gap with light emission capabilities within a specific composition range [1]. This material holds the promise to fill the gap between electronics and photonics industry using group IV semiconductors.

We use GaAs NWs with the wurtzite structure as a template to create both (1) core/shell and (2) trunk/branches heterostructures [2,3]. The GaAs-wurtzite is an ideal template to copy the structure by epitaxy and thus force the Ge to adopt the hexagonal crystal phase.

The growths were observed in real time at the atomic scale using in situ TEM. The microscope can be implemented either with molecular beam epitaxy (MBE) sources or with a gas injector for chemical vapor deposition (CVD). We show the different growth kinetics of Ge-2H on (1-100) lateral faces depending on temperature and precursor flow. We evidence the growth-related formation of original intrinsic stacking faults I3 [2] and discuss the correlation with the growth modes related to surface diffusion. In the paper we describe the characteristics of those defects. A possible scenario of I3 BSF formation is discussed. Understanding the nucleation of these defects is necessary to prevent their formation during epitaxy.

Additionally, the thermal evolution of I3 defects was also followed in situ. We evidence the expansion of the planar staking faults resulting in a complete cubic layer.

References:

- [1] E.M.T. Fadaly et al. *Nature* **2020**, 580, 205–209
- [2] L. Vincent et al. *Adv. Mat. Inter.* **2022**, 9-16, 2102340, doi.org/10.1002/admi.202102340
- [3] A. Li, et al. *Nanotechnology* **2022**, 34-1, 015601, doi.org/10.1088/1361-6528/ac9317

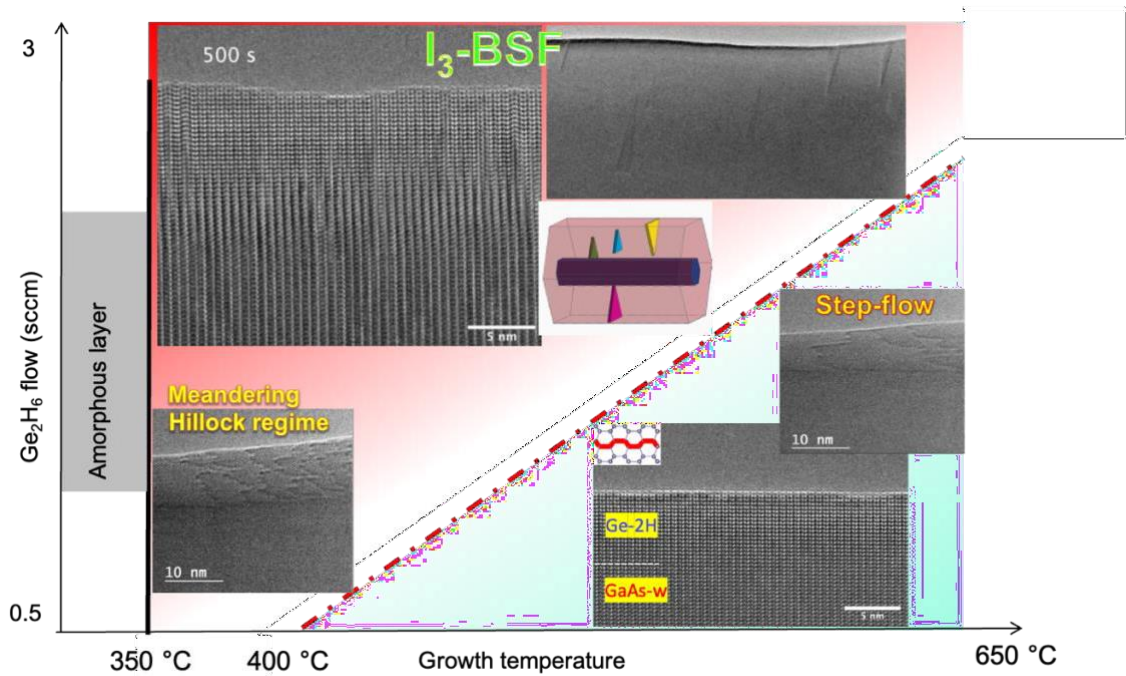


Fig. 1. Growth kinetics of Ge-2H on (1-100) sidewalls of GaAs-W. I_3 defects formed at low temperature and high precursor flow associated to the hillock regime

DLTS assessment of grown-in defects in hetero-epitaxial gate stacks for stacked silicon nanosheet channels

E. Simoen¹, S. Khelifi¹, H. Vrielinck¹, A. Akula² and R. Loo^{1,2}

¹ Ghent University, Depart. Of Solid State Sciences, Krijgslaan 281 S1, B-9000, Gent, Belgium

² Imec, Kapeldreef 75, B-3001, Leuven, Belgium

Email: eddy.simoen@ugent.be

The fabrication of state-of-the-art Gate-All-Around (GAA) silicon nanosheet transistors usually relies on the hetero-epitaxial growth of Si/SiGe structures, like in Fig. 1. Such a stack is formed by Chemical Vapor Deposition (CVD) in an epi reactor using higher order precursors and temperatures $\leq 500^{\circ}\text{C}$ [1]. This allowed the required two-dimensional epitaxial growth of smooth, fully strained SiGe/Si multi-stacks with Ge concentrations up to 50%. However, the low growth temperature results in an extremely long process duration and a concern for the incorporation of point defects in the active layers of the device. Improvements in the post-epi fabrication, especially the selective removal of SiGe, allow to reduce the Ge concentrations in the multi-stack. This opened the door to consider conventional process gases and higher growth temperatures for the epitaxial growth. The aim of the present work is to investigate the quality of these CVD gate stacks by Deep-Level Transient Spectroscopy (DLTS), probing electrically active defects and comparing high- and low-temperature deposited layers. The undoped epi-layers have been grown on 300 mm highly P-doped silicon wafers to a total thickness of around 107 nm. Al Schottky contacts have been evaporated on a wafer fragment enabling Capacitance-Voltage (C-V) measurements as shown in Fig. 2. Two distinct regions can be discerned in the bias range from $V_R = -2 \text{ V}$ to 0 V, corresponding with a different free carrier density in the n+ substrate and the SiGe/Si stack. It also defines the bias pulse voltages (V_R to V_P) for DLTS measurements, distinguishing the substrate region from the SiGe/Si hetero layers.

DLTS has been performed for a typical pulse period t_w of 51.2 ms and a filling pulse duration t_p of 100 μs . In the high-temperature sample, a clear electron trap peak is observed that shifts with the bias pulse towards lower peak position, when probing closer to the sample surface (Fig. 3). The corresponding Arrhenius plots in Fig. 4 confirm the reduction of the activation energy when probing closer to the sample surface. The change in the activation energy with probing depth could indicate a different local composition, as has been found previously for radiation-induced defects in relaxed $\text{Si}_x\text{Ge}_{1-x}$ with different composition x [2,3]. The nature of the observed point defects could be related to vacancy complexes, like, e.g., the E centre or P-V pair [4]. On the other hand, for the low-temperature sample in Fig. 5 a single broad peak is found when pulsing the gate stack region, while no detectable signal results from the silicon substrate. At the same time, logarithmic trap filling is found for the broad electron trap in Fig. 5, suggesting that extended defects (i.e., misfit and threading dislocations) are present in the low-T epi stack. This is confirmed by the results of Photoluminescence (PL) spectroscopy [1], demonstrating a partial relaxation of the low-T gate stacks.

References:

- [1] R. Loo *et al.*, SSDM 2023, abstract no. M-3-05, <https://doi.org/10.7567/SSDM.2023.M-3-05>.
- [2] H. av. Skardi, *et al.*, *Nucl. Instrum. Meth. In Phys; Res. B* **2002** 202, p. 195.
- [3] M. Mamor,*et al.*, *Phys. Rev. B* **2008** 77, p. 035213.
- [4] S. Ike, E. Simoen, *et al.*, *Jpn. J. Appl. Phys.* **2016** 55, p. 04EJ11.

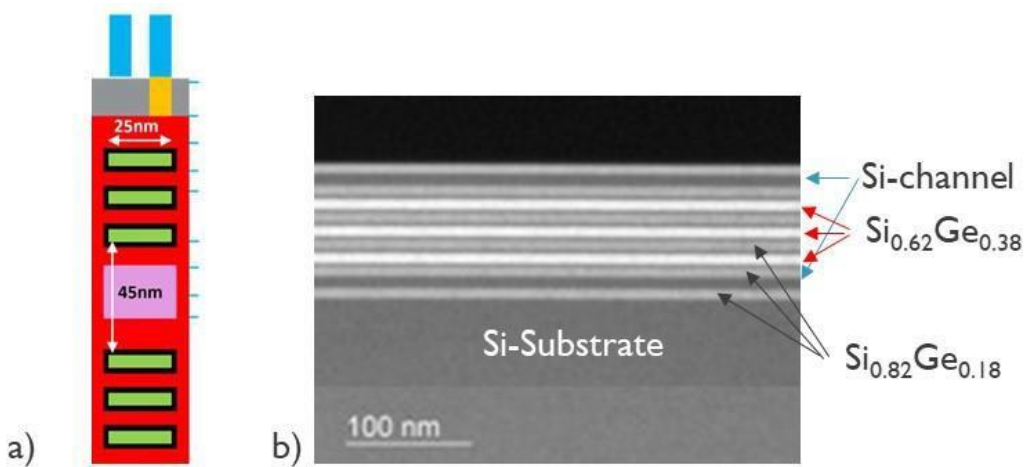


Fig. 1. Gate cross sections of a CFET Scheme and b) TEM image of a typical epi-stack used to fabricate CFET devices.

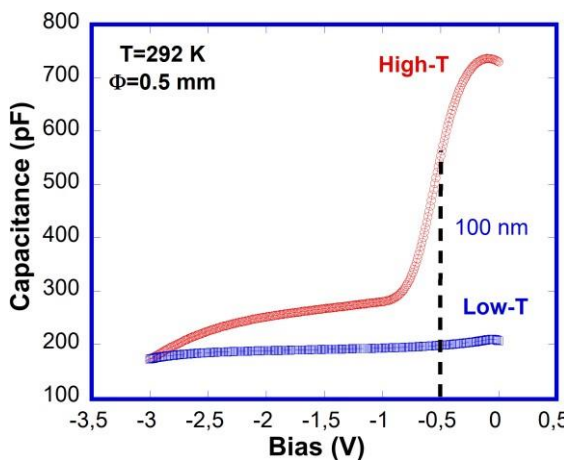


Fig. 2. Capacitance versus bias of a 0.5 mm diameter Al Schottky barrier on a low- and a high-temperature epi stack.

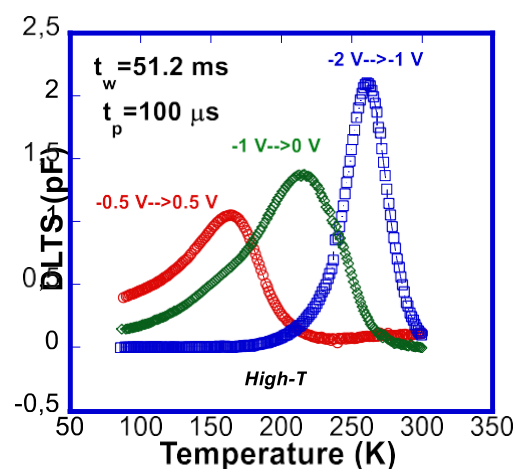


Fig. 3. DLTS spectrum of a high-temperature sample at different bias pulses. The pulse duration $t_p=100 \mu s$ and the pulse period $t_w=51.2 \text{ ms}$.

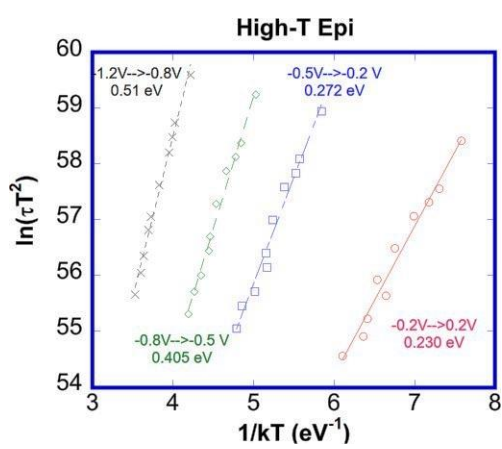


Fig. 4. Arrhenius plot of the high-temperature epi sample of Fig. 3, for different bias pulses.

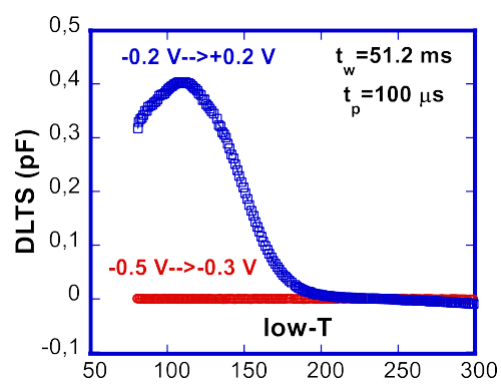


Fig. 5. DLTS of a low-temperature sample at different bias pulses. The pulse duration $t_p=100 \text{ ms}$ and the pulse period $t_w=51.2 \text{ ms}$.

Study of gettering in Silicon and SOI substrates

Alexandra Abbadie,¹ Cassandre Maljournal^{1, 2}, S. Kerdiles² and D. Boutry²

¹ STMicroelectronics 850 rue Jean Monnet, 38920, Crolles, France

² Univ. Grenoble Alpes, F-38000 Grenoble, France CEA, LETI, Minatec Campus, F-38054 Grenoble, France

Email: Alexandra.abbadie@st.com

The gettering topic has been widely studied these last years, addressing mainly the issue of contamination in silicon-based photovoltaic device [1]. This paper reviews the gettering efficiency on different kind of p-type Silicon Czochralski (Cz) substrates used for various applications in semiconductor industry.

The efficiency of metal contamination removal after voluntary contamination and anneals of Copper (Cu) and Nickel (Ni) is investigated on Si and Silicon-On-Insulator (SOI) substrates. The substrates differ by the intrinsic B doping and by deposited layers (called external gettering) such as poly Silicium or SiO₂ on Si. A protocol based on the use of Total X-ray Fluorescence (TXRF) is developed to enable comparison between all substrates (figure 1). Results presented in figure 2 on Si p- and p+ evidence the efficient gettering of Boron dopant on Cu contamination thanks to the formation of complexes Cu-B, likely enhanced by Bulk Micro Defects formation [2-4]. For most of substrates a different mechanism is proposed for Ni and Cu [5].

This paper investigates the monitoring of metallic contamination in advanced manufacturing lines and paves the way to the development of efficient gettering techniques.

References:

- [1] A. Liu, S. Pheng Phang and D. Macdonald, Solar Energy Materials and Solar Cells **2022**, 234, 111447
- [2] M.L. Polignano, G.F. Cerofolini, H. Bender, C. Claeys, J. Appl. Phys. **1988**, 64, 869.
- [3] W. Sugimura, T. Ono, S. Umeno, M. Hourai and K. Sueoka, ECS Transactions **2006**, 2(2), 95
- [4] B.C. Trzynadlowski and S. T. Dunham, J. Appl. Phys. **2013**, 114, 243508.
- [5] J. D. Murphy, K. Bothe, R. Krain, V. V. Voronkov and R. J. Falster, J. Appl. Phys. **2011**, 110, 053713

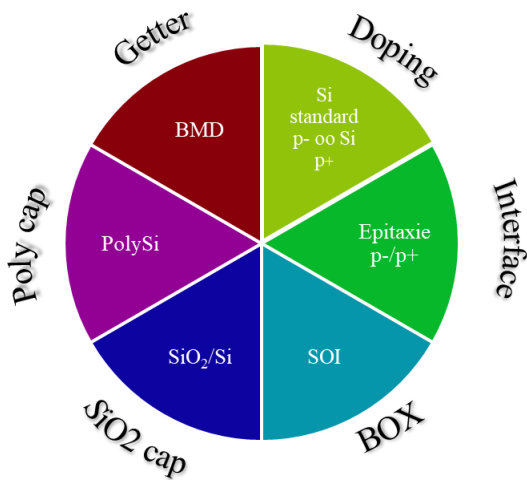


Fig. 1. List of substrates used in the study and nature of gettering

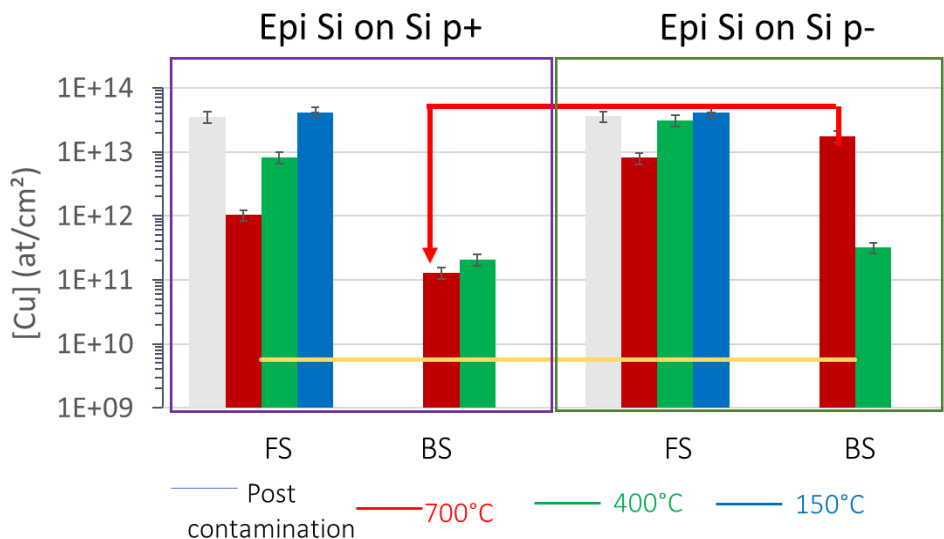


Fig. 2. TXRF results for Cu (at.cm⁻²) after a voluntary contamination and anneals on the Front-Side of the wafer. The analysis is made after on Front-side and Back-side to evaluate Cu diffusion.

The Diffusion Behavior of Sulfur in Silicon – A New Perspective

Felix Kipke,¹ Tim Böckendorf,¹ Joel Billermann¹ and Hartmut Bracht¹

¹ Institute of Materials Physics, University of Münster, Wilhelm-Klemm-Straße 10, 48149 Münster, Germany

Email; f.kipke@uni-muenster.de

Chalcogens such as sulfur, selenium, and tellurium, form deep double donors in silicon [1]. The low solubility of the chalcogens in silicon in combination with their high diffusivity [2,3] compared to group-III and group-V dopants [4] enables the realization of long-range and flat dopant profiles. These properties are advantageous for the realization of diode structures with a deep field-stop layer [5]. Pertermann et al. [5] report device simulations on the turn-off behavior of diodes doped with the deep double donor selenium and highlight the significance of a selenium doped deep field-stop layer. The deep double donor sulfur [2,6] diffuses faster than selenium [3] and may therefore be also a suitable candidate for applications in diode structures.

In this work, studies on the diffusion of sulfur in silicon are reported for temperatures between 920 °C and 1100 °C that were performed in closed evacuated quartz ampoules under a partial sulfur pressure of about 1 bar. After diffusion annealing, the resistivity profiles of sulfur are recorded by means of spreading resistance profiling. The resistivity profiles are converted into concentration profiles, considering either the impurity levels of single sulfur atoms or sulfur pairs. These energy levels can form during cooling to room temperature. Numerical simulations of sulfur diffusion based on interstitial-substitutional exchange mechanisms demonstrate the dominance of single sulfur atoms or pairs after cooling from the respective diffusion temperatures. The results are useful for specifically adjusting the sulfur species and the associated deep donor levels by diffusion annealing.

References:

- [1] P. Wagner, C. Holm, E. Sirtl, R. Oeder and W. Zulehner, in *Advances in Solid-State Physics*, edited by P. Grosse (Vieweg, Braunschweig, 1984), Vol. XXIV, 191-228.
- [2] F. Rollert, N. A. Stolwijk and H. Mehrer, *Appl. Phys. Lett.* **1993**, 63, 506–508.
- [3] H. Stümpel, M. Vorderwülbecke and J. Mimkes, *Appl. Phys. A* **1988**, 46, 159-163.
- [4] H. Bracht, H. H. Silvestri, I. D. Sharp, and E. E. Haller, *Phys. Rev. B*, **2007**, 75, 035211.
- [5] E. Pertermann, J. Lutz, H.-J. Schulze, H. P. Felsl, F.-J. Niedernostheide, S. Voß, H. Hüskens and R. Baburske, *Proc. ISPS*, **2012**, 11, 59-64.
- [6] N.A. Stolwijk, D. Grünebaum, M. Perret and M. Brohl, *Mater. Sci. Forum* **1989**, 38-41, 701-706.

For your remarks

Comparison of experimental and simulated results on the formation of N-related complexes in silicon

D. Kot,¹ G. Kissinger,¹ J. Dabrowski,¹ A. Sattler,² and T. Müller²

¹ IHP – Leibniz-Institut für innovative Mikroelektronik, Im Technologiepark 25, 15236 Frankfurt (Oder), Germany

² Siltronic AG, Einsteinstraße 172, 81677 München, Germany

Email: kot@ihp-microelectronics.com

Nitrogen is one of the most important co-dopants in the manufacturing of silicon crystals. This is due to its beneficial impact on crystal defects, what was extensively described in Ref. [1]. Nitrogen increases the strength of wafers and it has a strong impact on the size and distribution of grown-in defects [2]. In addition, nitrogen suppresses the size of voids in fast pulled CZ wafers [3]. The presence of nitrogen in CZ silicon leads to enhanced precipitation of oxygen and influences the width of the defect denuded zones [4].

It is well known that nitrogen exists in silicon mainly as N₂i complex but it can also form complexes with oxygen or vacancies. NO_x complexes with x=1-3 are particularly important because of their electrical activity. In this work we have used the binding energies determined by ab initio calculations and the law of mass action to simulate the equilibrium concentrations of the N species in silicon. We considered twelve N-related species, oxygen and vacancies. To verify the simulated equilibrium concentrations, several annealing experiments were carried out at different temperatures and for different annealing times. The annealing times used were assumed to be sufficient to reach equilibrium conditions [5]. Finally, we measured the absorption bands of NO_x (x=1-3) complexes at liquid helium temperature and the N₂, N₂O and N₂O₂ bands at liquid nitrogen temperature on 2 cm thick samples. The calibration factors of the complexes were used according to Ref [6] and from our own considerations. The initial concentrations of N and O were 6.5E14/cm³ and 5.5E17/cm³, respectively.

Fig. 1 shows a comparison between the experimental and simulated concentrations of the sum of measured N containing complexes (V containing complexes are not included). It can be seen that the summed concentrations, both experimental and simulated, are at the level of the initial N concentration in the range between 600°C and 800°C, and decrease at 1000°C and at 1100°C. This can be explained by the binding of N to vacancies. Unfortunately, as reported in ref [7], further experimental work is required to unambiguously assign certain IR bands to the corresponding N₂V₂O_n (n=1, 2) complexes. In our spectra, we found a weak IR band at 838 cm⁻¹ (Fig. 2). It is located in the range of wavenumbers where N₂V₂O_n (n=1, 2) could occur. In addition, the intensity of this band increases with increasing annealing temperature, which correlates with the increase in the vacancy contributions to the N complexes.

This work is a result of the BEYOND5 (www.beyond5.eu) project, which has received funding from the ECSEL Joint Undertaking (JU) under Grant 876124. The JU receives support from the European Union's Horizon 2020 research and innovation programme and from France, Germany, Turkey, Sweden, Belgium, Poland, Netherland, Israel, Switzerland, and Romania. The compute time provided by Gauss Centre for Supercomputing on the JUWELS cluster are acknowledged too.

References:

- [1] D. Yang, X. Yu, *Defect and Diffusion Forum* **2004**, 230-232, 199-220.
- [2] G. Kissinger, et al., *Solid State Phenom.* **2005**, 108-109, 17-24.
- [3] W. von Ammon, et al., *J. Cryst. Growth* **2001**, 226, 19-30K. Nakai, et al., *J. Appl. Phys.* **2001**, 89, 4301.
- [4] H. C. Alt and H. E. Wagner, *J. Appl. Phys.* **2009**, 106, 13511.
- [5] I. Okubo, H. Harada, T. Mikayama, D. Funao, N. Inoue, *Mat. Sci. Semicond. Proc.* **2003**, 5, 397.
- [6] E. N. Sgourou, N. Sarlis, A Chroneos and C. A. Londos, *Appl Sci.* **2024**, 14, 1631.

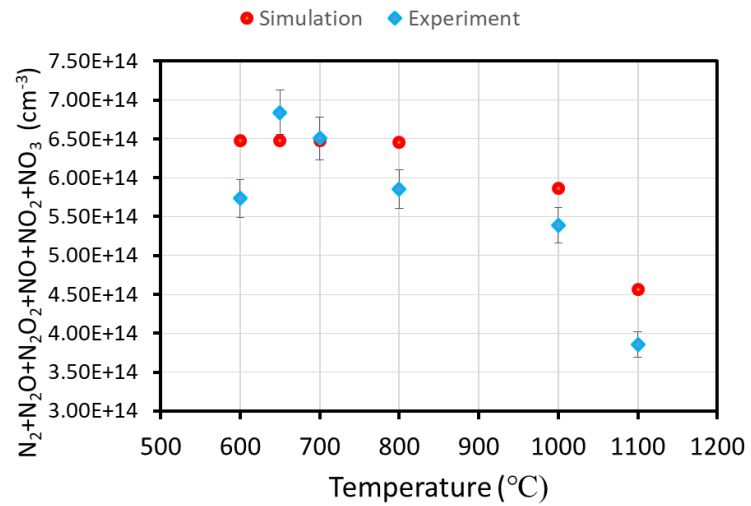


Fig. 1. Comparison between experimental and simulated concentrations of the sum of N-measured complexes at equilibrium concentrations at different temperatures.

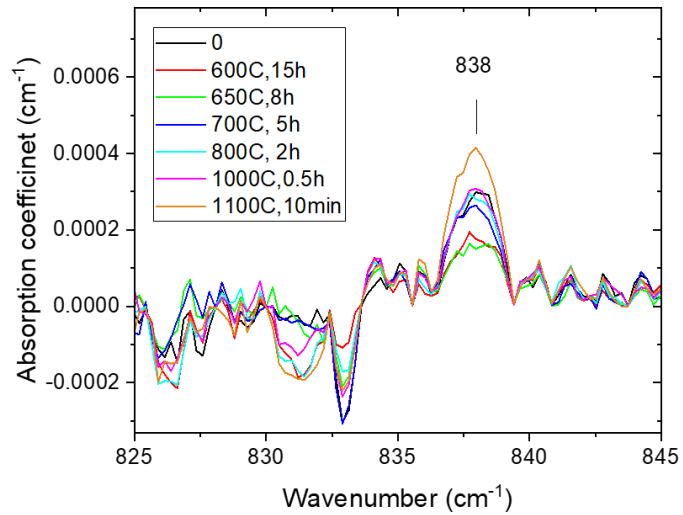


Fig. 2. FTIR spectra of a sample with a thickness of 2 cm, measured at 77 K.

Next Generation of Electronic Devices: Heterogenous Integration with Diamond

Martin Kuball¹

¹ Center for Device Thermography and Reliability, University of Bristol, United Kingdom

Email: Martin.Kuball@bristol.ac.uk

Current RF, but also power devices, suffer from a lack in efficient heat sinking/extraction, in particular, when considering wide and ultrawide bandgap semiconductors – these materials/devices are aimed at high power densities (and high voltages) and efficient heat sinking is essential to avoid severe degradation of device performance and/or early device failure. Most of these devices, for example, GaN devices, are presently either manufactured on SiC, Si substrates or engineered substrates such as QST. The substrate thermal conductivity is at best around 450 W/mK (for SiC); furthermore there are interfaces inside the device epitaxial structure such as AlGaN based strain relieve layers e.g. when GaN is grown on Si or QST substrates; all of these hinder/impact heat transport from the active device area, to the back of the substrate and ultimately the device package, keeping the electronics not as cool as optimally desired. Similar challenges exist in other material systems presently being considered, such as Al(Ga)N or Ga₂O₃ based device technologies (for RF and power applications). The bulk material with the highest known thermal conductivity to mankind is diamond. Diamond has been considered for active electronic devices, though this has proven very challenging in terms of the development of commercial products, in light of the difficulty of achieving a good doping capability, coupled with the need for a high carrier mobility. Diamond, however, is highly attractive to be used as substrate for wide and ultra-wide bandgap devices such as GaN or Ga₂O₃, either integrating polycrystalline diamond substrates by growth on the backside for example of a GaN devices (replacing its original Si substrate), integration using wafer bonding, or by growing active semiconductor devices such as Ga₂O₃ epitaxial device layers on top of diamond substrates. The latest developments in this field will be discussed, including approaches to assess device temperature and thermal conductivity of materials in this new technology.

For your remarks

Defect formation mechanisms and 2-DEG isolation induced by low- energy Ar, C, Fe ion implantation of $\text{Al}_{0.2}\text{Ga}_{0.8}\text{N}/\text{GaN}$ heterostructure

Antonino Scandurra^{1,2,3}, Paolo Ragonese¹, Cristiano Calabretta⁴, Khadisha Zahra⁵, Liam Soomary⁵, Fabrizio Roccaforte⁶, Giuseppe Greco⁶, Nicolò Piluso⁴, Maria Eloisa Castagna⁴, Ferdinando Iucolano⁴, Andrea Severino⁴, Elena Bruno^{1,2}, Salvo Mirabella^{1,2}

¹*Department of Physics and Astronomy "Ettore Majorana", University of Catania, via Santa Sofia 64, 95123 Catania, Italy*

²*Institute for Microelectronics and Microsystems of National Research Council of Italy (CNR-IMM, Catania University Unit), via Santa Sofia 64, 95123 Catania, Italy*

³*Research Unit of the University of Catania, National Interuniversity Consortium of Materials Science and Technology (INSTM-UdR of Catania), via S. Sofia 64, 95125 Catania, Italy;*

⁴*STMicroelectronics, Stradale Primosole 50, 95121 Catania, Italy*

⁵*Kratos Analytical Ltd, A Shimadzu Group Company, Wharfside, Trafford Wharf Road, Manchester, M17 1GP, UK*

⁶*Consiglio Nazionale delle Ricerche – Istituto per la Microelettronica e Microsistemi (CNR-IMM), Ottava Strada, 5 (Zona Industriale) - 95121 Catania (CT) Catania, Italy*

Email: Antonino.scandurra@dfa.unict.it

The defect creation and evolution in GaN produced by low-energy ion implantation are based on complex phenomena, still far to be fully understood. Two-dimensional electron gas (2- DEG) isolation by ion implantation is a process showing better performances than mesa isolation in terms of planarity and gate leakage current. In this contribution we report a comparative study of defects formation and isolation mechanisms of 2-DEG in $\text{Al}_{0.2}\text{Ga}_{0.8}\text{N}/\text{GaN}$ heterostructure by Ar, C or Fe ion implantation at room temperature. A time and cost-saving methodology has been employed [1]. The implants were done at 15, 20, 18 keV and fluences of 7×10^{13} , 1×10^{14} , $5 \times 10^{13} \text{ cm}^{-2}$, respectively. The experimental conditions for an effective and stable electrical isolation of $\text{Al}_{0.2}\text{Ga}_{0.8}\text{N}/\text{GaN}$ 2-DEG will be described in details. The thermal stability of the isolation was studied up to 900 °C by Rutherford Backscattering Spectrometry in Channeling mode, Photoluminescence, X-ray Diffraction, X- ray Photoelectron Spectroscopy and Capacitance Voltage profiling. The main effects of ion implantation were the thermally stable increase of the crystal lattice parameters, the formation of vacancies, non-radiative carrier traps at the GaN band edge and interstitial defects. As a result, a decrease in the number of occupied states in the lower side of the GaN valence band was observed. Furthermore, the diffusion of defects towards the surface by annealing at 900°C was observed. Due to the presence of the various defects, we estimated, using the capacitance-voltage profiling by mercury probe technique, that the concentration of the 2-DEG carrier, after ion implantation, is reduced from 10^{20} - 10^{21} to less than 10^{13} - 10^{14} cm^{-3} , after annealing at 900 °C for all the examined ions. The isolation of 2-DEG can be attributed to the significant carrier concentration reduction of the 2-DEG. We demonstrate that implantation of Ar, C, or Fe ions produces stable isolation up to 900 °C.

Reference:

- [1] A. Scandurra, M. Testa, G. Franzò, G. Greco, F. Roccaforte, M. E. Castagna, C. Calabretta, A. Severino, F. Iucolano, E. Bruno, S. Mirabella, Isolation of bidimensional electron gas in AlGaN/GaN heterojunction using Ar ion implantation, *Mater. Sci. Semicond.* **2023**, 168, 107871, <https://doi.org/10.1016/j.mssp.2023.107871>

For your remarks

Optical and electrical characteristics of the Fe_{Ga} defect in dilute Al_xGa_{1-x}N alloys

L.J. Sun^{1*}, P. Kruszewski², V.P. Markevich¹, A.R. Peaker¹, I.F. Crowe¹, J. Plesiewicz²,
 P. Prystawko², D. Binks¹, M.P. Halsall¹

¹ Photon Science Institute and Department of Electrical and Electronic Engineering,
 The University of Manchester, Manchester M13 9PL, United Kingdom

² Institute of High Pressure Physics, Polish Academy of Sciences, 01-142 Warsaw, Poland

Email: 1ijie.sun-3@postgrad.manchester.ac.uk

Both impurity-related and native lattice defects, which act as carrier traps or recombination centers, can play a pivotal role in influencing the performance and reliability of GaN/AlGaN devices. Therefore, identifying the properties and origin of such defects in actual devices is important [1]. Iron (Fe) is a ubiquitous impurity in the nitride family when grown by metal-organic vapor phase epitaxy (MOVPE). In this work, the properties of the Fe_{Ga} defect in high-quality dilute Al_xGa_{1-x}N samples grown by MOVPE on conductive native ammono-GaN substrates have been studied. The Al_xGa_{1-x}N (0 < x < 0.063) samples have been characterized using a combination of deep-level transient spectroscopy (DLTS), high-resolution Laplace DLTS (L-DLTS) and low-temperature photoluminescence (PL) spectroscopy.

In the conventional DLTS spectra, the E3 electron emission signal, assigned to an Fe_{Ga} acceptor level [2], shifts to higher temperatures (higher activation energy for electron emission) as Al content increases in the Al_xGa_{1-x}N samples. By using L-DLTS, the E3 signal in Al_xGa_{1-x}N is found to split into individual components, which is attributed to fluctuations in Al concentration within the second-nearest neighbor (2NN) shell around the Fe_{Ga} impurity atoms (Fig. 1a). The probabilities of there being a specific number of aluminum atoms in the 2NN shell of the Fe_{Ga} defect, calculated based on their being randomly distributed, align closely with experimental concentrations determined from L-DLTS peak intensities (Fig. 2). Furthermore, our findings demonstrate that the energy level of the Fe_{Ga} acceptor, with no Al atoms in the 2NN shell, shifts linearly with the Al concentration. This shift, relative to the corresponding energy level in GaN, was found to be +28 and +55 meV for samples with x = 0.025 and 0.05, respectively (Fig. 1b) [3].

It is observed that the position, shape and relative intensities of the PL peaks, related to the Fe_{Ga}(0/-) defect level, change with Al concentration (Fig. 3). The relative intensities of the PL peaks associated with different numbers of Al atoms in the 2NN shell, around the Fe_{Ga} defect are found to be consistent with a random distribution of Al and Fe atoms in these samples. The variation of the PL intensity with excitation energy has been used to determine the positions of the Fe_{Ga} acceptor levels relative to the valence band. It is further found that the alloying in dilute Al_xGa_{1-x}N does not significantly influence the Fe internal 3d-3d transition $^4T_1(G) \rightarrow ^6A_1(S)$ as evidenced from the lack of any significant shift in energy of the peak due to this transition in the PL spectra with Al content (Fig. 3).

References:

- [1] M. Meneghini et al. J. Appl. Phys. 130, 181101 (2021).
- [2] M. Horita, T. Narita, T. Kachi, and J. Suda. Appl. Phys. Express 13, 071007 (2020).
- [3] P. Kruszewski et al, Appl. Phys. Lett. 123, 222105 (2023)

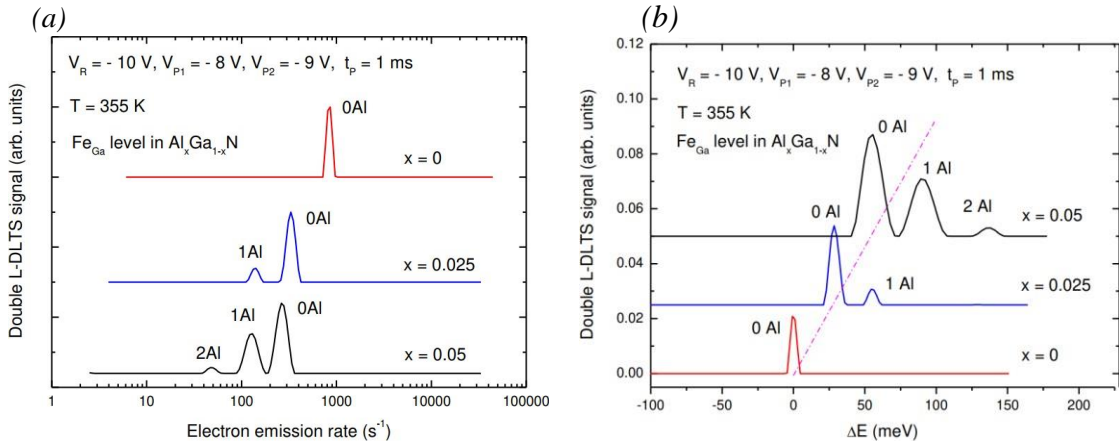


Figure 1: The Laplace DLTS spectra, which show (a) the electron emission signals due to Fe_{Ga} in $\text{Al}_x\text{Ga}_{1-x}\text{N}$ alloys with $x \leq 0.05$, (b) changes in electron emission energies from the Fe_{Ga} acceptor states in $\text{Al}_x\text{Ga}_{1-x}\text{N}$ ($x \leq 0.05$) samples relative to that in the GaN sample with no Al.

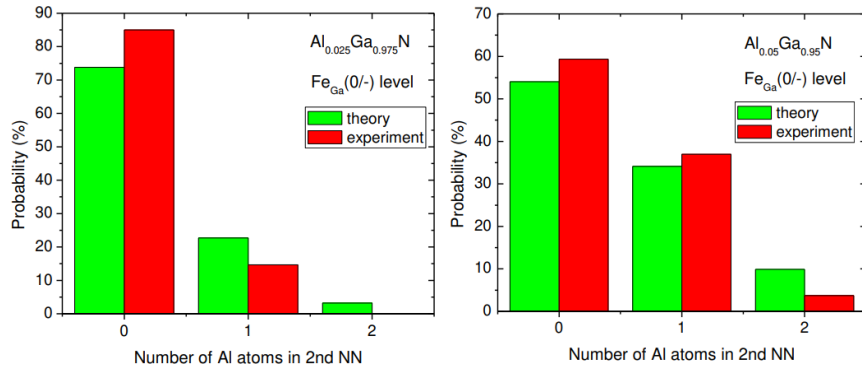


Figure 2: The green bars show probabilities of finding a given number of aluminum atoms in the 2NN shell of the Fe_{Ga} defect for the random distribution of Al in $\text{Al}_x\text{Ga}_{1-x}\text{N}$ samples having $x = 0.025$ (left side) and $x = 0.05$ (right side), respectively while red bars are experimental probabilities determined from L-DLTS peaks intensities.

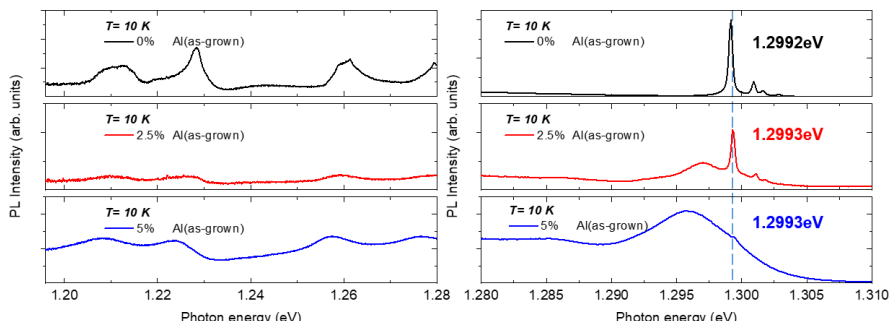


Figure 3: The PL spectra, which show emission lines associated with the Fe_{Ga} defect, in $\text{Al}_x\text{Ga}_{1-x}\text{N}$ samples with x equal to 0, 0.025 and 0.05.

Direct investigation of localized leakage currents in GaN on sapphire pin diodes with respect to structural defects and conduction mechanisms

Alexander D. Kinstler,^{1,2} Richard Neumann², Sven Besendörfer³, Elke Meissner^{1,3}, Frank Brunner⁴, Eldad B. Treidel⁴, and Jörg Schulze^{1,3}

¹ Friedrich-Alexander-Universität Erlangen-Nürnberg, Cauerstraße 6, 91058, Erlangen, Germany

² Infineon Technologies AG, Am Campeon 1-15, 85579 Neubiberg, Germany

³ Fraunhofer Institute for Integrated Systems and Device Technology IISB, Schottkystr. 10, 91058 Erlangen, Germany

⁴ Ferdinand-Braun-Institut gGmbH, Leibniz-Institut für Hochstfrequenztechnik, Gustav-Kirchhoff-Straße 4, 12489 Berlin, Germany

Email: alexander.kinstler@infineon.com

Literature currently has a limited understanding of localized leakage currents in gallium nitride (GaN) devices. Some groups seem to have identified responsible leakage mechanisms, others, the structural defects along which these currents flow [1-5]. Though few groups agree with one another, most have shown that dislocations are involved. This lack of understanding makes it difficult to understand and optimize performance and reliability issues in GaN devices [6].

One of the main challenges in determining the dominant leakage mechanisms and structural defects is the experimental methodology. All heteroepitaxial GaN devices are expected to contain structural defects, making an “ideal” reference for systematic comparison nearly unobtainable.

Our approach hinges on a design of GaN on sapphire pin diode that allows for direct comparison of device behavior and the presence of structural defects [7]. With a dislocation density in the range of 10^8 cm^{-2} , diodes with a diameter of 50 μm contain a large number of dislocations, however not all dislocations act as strong leakage sources and consequently impact device reliability [8]. It was therefore possible to obtain diodes with and without localized leakage currents, as seen in the electroluminescence images of fig. 1.

The dynamic IV measurements in fig. 2 record the response these leakage currents have to changes in electrical field and temperature, to which each conduction mechanism responds uniquely, revealing the mechanisms active in the diodes.

A combination of transition electron microscopy, electron channeling contrast imaging, and/or deep level transient spectroscopy provides further understanding of the structural defects over which the conduction mechanisms provide these localized leakage currents.

The measurements presented in this work enhance our understanding of localized leakage currents in GaN devices. By adopting a direct comparative approach in the optical and electrical measurements, we can more directly address the mechanisms and defects behind these localized leakage currents.

References:

- [1] D.V. Kuksenkov, et al., *Appl. Phys. Lett.*, **1998**, v. 72, n. 11, p. 1365–1367.
- [2] Y. Zhang, et al., *2015 IEEE International Electron Devices Meeting (IEDM)*, **2015**, p. 35.1.1
- [3] T. Hamachi, et al., *Scientific Reports*, **2023**, v. 13, n. 1, p. 2436.
- [4] Y. Ishikawa, et al., *Journal of Materials Science*, **2023**, v. 58, n. 22, p. 9221–9232.
- [5] T. Narita, et al., *2023 IEEE International Reliability Physics Symposium (IRPS)*, **2023**, p. 1–10.
- [6] M. Meneghini, et al., *Journal of Applied Physics*, **2021**, v. 130, nr. 18, p. 181101.
- [7] E. Brusaterra, et al., *IEEE Electron Device Letters*, **2023**, v. 44, n. 3, p. 388-391.
- [8] S. Besendörfer, E. Meissner, and J. Friedrich, *Appl. Phys. Express*, **2022**, 15, 95502.

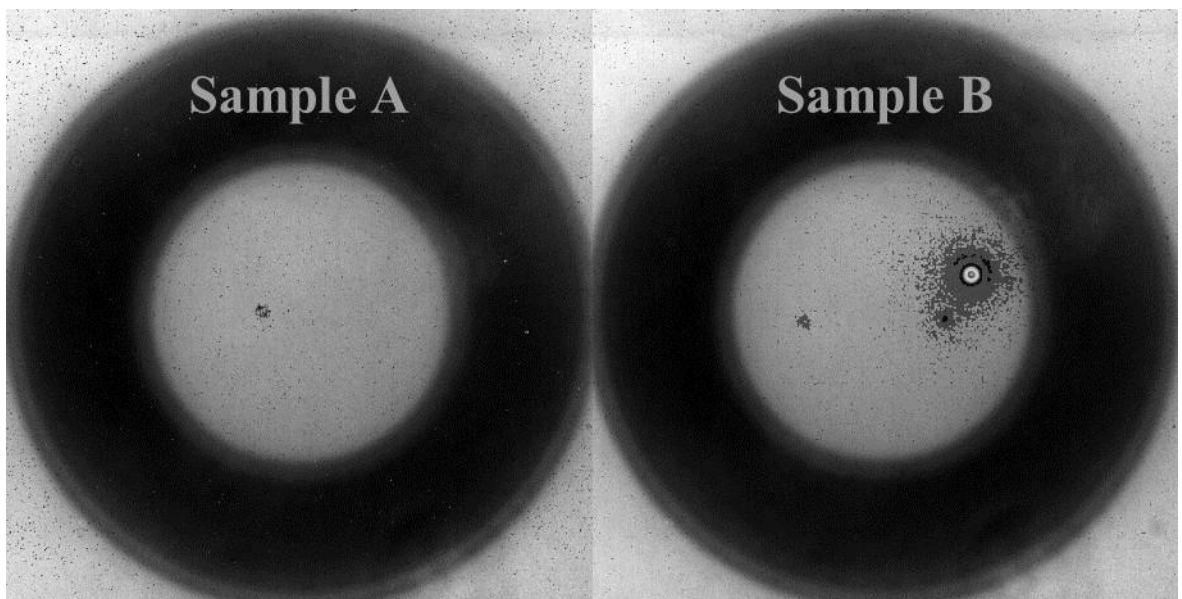


Fig. 1. Electroluminescence images of GaN on sapphire pin diodes under 300 V reverse bias showing an absence (left) and presence (right) of localized leakage currents.

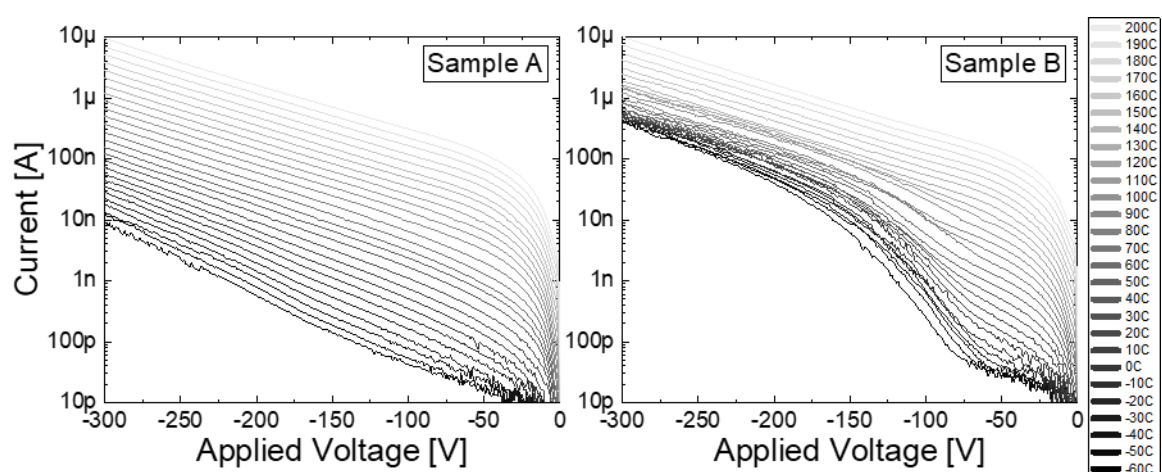


Fig. 2. IV curves in reverse bias of the diodes from fig. 1 over a temperature range from -60°C to 200°C showing the influence of localized leakage currents on device behaviour.

A novel deep acceptor in GaN

Stefan Schmult,¹ Steffen Wirth,² Andreas Großer,³ and Thomas Mikolajick^{1,3}

¹ TU Dresden, Institute of Semiconductors and Microsystems, Nöthnitzer Str. 64, 01187 Dresden, Germany

² Max-Planck-Institute for Chemical Physics of Solids, Nöthnitzer Str. 40, 01187 Dresden, Germany

³ Namlab gGmbH, Nöthnitzer Str. 64 a, 01187 Dresden, Germany

Email: stefan.schmult@tu-dresden.de

The presence of a hitherto undiscovered deep acceptor in GaN grown by molecular beam epitaxy (MBE) is reported. In ultra-pure GaN/AlGaN stacks (residual donor impurity level below 10^{17} cm^{-3}) hosting a 2-dimensional electron gas (2DEG), this deep acceptor limits the low-temperature electron mobility. Historically, the main factor limiting the 2DEG mobility is considered to be large angle Coulomb scattering on threading dislocations in the grown GaN/AlGaN stack [1]. By analyzing the transport and quantum life times in a 2DEG grown on dislocation-lean bulk GaN it was found that the 2DEG electron mobility is indeed limited by large angle scattering [2], which, however, cannot be accounted for by the low density of threading dislocations. A rough estimate on the concentration of the novel deep acceptor suggests a density around 10^{17} cm^{-3} .

On the other hand, this yet undisclosed defect leads to the absence of a 2DEG in ultra-pure GaN/AlGaN heterostructures with low aluminum mole fraction in dark environment. This behaviour can be explained by Fermi level pinning deep inside the band gap, which discloses important information about the binding energy of this defect [3].

Deep acceptors in GaN – such as carbon - contribute to a luminescence band around 2.2 eV, known as yellow luminescence (YL). In low-temperature cathodoluminescence (CL) investigations with high spatial resolution it was found, that one YL band is also present in intrinsic GaN. In carbon-doped material, on the other hand, 2 types of YL are found, separated by 120 meV (Fig. 1) [4]. This implies that this novel defect has a similar binding energy as carbon, but is also present in practically carbon-free GaN. The presentation reviews the current results and understanding.

References:

- [1] M. J. Manfra, S. Simon, K. W. Baldwin, A. M. Sergent, K. W. West, R. J. Molnar, and J. Cassie, Appl. Phys. Lett. **85**, 2004, 5278.
- [2] L. Krückeberg, S. Wirth, V.V. Solovyev, A. Großer, I.V. Kukushkin, T. Mikolajick and S. Schmult, J. Vac. Sci. Technol. B **38**, 2020, 042203.
- [3] T. Scheinert, T. Mikolajick, and S. Schmult, AIP Advances **9**, 2019, 125018.
- [4] S. Schmult, H. Schürmann, G. Schmidt, P. Veit, F. Bertram, J. Christen, A. Großer, T. Mikolajick, J. Cryst. Growth **586**, 2022, 126634.

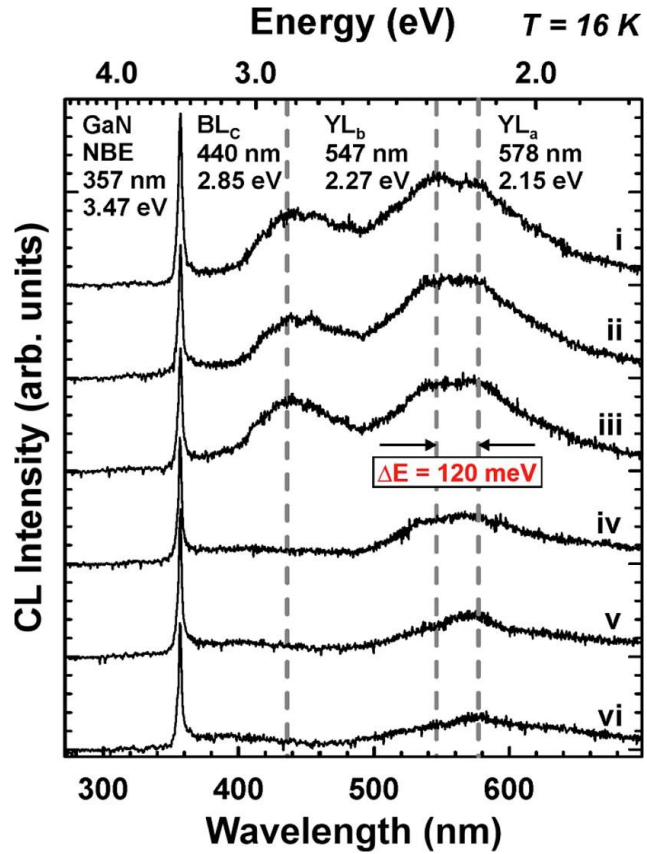


Fig. 1. Low-temperature cathodoluminescence spectra recorded from carbon-doped GaN grown by MBE (i - iii) and intrinsic GaN (iv - vi). In both layers one YL band at 2.15 eV is visible, while an additional band at 2.27 eV is clearly seen only in the carbon-doped GaN. The origin of both bands are transitions between donor and deep acceptor levels. Thus a hitherto undiscovered deep acceptor with a binding energy similar to that of carbon was revealed (adopted from [4]).

Investigation of dislocations introduced in Si wafers during flash lamp annealing by means of photoluminescence (PL) and μ -PL spectroscopy

D. Ryzhak,¹ G. Kissinger¹, A. Ehlert², A. Sattler², D. Spirito¹ and D. Kot¹

¹IHP – Leibniz-Institut für innovative Mikroelektronik, Im Technologiepark 25, 15236 Frankfurt (Oder), Germany

²Siltronic AG, Einsteinstraße 172, 81677 München, Germany

Email: ryzhak@ihp-microelectronics.com

Understanding defects in silicon (Si) is essential for Si-based semiconductor technology. Especially dislocations are crucial for engineering of advanced microelectronic devices and optimizing multi-crystalline Si for improvement of solar cell efficiency[1]. Dislocation-related recombination[2] and luminescence (D-lines) in Si have been investigated since decades[3,4]. In spite of many investigations, the origin of all D-lines is still not well understood.

In our study, dislocations were generated in Si wafers during flash lamp annealing at temperatures close to the melting point for 20 ms. Details of sample preparation are described in ref.[5]. The dislocation density was determined after Secco etching. Optical microscopy pictures of wafer surfaces with different densities of dislocations are shown in Fig.1 (a,b,c). In the PL spectra (Fig.1 d,e,f) from wafers with different defect densities, the presence of band-to-band (BB), BB Phonon Replica (BBPR), Boron dopant at 1.078eV[6], and sub-band-gap emissions (D-lines) were detected. The latter ones were identified as the previously mentioned D1, D2, D3, and D4 lines. All peak positions, despite of different defect densities, remain nearly constant. PL intensities of D1 and D2 rapidly decrease with decreasing dislocation density, in contrast to D3 and D4 as shown in Fig.1. The strong dependences of the lines D1 and D2 on the dislocation density could assign their origin to secondary defects generated in the vicinity of dislocations[7]. We also measured a single dislocation with micro-PL at 5 K (Fig.3). The D1 and D2 lines, indicative of secondary defects, are prominently observed in macro PL (Fig.1 d), but become almost imperceptible under micro-PL's finer focus (Fig.3), suggesting that these defects are relatively sparse and non-localized within the Si lattice, in contrast with the D4 and D3 lines. In conclusion, our study highlights the intricate relationship between dislocation density and luminescence in Si, providing valuable insights for engineering Si-based semiconductor devices.

References:

- [1] H.J. Möller, C. Funke, D. Kreßner-Kiel and S. Würzner, *Energy Procedia*, 3 (2011), 2–12
- [2] M. Trempa, G. Müller, J. Friedrich and C. Reimann, in *Handbook of Photovoltaic Silicon*, ed. by Deren Yang (Berlin, Heidelberg: Springer, 2018), pp. 1–48
- [3] Martin Kittler and Manfred Reiche, in *Crystalline Silicon - Properties and Uses*, ed. by Sukumar Basu (InTech, 2011)
- [4] V. Higgs, Edward C. Lightowers, Carl E. Norman and P. Kightley, *Materials Science Forum*, 83–87 (1992), 1309–14
- [5] G. Kissinger, D. Kot, M. A. Schubert and A. Sattler, *ECS Journal of Solid State Science and Technology*, 4.7 (2015), P195–99
- [6] AnYao Liu, H.T. Nguyen and D. Macdonald, *Physica Status Solidi (a)*, 213.11 (2016), 3029–32
- [7] H.T. Nguyen, F. E. Rougieux, F. Wang and D. Macdonald, *Energy Procedia*, 77 (2015), 619–25

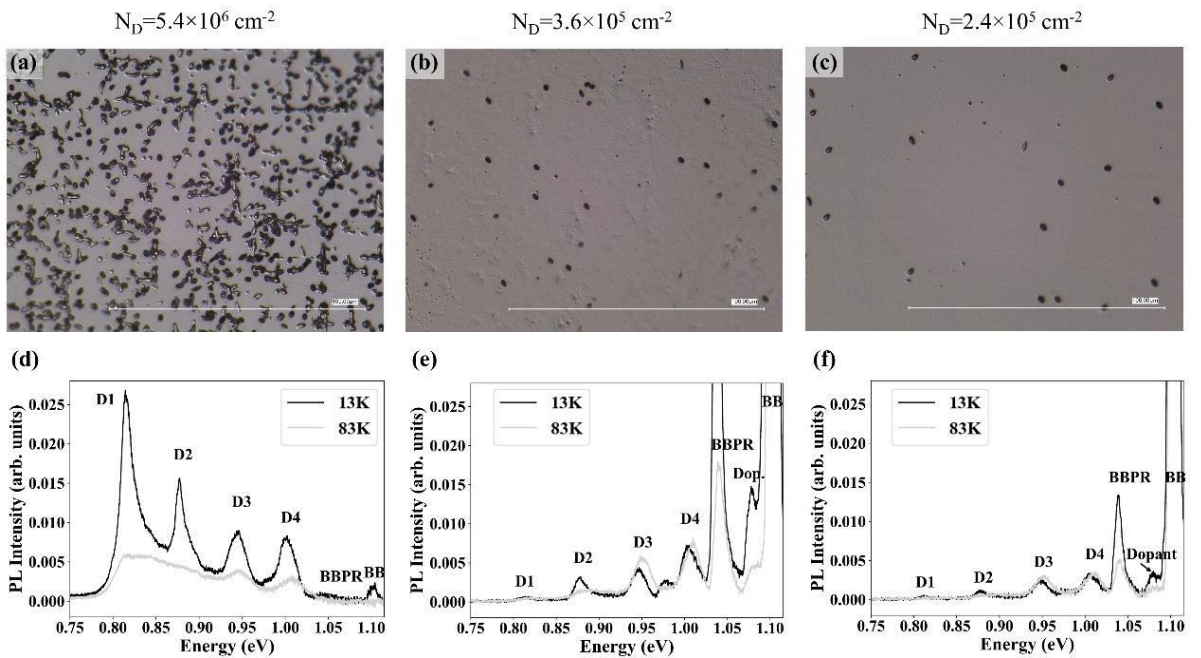


Fig. 1 Optical microscopy pictures (a,b,c) and macro PL spectra at 13 and 83K (d,e,f) of various density of dislocation a & d $N_D=5.4\times 10^6\text{ cm}^{-2}$, b & e $N_D=3.6\times 10^5\text{ cm}^{-2}$, and c & f $N_D=2.4\times 10^5\text{ cm}^{-2}$

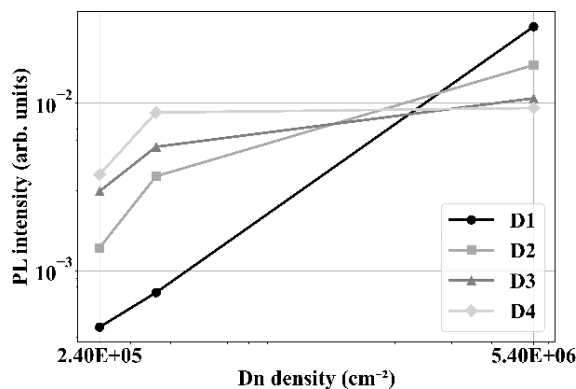


Fig. 2 PL intensity of D-lines for the different dislocation density.

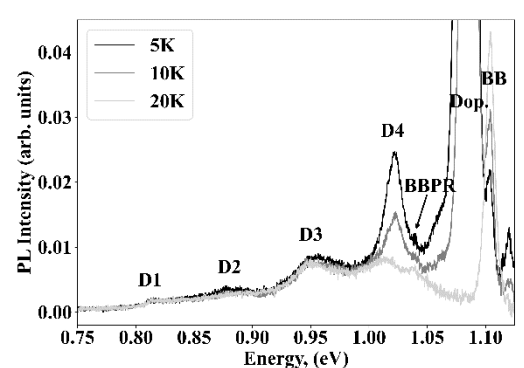


Fig. 3 Micro-PL spectra temperature dependence for $N_D=5.4\times 10^6\text{ cm}^{-2}$ sample dislocation

Influence of illumination spectrum on dissociation kinetic of iron-boron pairs in silicon

Oleg Olikh, Oleksandr Datsenko, Serhiy Kondratenko

Taras Shevchenko National University of Kyiv, 64/13, Volodymyrska Street, 01601, Kyiv, Ukraine

Email: olegolikh@knu.ua

The iron-boron pair is one of the most extensively examined defects in silicon. The complex's levels, carrier capture cross-sections, kinetic models, dissociation techniques, and even ultrasound influence on pairing have been established [1-3]. However, the exact mechanism underlying the second decay phase — iron ion recharge or a recombination-enhanced defect reaction (REDR) — remains debatable. We believe that investigation of the illumination spectrum impact on light-induced dissociation may reveal which proposed model is correct. An experimental study was undertaken to explore the efficiency of FeB pair dissociation in silicon solar cells (iron concentration of $8.7 \times 10^{12} \text{ cm}^{-3}$, doping level by boron of $1.4 \times 10^{15} \text{ cm}^{-3}$)

when different light sources are utilized. To achieve a varied illumination spectrum (see Fig.1), halogen lamps from three manufacturers — Orion, Osram, and General Electric (GE) — were used.

The characteristic time of FeB dissociation τ_{dis} was determined by measuring the dependence of the concentration of dissociated pairs on the illumination duration using a methodology referenced in [1]. It was observed that τ_{dis} was influenced not only by the light intensity W_{ill} and the carrier generation rate but also by the light source — see Table. It was found that as the photon wavelength decreases, the dissociation rate increases. Fig. 2 shows the average photon energy for different sources, correlating with the data in Table. The findings suggest that REDR is likely to be the dominant mechanism for pair decay.

References:

- [1] O. Olikh *et al.*, *J.Appl. Phys.* **2021**, *130*, 235703.
- [2] F. E. Rougieux, C. Sun, D. Macdonald, *Sol. Energy Mater. Sol. Cells* **2018**, *187*, 263.
- [3] C. Sun *et al.*, *Phys. Status Solidi RRL* **2021**, *15*, 2000520.

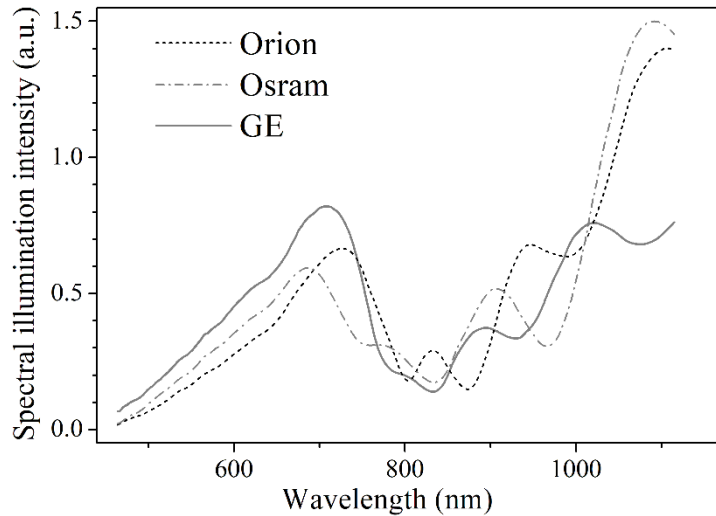


Fig. 1. The spectral composition of the sample illumination for different light sources, which is influenced by 1) the temperature of the filament; 2) the surface of the lamp reflector; and 3) the transmission characteristics of the optical fiber through which the illumination was conducted.

Table. The characteristic time of FeB dissociation for different illumination intensities and light sources

W_{ill} (mW)	τ_{dis} (s)		
	Orion	Osram	GE
200	42±3	20.0±0.7	15.1±0.5
300	15.7±0.6	12.4±0.1	6.5±0.2
400	8.8±0.3	6.1±0.3	3.6±0.3
500	5.5±0.2	4.5±0.2	
600	3.7±0.2	3.0±0.2	
700	2.4±0.2	2.4±0.2	

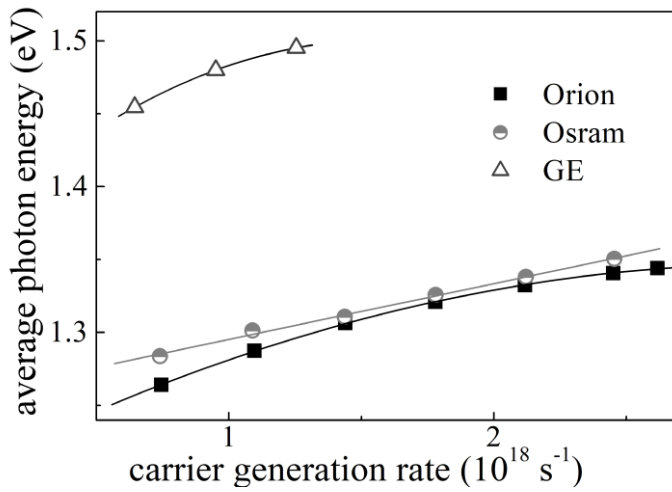


Fig. 2. Dependencies of the average photon energy on carrier generation rate for different light sources.

Point defect characterisation of proton irradiated *n*-type GaAs

Paul U. Feiler¹, Teimuraz Mchedlidze², Tobias Urban³ and Franziska C. Beyer¹

¹ Departement of Energy Materials and Test Devices, Fraunhofer Institute for Integrated Systems and Device Technology, Am Sankt Niclas Schacht 13, 09599 Freiberg, Germany

² Institute of Applied Physics, TU Bergakademie Freiberg, Leipziger Straße 23, 09599 Freiberg, Germany

³ 3-5 Power Electronics GmbH, Gostritzer Str. 61-63, 01217, Dresden, Germany

Email: Franziska.Beyer@iisb.fraunhofer.de

The characterisation of point defects in semiconductors has a long history and is mainly used to improve the device performance by increasing the carrier lifetime. However, for some applications a specifically designed defect structure is used to even improve device performance further, as lowering the carrier lifetime in a certain region of power devices [1] or even creating an isolation layer within doped material [2]. An appropriate option is to use protons for this purpose because the damage peak can be designed very narrow and in a wide depth range of several nm to up to 100 µm.

Deep level transient spectroscopy (DLTS) was used to characterize the effect of such a proton implantation on $\sim 2 \times 10^{14} \text{ cm}^{-3}$ Si-doped GaAs grown by MOVPE [3] on 4" GaAs substrate wafer with $1 \times 10^{18} \text{ cm}^{-3}$ n-type doping. Ohmic contact was realized by an alloy of AuGe/Ni/Ag/Ni (400 °C, 60 s) on rear side of the samples. The acceleration voltage was varied between 100 to 500 keV and fluence of $5 \times 10^{12} \text{ cm}^{-2}$ to $1 \times 10^{15} \text{ cm}^{-2}$ targeting the epi layer. Parts of the samples were covered during irradiation thus having reference diodes directly on the same sample piece. The Schottky contacts (alloy of Ti/Ni/Ag/Ni) with diameter of 500 µm were deposited on top of the irradiated and non-irradiated regions and the post irradiation annealing (200 °C-300 °C, 10 min) were performed in one sample series prior and the other after Schottky contact formation, thus the influence of the contact deposition can be studied as well.

DLTS spectra were recorded in the temperature range between 100 to 420 K, using -5 V reverse bias in combination with 4.8 V, filling pulse for 100 µs each, evaluating the traps for majority carriers. The well-known EL2 defect with $E_C - 0.8 \text{ eV}$, which is attributed to a complex involving the As antisite (As_{Ga}) [4], is detected in all samples, see Fig 1. The defect concentration is dominating compared to the second as-grown, shallow defect with $E_C - 0.4 \text{ eV}$ detected at 180 K on *n*-type GaAs, which may be attributed to is the EL6 defect, a combination of As_{Ga} and another point defect e.g. As-vacancy (V_{As}) [5-7]. The influences of the irradiation is seen by the appearance of irradiation induced defects besides the usually detected as-grown ones. The defect concentrations will be studied in dependence of the irradiation energy (100-300 keV) and doses ($5 \times 10^{12} \text{ cm}^{-2}$ - to $1 \times 10^{15} \text{ cm}^{-2}$).

This work is financially supported by the Federal Ministry for Economic Affairs and Climate Action (BMBK) within Central Innovation Programme for small and medium-sized enterprises with the grant "GaAs-IGBT" (KK5248102PR1).

References:

- [1] J. Lutz, H. Schlangenotto, U. Scheuermann, and R. Doncker, „*Semiconductor Power Devices*“ (Springer Berlin Heidelberg, Berlin, Heidelberg, 2011)
- [2] S. J. Pearton, *Materials Science Reports*, **1990**, 4, 313–363.
- [3] D. Lackner, T. Urban, R. Lang, C. Pellegrino, J. Ohlmann, and V. Dudek, *J. Cryst. Growth*, **2023**, 613, 127201.
- [4] H. J. von Bardeleben, D. Stiévenard, D. Deresmes, A. Huber, and J. C. Bourgoin, *Phys. Rev. B*, **1986**, 34, 7192–7202.
- [5] G. M. Martin, A. Mitonneau, and A. Mircea, *Electron. Lett.*, **1977**, 13, 191.
- [6] H. Shiraki, Y. Tokuda, and K. Sassa, *J. Appl. Phys.*, **1998**, 84, 3167–3174.
- [7] Ł. Gelczuk, J. Kopaczek, T. B. O. Rockett, R. D. Richards, and R. Kudrawiec, *Sci. Rep.*, **2017**, 7, 12824.

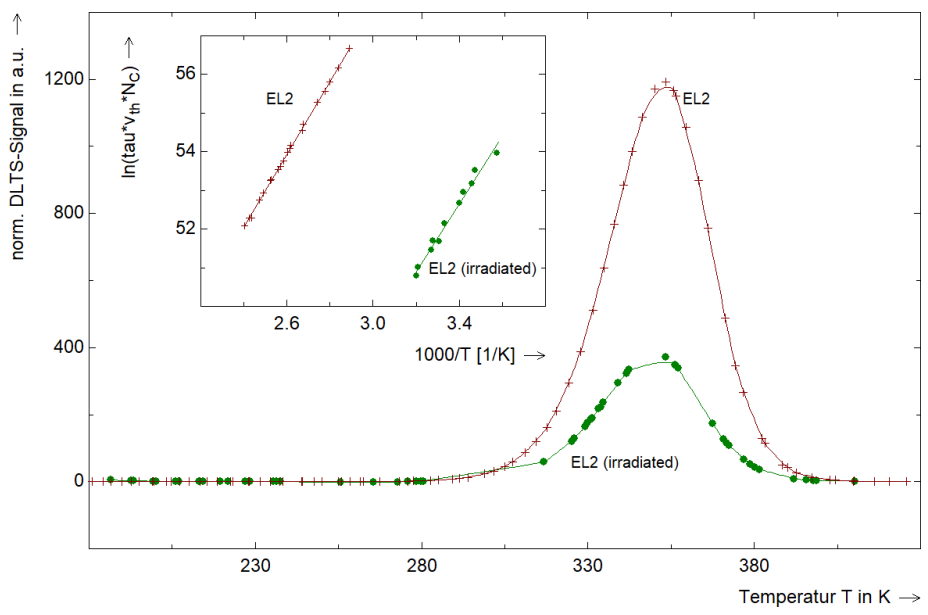


Fig. 1. Zoom of DLTS-spectra of *n*-GaAs with detection of the known EL2-level. The inset represents the Arrhenius plot of both DLTS curves for as deposit and irradiated *n*-GaAs.

In-situ observation of pressurized micro cracks in GaN

Blanco K.¹, Mazen F.¹, Colonel L.¹, Sediri A.¹, Giroud S.¹, Landru D.², Kononchuk O.²,
 Ben Mohamed N.², Rieutord F.²

¹CEA, LETI, MINATEC Campus, 17 rue des Martyrs, 38054 GRENOBLE Cedex 9, France.

²SOITEC, Parc Technologique des Fontaines, 38190 Bernin, France.

Email: katell.blanco@cea.fr

As a wide bandgap semiconductor, GaN is an interesting material in a broad range of applications such as for RF or high power electronic devices. Nowadays, most GaN substrates are epitaxially grown on a foreign substrate like SiC, sapphire or Si, with diameters up to 200mm. However due to the presence of thick buffers, used to manage stress and defects, and large thermal expansion mismatch in GaN heterostructures, major technical limitations still exist. The Smart Cut™ technology is a promising alternative to transfer thin GaN films onto another substrate that can be selected according to the targeted application or device [1]. This technology, used today to produce Silicon-On-Insulator (SOI) wafers, is based on implantation of light ions to create a buried damaged layer, formed by combination of point and extended defects and gas atoms. In silicon, upon annealing, these nano-sized defects grow to form pressurized micro cracks by capturing surrounding implanted atoms. A controlled fracture then occurs along the implanted layer at the wafer scale [2, 3]. In GaN, nanobubbles, assembled from vacancies clusters, were identified as the precursor nano-sized defects of the fracture [4] but the development and the growth mechanisms of these defects at the micrometre scale leading to the film exfoliation are still not understood.

In this work, we succeeded in characterizing the buried micro cracks in GaN, using confocal Infra-Red microscopy. To do so, structures of epitaxially grown GaN, implanted with light ions and bonded to silicon were designed to maximize the optical contrast linked to the buried defects (**Fig. 1**). It allowed us to obtain multiples images of micro cracks, recorded *in situ* during annealing, at different stages of their development, as shown in **Fig. 2**. Micro-cracks, detected when their diameter size is above 0.5 microns, grow during annealing until they reach a high surface coverage at the last stage before fracture. To investigate the growth mechanisms in GaN, we followed the evolution of micro cracks mean surface versus their density. It enables the comparison of micro cracks growths in materials with different annealing parameters, such as GaN and silicon. Micro cracks in both materials show similar evolution behaviour but in GaN, they reach bigger mean size at the final annealing stages (**Fig.3**). Thus, micro cracks in GaN and silicon grow with the same dominant mechanisms, which was experimentally shown to be coalescence events in silicon [3], but film exfoliation is triggered at different micro cracks maturation.

These experimental results give new insights on micro cracks growth mechanisms leading to the fracture in GaN and extend the validity of models, based on the mechanical analysis of pressurized penny-shaped micro cracks, established for silicon, to other materials.

References:

- [1] Guiot E., Caulmilone R., Baines Y., Frayssinet E., Cordier Y., *CS Mantech* **2018**.
- [2] Penot J.D., Massy D., Rieutord F., Mazen F., Reboh S., Madeira F., Capello L., Landru D., and Kononchuk O., *J. Appl. Phys.* **2013**, 114, 123513.
- [3] Colonel L., Mazen F., Landru D., Kononchuk O., Ben Mohamed N., Rieutord F., *Phys. Stat. Sol. A* **2021**, 218, 2100219.
- [4] Moutanabbir O., Chabal Y.J., Chicoine M., Christiansen S., Krause-Rehberg R., Shietekatte F., Scholz R., Seitz O., Senz S., Süsskraut F., Gösele U., *Nucl. Instrum. Methods Phys. Res. Sect B* **2009**, 267, 1264- 1268.

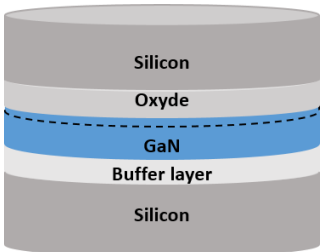


Fig. 1. Structure of epitaxially grown GaN on silicon, implanted with light ions and bonded on silicon. The dashed line represents the ions implantation depth, where the micro cracks are observed.

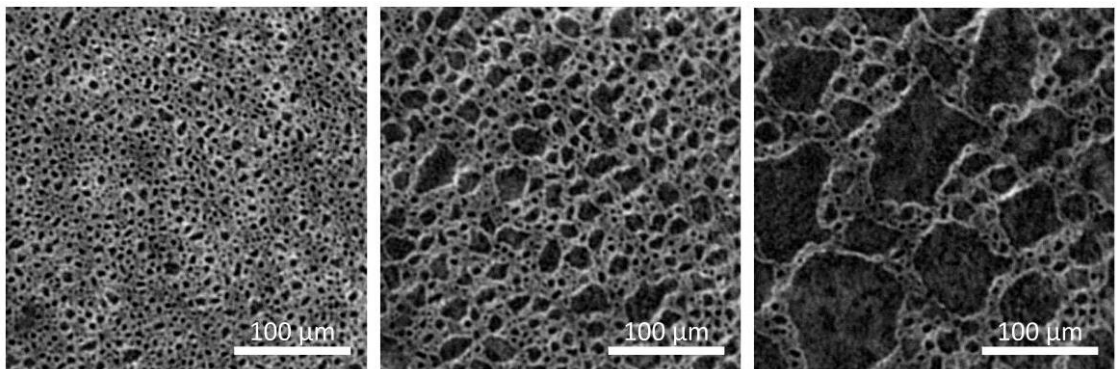


Fig. 2. In situ confocal infra-red microscopy images of micro cracks in GaN during annealing. Time runs from left to right.

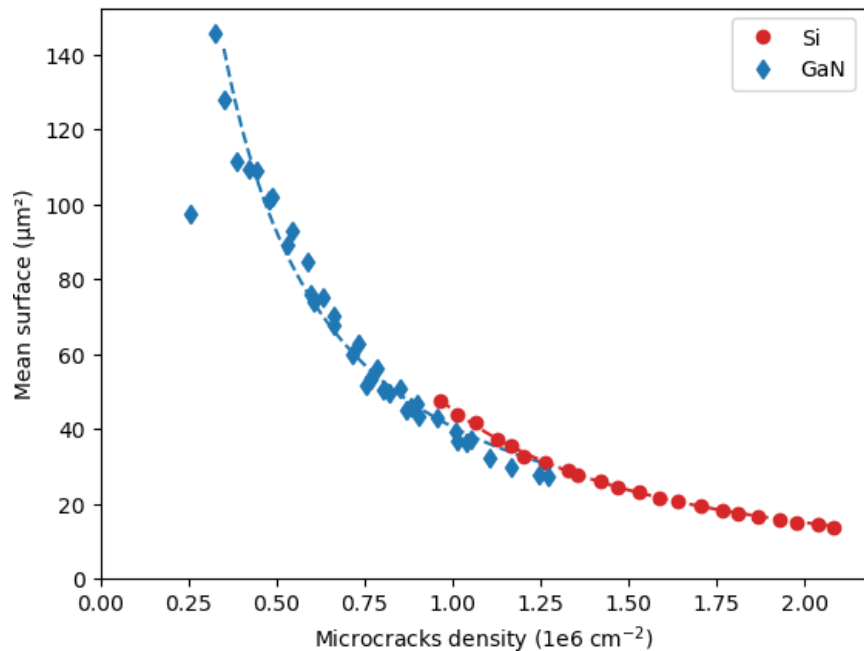


Fig. 3. Growth path of micro cracks in GaN and in silicon, starting from a high density of cracks with a small surface area (lower right corner) to a low density of larger cracks (upper left corner).

Experimental investigation of the interaction between structural defects and impurities in silicon for photovoltaic applications

Sirine Houam¹, Hadjer Ouaddah¹, Gabrielle Regula¹, Isabelle Périchaud¹, Guillaume Reinhart¹, Marisa Di Sabatino Lundberg², Lasse Vines³, Mathieu Silly⁴, Fabrice Guittonneau⁵, Laurent Barrallier⁵, Nathalie Mangelinck Noël¹

¹ Aix-Marseille Univ, Université de Toulon, CNRS, IM2NP, Marseille, France

² NTNU, Department of Materials Science and Engineering, Trondheim, Norway

³ University of Oslo, Department of Physics, Oslo, Norway

⁴ SOLEIL Synchrotron, CEA Paris-Saclay CNRS, Paris, France

⁵ Arts et Métiers Institute of Technology, MSMP, 2 cours des Arts et Métiers, 13617 Aix-en-Provence, France

Email: Sirine.houam@im2np.fr

During the fabrication of Si crystalline material for photovoltaic (PV) solar cells, several factors such as thermomechanical stresses, crucible and impurity contamination are at the origin of deformation, structural defects and impurity segregation [1,2] which can ultimately degrade the electrical properties.

In this work, we combine complementary structural, chemical and charge transport investigations that are respectively carried out by EBSD (Electron Backscattered Diffraction), SIMS (Secondary Ion Mass Spectrometry), FTIR (Fourier-Transform Infra-Red spectroscopy), PL (Photoluminescence) and SPV (Surface Photovoltage).

Correlating these techniques enables to better understand the strong dependence between structural defects, impurities and charge transport.

Figure 1 presents electrical and structural maps of the same region of a Si wafer characterised by the presence of sub-grain boundaries (sub-GBs). It can be seen that sub-GBs positions on the EBSD map (Figure 1 left) corresponds to high electrical recombination regions on the PL map (dark zones in Figure 1 right). Local higher recombination of excess electrical charges is thus directly related to the presence of these structural defects. Moreover, FTIR and μFTIR characterisations indicate that light impurities segregate preferentially at the level of the structural defects, forming micro-precipitates, whereas inside the grain, oxygen is predominantly found in interstitial position.

The experimental investigations conducted on Si material of several origin and with different levels of impurity contamination show how the presence of defects of different dimensions, from dislocation to grain size, influence the charge recombination in silicon, and consequently, degrade the solar cell quality and efficiency all the more as they interact with impurities.

References:

- [1] J. Huang *et al.*, Growth and Defects in Cast-Mono Si for Solar Cells: A Review, *physica status solidi (a)* (2022) 2200448.
- [2] K. Jiptner *et al.*, Thermal stress induced dislocation distribution in directional solidification of Si for PV application, *Journal of Crystal Growth* 408 (2014) 19.

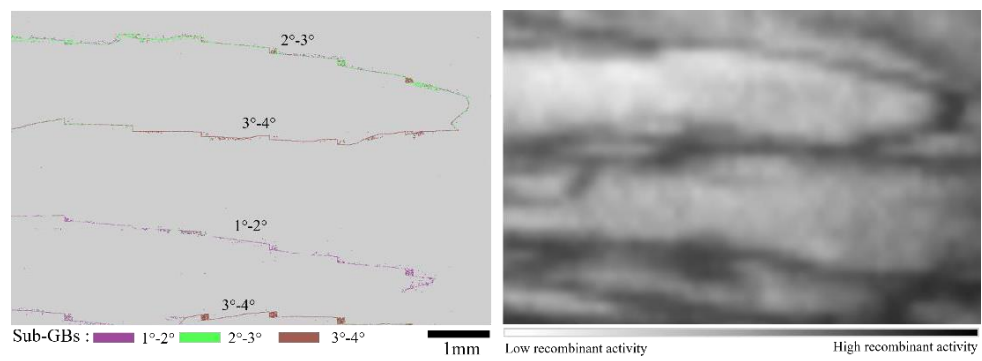


Fig. 1. Right: EBSD map. Left: Photoluminescence (PL) map of the same region.

I3 defects in hexagonal silicon germanium

M.F. Schouten,¹ W.H.J. Peeters¹, E. Scalise², A. Marzegalli², L. Miglio², L. Vincent³, F. Glas³, M.A. Verheijen¹, and E.P.A.M. Bakkers¹

¹ *Eindhoven University of Technology, De Groene Loper 19, 6512AP, Eindhoven, The Netherlands*

² *University of Milano Bicocca, Piazza dell'Ateneo Nuovo 1, 20126, Milano, Italy*

³ *Centre de Nanosciences et Nanotechnologies (C2N), CNRS, Univ. Paris-Sud, Université Paris-Saclay,, rue André Ampère, F91405 Orsay, France*

Email: m.f.schouten@tue.nl

Direct bandgap Group IV semiconductors are of general interest for the purpose of CMOS compatible photonics. In accordance to theoretical predictions, hexagonal silicon germanium alloys (hex-SiGe) have shown promising opto-electronic characteristics. Hex-SiGe nanowires have been realized using the crystal transfer method in which wurtzite gallium arsenide core nanowires are used as template for the epitaxial growth of hex-SiGe shells. Both core and shell are grown by Metal Organic Vapour Phase Epitaxy (MOVPE) [1].

In order to guarantee efficient optical activity, high crystal quality is required. The crystal quality is currently limited by the existence of I3 basal stacking faults, inserting a cubic layer in the otherwise hexagonal atomic stacking [2]. Ex-situ TEM analysis demonstrated that the cubic stacking is always bound by dislocation boundaries along the <11-20> directions. The cubic stacking of this so called “I3 defect” can occur in a triangular and elongated domain (Fig. 1) [2,3]. By means of in-situ TEM, a high-temperature-low-flux growth regime is identified, suitable for suppressing the nucleation of I3 defects [3]. Apart from nucleation, thermally activated back propagation of the I3 defect is suggested to explain the elongated shapes. The backpropagation mechanism is expected to be faster when using higher growth temperatures, which creates a trade-off with the reduced nucleation probability of I3 defects at high temperatures.

It is our challenge to increase understanding of the I3 defect behaviour. By experimental exploration of the growth parameter space, we aim to gain control of the crystal quality of hex-SiGe.

References:

- [1] E.M. Fadaly, et al., *Nature* **2020**, 580, 205-209.
- [2] E.M. Fadaly, et al., *Nano Letters* **2021**, 21, 3619–3625.
- [3] L. Vincent, et al., *Advanced Materials Interfaces* **2022**, 9.

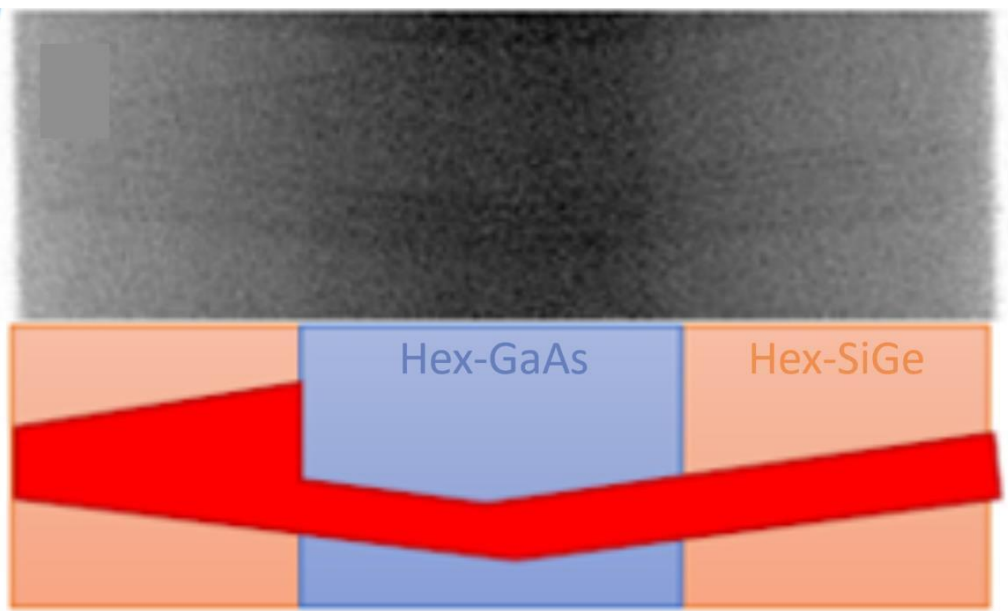


Fig. 1. TEM evidence of elongated defect shape I3 defect.

ALD-HfO₂ and ALD-SiO₂ as a Charge-lean Capping Layer Materials for Modulation Acceptor Doping of Silicon

Somayeh Shams,¹ Sourabh Seth,¹ Ingmar Ratschinski¹ and Daniel Hiller¹

¹*Institute of Applied Physics, Technical University Bergakademie Freiberg, Leipziger Straße 23, 09599, Freiberg, Germany*

Email: Daniel.Hiller@physik.tu-freiberg.de

Silicon nanowires (Si NWs) or nanosheets are the building blocks for future transistors but conventional impurity doping becomes increasingly inefficient for such ultra-small nanostructures. Impurity dopants require substitutional incorporation into the host lattice and subsequently ionization, which is typically accomplished by the thermal energy at room temperature. For nanostructures, however, both of these processes are impeded by e.g. confinement effects or the interaction with interface defects. Therefore, an alternative doping method is desirable that spatially separates the doping-induced free carriers from their parent dopant atoms.

In Ref. [1] we proposed modulation acceptor doping of silicon by using aluminum-induced acceptor states in an adjacent SiO₂ layer. Most recently, we demonstrated that modulation-doped Si NWs with Al-doped SiO₂-shells (SiO₂:Al) have several orders of magnitude lower electrical resistances than Si NWs with undoped SiO₂-shells [2,3]. The basic modulation doping stack just consists of a ~2 nm thick tunnel-SiO₂ coated with a few ALD cycles of Al₂O₃. Apparently, the conductivity of Si NWs that are modulation-doped with such stacks deteriorates over several days of storage time [2,3], which is attributed to the interaction with ambient air. Therefore, a capping layer is considered essential to protect the ultra-thin SiO₂:Al stack. On the other hand, the capping material should be charge-lean to avoid interactions with modulation doping mechanism.

Here, we present ALD-HfO₂ and ALD-SiO₂ thin films that were optimized for lowest fixed charge densities and sufficient electrical breakdown resistance. It will be shown that these ultra-thin capping layers extend the stability of the modulation-acceptors against ambient conditions.

References:

- [1] D. König et al., *Sci. Rep.* **2017**, *7*, 46703.
- [2] I. Ratschinski et al., *Phys. Status Solidi A* **2023**, *220*, 2300068.
- [3] S. Nagarajan et al., *Adv. Mater. Interfaces* **2024**, *11*, 2300600.

For your remarks

Shallow hydrogen-related donors after a dc H plasma treatment in Si

Katarzyna Gwozdz¹ and Vladimir Kolkovsky^{2,*}

¹*Department of Quantum Technologies Faculty of Fundamental Problems of Technology Wroclaw University of Science and Technology Wybrzeze Wyspianskiego 27, 50-370 Wroclaw, Poland*

²*Fraunhofer IPMS, EMT, Maria-Reiche Str. 2, 01109 Dresden, Germany*

Email: uladzimir.kalkouski@ipms.fraunhofer.de

Hydrogen is an abundant impurity in silicon wafers, easily introduced during various processing steps in the microelectronic industry. It diffuses at relatively low temperatures and interacts with various crystal imperfections, either passivating them or forming novel electrically active complexes. Despite numerous experimental studies investigating the electrical properties and origin of hydrogen-related defects in both n- and p-type Si, there are still several unanswered questions. In the present study, we analyse the electrical properties of shallow donors that arise after a dc hydrogen plasma treatment performed under broadband illumination. These defects were not observed after a dc H plasma treatment without illumination, and to our best knowledge, they were not previously reported in the literature. The concentration of the defects is maximal close to the surface and depends significantly on the oxygen concentration in Si samples. No traces of the defects were observed in Si samples with a C and O content below $5 \times 10^{15} \text{ cm}^{-3}$. The concentration of defects close to the surface reduces after an annealing step at around 350 K. We demonstrate that the defects are not correlated with COH defects observed at around 50-70 K as deep level transient spectroscopy peaks in the investigated samples. The origin of the defects will be discussed.

For your remarks

Surface photovoltage spectroscopy for evaluation of oxidation processes in the microelectronics industry

Vladimir Kolkovsky

Fraunhofer IPMS, EMT, Maria-Reiche Str. 2, 01109 Dresden, Germany

Email: uladzimir.kalkouski@ipms.fraunhofer.de

In the present study, the minority carrier diffusion length (MCDL), determined by surface photovoltage spectroscopy measurements, is compared in n- and p-type Si wafers after their oxidation under different conditions using various tools (horizontal and vertical furnaces, atomic layer deposition (ALD), low-pressure chemical vapor deposition, and plasma- enhanced chemical vapor deposition). We demonstrate that MCDL varies significantly depending on the design of furnaces, oxidation temperatures, the type of gases used before and during oxidation, and their flow ratios. The type and crystal growth method of Si wafers also play a significant role and influence MCDL. Additionally, we observed that MCDL after the deposition of alumina layers using atomic layer deposition (ALD) techniques is significantly larger compared to that observed after the thermal oxidation of Si. The larger values of MCDL after the ALD deposition of Al₂O₃ were detected independent of temperature and precursors used for the deposition. We discuss the origin of different MCDL values after various oxidation processes, with an emphasis on the formation of electrically active defects in Czochralski and Float-Zone grown Si wafers.

For your remarks

Spatially-Resolved Ion Beam Induced Phase Transition and Defect Analysis in Gallium Oxide

Umutcan Bektas¹, Maciej Oskar Liedke¹, Fabian Ganss¹, Nico Klingner¹, Rene Hübner¹,
Gregor Hlawacek¹

¹ Helmholtz-Zentrum Dresden-Rossendorf, Bautzner Landstraße 400, 01328, Dresden, Germany

Email: u.bektas@hzdr.de

Gallium Oxide (Ga_2O_3) is a promising ultra-wide bandgap semiconductor material that has garnered significant attention due to its easy large-scale production via melt growth and high breakdown voltage. Beta Ga_2O_3 is the most thermally and chemically stable polymorph among other polymorphs of Ga_2O_3 . Unfortunately, controlling and manufacturing other phases is immature due to the metastable structure of those phases.

Above a damage level (dpa), a polymorph conversion from the beta to gamma phase can be induced independent of the used primary ion species [1]. The formed polymorph is highly resistant against amorphization for very high damage levels up to 265 dpa. From the multi-species implantation experiments, we conclude that it is the induced strain by the defects and not the chemical nature of the implanted ions that drives the transition.

Here, we present a multi-method analysis approach to better understand and characterize the role of atomic defects before, during, and after the beta-to-gamma conversion. We use Helium Ion Microscopy (HIM) to locally irradiate Beta Ga_2O_3 substrate with Neon ions and create small structures to observe the resolution limit for phase conversion to gamma phase. Afterward, Transmission Electron Microscopy (TEM) is performed to observe the depth profile of the converted layer. We observed that with HIM, controlling and inducing well-defined gamma structure is possible at the nanoscale. Furthermore, broad beam irradiated samples are prepared for Positron Annihilation Lifetime Spectroscopy (PALS) and Doppler Broadening Variable Energy Positron Annihilation Spectroscopy (DB-VEPAS) to understand the defect structure during the phase transition. We see a reduction in defect concentration after the phase transition into the gamma phase, also changes in defect size depend on implanted ion fluence. This work is supported by the state of Saxony.

Reference:

- [1] A.Azarov, J.Fernandez, J. Zhao, Nature Communications **2023**, 14, 4855

For your remarks

Kinetics of carrier lifetime degradation in high-temperature 1 MeV electron-irradiated Cz n-Si associated with the formation of divacancy-oxygen defects

M. Kras'ko, A. Kolosiuk, V. Povarchuk and V. Voitovych

Institute of Physics of the NAS of Ukraine, 46 Nauki ave., 03028, Kyiv, Ukraine

Email: krasko@iop.kiev.ua

The study of the properties of radiation-induced defects in silicon is aimed at solving two main tasks: (i) increasing the radiation hardness and predicting the behavior of Si devices operating in radiation conditions (space, nuclear experiments, nuclear power and medicine); (ii) the use of these defects in device manufacturing technologies (for example, to control the minority carrier lifetime (τ) in Si power devices).

In Czochralski-grown (Cz) Si, the divacancy-oxygen (V_2O) are the dominant electrically active defects which are formed after high-dose irradiation [1] or after low-dose irradiation and subsequent annealing above 200 °C when a mobile V_2 is trapped by an interstitial O_i atom [2]. Recently [3], we found that in γ -irradiated Cz n-Si, τ decreases after annealing in the range 180–280 °C, and this effect is associated with the V_2O formation (Fig. 1a).

In this paper, the kinetics of τ degradation in 1 MeV electron-irradiated Cz n-Si was investigated at different temperatures in the range 20–285 °C: at 20 °C – the main introduced defects of VO and V_2 are stable; at 220 °C – VO remain stable while V_2 are transformed to V_2O ; at 270, 285 °C – VO are practically stable, and V_2O are already annealing. In addition to studying the recombination properties of V_2O , such studies are interesting because the simultaneous action of irradiation and high temperature does not lead to such an accumulation of defects as the sequential action of these factors [4].

It was established that changes in τ are qualitatively and quantitatively determined by the temperature of electron irradiation (Fig. 1b). Analysis of experimental data showed that the main mechanism of τ degradation in our experiment is the formation of recombinational active V_2O and VO (Fig. 2).

References:

- [1] Y.-H. Lee and J. W. Corbett, *Phys. Rev. B* **1976**, 13, 2653.
- [2] V.P. Markevich, A.R. Peaker, S.B. Lastovskii, L.I. Murin, and J.L. Lindström, *J. Phys.: Condens. Matter* **2003**, 15, S2779.
- [3] M. Kra'sko, A. Kolosiuk, V. Voitovych, and V. Povarchuk, *Phys. Status Solidi A* **2019**, 216, 1900290.
- [4] M.M. Kras'ko, A.G. Kolosiuk, V.B. Neimash, V.Yu. Povarchuk, I.S. Roguts'kyi, and A.O. Goushcha, *Journal of Materials Research* **2021**, 36, 1646

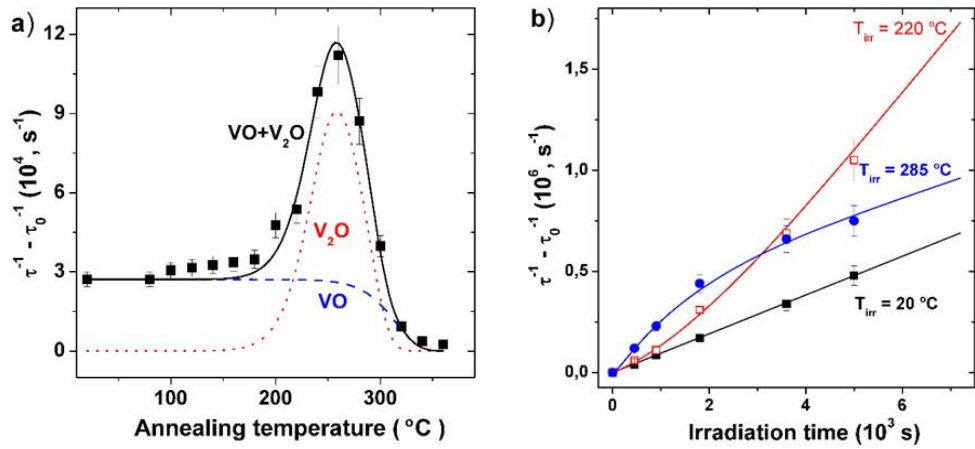


Fig. 1. **a)** Isochronal (20 min) annealing of carrier lifetime in Cz n-Si [$P \sim 1E15 \text{ cm}^{-3}$] after ^{60}Co γ -irradiation with a fluence of $7E14 \text{ cm}^{-2}$. τ_0 – the initial carrier lifetime, τ – the carrier lifetime in samples subjected to irradiation and subsequent annealing steps; **b)** Dependences of $1/\tau - 1/\tau_0$ on the irradiation time with 1 MeV electrons at different temperatures (τ – the carrier lifetime after irradiation). Symbols – experiment, lines – calculated Shockley-Read-Hall lifetime ($\Delta n \ll n_0$) for cumulative contribution of VO and V₂O.

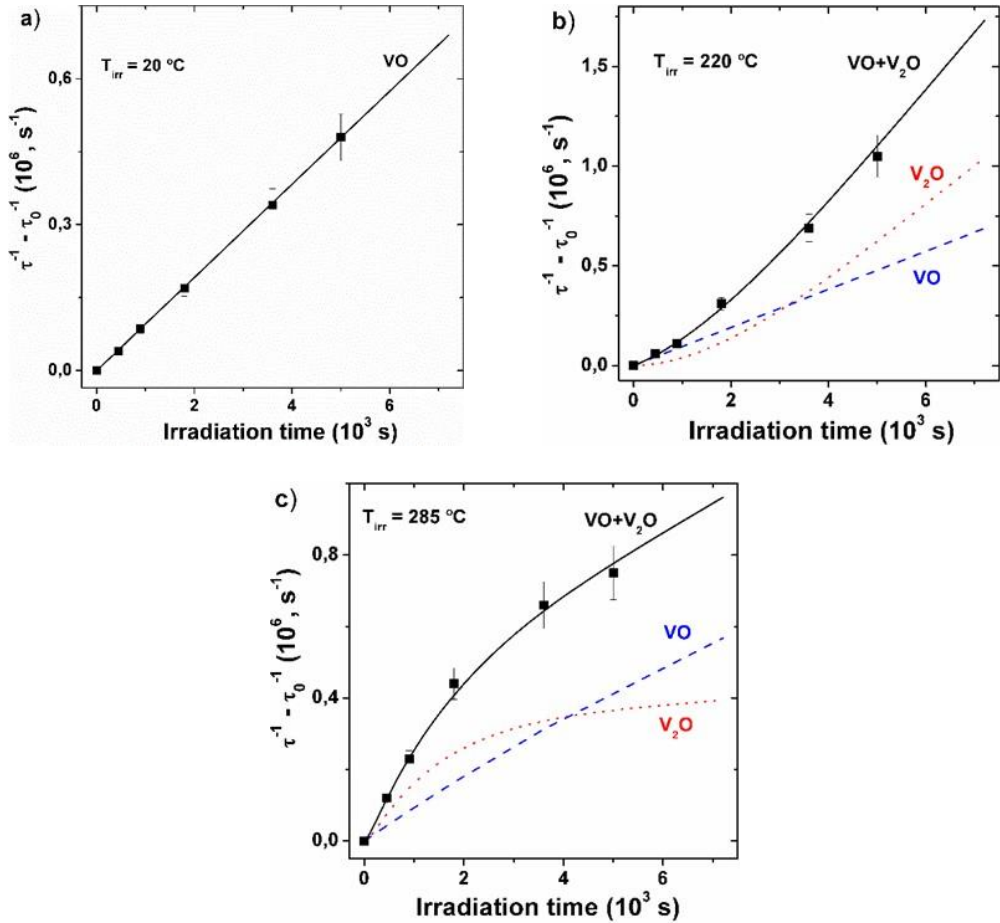


Fig. 2. Partial contributions of VO and V₂O in the degradation of carrier lifetime for the dependences in Fig. 1b. Symbols – experiment, lines – calculated Shockley-Read-Hall lifetime ($\Delta n \ll n_0$).

Efficient surface passivation of germanium by porous Ge layer

Mariia Terletskaya¹, Joonas Isometsä¹, Mikko Miettinen², Pekka Laukkanen², Ville Vähänissi¹, Hele Savin¹

¹ Aalto University, Tietotie 3, 02150, Espoo, Finland

² University of Turku, Vesilinnantie 5, 20014, Turku, Finland

Email: mariia.terletskaya@aalto.fi

Germanium (Ge) is considered a promising semiconductor material for optoelectronic applications in near-infrared (NIR) range. Since most of the applications are based on minority carriers, the amount of recombination active defects both in the bulk of the material and at the surfaces should be minimised. While the Ge bulk can be made of high quality, its surface passivation is more complicated. Indeed, plenty of efforts have been done to minimize surface recombination activity both on planar and textured Ge surfaces. [1-3] This research started with a surprising observation: our nanotextured Ge surface prepared by metal-assisted chemical etching (MACE) without any intentional passivation layer exhibited passivation comparable to state-of-the-art atomic layer deposited (ALD) Al₂O₃ [2] (Fig.1a). This result triggered us to study whether such MACE solution could be used for surface passivation. Investigation of the influence of the MACE solution components on Ge showed that HF:H₂O₂ mixture diluted with water clearly formed a film on the surface, which, based on the minority-carrier lifetime measurements, provided excellent passivation (Fig 1a). To study the composition and structure of this film, we carried out X-ray photoelectron spectroscopy (XPS) and scanning electron microscopy (SEM). In case of original MACE solution, XPS revealed the presence of GeO₂ (Fig. 1b) known to provide low interface defect density but simultaneously being unstable and water-soluble [1, 3]. Meanwhile, XPS for the modified solution surprisingly indicated the presence of GeO_x which has tendency to form defective GeO_x/Ge interface [5, 6]. Based on SEM the film possessed a sponge-like structure, which was possibly composed of porous germanium (PGe) [4] and GeO_x. Finally, the structure was shown to retain stable passivation performance for at least several days (Fig. 2). Thus, the modified MACE solution could be considered as a potential method for Ge surface passivation, although the exact mechanisms require further studies.

References:

- [1] W.J.H. Berghuis, J. Melskens, B. Macco, et al., *Journal of Materials Research* **2021**, 36, 571–581.
- [2] J. Isometsä, T. H. Fung, T. P. Pasanen, et al., *APL Materials* **2021**, 9.
- [3] T. H. Fung, J. Isometsä, J.-P. Lehtio, et al., *Nanotechnology* **2023**, 34.
- [4] T. Hanuš, J. Arias-Zapata, B. Ilahi, et al., *Adv. Mater. Interfaces* **2023**, 10.
- [5] J. Isometsä, Z. J. Rad, T. H. Fung, et al., *Crystals* **2023**, 13, 667.
- [6] L. Zhou, X. Wang, X. Ma, et al., *Semicond. Sci. Technol.* **2018**, 33.

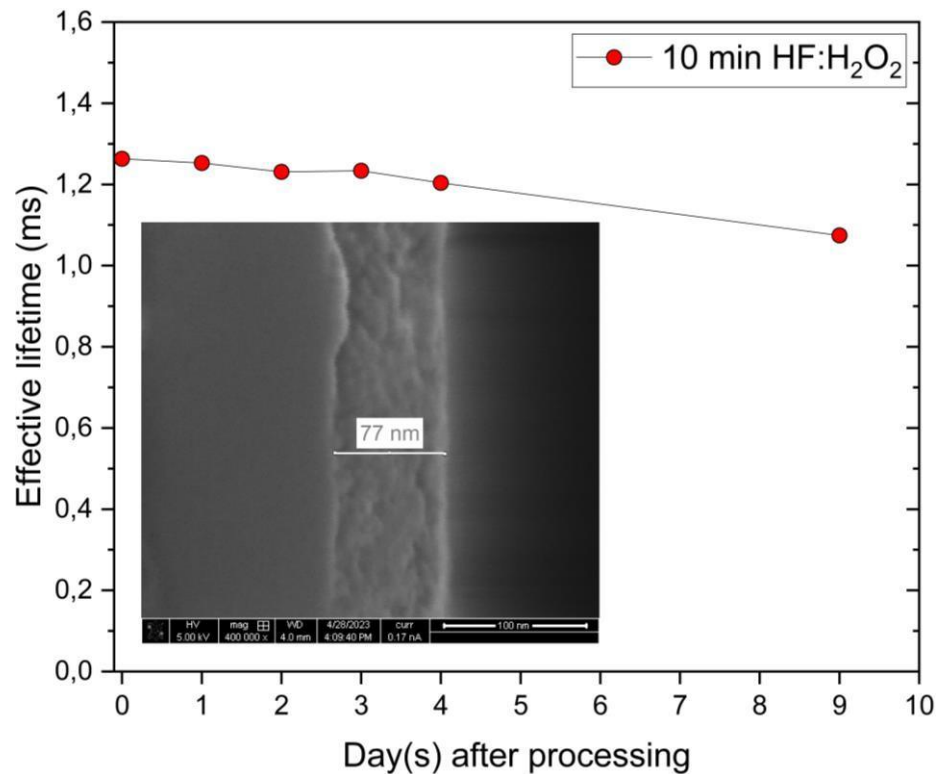
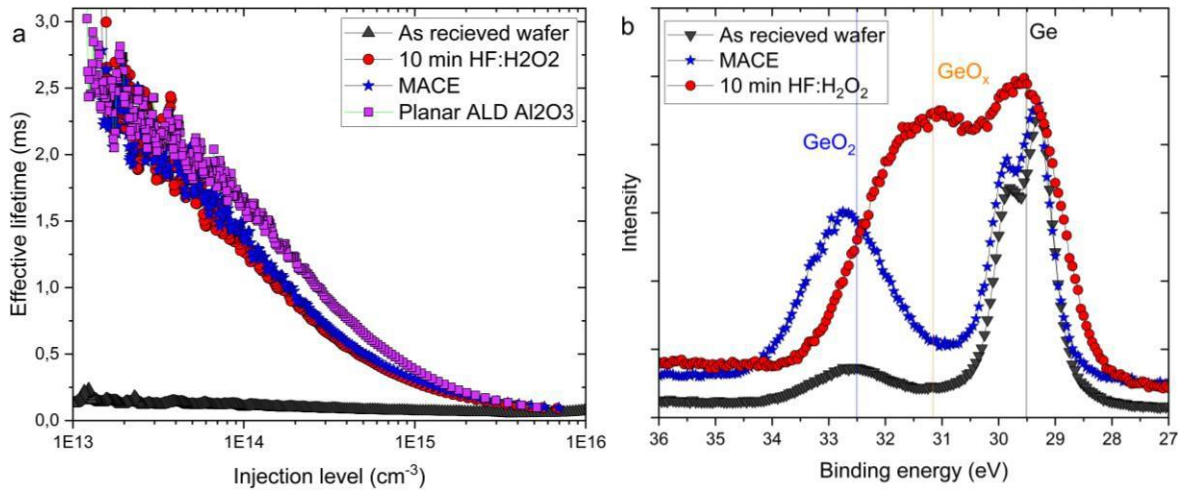


Fig. 2. Stability test for the sample after modified MACE treatment. The effective lifetime is taken at an injection level of 1E14 cm⁻³. The inset shows an SEM image of the sample surface revealing a sponge-like structure of the film.

Pros for using MFIA in deep level transient spectroscopy studies

Teimuraz Mchedlidze

Institute for Applied Physics, Technical University Bergakademie Freiberg, Freiberg 09599, Germany

Email: teimuraz.mtchedlidze@physik.tu-freiberg.de

Utilization of a multi-functional Impedance analyser and dual-phase digital lock-in amplifier (MFIA) from Zurich Instruments for deep-level transient spectroscopy (DLTS) measurements, allows substantial improvements in the measurement parameters (i.e., a decrease of instrumental recovery time and an increase of transient sampling rate). Usually, DLTS allows trap-associated defect identification based on their “signature” obtained from the Arrhenius plot [1], [2] and determining trap concentrations based on the amplitude of the related capacitance transients. The MFIA-based system is especially useful for determining DLTS “signatures” of traps with specific properties (i.e., strong temperature-dependent carrier cross-section, extended structure, etc.). For such traps, the initial portion of the capacitance transient (in the interval before 2 ms after the filling pulse) has crucial importance and substantially affects the obtained DLTS “signatures” (see Fig.1 and 2). Using the MFIA-based system we corrected the DLTS “signature” of traps related to reconstructed dislocations in Si [3]. We also obtained extended dependence of transient response on the duration of the filling pulse for the point-like and extended defects (see Fig.3). The studies were performed using crystalline silicon samples contaminated with gold [4].

References:

- [1] P. Blood and J. Orton, "Deep Level Transient Spectroscopy of Majority Carrier Traps," in The Electrical Characterization of Semiconductors: Majority Carriers and Electron States, vol. 14 (N. March, Ed., San Diego, CA: Academic Press Inc, 1992), pp. 399-465.
- [2] M. K. Juhl, et al., IEEE J. Photovoltaics, **2023**, 13, 524.
- [3] V. Kveder, Et al., PSS(a), **1982**, 72, 701.
- [4] K. Gwozdz, et al., J. Applied Phys., **2018**, 124, 015701.

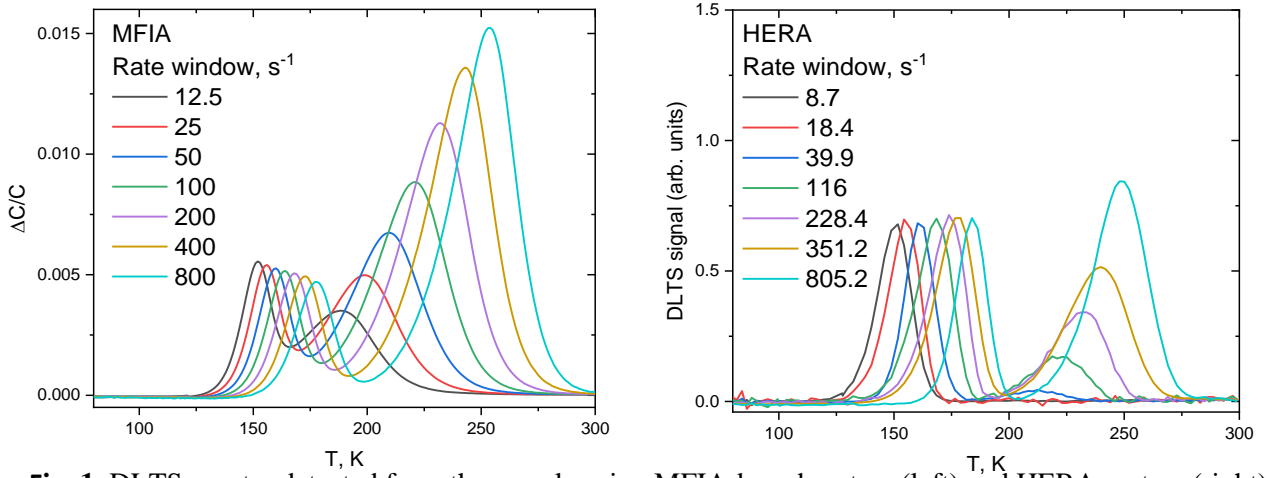


Fig. 1. DLTS spectra detected from the sample using MFIA-based system (left) and HERA system (right) for the same sample.

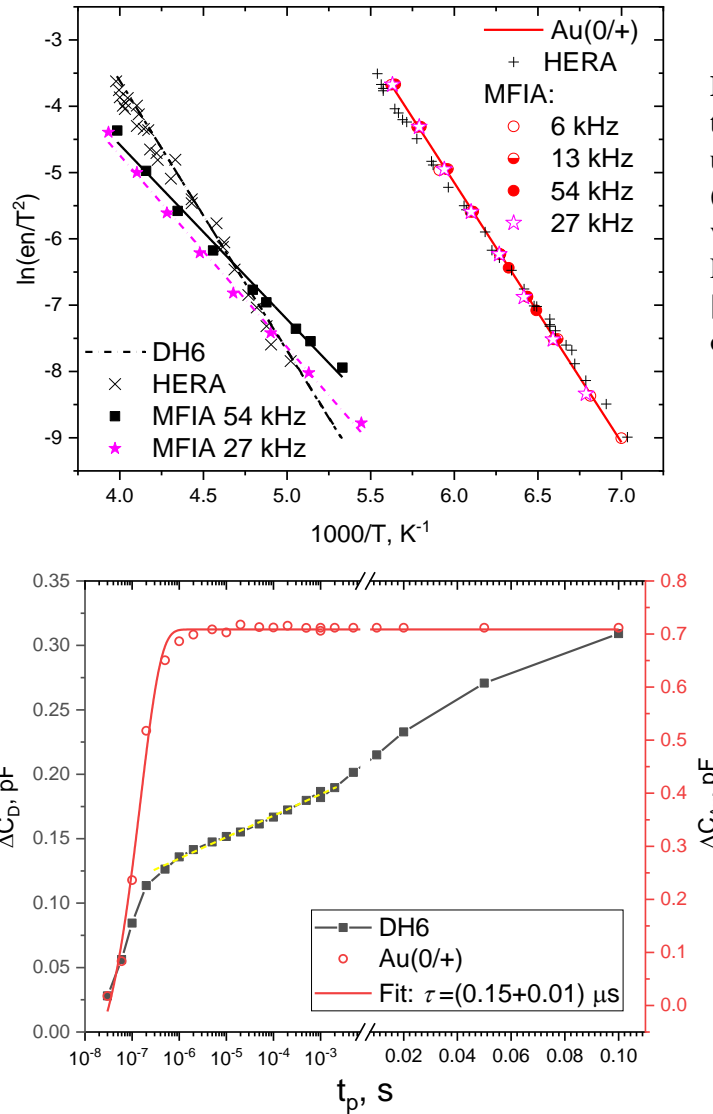


Figure 2. Arrhenius plots (symbols) for the DLTS peaks detected in the sample using HERA and MFIA systems (attributions are indicated in the figure, various settings of MFIA were used). Lines present data from the references [3], [4] and our fit for the DH6 trap data obtained on the MFIA DLTS system.

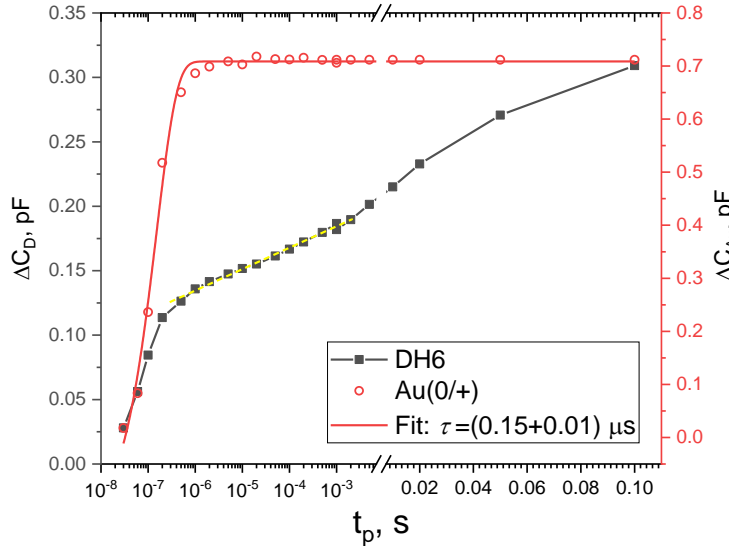


Figure 3. Symbols show dependencies of transient amplitudes on the filling pulse duration for the signals from dislocation-related traps (DH6) and gold-related traps $\text{Au}(0+)$. The red curve presents fitted dependence for $\text{Au}(0+)$ trap, yellow dotted curve presents that for the DH6 trap [3].

Edge inspection of Si wafers for Bulk Microdefects

Tamás Szarvas¹, Szilárd Pothorszky¹ and György Nádudvari¹

¹Semilab Co. Ltd., 2 Prielle K. str., 1117 Budapest, Hungary

Email: tamas.szarvas@semilab.hu

Although the detection of Bulk Microdefects (BMD) is well established in the internal region of Si wafers, and the surface scatters on the edge as well, not much attention has been given to BMDs in the regions close to the edge along the wafer periphery.

The industry-standard machine for BMD detection in the internal region of the Si sample is the Semilab Light Scattering Tomograph (LST) [1]. It detects BMDs in half Si wafers by applying a focused laser illumination to the front surface of the half wafer, around 50 µm behind the cleaved surface. Scattered light from BMDs is collected via the cleaved surface by a microscope system.

To serve Integrated Device Manufacturer (IDM) needs, Semilab has developed a metrology solution called Light Scattering tomograph enhanced with Low-angle illumination (LSL) [2- 3]. It can detect BMDs even in the presence of metallization on the front surface of the wafer by applying an additional, low-angle illumination unit.

This unique feature opens the way to detect BMDs via a flat apex of the wafer periphery. BMDs this close to the wafer edge may greatly impact the electrical characteristics of the microdevices close to the wafer edge. The distribution of the BMDs in this region may not follow patterns, which are well-described in the inner region, since the presence of surface cracks, grinding damages, local stress fields could have an intense effect on BMD formation. The optical design of the system is presented in Fig. 1. A rotary stage is used to scan around the wafer. The detection is executed with a high magnification microscope objective, therefore active focus tracking is applied in the optical axis. A line-focused Infrared (IR) laser beam illuminates the sample in low angle. The focal plane is situated 50-100 µm behind the wafer edge coinciding with the illumination line. BMDs here are well-focused as Fig. 2 depicts. Large surface particles on the edge may appear as defocused diffraction patterns depending on the sample cleanliness and edge quality.

Apart from BMDs, the system can easily detect surface particles and cracks as well, allowing customers to discover edge quality and cleanliness before real bulk measurements are taken. As an example, Fig. 3 shows a typical image about dust particles and microcracks.

References:

- [1] Ferenc Korsós et al., “Efficiency limiting crystal defects in monocrystalline silicon and their characterization in production”, *Solar Energy Materials and Solar Cells* **2018**, 186, 217–226
- [2] Tamás Szarvas et al., “Bulk micro-defect detection with low-angle illumination”, *Review of Scientific Instruments* **2021**, 92, 043701
- [3] Tamás Szarvas, “Application of low-angle illumination for light scattering-based bulk micro defect detection in patterned wafers”, *GADEST 2022, oral presentation*

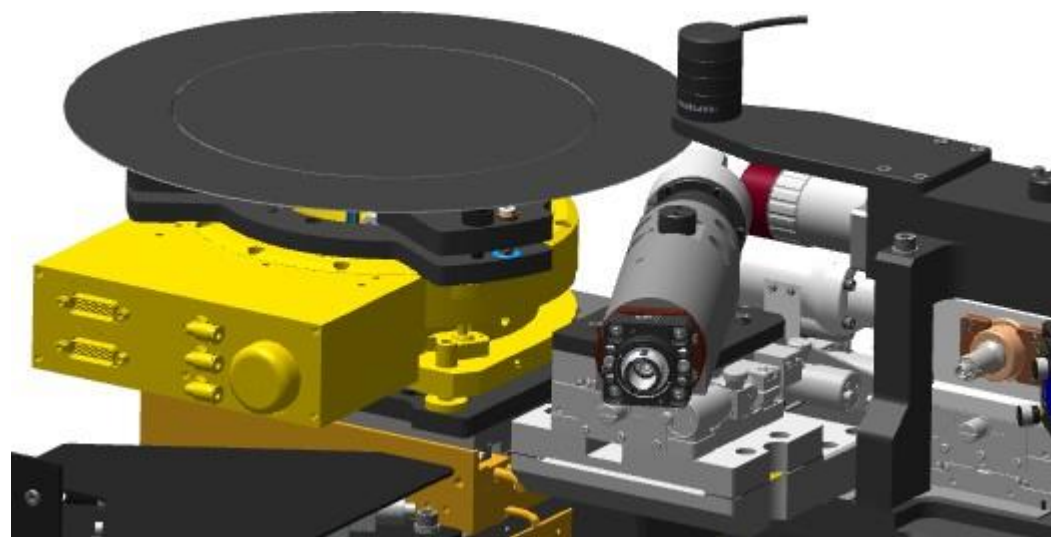


Fig. 1. Optical system design.

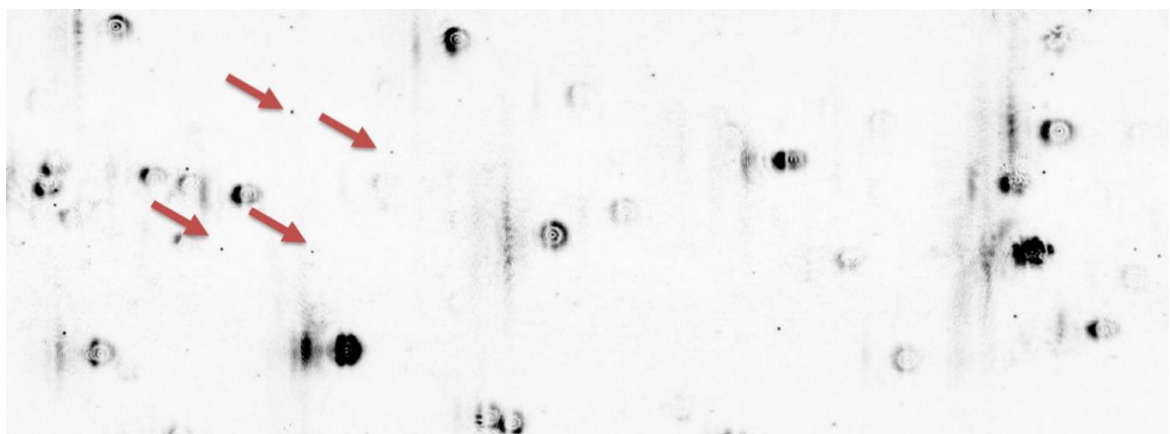


Fig. 2. BMDs few tens of microns behind the flat apex of a Si wafer periphery.

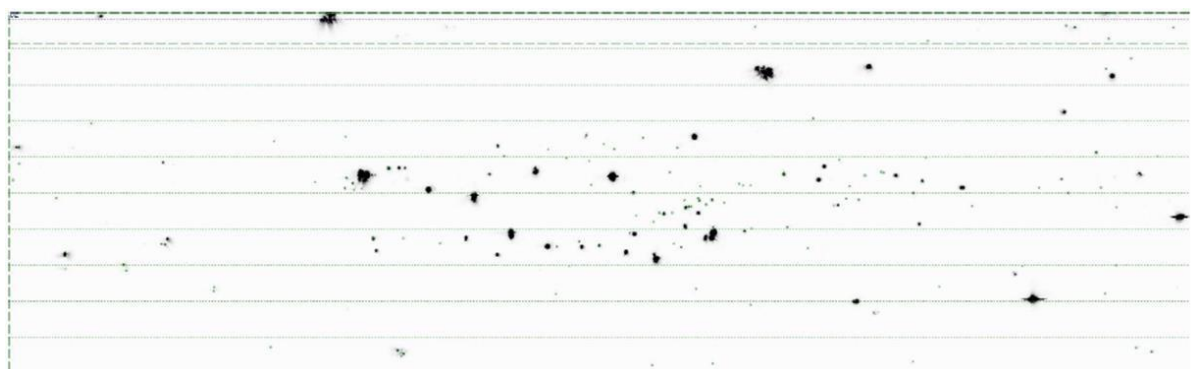


Fig. 3. Surface particles on Si wafer edge. They can be either dust particles or microcracks.

Detection of defect transitions in ultra-wide bandgap semiconductors by dc and ac surface photovoltage spectroscopy

Steffen Fengler¹, Thomas Dittrich²

¹Freiberg Instruments GmbH, Delfter Str. 6, 09599 Freiberg, Germany

²Helmholtz-Zentrum Berlin für Materialien und Energie GmbH, Schwarzschildstr. 8, 12489 Berlin, Germany

Email: steffen.fengler@freiberginstruments.com

Surface photovoltage spectroscopy (SPV) allows for the detection of electronic defect transitions in semiconductors without the need for contact preparation, i.e. defect transitions can be characterized at different stages of technology. The relatively fast, highly sensitive and robust characterization of defects in ultra-wide bandgap semiconductors over wide ranges of photon energies is still challenging. In addition, SPV measurements can give access to the characterization of buried interfaces.

We developed a SPV set-up suitable for highly sensitive dc and ac SPV measurements with the same electrode on ultra-wide bandgap semiconductors such as $\beta\text{-Ga}_2\text{O}_3$ [1] or diamond [2, 3, 4]. The SPV set-up allows for measurements on semiconductors, insulators, thin films, powders and molecular monolayers [5]. The study of defects in ultra-wide bandgap semiconductors by SPV techniques requires the continuous variation of photon energies from the near infrared to the deep ultra-violet. For this purpose, we use single (SPM2, Carl Zeiss Jena) and double (DPM100, Freiberg Instruments) prism monochromators based on fused silica.

Here we show examples for the characterization of defect transitions by dc (Kelvin probe regime) and ac (modulated regime) SPV measurements in single crystals, epitaxial layers and thin films of $\beta\text{-Ga}_2\text{O}_3$, diamond and AlN (provided by the FBH Berlin).

References:

- [1] T. Dittrich, S. Fengler and N. Nickel, *Phys. Stat. Sol. A* **2021**, 218, 2100176.
- [2] T. Dittrich, *AIP Advances*, **2022**, 12, 065206.
- [3] T. Dittrich and S. Fengler, *Semicond. Sci. Technol.* **2023**, 38, 015015.
- [4] A. Chemin, I. Levine, M. Rusu, R. Vaujour, P. Knittel, P. Reinke, K. Hinrichs, T. Unold, T. Dittrich and T. Petit, *Small Methods* **2023**, 7, 2300423.
- [5] see also T. Dittrich and S. Fengler, "Surface photovoltage analysis of photoactive materials" (World Scientific, New Jersey, London, Singapore, Beijing, Shanghai, Hong Kong, Taipei, Chennai, Tokyocity, year), p. 113.

For your remarks

First Principles Calculation of Electron Absorption and Recombination in Strained GeSn

Kevin Sewell¹ and Felipe Murphy-Armando¹

¹ Tyndall National Institute, University College Cork, Lee Maltings Complex Dyke Parade, T12R5CP, Cork, Ireland.

Email:
 kevin.sewell@tyndall.ie
 philip.murphy@tyndall.ie

Radiative recombination in semiconductors with an indirect absorption edge is slower than in direct-gap materials since it can only occur through the absorption or emission of phonons. Optical transitions in such semiconductors are orders of magnitude weaker than direct transitions [1]. This is why LEDs and laser diodes are usually made with direct-gap materials. Germanium has a pseudo-direct band-gap nature, whereby the difference between the L and Γ -valley conduction-band minima is only around 150 meV [2]. A direct bandgap can be achieved either by applying <1.5% biaxial tensile strain [3,4], or by alloying Ge with 6-11% Sn [5-8]. In addition to enabling direct absorption, the direct gap has the potential of dramatically enhancing the electron mobility, in a similar way to strain in Ge [9,10]. In our calculations (see companion presentation), we find that at a Sn concentration $\approx 21\%$, unstrained GeSn has high electron mobility ($\approx 34,000 \text{ cm}^2 \text{V}^{-1} \text{s}^{-1}$). This mobility can be further enhanced by applying 1% biaxially tensile strain to GeSn, resulting in a mobility of $\approx 41,000 \text{ cm}^2 \text{V}^{-1} \text{s}^{-1}$ at 14.85% Sn. This, along with its tuneable bandgap makes (strained) GeSn an attractive alternative to III-V materials in such devices.

We calculate the absorption and emission properties of unstrained and biaxially tensile-strained GeSn due including phonon and alloy disorder. We employ first-principles electronic-structure methods [11] to calculate the Sn composition and strain dependence of the dielectric function $\epsilon(\omega)$, the absorption coefficient $\alpha(\omega)$, the spontaneous emission $S(\omega)$ and the stimulated emission spectra, where ω are the photon frequencies [1]. Given the changing bandgap nature of strained GeSn, electrons are absorbed directly and indirectly. We employ degenerate perturbation theory at the indirect-to-direct bandgap transition, where L and Γ -valleys are near-equal in energy, and at low Sn concentration (and low strain) when electrons near the L valley gain energy close to that of the Γ -valley. We expect alloy disorder and strain to increase electron absorption and emission. Finally, we introduce circularly polarised light to examine the changes in spin polarisation with alloy content as well as phonons.

The electronic structure calculations are performed using DFT corrected by the GW approximation [12]. All first principles calculations are performed in a plane-wave pseudopotential formalism using Density Functional Theory with the ABINIT code [13].

References:

- [1] Edition, Springer (2001).
- [2] M. Fischetti and S. Laux, “Band structure, deformation potentials, and carrier mobility in strained Si, Ge, and SiGe alloys”. *J. Appl. Phys.* **80**, 2234 (1996).
- [3] M. El Kurdi et al, “Band structure and optical gain of tensile-strained Ge based on a 30-band k.p formalism”, *J. Appl. Phys.* **107**.1 (2010).
- [4] Kuo-Hsing Kao et al. “Tensile strained Ge tunnel field-effect transistors: k· p material modelling and numerical device simulation”. In: *Journal of Applied Physics* **115**.4 (2014). .
- [5] S. Gupta, B. Magyari-Köpe, Y. Nishi & K.C. Saraswat, “Achieving direct band gap in germanium through integration of Sn alloying and external strain”. *J. Appl. Phys.* **113**, 073707 (2013).
- [6] P. Moontragoon, Z. Ikonić, & P. Harrison, “Band structure calculations of Si-Ge-Sn alloys: achieving direct band gap materials”. *Semicond. Sci. Technol.* **22**, 742–748 (2007).
- [7] W.J. Yin, X.G. Gong & S.H Wei, “Origin of the unusually large band-gap bowing and the breakdown of the band-edge distribution rule in the $\text{Sn}_x\text{Ge}_{1-x}$ alloys”. *Phys. Rev. B* **78**, 161203 (2008).
- [8] Y. Chibane & M. Ferhat, “Electronic structure of $\text{Sn}_x\text{Ge}_{1-x}$ alloys for small Sn compositions: Unusual structural and electronic properties”. *J. Appl. Phys.* **107**, 053512 (2010).
- [9] F. Murphy-Armando and S. Fahy, “Giant enhancement of n-type carrier mobility in highly strained germanium nanostructures”, *J. Appl. Phys.* **109**, 113703 (2011).
- [10] M.B. Clavel *et al.*, “Multivalley Electron Conduction at the Indirect-Direct Crossover Point in Highly Tensile-Strained Germanium”, *Phys. Rev. Applied* **18**, 064083 (2022)
- [11] M. Hudait et al, “Design, Theoretical and Experimental Investigation of Tensile-Strained Germanium Quantum-Well Laser Structure”. *ACS Appl. Electron. Mater.* **3**, 4535-4547, (2021).
- [12] W.G. Aulbur, I. Jonsson and J.W. Wilkins, “Solid State Physics”, **54**:1-218, (2000).
- [13] Beuken, J-M. The ABINIT Group. <https://www.abinit.org/>

The Nanoscopic Electronic Structure Shift Induced by Anions at Surfaces (NESSIAS) to replace doping in nano-Si for VLSI

Dirk König¹, Michael Frentzen², Daniel Hiller³, Noël Wilck², Giovanni Di Santo⁴, Luca Petaccia⁴, Igor Piš⁵, Federica Bondino⁵, Elena Magnano⁵, Joachim Mayer⁶, Joachim Knoch², and Sean C. Smith¹

¹ Integrated Materials Design Lab, Australian National University, Canberra, ACT 2601, Australia

² Institute of Semiconductor Electronics, RWTH Aachen University, 52074 Aachen, Germany

³ Institute of Applied Physics, Technische Universität Bergakademie Freiberg, 09599 Freiberg, Germany

Elettra Sincrotrone Trieste, Strada Statale 14 km 163.5, 34149 Trieste, Italy

⁵ IOM-CNR, Instituto Officina dei Materiali, Area Science Park S.S. 14 km 163.5, 34149 Trieste, Italy

⁶ Ernst-Ruska Centre for Electron Microscopy, RWTH Aachen University, 52074 Aachen, Germany

Email: solidstatedirk@gmail.com

The NESSIAs causes the electronic structure of SiO₂- versus Si₃N₄-coated low nanoscale intrinsic silicon (Si) to shift away from versus toward the vacuum level E_{vac} [1-5]. The experimentally derived impact length into Si of dNESSIAS of 1.4 nm/ 2.8 nm/ 4.2 nm for nanowells (NWells)/ nanowires (NWires)/ nanocrystals (NCs) renders Si NWells with dwell ≤ 2.8 nm, NWires with dwire ≤ 5.6 nm, and NCs with dNC ≤ 8.4 nm to be dominated by NESSIAs [4]. We explain the origin of NESSIAs by the quantum chemical properties of the elements involved, and delimit it against known interface effects such as interface dipoles or the push-back/pillow effect. Deriving an analytic quantum-chemical parameter Λ to predict the highest occupied energy level of nano-Si, we can predict the energy offset of nano-Si as a function of its dielectric embedding (boride, carbide, nitride, oxide, fluoride, sulfide) [5]. Such predictions are confirmed by various hybrid-density functional calculations carried out with Si nanocrystals (NCs) over a wide size range.

First experimental data of Si nanowells (NWells) [5,6] embedded in SiO₂ versus Si₃N₄ were measured by X-ray absorption spectroscopy in total fluorescence yield mode (XAS-TFY), complemented by ultraviolet photoelectron spectroscopy (UPS), characterizing their conduction band and valence band edge energies E_c and E_v, respectively. Band offsets of $\Delta E_c = 0.56$ eV and $\Delta E_v = 0.89$ eV were measured for 1.9 nm thick Si NWells in SiO₂ versus Si₃N₄, demonstrating an intrinsic Si type II homojunction [5].

This p/n junction generated by NESSIAs eliminates any deteriorating impact of impurity dopants in nano-Si – density fluctuations, self-purification and clustering, out-diffusion, finite thermal energy (temperature) required for dopant ionization, loss of power (heat generation) and carrier mobility by inelastic Coulomb scattering. As a result, the NESSIAs offers undoped ultrasmall Si electronic devices with much reduced physical gate lengths and CMOS-compatible materials and logic operating with ultra-low power demand and full cryo-functionality [7]. A strong preference of nano-Si for holes (p-type) or electrons (n- type) is simply achieved by Si₃N₄- or SiO₂ coating.

References:

- [1] D. König et al, *Adv. Mater. Interfaces* **2014**, 1, 1400359.
- [2] D. König et al, *Beilstein J. Nanotechnol.* **2018**, 9, 2255.
- [3] D. König et al, *Phys. Rev. Appl.* **2019**, 12, 054050.
- [4] D. König et al, *ACS Appl. Mater. Interfaces* **2021**, 13, 20479
- [5] D. König et al, *Adv. Phys. Research* **2023**, 2, 2200065
- [6] M. Frentzen et al., *Phys. Stat. Sol. A* **2023**, 220, 2300066.
- [7] J. Knoch et al., *Phys. Stat. Sol. A*, **2023**, 220, 2300069

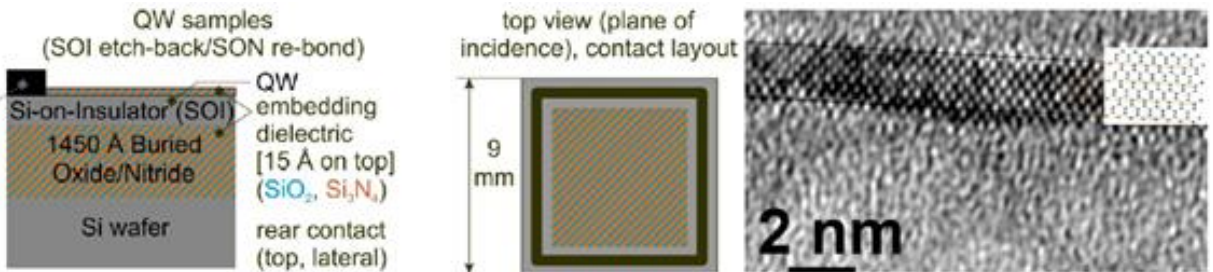


Fig. 1: (left) Layout of Si_3N_4 - and SiO_2 -embedded Si NWell samples for synchrotron UPS and XAS-TFY, shown in X-section and top view. **(right)** X-section view of 1.7 nm (001)-Si NWell in Si_3N_4 seen along the $\langle 110 \rangle$ vector class as obtained by TEM [5,6].

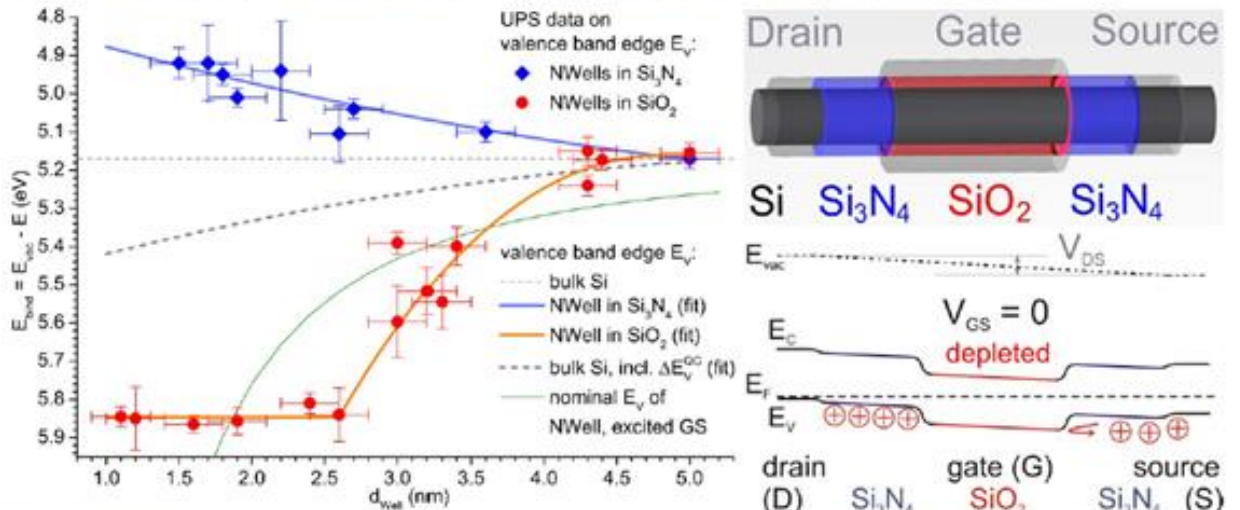


Fig. 2: (left) E_v for Si NWells embedded in SiO_2 (red symbols, orange residual fit) or Si_3N_4 (blue symbols, blue residual fit) over d_{NWell} obtained by synchrotron UPS. Error bars show standard deviations in d_{NWell} and E . Thin dashed grey line shows E_v of bulk Si. Thick dashed grey line shows E_v with intrinsic quantum confinement $E_v^{\text{QC}}(d_{\text{NWell}})$, ignoring NESSIAs. Green line shows E_v of the nanowell for photon absorption (including exciton binding energy, excluding lattice relaxation; unrelaxed excited state) per existing theory [5]. **(right)** Application of NESSIAs at self-blocking NWire MISFET (scheme, band diagram) [2].

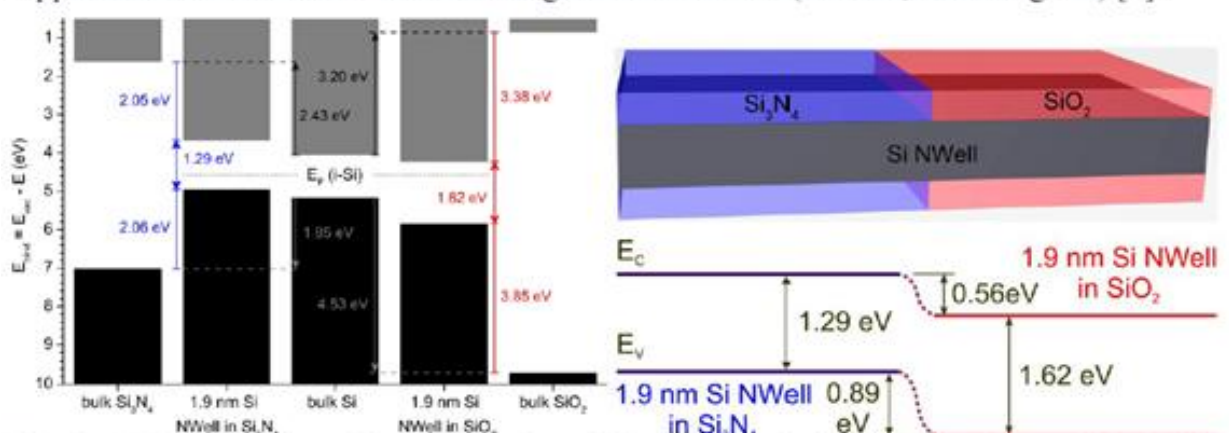


Fig. 3: (left) Fundamental band gaps for – left to right – bulk Si_3N_4 , a 1.9 nm Si-NWell in Si_3N_4 , intrinsic bulk Si, a 1.9 nm Si- NWell in SiO_2 , and bulk SiO_2 . Band offsets to dielectrics are shown by labelled red (blue) lines for NWells in SiO_2 (Si_3N_4), and in gray/black for bulk Si. Values of band edges for bulk solids are from experimental data in the literature, data for NWells were obtained by UPS and XAS-TFY [5]. **(right)** Layer system comprising a 1.9 nm thick Si NWell coated with 1.0 nm Si_3N_4 and SiO_2 , and its band diagram with energies in units of eV, derived from experimental data in left graph [5].

Advanced device designs for group IV double-heterostructure light-emitting diodes operating at room temperature

A. Salomon,¹ J. Aberl¹, E. Prado-Navarrete¹, Diego Haya Enriquez¹, Christoph Wilflingseder¹, Merve Karaman¹, T. Fromherz¹, M. Brehm¹

¹*Institute of Semiconductor and Solid-State Physics,
 Johannes Kepler University Linz, Altenbergerstr. 69, A-4040 Linz, Austria*

Email: andreas.salomon@jku.at

For integrating optoelectronic components such as light-emitting diodes (LEDs) or lasers into existing CMOS-based technology, it would be of great advantage if the components could be processed using Si technology. However, Si and Ge are intrinsically poor light emitters due to their indirect band gap, and Ge/Si heterostructures are of type-II band alignment, i.e., charge carrier separation further hinders light emission.

Here, we show that double-heterostructures (DHS) LEDs made from Si/SiGe/Si layer stacks emit light at telecom wavelengths and room temperature and above. However, such room temperature operation is only possible if the SiGe layer thickness is far higher than conventional experimental limits for layer relaxation. The samples were grown in an MBE system on a n-doped Si-substrate followed by a n-doped Si buffer-layer, the p-n-junction is formed by a n-doped and a p-doped SiGe layer with a sufficiently high layer thickness (≥ 16 nm) to avoid quantum confinement and finally capped by a final p-doped Si layer. The growth at a very low pressure of $\leq 10-10$ mbar and at ultra-low temperature of $\sim 300^\circ\text{C}$ is an essential prerequisite for a defect-free, pseudomorphic growth of sufficiently thick Si0.6Ge0.4 layers (≥ 16 nm) on a Si buffer layer [1]. Transmission electron microscope (TEM) measurements and obtained device parameters confirm a perfect lattice quality attributed to the aforementioned growth parameters.

The main benefit of this newly developed group-IV DHS is the conversion from type-II to type-I band offsets for higher applied bias voltage [2,3]. Consequently, electroluminescence measurements of our Si/Si0.6Ge0.4/Si DHS samples show a high emission rate at telecom wavelengths, adjustable by the Ge content. Adding quantum dots to form a dot-in-well heterostructure stabilizes the emission intensity and the spectral position of the emitted light from low temperatures (10 K) up to 360 K, which corresponds to the maximum available sample temperature without relevant thermal quenching [3].

Furthermore, device simulations suggest that the DHS structures can have a high internal quantum efficiency. As a first step towards reducing the losses, we addressed current crowding by making design adjustments. Additionally, we were able to improve the line width and temperature stability by embedding quantum dots [3].

Thus, we present the first successful demonstration of these group-IV and type-I electrically-pumped double heterostructure light sources that emit in the telecom wavelength range and can be operated from low temperatures up to room temperature and beyond.

References:

- [1] A. Salomon et al., Phys. Status. Solidi A., doi:10.1002/pssa.202200154 (2022).
- [2] Patent in preparation.
- [3] A. Salomon et al., in preparation

For your remarks

Optical characterization of colour centres in AlN

A. Albrecht¹, J. Beyer¹, C. Röder^{1,2}, G. Lukin², A. Lesnik², S. Besendorfer², E. Meißner²,
 J. Friedrich², F. C. Beyer², and J. Heitmann^{1,2}

¹TU Bergakademie Freiberg, Institut für Angewandte Physik, Leipziger Straße 23, 09599 Freiberg

²Fraunhofer-Institut für Integrierte Systeme und Bauelementetechnologie (IISB), Schottkystraße 10, 91058 Erlangen

Email: amy.albrecht@physik.tu-freiberg.de

Aluminium nitride (AlN) is a promising wide band-gap host material for colour centres for quantum information and sensing applications. Using density functional theory (DFT), calculations of the energy level structure of point defects and defect complexes related to transition metals and vacancies show the potential formation of triplet ground states that are localized within the band-gap of AlN and are suitable for quantum applications [1]. Experimental studies of AlN demonstrate promising results on defect species with radiative recombination behaviour which may serve as single photon sources [2; 3].

In this study, pieces of epi-ready AlN wafers were optically characterized using photoluminescence (PL) spectroscopy. For this purpose, PL spectra and mappings with a local resolution down to a few μm were recorded. The investigated free-standing AlN wafers were prepared from AlN single crystals with wurtzite structure and grown by physical vapour transport (PVT) [4].

First micro- and macro-PL mappings excited by laser illumination in the visible spectral range (442 – 800 nm) revealed localized regions with distinct PL features. To investigate the saturation behaviour of radiative recombination channels and brightness of the colour centres, the PL intensity was measured in dependence on the laser power density. Furthermore, PL excitation spectroscopy was performed for a better understanding of the involved energetic levels of radiative recombination centres. The colour centres identified in the mappings were further characterized optically to evaluate their potential as quantum sensors. The identification of single photon sources will be carried out by determining the autocorrelation function.

References:

- [1] J. B. Varley, A. Janotti und C. G. van de Walle, *Physical Review B* **2016**, 93, 161201.
- [2] S. G. Bishop, J. P. Hadden, F. D. Alzahrani, R. Hekmati, D. L. Huffaker, W. W. Langbein und A. J. Bennett, *ACS Photonics* **2020**, 7, 1636–1641.
- [3] J. K. Cannon, S. G. Bishop, J. P. Hadden, H. B. Yağcı und A. J. Bennett, *Applied Physics Letters* **2023**, 122, 1721041–1721044.
- [4] T. Wicht, S. Müller, R. Weingärtner, B. Epelbaum, S. Besendorfer, U. Bläss, M. Weisser, T. Unruh und E. Meißner, *Journal of Applied Crystallography* **2020**, 53, 1080–1086.

For your remarks

Process Mode Engineering of Atomic Layer Etching of Wide-Bandgap Materials

Ch. Miersch¹, S. Seidel¹, A. Schmid², J. Heitmann², F. C. Beyer¹

¹ Departement of Energy Materials and Test Devices, Fraunhofer Institute for Integrated Systems and Device Technology, Am Sankt Niclas Schacht 13, 09599 Freiberg, Germany

² Department of Applied Physics, Technical University Bergakademie Freiberg, Freiberg, Germany

Email: christian.miersch@iisb.fraunhofer.de

The demands on semiconductor devices range from smaller structure sizes, high power densities and switching frequencies to atomically smooth surfaces i. e. for quantum devices or electromobility. Wide-bandgap semiconductors like SiC, GaN or AlN are indispensable to meet the requirements. AlGaN/GaN high electron mobility transistors (HEMTs) can be used for both high frequency and power applications [1–4]. This normally-on transistors are desirable normally-off, fitting to the established MOSFET circuit design. Recess etching of the gate contact into the AlGaN barrier, is one way to shift the threshold voltage V_{th} in positive direction (Fig. 1)[5]. For this purpose, atomic layer etching (ALE) offering a high controllable and precise etching rate with low damage. ALE generally consists of two independent steps forming a repeatable cycle with a distinct etch per cycle (EPC) [6]. A conventional ALE approach on a AlGaN/GaN heterostructure starts with modifying the surface by chlorine etching chemistry, producing a thin layer, ideally on an atomic scale, of volatile GaCl_x and AlCl_x products. In the following removal step, the modified layer is removed by accelerated low energy Argon-ions, without sputtering the unmodified material below. A purging in between the steps is typically applied, which increases the cycle time and influencing the processing costs, too. The implementation of other ALE methods (i.e. pulsed-bias[7]) can be beneficial.

In this study, we develop an ALE recipe for the $\text{Al}_{25}\text{Ga}_{75}\text{N}$ barrier layer and optimized it in respect to the cycle times and the plasma damage. Furthermore, we compare different ALE methods: with purging in between the steps, purge-free[5], continuous plasma and a bias- pulsed[7] option. The evaluation of the developed processes will be performed by morphological and electrical characterization (gate recessed HEMTs). The induced damage will be investigated by structural and defect spectroscopical analysis. Finally we will transfer and modify the recipe for ALE on SiC with the focus on damage-free surface for quantum device nanofabrication [7].

This work was financially supported by the Fraunhofer Internal Programs under Grant No. Attract 079-600865.

References:

- [1] R. S. Pengelly, et al., IEEE T. Microw. Theory **2012**, 60, 1764.
- [2] N. Ikeda, et al., Proc. IEEE **2010**, 98, 1151.
- [3] M. Ishida, T. Ueda, T. Tanaka, and D. Ueda, IEEE T. Electron Dev. **2013**, 60, 3053.
- [4] V. Kumar, et al., Solid State Electron. **2003**, 47, 1577.
- [5] C. Miersch, et al., J. Vac. Sci. Technol. A **2024**, 42, 022604.
- [6] K. J. Kanarik, et al., J. Vac. Sci. Technol. A **2015**, 33, 20802.
- [7] J. A. Michaelset al., J. Vac. Sci. Technol. A **2023**, 41, 032607.

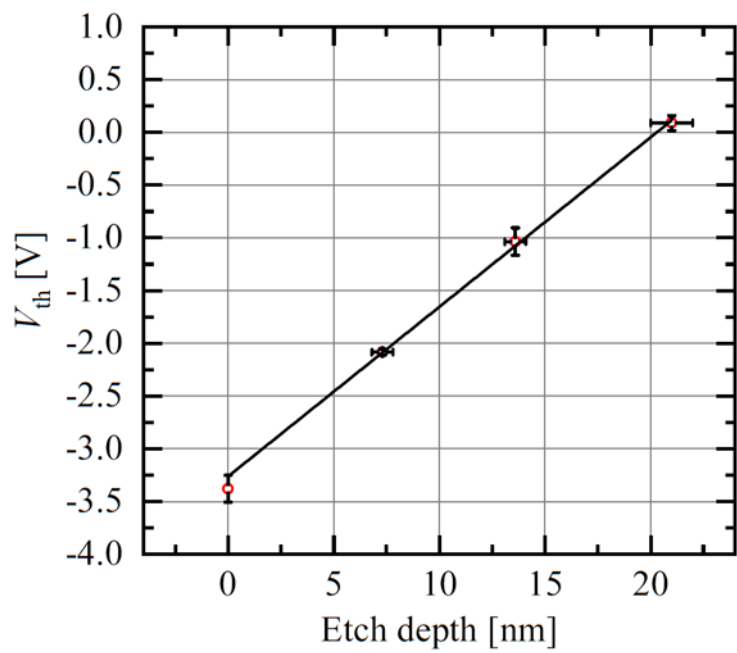


Fig. 1: Threshold voltage V_{th} shift due to recess etch of the gate contact in to the $\text{Al}_{25}\text{Ga}_{75}\text{N}$ barrier. V_{th} extracted from step in gate capacitance. V_{th} increases linearly with etch depth.[5].

**Falp® (Fast Atomic Layer Processing) a Chamber for Combined PEALD
and ALE Processes at low temperatures**

Stephan Wege,¹ Aditya Kumar Soni², Vardhman Singh Chaudhary³, Elias Ricken⁴

¹plasway-Technologies GmbH, Maria-Reiche-Str. 3, 01109, Dresden, Germany

Email: stephan.wege@plasway.de

Atomic Layer Etching and (Plasma Enhanced) Atomic Layer deposition are processes that are needed for the advanced nanometer silicon processing technologies. The new FALP (Fast Atomic Layer Processing) tool is able to run both processes in one chamber. Based on a dual frequency CCP concept with low chamber volume, a highly symmetric turbo pumping and a patented new gas inlet ring, we are able to achieve a very fast exchange of the gases. Therefore, the FALP (Fast Atomic Layer Processing) tool is also high productive. This Tool can handle even heavy optical 17" substrates (20mm thick 8kg heavy) and is able to deal with 8", 6", 4" small wafer sizes. For 300mm, we have a special version for 300mm with Electrostatic Chuck (ESC). This bipolar ESC is also developed by Plasway-Technologies. Also, for high power application with GaAs, GaN this type of application is getting more and more importance. Even for optical applications extremely high quality and thick films are of interest. Our new Tool FALP combines low temperature (20°C-120°C) PEALD and ALE(In-Situ) with high throughput and better electrical quality. Even during PEALD, we are able to have a good controlled additional kinetic energy knob to get even at low temperatures 20°C high quality film. Based on 17" capable design, we will present results of thick ~500nm SiO₂ films with a very good index of refraction. On 300mm with ESC, we will present some first results of integrated ALE and PEALD on GaAs Substrates and low temperature film deposition. In addition, results on 300mm with Al₂O₃ and SiO₂. We also performed some first experiments of ion energy supported PEALD. It seems that we can change significantly the film structure. We usually deposit amorphous Al₂O₃. But with some additional ion energy we can change the system to poly-crystalline. We will also present some first thin sandwich stacks e.g., 2nm Al₂O₃/ 2 nm SiO₂ maybe even with additional kinetic energy.

For your remarks

Exceptional phonon point versus free phonon coupling in CdZnTe semiconductor mixed crystals under pressure

T. Alhaddad,¹ M.B. Shoker,² O. Pagès,¹ A. Polian,³ V.J.B. Torres,⁴ Y. Le Godec,⁵ J.-P. Itié,⁵ C. Bellin,³ K. Béneut,³ S. Diliberto,⁶ S. Michel,⁶ A. Marasek,⁷ and K. Strzałkowski⁷

¹ Université de Lorraine, LCP-A2MC, ER 4632, F-57000 Metz, France

² University of Luxembourg, Department of physics and materials science, 41 rue du Brill, 4422 Belvaux, Luxembourg

³ Institut de Minéralogie, de Physique des Matériaux et de Cosmochimie, Sorbonne Université — UMR CNRS 7590, F-75005 Paris, France

⁴ Departamento de Física and I3N, Universidade de Aveiro, 3810 – 193 Aveiro, Portugal

⁵ Synchrotron SOLEIL, L'Orme des Merisiers Saint-Aubin, BP 48 F-91192 Gif-sur-Yvette Cedex, France

⁶ Institut Jean Lamour, UMR CNRS 7198, Campus Artem, Université de Lorraine, 57078, Metz, France

⁷ Institute of Physics, Faculty of Physics, Astronomy and Informatics, Nicolaus Copernicus University in Toruń, ul. Grudziądzka 5, 87-100 Toruń, Poland

Email: olivier.pages@univ-lorraine.fr

We investigate the local atomic bond strength of high quality and purity $\text{Cd}_{1-x}\text{Zn}_x\text{Te}$ single cubic crystals under pressure by Raman scattering and Pseudopotential-Density Functional Theory. This cubic semiconductor alloy (SCA) has two bond types, Cd-Te and Zn-Te bonds. The Raman spectra at ambient pressure show a two-mode Zn-Te phonon behavior, which within our so-called percolation model (PM) [1] points out that the Zn-Te bond vibrates at two different frequencies depending on its “same” or “alien” environment, denoted by $(\text{Zn- Te})^{\text{Zn}}$ and $(\text{Zn-Te})^{\text{Cd}}$, respectively. The PM has been applied so far successfully to all tested binary and ternary SCA [2], suggesting its universality. This was lately completed by a predictive PM-based bipartition of II-VI and III-V ternaries depending on whether the percolation-type Raman doublet converges or diverges under pressure [3], as fixed by the relative hardening rates of the “same” or “alien” environments [4]. The case of convergence, in which the two sub-modes forming a percolation doublet are forced into proximity by pressure, is particularly interesting. In previous studies done at moderate content of the bond supporting the doublet, an exceptional phonon point was achieved at the resonance. In this scenario 1, only the sub-mode due to the “alien” environment survives from the resonance onwards; that due to the “same” environment is killed [5]. When the bond supporting the doublet is matrix-like, this scenario is not physically realistic. Another scenario (2) must emerge, currently investigated by addressing the high-pressure Raman behavior of cubic- $\text{Cd}_{1-x}\text{Zn}_x\text{Te}$ at large content ($x \sim 0.9$) with a focus on the dominant (Zn-Te) bond [2,6].

References:

- [1] O. Pagès *et al.*, *J. Appl. Phys.* **99**, 063507 (2006).
- [2] T. Alhaddad *et al.*, *J. Appl. Phys.* **133**, 065701 (2023), and Refs. therein.
- [3] M.B. Shoker *et al.*, *Scientific Reports*, **10**, 19803 (2020).
- [4] N. E. Christensen *et al.*, *Phys. Rev B*, **36**, 2 (1987).
- [5] M.B. Shoker *et al.*, *Scientific Reports* **12**, 753 (2022).
- [6] T. Alhaddad *et al.*, <https://doi.org/10.48550/arXiv.2306.14539>.

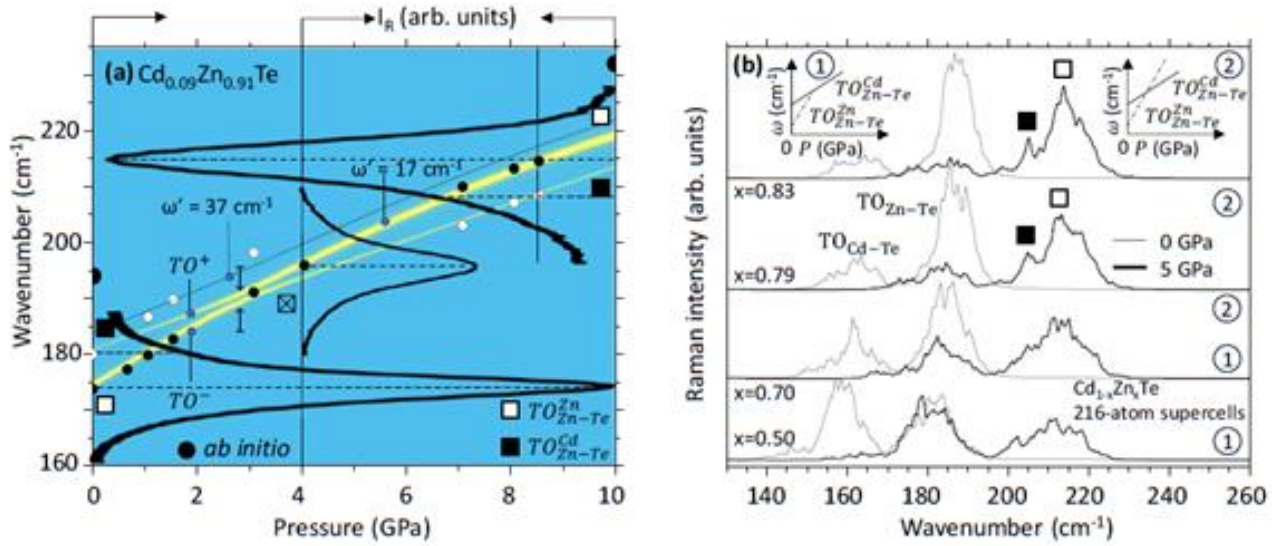


Fig. 1. High-pressure TO Raman insight into the $\text{Cd}_{1-x}\text{Zn}_x\text{Te}$ bond mechanic properties ($x \sim 0.9$). (a) Selected high-pressure $\text{Cd}_{1-x}\text{Zn}_x\text{Te}$ -zincblende ZnTe-like TO Raman spectra taken at minimal (left, tilted- 90°), intermediary (central) and maximum (right) pressures in the upstroke at large Zn content ($x=0.91$). Fair contour modeling of the bimodal Raman frequencies (thick-clear curves, circles) and intensities (brightness of curves) is achieved by involving a weak mechanic coupling (17 cm^{-1}) between $\text{TO}_{\text{Zn-Te}}^{\text{Zn}}$ (symbolized □, hollow circles) and $\text{TO}_{\text{Zn-Te}}^{\text{Cd}}$ (■, filled circles) when forced to proximity by pressure. The coupling culminates at the resonance (37 cm^{-1}) manifested by anticrossing (opposite arrows) of the coupled TO^- and TO^+ features. A proper $\text{TO}_{\text{Zn-Te}}^{\text{Zn}} \leftrightarrow \text{TO}_{\text{Zn-Te}}^{\text{Cd}}$ inversion is completed post resonance. **(b)** *Ab initio* (AIMPRO code) $\text{Cd}_{1-x}\text{Zn}_x\text{Te}$ high-pressure Raman spectra calculated on large (216-atom) disordered zincblende-supercells. An inversion is revealed when the Zn-Te bond is matrix-like ($x \geq x_{\text{Cd-Te}}$), in line with scenario (2), as sketched out. The inversion disappears on crossing the Cd-Te bond percolation threshold ($x_{\text{Cd-Te}} = 0.81$), *i.e.*, when Zn-Te is dispersed in chains ($x \leq x_{\text{Cd-Te}}$), suggesting the achievement of a phonon exceptional point at the resonance, in line with scenario (1), as sketched out.

Process Model for SiC Oxidation for a Large Range of Conditions

Christoph Zechner,¹ Anna Johnsson¹, Tamara Fidler², and Patrick Schmid²

¹*Synopsys GmbH, Karl-Hammerschmidt-Str. 34, 85609 Aschheim/Dornach, Germany*

²*centrotherm international AG, Würtemberger Str. 31, 89143 Blaubeuren, Germany*

Email: zechner@synopsys.com

The oxidation rate of 4H-SiC has been studied. A comprehensive process model for SiC oxidation has been created and calibrated for a wide range of process conditions.

Following Deal and Grove [1], oxidation is described by modelling oxidants (O_2 or H_2O) diffusing through the oxide and reacting at the oxide/SiC interface. For thin oxides, to account for oxidation rates higher than predicted by the Deal and Grove model, we use a suggestion of Massoud [2] and include empirical correction terms which add to the oxidation rate and asymptotically approach zero with increasing oxide thickness.

A process simulation model has been calibrated against data from publications [3]-[12] and against a large, so-far unpublished collection of oxidation data from experiments performed at Centrotherm. The model reproduces measured oxide thickness data of Si-face, C-face, and a-face SiC wafers, in the temperature range $950^\circ\text{C} - 1500^\circ\text{C}$, in the pressure range $0.25 \text{ atm} - 4.0 \text{ atm}$, in the thickness range $3 \text{ nm} - 1600 \text{ nm}$, and for SiC doping ranging between 10^{19} cm^{-3} n-type and 10^{19} cm^{-3} p-type.

The model has been calibrated with Synopsys' Sentaurus Calibration Workbench [13] and integrated to the process simulator Synopsys' Sentaurus Process [14]. Beyond parameter optimization, computer-aided calibration supported our selection from various model options by a just comparison of the maximum accuracy achievable with each candidate formula. Figures 1-3 show comparisons between selected experiments and simulation results.

For dry oxidation, we report a remarkable discovery: While for thick oxides, the oxidation rate scales linearly with the partial pressure of O_2 , the correction terms for thin oxides serve the overall model accuracy best when scaling with the square root of the partial pressure of O_2 . This pressure dependence suggests that the atomistic processes contributing to the fast initial growth of oxides involve the splitting of O_2 molecules into two O atoms. That different reaction chemistry may be a reason for the higher rate of carbon interstitial injection into SiC at the initial stage of oxidation [15], important for the elimination of carbon vacancies in the SiC bulk and possibly relevant for oxidation enhanced diffusion of dopants in SiC.

References:

- [1] B. E. Deal and A. S. Grove, J. Appl. Phys. 36, 12, 3770, 1965
- [2] H. Z. Massoud et al., 1985 J. Electrochem. Soc. 132, 2693
- [3] B. K. Daas et al., IEEE Trans. On Elec. Dev., Vol. 58, No. 1, 2011.
- [4] D. Goto et al., J. Appl. Phys. 117, 095306 (2015).
- [5] R. Hasanuma et al., ECS Transactions, 75 (12) 201-206 (2016)
- [6] T. Hosoi et al., Jap. J. App. Phys. 54, 098002 (2015)
- [7] K. Kita et al., ECS Trans. 61(2), 135-142 (2014)
- [8] T. Kobayashi et al., 2014 IEEE Int. Meeting for Future of El. Dev., Kansai (IMFEDK), Kyoto, Japan, 2014, pp. 1-2
- [9] K. Kouda et al., J. Appl. Phys. 112, 024502 (2012)
- [10] S. Kumar and J. Akhtar, SiC - Materials, Processing and Appl.in El. Devices. InTech, Oct. 10, 2011.
- [11] Ray et al, J. Appl. Phys. 103, 023522 (2008)
- [12] Y. Song et al., J. Appl. Phys., 95, 9, (2004).
- [13] Synopsys, Inc, Sentaurus™ Calibration Workbench User Guide, Mountain View, CA, USA, Dec 2023
- [14] Synopsys, Inc, Sentaurus™ Process User Guide, Mountain View, CA, USA, March 2024
- [15] C. Zechner et al., J. Appl. Phys. 132, 035702 (2022)

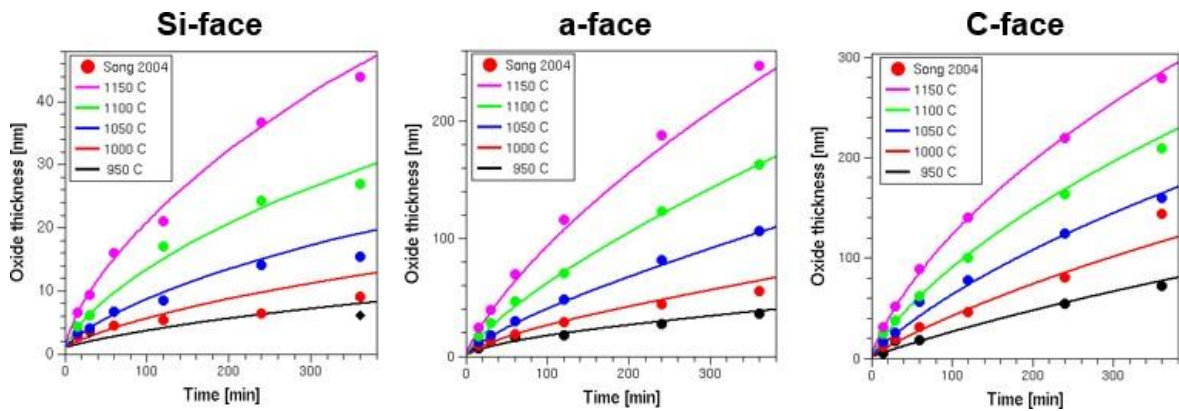


Fig. 1. Oxide thickness after dry oxidation of SiC as a function of time, for various temperatures and surface orientations. Measured data (adapted from Song et al., JAP 2004, v.95, n.9, (2004), <https://doi.org/10.1063/1.1690097>, with permission of AIP publishing; symbols) are compared to TCAD results (lines).

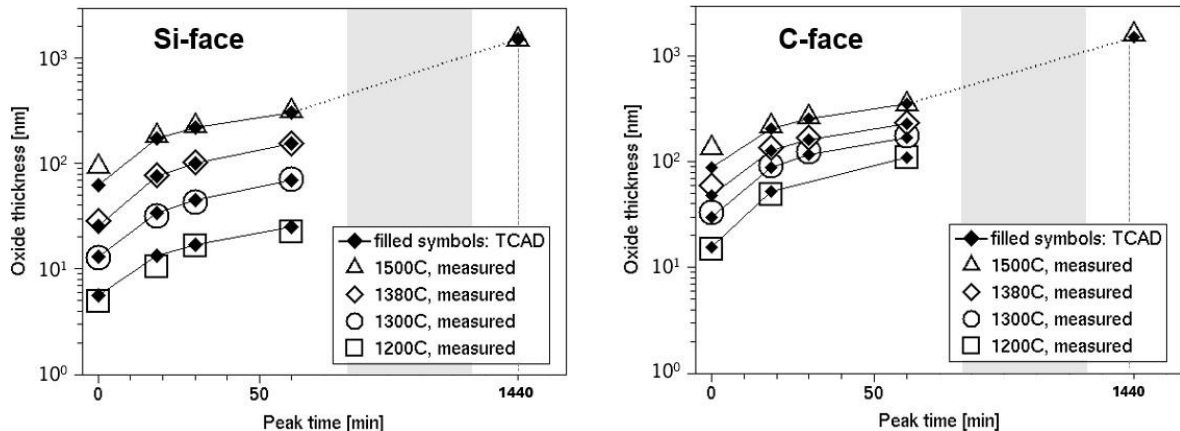


Fig. 2. Measured oxide thickness after dry oxidation of SiC (open symbols) compared to process simulation results (filled symbols), for various temperatures, times, and surface orientations.

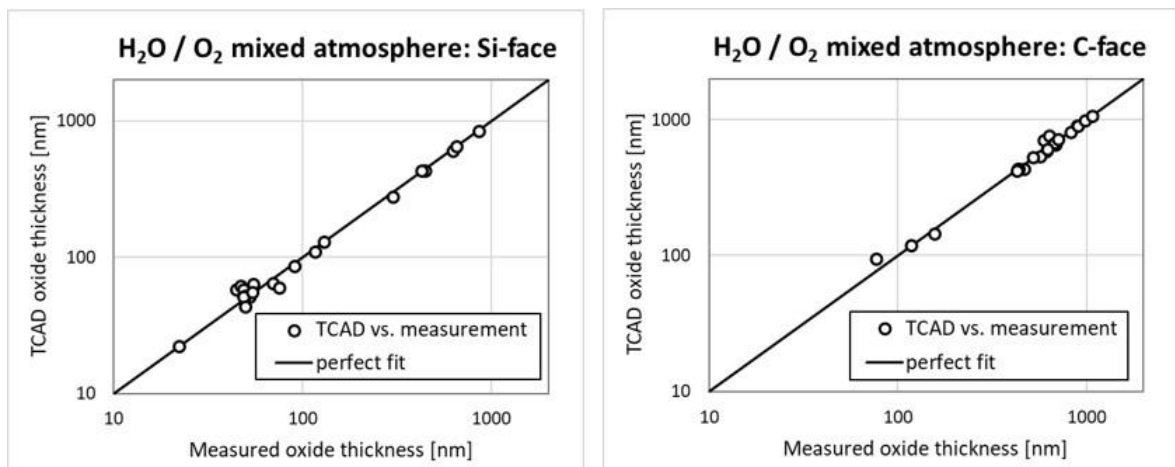


Fig. 3: Oxide thickness after oxidation in mixed H₂O / O₂ atmosphere. The TCAD model reproduces the measured value for a wide range of process conditions (temperature range: 1000°C – 1500°C; variation in time and pressure) with an average mismatch of less than 10%.

Synthesis of MoS₂ layers by sputter deposition and pulsed laser annealing

Alessandro Tonon¹, Enrico Di Russo^{1,2,3}, Francesco Sgarbossa^{1,2}, Emma Coleman⁴, Farzan Gity⁴, Brendan Sheehan⁴, Vasily A Lebedev⁵, Davide De Salvador^{1,2}, Ray Duffy⁴, and Enrico Napolitani^{1,2,6,*}

¹Dipartimento di Fisica e Astronomia, Università di Padova and CNR-IMM and LNL-INFN, Via Marzolo 8, I-35131 Padova, Italy

²Istituto Nazionale di Fisica Nucleare, Laboratori Nazionali di Legnaro, viale dell'Università 2, 35020 Legnaro (PD), Italia.

³CNR-IMM, Via Gobetti 101, Bologna, 40129, Italy.

⁴Tyndall National Institute, University College Cork, Lee Maltings, Cork, T12 R5CP, Ireland.

⁵Bernal Institute, University of Limerick, V94T9PX Limerick, Ireland.

⁶CNR-IMM, Via S. Sofia 64, 95123 Catania, Italy.

Email: enrico.napolitani@unipd.it

The wafer-scale synthesis of layered transition metal dichalcogenides presenting good crystal quality and uniform coverage is a challenge for the development of next generation nanoelectronic devices. This work explores a fairly new and unconventional growth method based on a two-step process consisting in sputter deposition of stoichiometric MoS₂ on Si/SiO₂ substrates followed by nanosecond UV (248 nm) pulsed laser annealing.[1,2] Large scale 2H-MoS₂ multi-layer films were successfully synthetized in N₂ rich atmosphere thanks to a fine-tuning of the laser annealing parameters by varying the number of laser pulses and their energy density. The identification of the optimal process led to the success in achieving (002)-oriented nanocrystalline MoS₂ film without performing post-sulfurization. A broad investigation is reported involving state-of-the techniques such as Raman, XRD, RBS, AFM, TEM/EDS, back-gated FET characterization, coupled with Heat Flow calculations of the laser process temperature profiles. It is noteworthy that the spatial and temporal confinement of laser annealing keeps the Si/SiO₂ substrate temperature well below the back-end-of-line temperature limit of Si CMOS technology (770 K). The synthesis method described here present large spaces of further development and improvement in terms selective crystallization and doping of MoS₂ layers, and can speed up the integration of large-area 2D- materials with Si-based devices, paving the way for many important applications.

References:

- [1] A. Tonon, E. Di Russo, F. Sgarbossa, L. Bacci, N. Argiolas, C. Scian, Y.P. Ivanov, G. Divitini, B. Sheehan, D. De Salvador, A. Gasparotto, V. Morandi, R. Duffy, E. Napolitani, Laser induced crystallization of sputtered MoS₂ thin films, Mater. Sci. Semicond. Process. 164 (2023) 107616. <https://doi.org/10.1016/j.mssp.2023.107616>.
- [2] E. Di Russo, A. Tonon, A. Mischianti, F. Sgarbossa, E. Coleman, F. Gity, L. Panarella, B. Sheehan, V.A. Lebedev, D. De Salvador, R. Duffy, E. Napolitani, Synthesis of Large-Area Crystalline MoS₂ by Sputter Deposition and Pulsed Laser Annealing, ACS Appl. Electron. Mater. 5 (2023) 2862–2875. <https://doi.org/10.1021/acsaelm.3c00362>
- E. Di Russo, F. Sgarbossa, P. Ranieri, G. Maggioni, S. Ndiaye, S. Duguay, F. Vurpillot, L. Rigutti, J.-L. Rouvière, V. Morandi, D. De Salvador, E. Napolitani, Synthesis of relaxed Ge0.9Sn0.1/Ge by nanosecond pulsed laser melting, Appl. Surf. Sci. 612 (2023) 155817. <https://doi.org/10.1016/j.apsusc.2022.155817>.

For your remarks

Towards a silicon semiconductor vacuum: donor spin decoherence in isotopically engineered 28-silicon

Shao Qi Lim,¹ Ravi Acharya,^{2,3} Nicholas Gillespie,² Brett C. Johnson,⁴ Alexander Malwin Jakob,¹ Daniel L. Creedon,^{2,5} Sergey Rubanov,⁶ Jeffrey C. McCallum¹ and David N. Jamieson¹

¹ Centre of Quantum Computation and Communication Technology, School of Physics, The University of Melbourne, Parkville 3010 Victoria, Australia.

² School of Physics, The University of Melbourne, Parkville 3010 Victoria, Australia.

³ Department of Electrical and Electronic Engineering, University of Manchester, United Kingdom.

⁴ School of Science, RMIT University, Melbourne 3000 Victoria, Australia.

⁵ CSIRO Manufacturing, Clayton 3168 Victoria, Australia.

⁶ Bio21 Institute, Electron Microscopy Unit, University of Melbourne, Parkville, VIC 3010, Australia.

Email: qi.lim@unimelb.edu.au

Ion implanted group V donors in silicon is a promising platform for realizing scalable quantum computers [1]. One of the many advantages of using silicon is that its most abundant isotope, ²⁸Si, has zero nuclear spin and thus provides a “semiconductor (magnetic) vacuum” for donor spin qubits in silicon. Natural silicon, however, contains ~5% of ²⁹Si which has a non-zero nuclear spin. These naturally occurring ²⁹Si atoms give rise to local magnetic perturbations in bulk silicon and subsequently result in a greater degree of donor spin decoherence. In our previous work, we demonstrated isotopic enrichment of silicon surface layers by high fluence ($>1\times10^{18} \text{ cm}^{-2}$) ion implantation of ²⁸Si ions into natural silicon (^{nat}Si) substrates [2], thus providing a means of greatly diminishing this source of decoherence. Recently, we have also demonstrated the ability to fabricate large arrays (>250) of individual near-surface dopant atoms using deterministic single ion implantation [3]. This addresses the issue of scale-up, which is one of the biggest challenges faced by the quantum computing research community.

We are currently developing the technique of Electrically Detected Magnetic Resonance (EDMR) as a fast-turn-around process for measuring the “quantum environment” of the enriched layer to assess the lifetime of donor electron spins, and the potential impact of residual defects and other factors for applications of the enriched material as a platform for realizing scalable quantum computers. This talk will first cover our previous and ongoing works on the isotopic enrichment of bulk silicon and silicon-on-insulator substrates, and deterministic single ion implantation of group V donors in silicon. The second part of this talk will focus on our efforts on performing EDMR measurements on devices fabricated from both ^{nat}Si and ²⁸Si enriched substrates implanted with group V donors. EDMR is an electrical technique that is widely used to study paramagnetic defects in semiconductors and has the advantage of providing the required high sensitivity for donor electrons in silicon without the need for sophisticated device architectures [4, 5]. Through pulsed magnetic resonance experiments, donor spin coherence times in our isotopically enriched ²⁸Si material can be extracted and will be compared directly to coherence times of donor spins in ^{nat}Si.

References:

- [1] B. C. Johnson, J. C. McCallum, and T. Botzem, *Appl. Phys. Rev.* **2021**, 8, 031314.
- [2] D. Holmes et al., *Phys. Rev. Materials* **2021**, 5, 014601.
- [3] A. M. Jakob et al., *Adv. Materials* **2022**, 34, 2103235.
- [4] D. R. McCamey et al., *Appl. Phys. Lett.* **2006**, 89, 182115.
- [5] F. Hoehne et al., *Rev. Sci. Instr.* **2012**, 83, 043907.

For your remarks

Engineered Donor-Qubit Arrays for Silicon Quantum Computing

A.M Jakob¹, S.G. Robson¹, H. Firgau², V. Mourik², V. Schmitt², D. Holmes², M. Posselt³, E. Mayes⁴, D. Spemann⁵, A. Morello², D. Jamieson¹

¹ School of Physics, University of Melbourne, 3010, Australia

² School of Electrical Engineering and Telecommunications, UNSW Sydney, 2052, Australia

³ Helmholtz-Zentrum Dresden-Rossendorf (HZDR), 01328 Dresden, Germany

⁴ RMIT University, Melbourne, 3052, Australia

⁵ Leibniz-Institute of Surface Engineering (IOM), 04318 Leipzig, Germany

Email: alexander.jakob@unimelb.edu.au

Semiconductor spin qubits combine excellent quantum performance [1] with the prospect of manufacturing quantum devices using industry-standard metal-oxide-semiconductor (MOS) processes [2]. This applies also to ion-implanted donor spins, which further afford exceptional coherence times and large Hilbert space dimension in their nuclear spin [3,4]. Here we demonstrate and integrate multiple strategies to manufacture scale-up donor-based quantum computers [5]. We use $^{31}\text{PF}_2$ molecule implants to triple the placement certainty compared to ^{31}P ions, while attaining 99.99% confidence in detecting the implant [6]. Similar confidence is retained by implanting heavier atoms such as ^{123}Sb and ^{209}Bi , which represent high-dimensional qudits for quantum information processing [4], while Sb_2 molecules enable deterministic formation of closely spaced qudits [6]. We demonstrate the deterministic formation of regular arrays of donor atoms with 300nm spacing, using step-and-repeat implantation through a nano aperture [6]. These methods cover the full gamut of technological requirements for the construction of donor-based quantum computers in silicon.

References:

- [1] F. A. Zwanenburg, A. S. Dzurak, A. Morello, M. Y. Simmons, L. C. Hollenberg, G. Klimeck, S. Rogge, S. N. Coppersmith, and M. A. Eriksson, *Reviews of modern physics*, 2013, 85, 961
- [2] A. Chatterjee, P. Stevenson, S. De Franceschi, A. Morello, N. P. de Leon, and F. Kuemmeth, *Nature Reviews Physics* 3, 2021, 157
- [3] J. T. Muhonen, J. P. Dehollain, A. Laucht, F. E. Hudson, R. Kalra, T. Sekiguchi, K. M. Itoh, D. N. Jamieson, J. C. McCallum, A. S. Dzurak et al., *Nature nanotechnology*, 2014, 9, 986
- [4] H. G. Stemp, S. Asaad, M. R. van Blankenstein, A. Vaartjes, M. A. Johnson, M. T. Mądzik, A. J. Heskes, H. R. Firgau, R. Y. Su, C. H. Yang, A. Laucht, C. I. Ostrove, K. M. Rudinger, K. Young, R. Blume-Kohout, F. E. Hudson, A. S. Dzurak, K. M. Itoh, A. M. Jakob, B. C. Johnson, D. N. Jamieson, A. Morello, arXiv preprint:2309.15463 2023
- [5] G. Tosi, F. A. Mohiyaddin, V. Schmitt, S. Tenberg, R. Rahman, G. Klimeck, and A. Morello, *Nature Communications*, 2017, 8, 450
- [6] A. M. Jakob, S. G. Robson, H. R. Firgau, V. Mourik, V. Schmitt, D. Holmes, M. Posselt, E. L. Mayes, D. Spemann, A. Morello, D. N. Jamieson, arXiv preprint:2309.09626 2023.

For your remarks

Exploring $\text{As}_i\text{-Si}_i$ -defects as qubits

Kevin Lauer,^{1,2} Katharina Peh,² Robin Müller,² Dirk Schulze,² Rüdiger Schmidt-Grund,² Stefan Krischok,² Aaron Flötotto,² Wichard Beenken,² Erich Runge,² Anna Reinhardt,¹ Mario Bähr,¹ Stephanie Reiß,¹ Andreas Frank¹ and Thomas Ortlepp¹

¹ CiS Forschungsinstitut für Mikrosensorik GmbH, Konrad-Zuse-Str. 14, 99099 Erfurt, Germany

² Technische Universität Ilmenau, Institut für Physik, Weimarer Str. 32, 98693 Ilmenau, Germany

Email: klauer@cismst.de

In present days extensive research is undertaken to identify defects in silicon, which could work as qubit. [1] Such defects may open the path to fully integrate quantum processors in silicon by using the large knowledge on silicon processing technology.

In this contribution the ability of $\text{As}_i\text{-Si}_i$ -defects to act as qubit is explored by considering reported experimental results related to this defect category. $\text{As}_i\text{-Si}_i$ -defects consist of an acceptor atom (e.g. B, Al, Ga, In or Tl) and a silicon atom which are located together in the space near one lattice position. [2] Defects of this category are able to exist in different configurations or modes. Some of these modes are known to emit bright luminescence. [3] One possibility to realize a qubit is by using the spin of e.g. an electron, which occupies a state caused by the defect. An indication, that a spin is involved in the electron transition responsible for the luminescence line, can be the splitting of the line in an applied magnetic field. Amongst others a specific luminescence feature of the $\text{Tl}_{\text{Si}}\text{-Si}_i$ -defect, called A-line, shows for specific parameters of the magnetic field a twofold splitting. [4]

The existing knowledge for this defect category is ploughed through for hints related to the ability of $\text{As}_i\text{-Si}_i$ -defects to act as qubit. These results will be summarized and discussed.

References:

- [1] D. B. Higginbottom et al., *Optical Observation of Single Spins in Silicon*, Nature **607**, 7918 (2022).
- [2] K. Lauer, K. Peh, D. Schulze, T. Ortlepp, E. Runge, and S. Krischok, *The $\text{As}_i\text{-Si}_i$ Defect Model of Light-Induced Degradation (LID) in Silicon: A Discussion and Review*, Phys. Status Solidi A **219**, 2200099 (2022).
- [3] K. Lauer, C. Möller, D. Schulze, and C. Ahrens, *Identification of Photoluminescence P Line in Indium Doped Silicon as InSi-Si_i Defect*, AIP Adv. **5**, 017101 (2015).
- [4] H. Conzelmann, A. Hangleiter, and J. Weber, *Thallium-Related Isoelectronic Bound Excitons in Silicon. A Bistable Defect at Low Temperatures*, Phys. Status Solidi B **133**, 655 (1986).

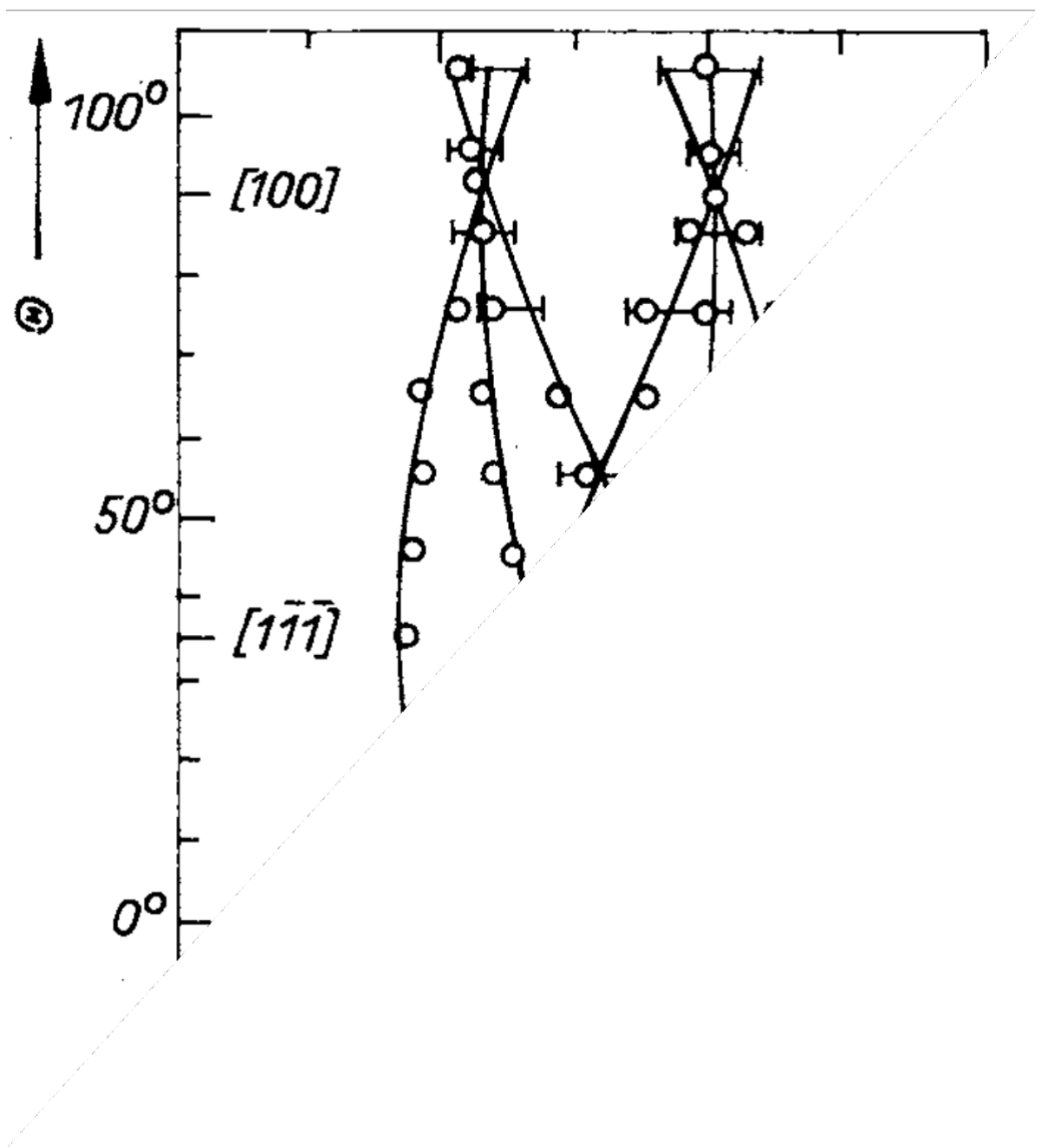


Fig. 1. Splitting of the A_0^0 -line of the Tl_{Si} - Si_i -defect under an applied magnetic field of 5.3T in different crystal directions. [4]

Fabrication and vertical position control of silicon colour centres via ultra-low temperature molecular beam epitaxy

Johannes Aberl¹, Enrique Prado Navarrete¹, Merve Karaman¹, Diego Haya Enriquez¹,
 Christoph Wilflingseder¹, Andreas Salomon¹, Petter Ström², Daniel Primetzhofer², Markus
 Andreas Schubert³, Giovanni Capellini^{3,4}, Thomas Fromherz¹, Peter Deák⁵, Ádám Gali^{5,6,7}
 and Moritz Brehm¹

¹ Institute of Semiconductor and Solid State Physics, Johannes Kepler University, Altenberger Straße 69, Linz
 4040, Austria

² Department of Physics and Astronomy, Uppsala University, Box 516, 75120 Uppsala, Sweden

³ IHP—Leibniz-Institut für innovative Mikroelektronik, Frankfurt (Oder), Germany

⁴ Dipartimento di Scienze, Università degli Studi Roma Tre, Rome, Italy

⁵ Wigner Research Centre for Physics, P.O. Box 49, H-1525, Budapest, Hungary

⁶ Department of Atomic Physics, Institute of Physics, Budapest University of Technology and Economics,
 Műegyetem rakpart 3., Budapest H-1111, Hungary

⁷ MTA-WFK Lendület “Momentum” Semiconductor Nanostructures Research Group, P.O. Box 49, H-1525,
 Budapest, Hungary

Email: johannes.aberl@jku.at

Recent demonstrations of high-purity single photon emission from isolated silicon (Si) colour centres (CCs) [1,2] triggered a renewed interest in this fairly-known defect class [3], holding the prospect of scalable deterministic group-IV based quantum light sources [4] operating in the telecom wavelength range. Just obtained results for the carbon (C) based G- and T-centres further outline their promising spin properties [5,6] for the realization of spin-photon interfaces on a scalable Si quantum photonics platform. However, towards their high-yield photonic integration, a severe obstacle remains, which is their common fabrication process based on single- or two-step ion implantation [1,7]. Here, the broad ion implantation profile entails a decisive lack of control over the vertical emitter position which significantly degrades the coupling efficiency to photonic structures such as resonators or waveguides.

In this contribution we present a completely different, all-epitaxial approach for the fabrication of variable Si CCs [8], which enables us to restrict their formation to a specific epilayer and hence control their vertical position in a structure with even sub-nm precision. They self-assemble *in-situ* during ultra-low temperature (ULT) growth [9] of thin Si:C layers deposited at $T_G=200^\circ\text{C}$ via molecular beam epitaxy (MBE). While the ULT growth just allows for the lattice disorder required for their formation, exceptionally pristine chamber conditions ensure a high optical quality of the CCs and allow fully crystalline Si overgrowth at higher T_G . To verify the vertical position control, we compare the photoluminescence (PL) signal of the created CCs for a systematic variation of T_G of active layer and cap vs. undoped references. The emitter density can be conveniently controlled via C doping concentration and Si:C layer thickness. Furthermore, we show first results for electrically-pumped CCs by integration of the Si:C nanolayers into ULT-grown p-i-n light emitting diodes.

References:

- [1] W. Redjem, *et al.*, Nat. Electron. 3, 738 (2020)
- [2] M. Hollenbach, *et al.*, Opt. Express 28, 26111 (2020)
- [3] G. Davies, Phys. Rep. 176, 83 (1989)
- [4] M. Khouri and M. Abbarchi, J. Appl. Phys. 131, 200901 (2022)
- [5] P. Udvarhelyi, *et al.*, Phys. Rev. Lett. 127, 196402 (2021)
- [6] D. B. Higginbottom, *et al.*, Nature 607, 266 (2022)
- [7] Y. Baron, *et al.*, Appl. Phys. Lett. 121, 084003 (2022) [8]
J. Aberl, *et al.*, arXiv, 2402.19227 (2024)
- [9] A. Salomon, *et al.*, Phys. Status. Solidi A. 219, 2200154 (2022)

Multi-physical modeling of bulk crystal growth: from furnace design to defect engineering

Kaspars Dadzis¹

¹Leibniz-Institut für Kristallzüchtung (IKZ), Max-Born-Str. 2, 12489, Berlin, Germany

Email: kaspars.dadzis@ikz-berlin.de

Crystal growth processes often take place at high temperatures, in controlled atmospheres of vacuum-sealed furnaces. While defects in the produced crystalline material usually occur on microscopic or atomistic scales, understanding the growth environment requires a different perspective that considers a set of macroscopic multi-physical phenomena:

- Heat transport inside the furnace by conduction, convection in liquid and gaseous phases as well as heat radiation determines the phase changes involved in the growth process and relevant parameters such as growth rate and thermal gradients;
- Electromagnetic fields related to the heating system may additionally generate forces in electrically conductive melts driving a flow;
- Flows in the liquid and gaseous phases influence the transport of the target material as well as various impurities;
- Stresses in the crystal arise from both thermal or compositional gradients.

Considering the limited possibilities of in-situ measurements in growth furnaces, how to investigate, control and optimize these phenomena?

Numerical simulation is a widely available tool today, which has been applied also to the complex, multi-physical, three-dimensional phenomena during crystal growth [1]. However, the underlying models contain many parameters and assumptions, which need to be validated using experimental data [2]. Therefore, the NEMOCRYS project [3] starts the model development from a physically similar model experiment designed for convenient in-situ access. The application of infrared cameras for temperature distributions, sensors for magnetic field, liquid flow velocity and many other fields allow one to validate the numerical models and subsequently use them for reliable simulation of the target process.

The present contribution is focused on the growth of bulk crystals from the melt using the Czochralski and Floating Zone techniques with various heating concepts. These methods have been applied not only to produce silicon in the microelectronics industry, but also a large variety of other crystalline materials such as high-melting oxides. A new model furnace with a flexible hotzone will be presented together with validated multi-physical models based on open source software packages. Although main experimental and theoretical results lie here on a macroscopic scale, the discussion of relations between thermal stresses and dislocation density or between melt flow pattern and impurity distribution will allow to build a bridge to defect engineering.

References:

- [1] K. Dadzis, P. Bönisch, L. Sylla, and T. Richter, *Journal of Crystal Growth* **2017**, 474, p. 171.
- [2] A. Enders-Seidlitz, J. Pal, and K. Dadzis, *Journal of Crystal Growth* **2022**, 593, p. 126750.
- [3] Next Generation Multiphysical Models for Crystal Growth Processes: <https://nemocrys.github.io/>

Acknowledgement: This work has been funded by the European Research Council (ERC) under the European Union's Horizon 2020 research and innovation programme (grant agreement No 851768).

For your remarks

Growth stability and defect generation of grain boundaries during directional solidification

Shuai Yuan^{1,2}, Xuegong Yu¹, Deren Yang^{1,2}

¹State Key Laboratory of Silicon and Advanced Semiconductor Materials and School of Materials Science and Engineering, Zhejiang University, Hangzhou 310027, PR China

²Shangyu Institute of Semiconductor Materials, Shaoxing, 312300, PR China

Email: shuaiyuan@zju.edu.cn

Seed joint defect had been a significant defect source in industrial cast monocrystalline silicon (CM-Si) materials since reported [1] because seeds as large as the crucible are hard to prepare. To date, the splicing of seeds still cannot be avoided. Seed splicing sabotages lattice integrity, causing the formation of a series of structural defects. The influence of the seed gap was reported by Ervik et al. [2]. While for boundaries themselves across the crystal, Hu et al. confirmed they are small angle grain boundaries (SAGBs), and then achieved the avoidance of SAGB formation in industrial ingot by setting large-angle grain boundaries (LAGBs) at seed joints [3]. Many works on various intentional LAGBs have been reported [4-7]. Trempa et al. investigated various types of CSL GBs ($\Sigma 3$, $\Sigma 9$, $\Sigma 33$, $\Sigma 41$) in multicrystalline silicon [4]. Kutsukake et al. reported stable $\Sigma 5$ GBs at ingot edge [5]. Wu et al. reported GBs with various tilt angles (0, 10°, 20°, 30°, 40°) [6]. Zhang et al. reported $\Sigma 13$ GB as seed joint boundaries [7]. So far, the common knowledge is that LAGBs are much more stable than SAGBs [5-7], but still can cause the formation of structural defects [4, 6, 7]. Interestingly, dislocations are formed at $\Sigma 33$ & $\Sigma 41$ GBs [4], and twins are formed at $\Sigma 13$ GBs [7]. However, there is no mature model or mechanism to explain: 1, why SAGB cannot stably grow and how SAGBs propagate; 2. The difference in growth behaviours between various types of LAGBs.

In this work, the physical model of SAGBs and LAGBs at the seed joints of CM-Si is given based on observations on behaviours shown in growth experiments. It is found that tilt angle deviation against aimed metastable state causes the rotation movement of seed joint grain boundaries during growth. Deviated grain boundary gradually grows into a curved surface; meanwhile, the relationship between the two sides changes from pure tilt into superposed tilt & twist. And the model is explained from the perspective of grain boundary energy. Curved GBs are an important deleterious defect source in CM-Si. When deviated from the original plane, the GB interface is not parallel with the growth direction. Solidification happens on the interface so that the imperfect lattice at GB might become a defect source. Various types of LAGBs and related defects were compared through experiments, which helps to conclude the influence of LAGB selection on the formation of deleterious defects.

References:

- [1] N. Stoddard, B. Wu, I. Witting et al., *Solid State Phenom.* **2008**, *131*, 1-8.
- [2] T. Ervik, G. Stokkan, T. Buonassisi et al., *Acta Mater.* **2014**, *67*, 199-206.
- [3] D. Hu, S. Yuan, L. He et al., *Sol. Energy Mater. Sol. Cells* **2015**, *140*, 121-125.
- [4] M. Trempa, C. Reimann, J. Friedrich et al., *Cryst. Res. Technol.* **2015** *50*(1), 124-132.
- [5] K. Kutsukake, N. Usami, Y. Ohno et al., *IEEE J. Photovolt.* **2014**, *4*, 84-87.
- [6] Y. Wu, A. Lan, C. Yang et al., *Cryst. Growth Des.* **2016**, *16*(11), 6641-6647.
- [7] F. Zhang, X. Yu, C. Liu et al., *Sol. Energy Mater. Sol. Cells* **2019**, *200*, 109985.

For your remarks

Phosphorus gettering effect on iron-related defects around dislocations with different densities in N-type cast-mono silicon

Jie Huang, Ruokai Wu, Xuegong Yu,^{*} Shuai Yuan and Deren Yang^{*}

*State Key Laboratory of Silicon and Advanced Semiconductor Materials, Zhejiang University, Hangzhou
310027, P. R. China*

Email: yuxuegong@zju.edu.cn; mseyang@zju.edu.cn

In the past few years, with the development of high-efficiency silicon solar cell architectures, the demand for high-performance N-type silicon wafers in the photovoltaic market has increased significantly. As a potential cell substrate, cast-mono silicon (CM-Si) may better meet this demand due to its high yield and low costs. However, iron, as the most common metal impurity in CM-Si, can introduce trap levels and interact with dislocations to form iron-related defects, which seriously affects the CM-Si performance.

In this work, the electrical properties of iron-related defects around dislocations with different densities as well as the phosphorus gettering effect on them have been studied in N-type CM-Si using deep level transient spectroscopy (DLTS) and electron beam induced current (EBIC). DLTS results reveal two trap levels related to iron complexes and clusters around low-density scattered dislocations: E1 (E_c - 0.212 eV) and E2 (E_c - 0.491 eV) [1], both of which are identified as extended localized states [2]. EBIC results show phosphorus gettering can effectively remove the above iron-related traps but not work on denser dislocations like dislocation arrays (DAs) and the already formed sub-grain boundaries (sub-GBs), which is possibly due to the severe competitive gettering influence from denser defects.

This work could offer a deeper understanding of the gettering effects on iron-related defects around dislocations and further promote the application of CM-Si to high-efficiency solar cells like HJT, TOPCon, or HBC.

Reference:

- [1] S. Gao, S. Yuan, Z. Hu, X. Yu, X. Zhu and D. Yang, *Applied Physics Express* **2021**, *14*(3), 035502.
 [2] W. Schröter, J. Kronewitz, U. Gnauert, F. Riedel and M. Seibt, *Physical Review B* **1995**, *52*, 13726.

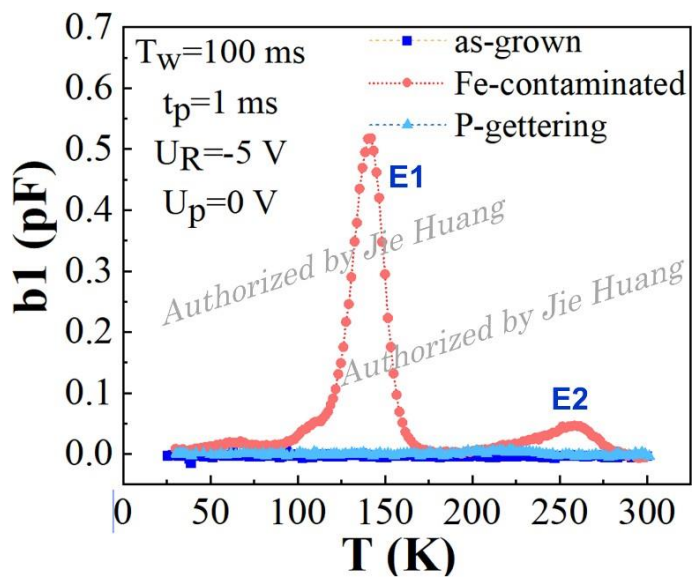


Fig. 1. DLTS spectra of the N-type CM-Si sample at as-grown, Fe-contaminated, and P-gettering states, respectively. Related parameters of the DLTS measurements: reverse bias $U_R = -5$ V, filling pulse bias $U_p = 0$ V, period width $T_w = 100$ ms, and the filling pulse duration $t_p = 1$ ms.

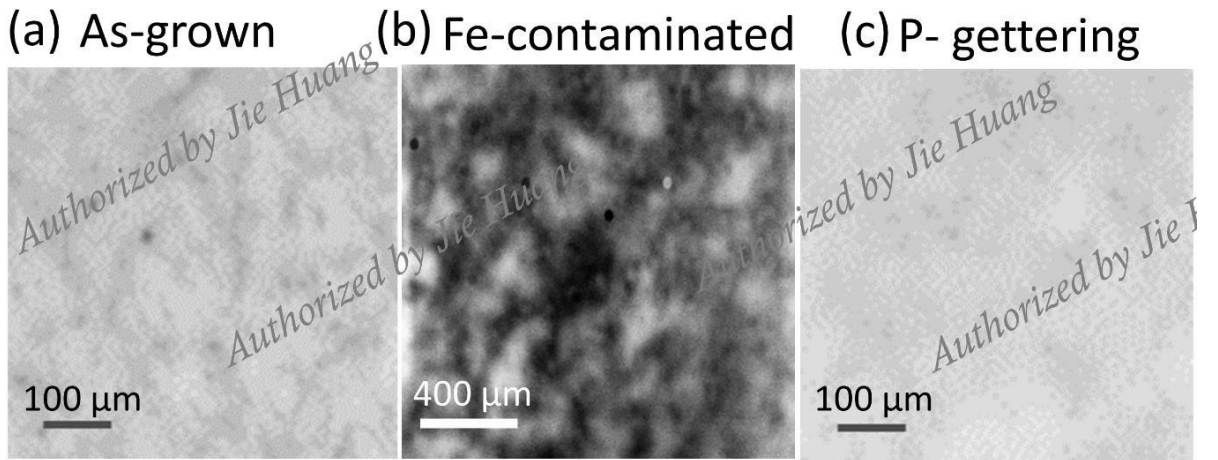


Fig. 2. EBIC images of the N-type CM-Si sample measured at room temperature: (a) As-grown; (b) Fe-contaminated; (c) P-gettering states.

Characterization of electrically active defects in semiconductor-grade Cz-Si by photoluminescence imaging

Katja Mustonen¹ and Hele Savin²

¹ Okmetic, Piitie 2, 01510 Vantaa, Finland

² Aalto University, Department of Electronics and Nanoengineering, Tietotie 3, 02150 Espoo, Finland

Email: katja.mustonen@okmetic.com

Photoluminescence imaging (PLI) is a widely accepted, fast and non-destructive method for detecting crystal defects in crystalline silicon solar cells [1][2]. PLI is less known by semiconductor wafer manufacturers despite the similarities between photovoltaic and semiconductor wafers. We study its application in characterizing defects in high-quality Czochralski silicon (Cz-Si) wafers, with a focus on detecting electrically active microcracks, slip lines, oxygen induced stacking faults (OISF) and bulk microdefects, benchmarked against current methods (see e.g. [3],[4],[5]).

Our results show that heavily doped wafers (resistivity below 0.1 Ωcm) are not sensitive to surface finish, e.g. acid-etched (Fig. 1a), and defects are clearly visible with PLI, regardless of the process stage. This can be explained by the excited carriers recombining in the bulk due to strong Auger recombination. As wafer resistivity increases to ~1 Ωcm and above, dopant-induced recombination weakens, and surface recombination begins to affect the PL signal. However, several process steps, e.g. lapping, yield a uniform enough background signal to distinguish crystal defects, regardless of wafer resistivity (Fig. 1b).

Like microcracks, the visibility of slip lines with PLI appears to depend on material parameters and surface finish. While x-ray diffraction imaging (XRDI) [3] excels in slip line detection, PLI can also reveal short and slender slip lines with an appropriate surface finish. In specific wafers, much faster PLI is able to show slip lines less visible by XRDI (Fig. 2a,2b). As a reference, Makyoh topography [4] only detects clustered slip lines (Fig. 2c).

OISFs that are revealed after destructive Wright etching [5], could potentially be detected with PLI even without thermal oxidation. The detection of OISF inducing nuclei by PLI is discussed in the presentation.

Finally, it is important to note that the visibility of all crystal defects in PLI will be limited by (metal) contamination, which causes bulk recombination in the wafers. Therefore, for effective crystal defect detection, wafers should be free of such contamination.

References:

- [1] T. Trupke, R.A. Bardos, M.C. Schubert, W. Warta, Photoluminescence imaging of silicon wafers. *Appl. Phys. Lett.* **2006**, 89, 44107.
- [2] T. W. Teo, Z. Mahdavipour and M. Z. Abdullah, Recent advancements in micro-crack inspection of crystalline silicon wafers and solar cells, *Measurement Science and Technology* **2020**, 31(8), pp. 1-16.
- [3] A. R. Lang, Direct Observation of Individual Dislocations by X-Ray Diffraction, *J. Appl. Phys.* **1958**, 29(3), pp. 597-598.
- [4] F. Riesz, Makyoh topography: A simple yet powerful optical method for flatness and defect characterisation of mirror-like surfaces, *Proceedings of SPIE - The International Society for Optical Engineering* **2004**, 5458, pp. 86-100.
- [5] M. W. Jenkins, A new preferential etch for defects in silicon crystals, *Journal of the Electrochemical Society* **1977**, 124(5), p. 757.

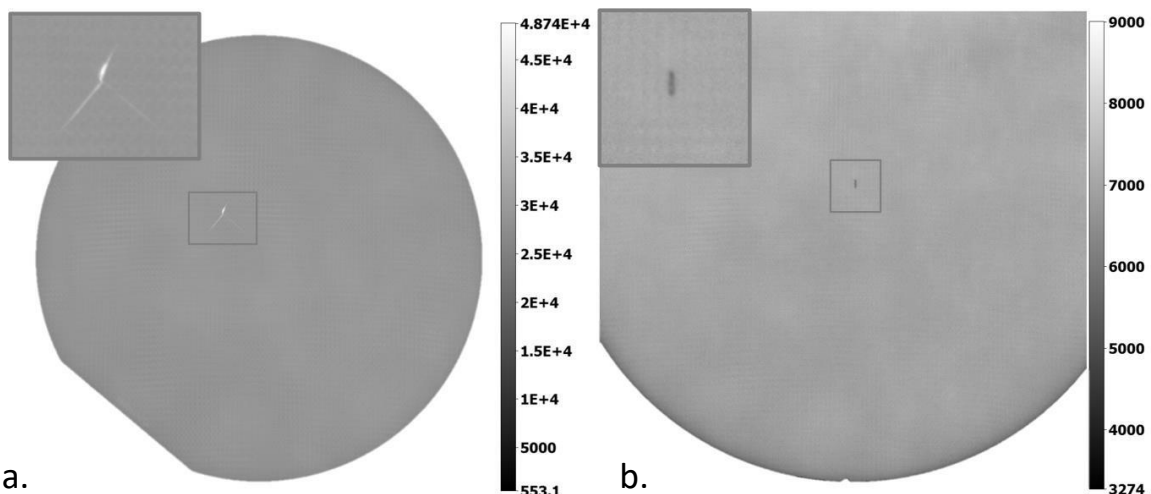


Fig. 1. Examples of photoluminescence images (PLI) measured from a) a 150 mm boron-doped Cz-Si (100) wafer with a resistivity of $0.01 \Omega\text{cm}$ and thickness of $625 \mu\text{m}$ *after acid etching*, and b) a 200 mm boron-doped Cz-Si (100) wafer with resistivity of $3.7 \Omega\text{cm}$ and thickness of $300 \mu\text{m}$ directly *after lapping*. The data shows the number of emitted PL counts when using excitation photon flux of $2\text{e}18 \text{ cm}^{-2}\text{s}^{-1}$ and exposure time of 5 s and 10 s in (a) and (b), respectively. The inset shows the zoomed image of the detected crystal defects (microcracks).

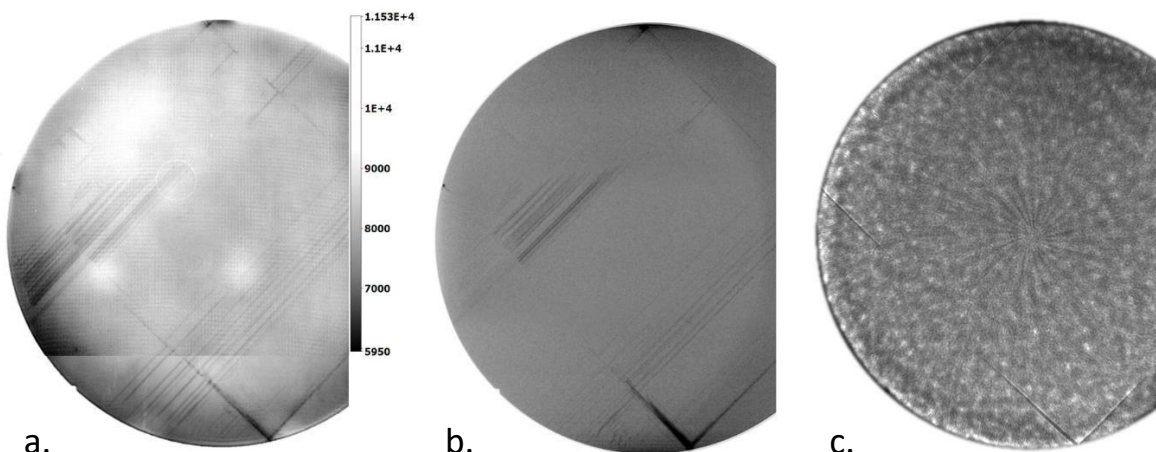


Fig. 2. Appearance of slip lines via a) PLI, b) XRDI, and c) Makyo topography in the same 200 mm boron-doped Cz-Si (100) wafer with a resistivity of $>5000 \Omega\text{cm}$ and thickness of $725 \mu\text{m}$. PLI image is constructed from two separate 150 mm images taken with the same exposure time of 170 s and photon flux of $2\text{e}18 \text{ cm}^{-2}\text{s}^{-1}$.

Insight into the Defects that Govern Degradation of Silicon Heterojunctions Solar Cells

Martiana Bertoni

*Defect Lab, School of Electrical, Computer and Energy Engineering, Arizona State University,
USA*

Email: mariana.bertoni@asu.edu

Silicon Heterojunction (SHJ) is an established solar technology with a record power conversion efficiency of ~27%, however, its widespread adoption in the photovoltaic (PV) market is still lacking. Studies have shown that the greatest contributor to loss in SHJ performance in the field emanates from the drop in open-circuit voltage (V_{oc}). This hints towards a possible loss of passivation at the interfaces under light and elevated temperature (T) in the field. While the deposition conditions and the structural and optical properties of amorphous silicon have been studied for optimizing the passivation of crystalline silicon surface, they have never been investigated for long-term stability. In this presentation, I will share how the passivation quality of the amorphous silicon/ crystalline silicon stacks behave through time under various stressing conditions (T and Δn). Parametrization of the defect density at the interface show that the bond energies of a large fraction of the Si atoms, especially those close to the interface, are weakened by stretching and twisting. This suggests that the defect generation is controlled by a broad distribution of energy barriers instead of a narrow one, as is customary to expect when thinking about the degradation of chemical passivation processes. I will also discuss changes at the transparent conductor/a-Si interface and some interesting behavior of the hydrogenated films under operation.

For your remarks

Relationship between the P-line in indium-doped silicon spectra and the recent ASi-Sii defect model

Katharina Peh,¹ Dominik Bratek,¹ Kevin Lauer,^{1,2} Robin Müller,¹ Dirk Schulze,¹ Aaron Flötotto¹ and Stefan Krischok¹

¹ TU Ilmenau, Institut für Physik und Institut für Mikro- und Nanotechnologien, 98693 Ilmenau, Germany

² CiS Forschungsinstitut für Mikrosensorik GmbH, Konrad-Zuse-Str. 14, 99099 Erfurt, Germany

Email: katharina.peh@tu-ilmenau.de

Despite intensive studies of the P-line, located at around 1.118 eV, in indium-doped silicon by low-temperature photoluminescence spectrum for decades its origin is still not fully understood. Lauer et al. [1] describe in their recent review the following three key observations for indium-doped silicon [2 – 6]: (i) The appearance of the P-line is dependent on the presence or absence of silicon interstitial density. (ii) The intensity of the P-line changes with moderate illumination and annealing treatments along the treatments of the LID cycle. (iii) The P-line disappears when hydrogen-rich silicon nitride layers are applied to indium-doped silicon and annealed at 200 °C for 10 minutes.

Therefore, we assume that the silicon interstitial as part of the ASi-Sii defect plays an important role for Light Induced Degradation (LID) and the P-line can serve as a fingerprint. The different involved defect states, can also be passivated by hydrogen by forming an InSi-Sii-H defect. After deriving a configuration-coordinate energy diagram for the ASi-Sii defect model, we assumed that the illumination and annealing step leads to a configuration change of the silicon interstitial itself. Here the P-line intensity indicates the intermediate state of the model. Therefore, by analysing the intensity of the P-line, we can draw conclusions about the defect density in the intermediate state. This is evidence that the defects can also exist in different configurations. In this work we take a closer look at the annealing behaviour and configuration change of the LID defect in indium-doped silicon. A sequence of short annealing steps after an initial long illumination of the sample shows an increase in P-line intensity in the experiment. This is followed by a successive decrease in intensity with further annealing steps (see *Fig. 1*). We are able to determine the second energy barrier for this configuration change (see *Fig. 2*). The rate constants for the decay and an energy barrier of Ebarrier= 0.62±0.06 eV could be calculated from the decay of the P-line intensities. Both indium as grown Czochralski (CZ) and implanted float zone (FZ) silicon wafers are examined and their behavior is compared. The ASi-Sii defect model is used to discuss the results.

References:

- [1] K. Lauer, K. Peh, D. Schulze, T. Ortlepp, E. Runge, and S. Krischok, “The ASi-Si_i Defect Model of Light - Induced Degradation (LID) in Silicon: A Discussion and Review,” *Physica Status Solidi (a)* 219(19), 2200099 (2022).
- [2] C. Möller, and K. Lauer, “Light-induced degradation in indium-doped silicon,” *Physica Status Solidi (RRL) - Rapid Research Letters* 7(7), 461–464 (2013).
- [3] C. Möller, and K. Lauer, “ASi-Sii-defect Model of Light-induced Degradation in Silicon,” *Energy Procedia* 55, 559–563 (2014).
- [4] K. Lauer, C. Möller, D. Schulze, and C. Ahrens, “Identification of photoluminescence P line in indium doped silicon as InSi-Sii defect,” *AIP Advances* 5(1), 017101 (2015).
- [5] K. Lauer, C. Möller, D. Schulze, C. Ahrens, and J. Vanhellemont, “Discussion of ASi-Sii-defect model in frame of experimental results on P line in indium doped silicon,” *Solid State Phenomena* 242, 90 (2015).
- [6] K. Lauer, C. Möller, C. Tessmann, D. Schulze, and N.V. Abrosimov, “Activation energies of the InSi-Sii defect transitions obtained by carrier lifetime measurements,” *Physica Status Solidi (c)* 14(5), 1600033 (2017).

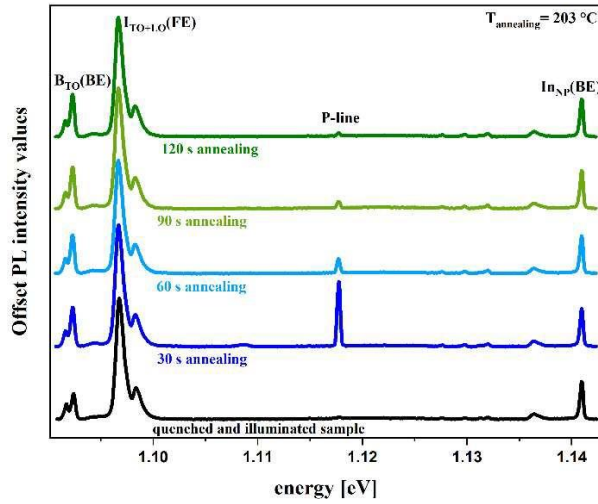


Fig. 1: PL spectra for different annealing times after an initial quenching and a long illumination step. Measuring temperature $T = 4.2 \text{ K}$. The spectra are normalized with respect to the height of indium non phonon $\text{In}_{\text{NP}}(\text{BE})$ peak. All 5 spectra were measured consecutively on the same sample: FZ Si:In. The order of the measurements is from bottom to top.

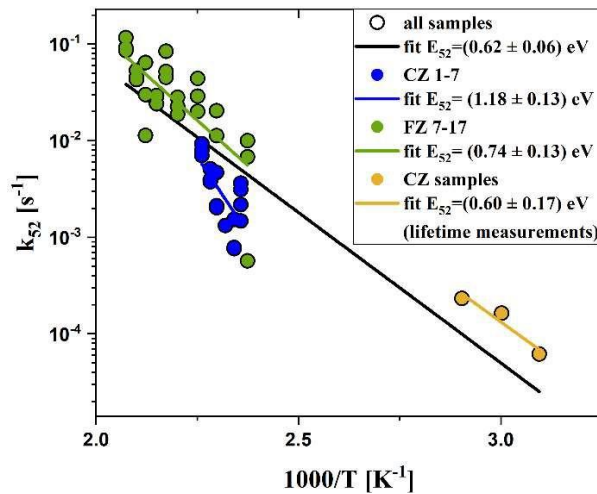


Fig. 2: Measured transition rates as a function of inverse temperature (Arrhenius plot). The calculated energy barriers E_{52} of samples are given in the legend.

Resolving the defects in polycrystalline metal halide perovskite by photoluminescence technique

Zhenyi Ni¹

¹ Zhejiang University, Hangzhou, China

Email: zyni@zju.edu.cn

Understanding carrier recombination processes in metal halide perovskites are fundamentally important to further improving the efficiency of perovskite solar cells, yet the accurate recombination velocity at grain boundaries (GBs) has not been determined. Here we report the determination of carrier recombination velocities at GBs (S_{GB}) of polycrystalline perovskites by mapping the transient photoluminescence pattern change induced by the non- radiative recombination of carriers at GBs. Charge recombination at GBs is revealed to be even stronger than at surfaces of unpassivated films, with average S_{GB} reaching 2200 – 3300 cm/s. Regular surface treatments do not passivate GBs, due to the absence of contact at GBs. We find a surface treatment using tributyl(methyl)phosphonium dimethyl phosphate which can penetrate into GBs by partially dissolving GBs and converting it into one-dimensional perovskites. It reduces the average S_{GB} by four times, with a lowest S_{GB} of 410 cm/s which is comparable to surface recombination velocities after passivation. [1].

References:

- [1] Z.Y. Ni, S. Xu, H.Y. Jiao, H.Y. Gu, C.B. Fei, J.S. Huang "High grain boundary recombination velocity in polycrystalline metal halide perovskites", *Science Advances*, 8, abq8345 (2022).

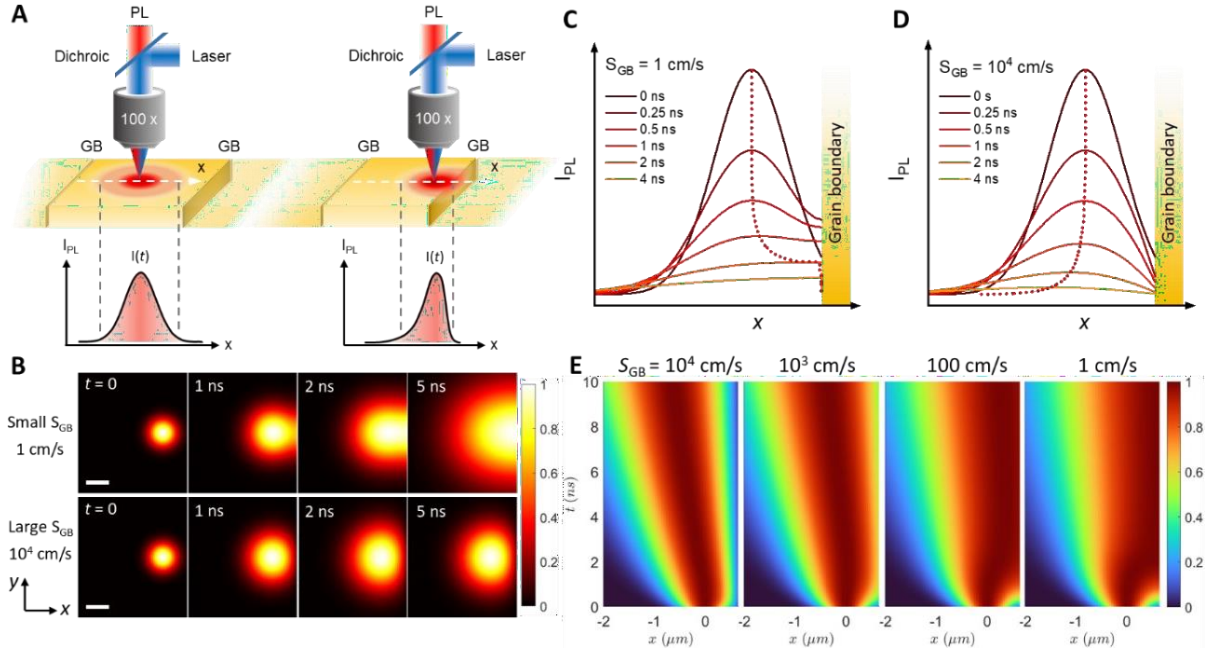


Fig. 1. Determination of GB charge recombination velocities. (A), schematic diagram of using PL mapping and carrier diffusion imaging to measure GB recombination velocities. (B), simulated 2D (x - y) carrier diffusion images of perovskite crystals with small (top) and large (bottom) S_{GB} at time frames of 0, 1, 2 and 5 ns. The I_{PL} is normalized to its peak value at each frame. Simulated linear PL profiles along one direction (x) of the perovskite crystals with (C) $S_{GB} = 1 \text{ cm/s}$ and (D) 10^4 cm/s at different times after laser excitation. The red dashed lines denote the shifts of the peak positions of the profile curves. The yellow blocks denote the locations of GBs. (E), simulated linear carrier diffusion profiles along the normal direction of crystal edges of MAPbI_3 single crystals with different S_{GB} . The crystal edge is at the right edge of each figure.

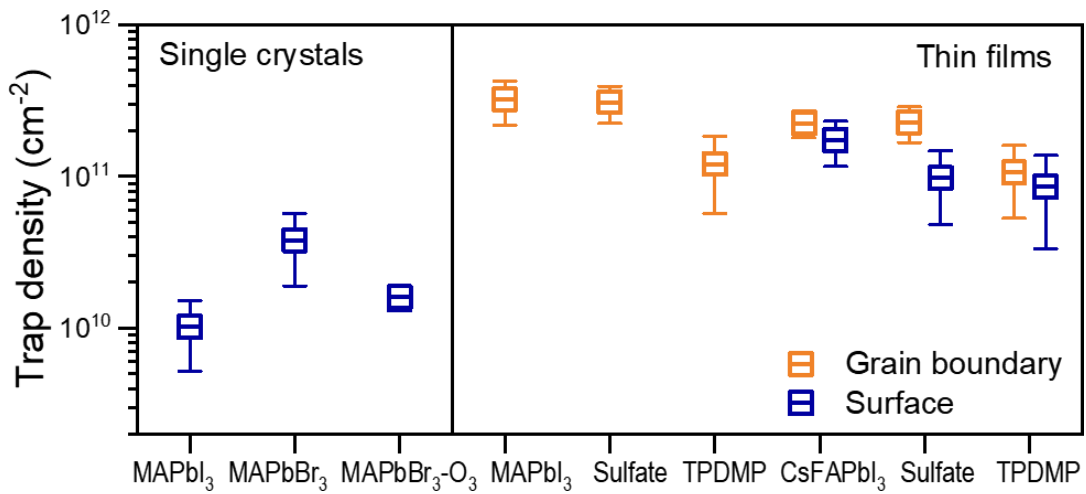


Fig. 2. Measured surface and GB trap densities of perovskite single crystals and polycrystalline thin films.

The role of Electron Trapping and Ion Drift on Photo-Induced Current Transient Spectroscopy of Metal Halide Perovskites

Daniela Cavalcoli, Giovanni Armaroli, Lorenzo Maserati, Andrea Ciavatti, Beatrice Fraboni

¹Department of Physics and Astronomy, University of Bologna, Viale Berti Pichat 6/2, 40127 Bologna, Italy

Email: daniela.cavalcoli@unibo.it

Metal-halide perovskites (MHPs) have demonstrated the potential to greatly impact optoelectronic devices. The presence of electronic trap states represents a significant material's science challenge in these materials, as they are difficult to characterize and mitigate. Various attempts have been made to use electronic spectroscopies to study the defect states in bulk crystals of MHPs. However, due to the mixed nature of electronic and ionic conductivity in MHPs, the results of these experiments often present a high level of uncertainty in distinguishing between electronic and ionic charge contributions.

In this study, we employ a method called photo-induced current transient spectroscopy (PICTS) [1], which was previously used in highly resistive inorganic semiconductors [2], to analyze single crystals of two types of MHPs: lead bromide 2D-like $((\text{PEA})_2\text{PbBr}_4)$ and standard "3D" (MAPbBr_3) perovskites. The method is usually based on the detection of photocurrent transients at varying temperatures, from which the trap parameters are obtained (see fig.1). The different ion mobility of "2D" and "3D" MHPs allowed us to differentiate between the electronic and ionic contributions to the photocurrents. Our experimental findings reveal that the PICTS method allows for the detection of electronic trap states in the 2D perovskite $((\text{PEA})_2\text{PbBr}_4)$, which has limited ion mobility, while it allows for the detection of parameters related to ion diffusivity in 3D (MAPbBr_3) perovskites.

Therefore, our results establish new boundaries for the use of PICTS in studying 3D perovskites, which exhibit greater ionic diffusion [3].

References:

- [1] P. Blood, and J.W. Orton, The Electrical Characterization of Semiconductors: Majority Carriers and Electron States (Academic Press, 1992) p.70.
- [2] J.C. Balland, J.P. Zielinger, C. Noguet, and M. Tapiero, "Investigation of deep levels in high-resistivity bulk materials by photo-induced current transient spectroscopy. I. Review and analysis of some basic problems," *J. Phys. D: Appl. Phys.* 19(1), 57 (1986).
- [3] G. Armaroli, L. Maserati, A. Ciavatti, P. Vecchi, A. Piccioni, M. Foschi, V. Van der Meer, C. Cortese, M. Feldman, V. Foderà, T. Lemercier, J. Zaccaro, J. Guillén, E. Gros-Daillon, B. Fraboni, and D. Cavalcoli, "Photo-Induced Current Transient Spectroscopy on Metal Halide Perovskites: Electron Trapping and Ion Drift," (2023) *ACS Energy Letters* **2023** 8, 4371.

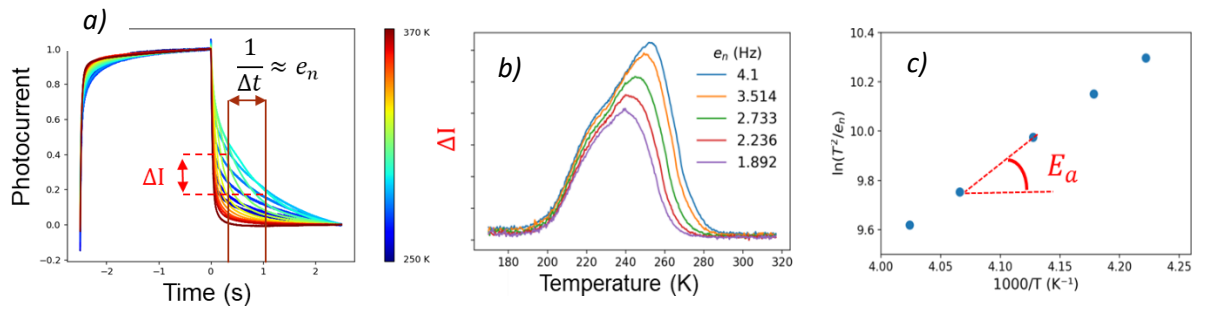


Fig. 1. Schematics of the PICTS (Photoinduced Current Transient Spectroscopy) experiments. The signals ΔI related to the photoinduced decay transients, detected over a time interval Δt (*a*), are plotted vs temperature (*b*). The plot of the emission rate e_n vs inverse temperature (*c*) allows for the evaluation of the trap activation energy E_a .

Muon probes of charge carrier kinetics in semiconductors

Koji Yokoyama¹

¹ ISIS Neutron and Muon Facility, STFC Rutherford Appleton Laboratory, Didcot, OX11 0QX, UK Email:

Email: koji.yokoyama@stfc.ac.uk

Positively charged muons, as a bulk probe of materials, have been used to study the charge carrier kinetics in tetrahedral semiconductors. The photoexcited muon spin spectroscopy technique (“photo- μ SR”) [1] can optically generate excess carriers in semiconductor materials, while muons can measure the excess carrier density. A hydrogen-like muonium atom, $\text{Mu} = \mu^+ + e^-$, are formed in many semiconductor materials. They interact with free carriers via carrier exchange interaction, which in turn induces muon spin relaxation via $\mu^+ - e^-$ hyperfine interaction. Hence, the spin relaxation rate can be used as a measure of the excess carrier density. With a pulse delay between a muon (~ 60 ns) and laser (~ 10 ns) pulse, a carrier recombination lifetime spectrum can be obtained. So far, we have applied and successfully demonstrated the method in Si [2], Ge [3], and SiC. To further explore the capability of the method, we varied the muon implantation depth and demonstrated a depth-dependent carrier lifetime measurement [4]. The measurements can allow us to de-convolute the bulk and surface recombination properties by applying a simple one-dimensional diffusion model. These advantages can be useful in measuring carrier lifetimes in completed silicon solar cells [5] and eventually optimising their device performance. I will start the presentation with a short introduction to the muon spin spectroscopy technique and illustrate the methods with its advantages and limitations. If time allows, I wish to introduce our recent attempt in measuring fast carrier recombination in direct gap semiconductors [6].

References:

- [1] K. Yokoyama, J.S. Lord, P. Murahari, K. Wang, D.J. Dunstan, S.P. Waller, D.J. McPhail, A.D. Hillier, J. Henson, M.R. Harper, P. Heathcote, and A.J. Drew, *Review of Scientific Instruments* **2016**, 87(12), 125111.
- [2] K. Yokoyama, J.S. Lord, J. Miao, P. Murahari, and A.J. Drew, *Phys. Rev. Lett.* **2017**, 119(22), 226601.
- [3] K. Yokoyama, J.S. Lord, P.W. Mengyan, M.R. Goeks, and R.L. Lichteni, *Appl. Phys. Lett.* **2019** 115(11), 112101.
- [4] K. Yokoyama, J.S. Lord, J. Miao, P. Murahari, and A.J. Drew, *Appl. Phys. Lett.* **2021**, 118(25), 252105.
- [5] J.D. Murphy, N.E. Grant, S.L. Pain, T. Niewelt, A. Wratten, E. Khorani, V.P. Markevich, A.R. Peaker, P.P. Altermatt, J.S. Lord, and K. Yokoyama, *Journal of Applied Physics* **2022**, 132(6), 065704.
- [6] K. Yokoyama, J.S. Lord, P.W. Mengyan, M.R. Goeks, and R.L. Lichteni, *Preprint (under review)* **2023** at <https://doi.org/10.48550/arXiv.2305.05513>.

For your remarks

Photo-elastic Characterization of Twin Structures and Growth Striations in InP and GaAs Crystals

Martin Herms¹⁾, Laura Narvaez¹⁾
Christiane Frank-Rotsch²⁾, Uta Juda²⁾
Dmitri Suptel³⁾

¹⁾ PVA Metrology & Plasma Solutions GmbH, Im Westpark 10-12, D-35435 Wettenberg, Germany

²⁾ Leibniz-Institut für Kristallzüchtung (IKZ), Max-Born-Str. 2, D-12489 Berlin, Germany

³⁾ Freiberger Compound Materials GmbH, Am Junger-Löwe-Schacht 5, D-9599 Freiberg, Germany

Email: martin.herms@pvatepla.com

Extended defect structures such as twin lamellae and growth striations in InP and GaAs crystals grown by Vertical Gradient Freezing (VGF) [1] technique are characterized using Defect Selective Etching (DSE) [2, 3] and Scanning Infrared Depolarization (SIRD) [4]. Both methods reveal congruent defect patterns, although the origins of contrast differ. Moreover, SIRD works non-destructive. In particular, the multi-polarization analysis (MPA) allows for determining the maximum value and principal direction of birefringence [5]. The lines of isostatics highlight a notable difference between twin boundaries and growth striations (see figure 1). The local contrast of birefringence across growth striations is stress-induced. The principal direction of stress is alternatingly aligned parallel and perpendicular to the phase boundary. In contrast, twin boundaries separate areas of native anisotropy according to the crystallographic orientation but presumably without a contribution of shear stress.

References:

- [1] C. Frank-Rotsch, N. Dropka, A. Glacki, and U. Juda, *Journal of Crystal Growth* (**2014**) 401, 702-707, DOI: 10.1016/j.jcrysgro.2013.12.063
- [2] M. S. Abrahams, C.J. Buiocchi, *J. Appl. Phys.* (**1965**), 36(9), 2855-63, DOI: 10.1063/1.1714594.
- [3] J.L. Weyher, P.J. van der Wel, G. Frigerio, C. Mucchino, *Proceedings of the Sixth Conference on Semi-insulating III-V Materials*, Toronto, Canada, (**1990**) p. 161, ISBN: 9780750300667
- [4] M. Herms, M. Wagner, A. Molchanov, P. Lin, I. De Wolf, and M. Zhao, *Phys. Status Solidi C* **12** (**2015**), No. 8, 1085–1089, DOI: 10.1002/pssc.201400356.
- [5] M. Herms, G. Irmer, G. Kupka, N. Kirchner, and M. Wagner, *Journ. Electronic Mater.* (**2020**), DOI: 10.1007/s11664-020-08141-7.

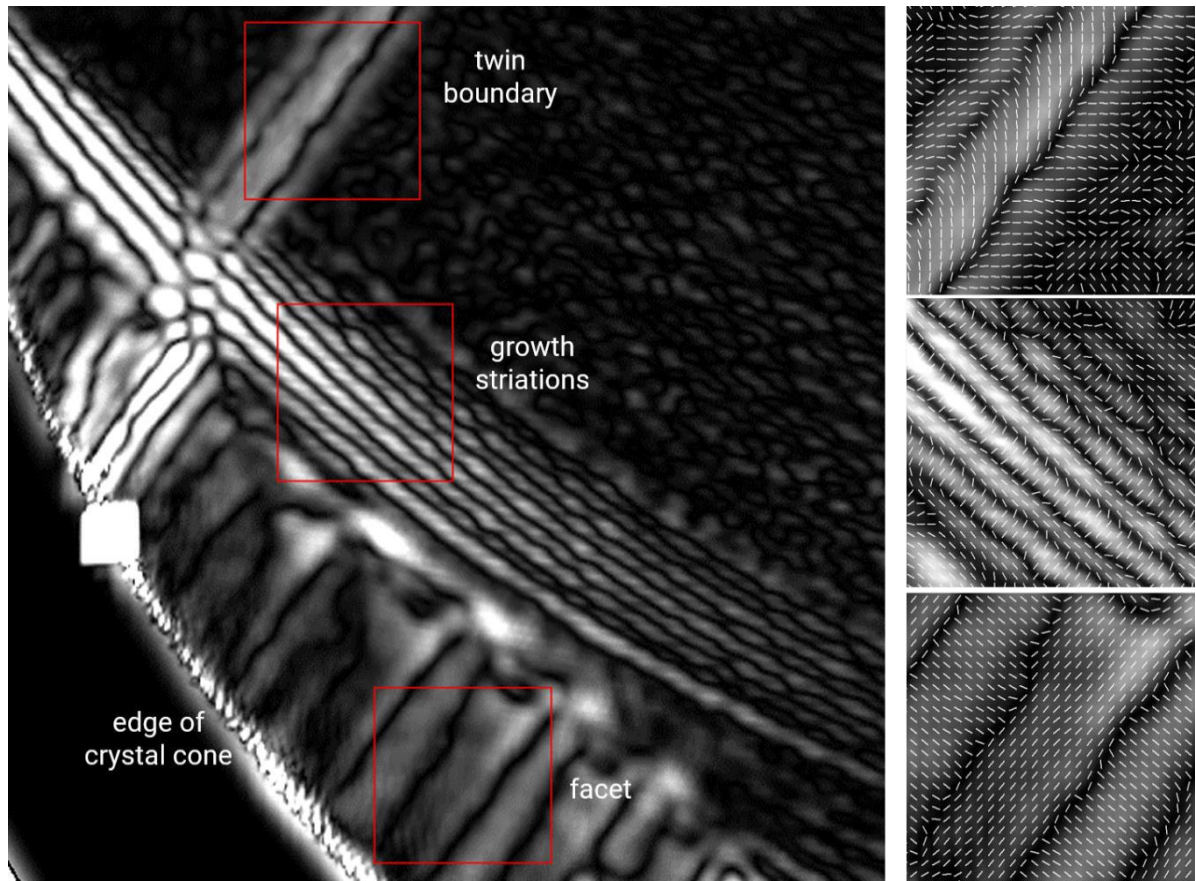


Fig. 1. Birefringence map of a (110) slice cut from a InP crystal, displaying the cone area ($10\text{mm} \times 10\text{mm}$) and three magnified details ($2\text{mm} \times 2\text{mm}$). The white lines indicate the direction of the fast principal axis of birefringence.

Characterization of electrically active defects in elemental and compound semiconductors by means of Scanning Spreading Resistance Microscopy

Tim Böckendorf¹, Felix Kipke¹, Jan Tröger^{1,2}, and Hartmut Bracht¹

¹Institute of Materials Physics, University of Münster, Wilhelm-Klemm-Straße 10, D-48149 Münster, Germany

²Tascon GmbH, Mendelstraße 17, D-48149 Münster, Germany

Email: tim.boeckendorf@uni-muenster.de

Today the characterization of electrically active defects and their distribution in semiconductor structures is a challenge, as the dimensions of electronic structures have reached the nanometer range. Secondary ion mass spectrometry and atom probe tomography offer nanometer-scale depth resolution, but these techniques only provide information about the chemical composition of the material within their specific detection limits. No information is available on the electrical behavior of intentionally or unintentionally introduced electrically active defects. Scanning spreading resistance microscopy (SSRM) measures the resistance of the semiconductor with nanometer depth resolution. By means of careful calibration and numerical simulations of the 2D SSRM resistance map the charge carrier distribution of electrically active defects can be determined.

SSRM has been successfully applied on silicon (Si) and germanium (Ge) [1,2,3] as well as on compound semiconductors such as gallium arsenide (GaAs) and silicon carbide (SiC) [4,5,6]. When performing SSRM on GaAs and SiC, the polarity of the applied bias voltage and the voltage level must be carefully adjusted, as the measured resistance strongly depends on the applied bias voltage. This is a consequence of the Schottky-like contact between probe and sample. We report SSRM analyses on elemental and compound semiconductor nanostructures that demonstrate the impact of surface and interface states. Current-voltage curves reveal the nature of the contact barrier between probe and sample. Most suitable bias settings are utilized to quantify the concentration of electrically active defects in the various semiconductor structures.

References:

- [1] A. Schulze, T. Hantschel, P. Eyben, A.S. Verhulst, R. Rooyackers, A. Vandooren and W. Vandervorst, *Ultramicroscopy* **2013**, *125*, 18-23.
- [2] J.K. Prüßing, G. Hamdانا, D. Bougeard, E. Peiner and H. Bracht, *Journal of Applied Physics* **2019**, *125*(8), 085105.
- [3] J. K. Prüßing, T. Böckendorf, F. Kipke, J. Xu, P. Puranto, J. Lundsgaard Hansen, D. Bougeard, E. Peiner, and H. Bracht, *Journal of Applied Physics* **2022**, *131*(7), 075702.
- [4] R. P. Lu, K. L. Kavanagh, St. J. Dixon-Warren, A. Kuhl, A. J. SpringThorpe, E. Griswold, G. Hillier, I. Calder, R. Arés and R. Streater, *Journal of Vacuum Science & Technology* **2001**, *19*(4), 1662-1670.
- [5] O. Dixon-Luinenburg, U. Celano, W. Vandervorst and K. Paredis, *Ultramicroscopy* **2019**, *206*, 112809.
- [6] J. Osterman, A. Hallén and S. Anand, *Applied Physics Letters* **2002**, *81*(16), 3004-3006.

For your remarks

Positively charged defects in Ta₂O₅ and Nb₂O₅: are they correlated with sodium ions?

Vladimir Kolkovsky* and Eberhard Kurth

Fraunhofer IPMS, Maria-Reiche Str. 2, 01109 Dresden, Germany

Email: uladzimir.kalkouski@ipms.fraunhofer.de

Stack structures of Ta₂O₅ (Nb₂O₅) and SiO₂ are promising candidates for applications as gate insulators in ion-sensitive field-effect transistors and various actuator applications. Defects unintentionally introduced into these layers during deposition or subsequent wafer treatments could be responsible for severe degradation of the devices. Through capacitance-voltage and triangular voltage sweep (TVS) measurements, we observed mobile positively charged defects in both Ta₂O₅ and Nb₂O₅ layers deposited on thin SiO₂ layers. These defects were not detected in the SiO₂ layers before the deposition of high-k oxides, and their concentration significantly depends on the purity of the targets. We found the electrical properties of these defects to be similar to those of positively charged Na⁺ in SiO₂. Vapor-phase decomposition inductively coupled plasma mass spectrometry measurements show that Na is a dominant signal besides Ta and Nb after the deposition of Ta₂O₅ and Nb₂O₅, respectively. Considering these findings, we discuss the origin of the positively charged defects with an emphasis on their correlation with Na⁺.

For your remarks

Secondary phases detection in CuInS₂ single crystal

Samira Khelifi,¹ Henk Vrielinck¹

¹ Ghent University, Department of Solid State Sciences, Krijgslaan 281, S1, 9000, Ghent ,Belgium

Email: samira.khelifi@ugent.be

The presence of secondary phases in the absorbers during the fabrication of solar cells is known to have a strong effect on the device performance, since their formation during the crystal or the film growth is inevitable [1]. Ternary chalcopyrite CuInS₂ based solar cells have so far reached an efficiency of 11-12% [2,3], which is still below the theoretical efficiency. Therefore, the enhancement of the device performance requires a better understanding of the microstructure of the absorber material and its dependence on the fabrication processes. In this work, the microstructure of single crystal CuInS₂, fabricated by melt-growth method (Bridgman), is investigated using two non-destructive characterization techniques, X-Ray diffraction (XRD) analysis and Fourier-Transform Infrared spectroscopy. The XRD measurements were performed on powder samples obtained from the CuInS₂ single crystal, while the FTIR spectra were recorded on pressed pellet prepared by mixing CuInS₂ powder with polyethylene. The combination of both techniques has allowed the identification of CuIn₅S₈ secondary phase which is also known as nonstoichiometric ordered defect compounds (ODC). For comparison, results obtained on chalcopyrite thin-film absorbers prepared using different deposition techniques are discussed. Subsequently, the effect of the presence of the ODC secondary phase on the solar cell performance is investigated using numerical modelling and simulation [4].

References:

- [1] S. Khelifi et al., Solar Energy Materials and Solar Cells, 2021, 219, 110824
- [2] K. Siemer, J. Klaer, I. Luck, J. Bruns, R. Klenk, D. Bräunig, Sol. Energy Mater. Sol. Cells, 2001, 67, 159-166.
- [3] K. Siemer, J. Klaer, I. Luck, J. Bruns, R. Klenk, D. Bräunig, Semicond. Sci. Technol. 1998, 13, 1456-1458.
- [4] M. Burgelman, K. Decock, S. Khelifi, A. Abass, Thin Solid Films, 2013, 535, 296–301.

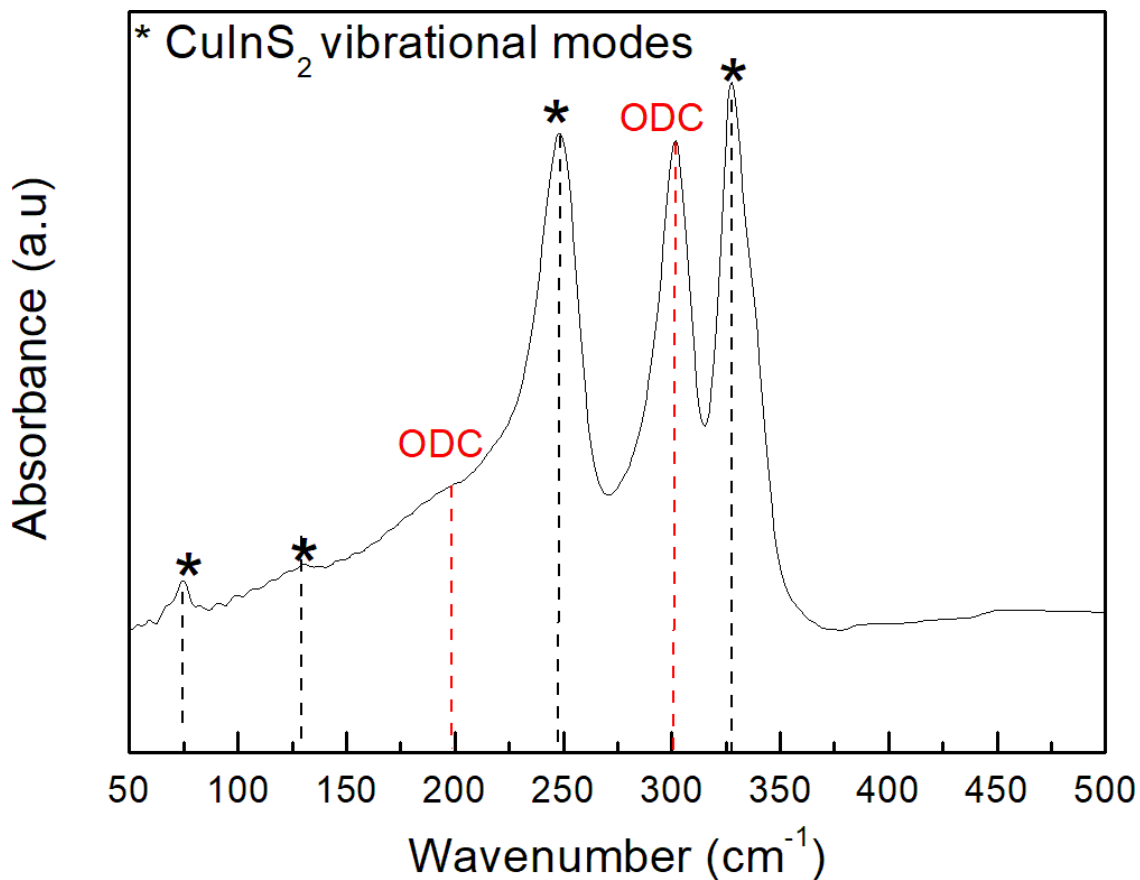


Fig. 1. FTIR absorbance spectrum recorded on pressed pellet prepared from powder single crystal CuInS_2 . The IR active modes of the chalcopyrite lattice having E/B symmetry modes are shown by star symbol (black dash lines). The peak related to the CuIn_5S_8 (ODC secondary phase) can be seen at 302 cm^{-1} wavenumber (red dash line).

Threading dislocation line mapping in aluminum nitride wafers using X-ray topography in reflection geometry

Roland Weingärtner,¹ Andreas Lesnik,¹ Gleb Lukin,¹ Elke Meissner,¹ Leon Schiller¹
 Jochen Friedrich¹ and Sven Besendörfer¹

¹ Fraunhofer Institute for Integrated Systems and Device Technology (IISB), Schottkystr.10, 91058, Erlangen, Germany

Email: roland.weingaertner@iisb.fraunhofer.de

Aluminum nitride (AlN) bulk crystals of approximately 5 mm height were grown by physical vapor transport method as described in [1-3]. C-plane-oriented slices with a typical diameter of around 35 mm and a thickness of 450 µm have been prepared from these bulk crystals with atomic flat surfaces and threading dislocation densities typically below 1000 cm⁻².

We present a method based on X-ray topography (XRT) for the determination of the orientation of the threading dislocation lines across the full sample size. As an application the direction map of the dislocations give insight into the growth process of AlN.

Topographs are measured in reflection geometry with an XRTmicron tool from Rigaku company equipped with copper/molybdenum (Cu/Mo) anode powered at 1200 W. Usually topographs of the (0004) reflex with Cu anode are used to map the c-plane. Dislocation lines are seen as slightly distorted dark spots, where the degree of distortion depends on the interaction depth of the measurement. Our innovative approach uses the Mo anode instead of the Cu anode in order to enhance the penetration depth of the X-rays into the AlN wafer, resulting in a stronger distortion of the dark spot (see Fig 1). The dark spot itself and its shape is correlated to the orientation of the dislocation line and essential for the determination of the direction. This offers the chance to derive a semi-empirical formulation for the calculation of the line direction of a threading dislocation. The theory considers the diffraction geometry as well as the intensity distribution of the dark spot. We demonstrate the validity of our method with two different measurement procedures. First, we measured a series of symmetric reflection topographs of the c-plane at different wafer rotation angles around the c-axis, leading to a systematic non-trivial change of the distortion of the dark spots. At the same time their intensity distribution changes, which can be consistently described by our method. Second, we apply three-dimensional section topography using the (11-20) reflex (Mo anode) in transmission geometry to have a three-dimensional model of some selected threading dislocations and compare their directions with the results obtained from our novel approach. Please note that although the three-dimensional section topography method can in principle obtain the direction information of threading dislocations, it is not feasible to apply it to a whole wafer, which is the mayor benefit of our new method shown here.

References:

- [1] T. Wicht, S. Müller, R. Weingärtner, B. Epelbaum, S. Besendörfer, U. Bläß, M. Weisser, T. Unruh, E. Meissner, *J. Appl. Cryst.*, **2020**, 53, 1080.
- [2] B. M. Epelbaum, C. Seitz, A. Magerl, M. Bickermann, A. Winnacker, *J. Crystal Growth*, 2004, **265**, 577.
- [3] www.iisb.fraunhofer.de/de/research-areas/materialien/gan-aln.html.

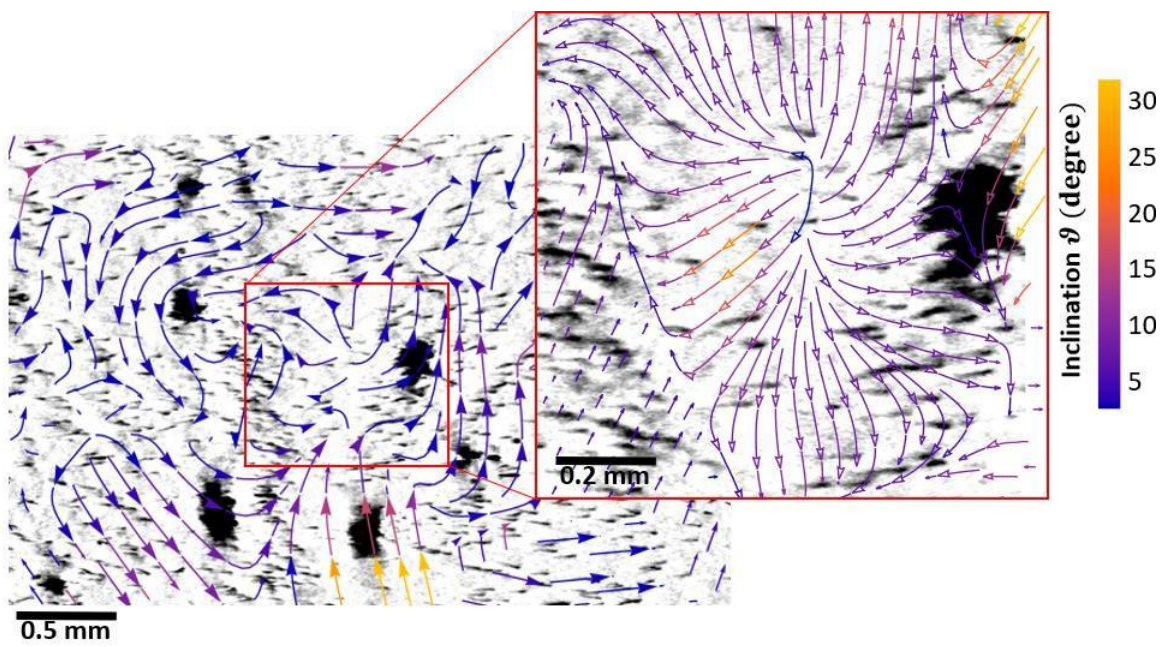


Fig. 1. XRT-topograph of the c-plane (0008) reflex with Mo-anode of an aluminum nitride wafer. The region of interest shows single threading dislocations as elongated dark spots in the neighbourhood of large defect clusters. Effective inclination stream field for the dislocation direction of threading dislocations is overlaid.

Investigating the surface quality of wide bandgap materials using surface photovoltage spectroscopy

Viktoriia Nikonova,¹ Nadine Schüler,¹ Thomas Clausen,¹ Knut Gottfried,² Imme Ellebrecht² and Kay Dornich¹

¹ Freiberg Instruments GmbH, Delfter Strasse 6, 09599, Freiberg, Germany

²ErzM-Technologies UG, Technologie-Campus 1, 09126, Chemnitz, Germany

Email: viktoria.nikonova@freiberginstruments.com

The contactless optoelectronic characterization of wide band gap semiconductors (SiC, GaN, AlN and others) and heterostructures under production conditions and in fields of R&D is often challenging. Surface photovoltage (SPV) techniques are powerful tools for the characterization of photoactive materials in research and technology and analysis of dominating processes. SPV spectroscopy provides information about preferential directed charge separation in relation to electronic transitions and carrier dynamics. [1, 2]

The measurements of the SPV signal height maps have been done using the new compact non-contact high resolution SPV spectroscopy (HR-SPS) tool with fixed energy excitation sources produced by Freiberg Instruments GmbH. It detects the samples automatically and allows it to work with wafers up to 300 mm in diameter. The major advantage of HR-SPS is its high flexibility, which for example enables the integration of up to four lasers in the measurement head, either for injection level dependent SPV measurements ranging from very low to high injection or extracting depth information by using different laser wavelengths.

The experiments (eg. Fig. 1) show the difference in maps between surface quality of wafers: polished wafers (unetched), etched roughened surface, fine and coarse grinding surfaces. Thus, the presented technique can be used to make quantitatively based decisions on the goodness of surface treatment methods without damaging the samples and to improve production based on wide bandgap materials.

References:

- [1] Th. Dittrich, S. Fengler “Surface photovoltage analysis of photoactive materials” (World Scientific, 2020), p. 287.
 [2] Th. Dittrich, S. Fengler, N. Nickel, *Phys. Stat. Sol. A* **2021**, 11, 2100176.

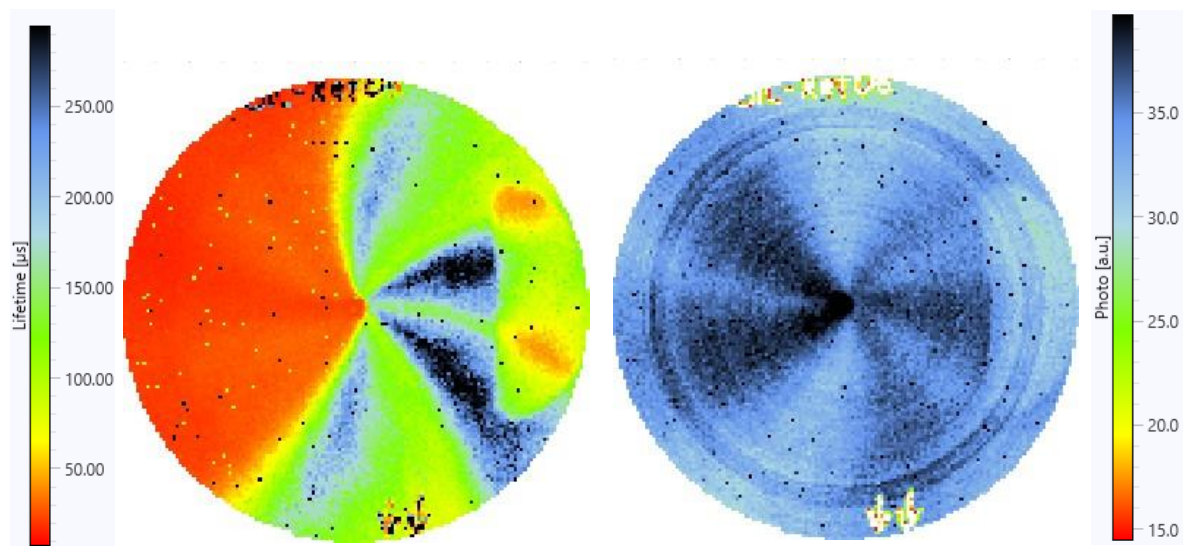


Fig. 1. SPV lifetime (left) and signal height (right) maps of SiC wafer with pattern from polishing wheel measured with UV laser 355 nm.

Enhanced emission in erbium and ytterbium doped gallium oxide devices based on the sensitization of oxygen vacancies

Houwei Pang,¹ Dongsheng Li¹ and Deren Yang¹

¹*State Key Laboratory of Silicon and Advanced Semiconductor Materials and School of Materials Science and Engineering, Zhejiang University, 310027, Hangzhou, P. R. China*

Email: mseyang@zju.edu.cn

Gallium oxide (Ga_2O_3) has aroused extensive interest in the field of power devices, solar-blind detectors, and transparent conductors, due to its ultrawide bandgap, high breakdown field, as well as outstanding stability [1]. For the most stable β - Ga_2O_3 phase, progresses in the aspects of bulk crystal growth, film epitaxy, and the demonstration of electronic devices have been made. In view of the frequent deviation of the composition from the stoichiometry, abundant native point defects exist in β - Ga_2O_3 . Among all the point defects, donor oxygen vacancies seem to play significant roles in the electrical properties of native β - Ga_2O_3 . Furthermore, oxygen vacancies can act as luminescence centers via the donor-acceptor pair recombination, which can be transferred to other activators for emission, such as rare earth ions. As a result, the sensitizing effect of oxygen vacancies can realize luminescence in Ga_2O_3 based devices.

We deposited erbium (Er) doped Ga_2O_3 films on silicon substrates by sputtering. The existence of oxygen vacancies was identified by means of photoluminescence (PL), and the energy transfer between oxygen vacancies and Er^{3+} ions was demonstrated. We fabricated light-emitting devices based on the Er doped Ga_2O_3 films and realized the Er^{3+} ions related electroluminescence in visible and communication wavelengths assisted by oxygen vacancies [2]. The concentration of oxygen vacancies within the Ga_2O_3 hosts could be tuned by changing the sputtering and annealing ambient [3]. To enhance the emission intensity, ytterbium (Yb) doped Ga_2O_3 interlayers were inserted. It was found that with the appropriate concentration ratio and ionic distance of Er^{3+} and Yb^{3+} , intense electroluminescence (EL) of Er^{3+} could be achieved. We analysed the interaction mechanism of Er^{3+} and Yb^{3+} ions via the time-resolved EL spectra, demonstrating the effective electron transfer and energy transfer between the two kinds rare earth ions.

References:

- [1] J. Zhang, P. Dong, K. Dang, Y. Zhang, Q. Yan, H. Xiang, J. Su, Z. Liu, M. Si, J. Gao, M. Kong, H. Zhou, and Y. Hao, *Nature Communication* **2022**, *13*, 3900.
- [2] H. Pang, M. He, J. Hu, Y. Fan, H. Shang, D. Li, and D. Yang, *Optical Materials* **2022**, *129*, 112462.
- [3] H. Pang, Y. Fan, Y. Wang, Y. Wu, D. Li, and D. Yang, *Materials Science in Semiconductor Processing* **2024**, *171*, 108029.

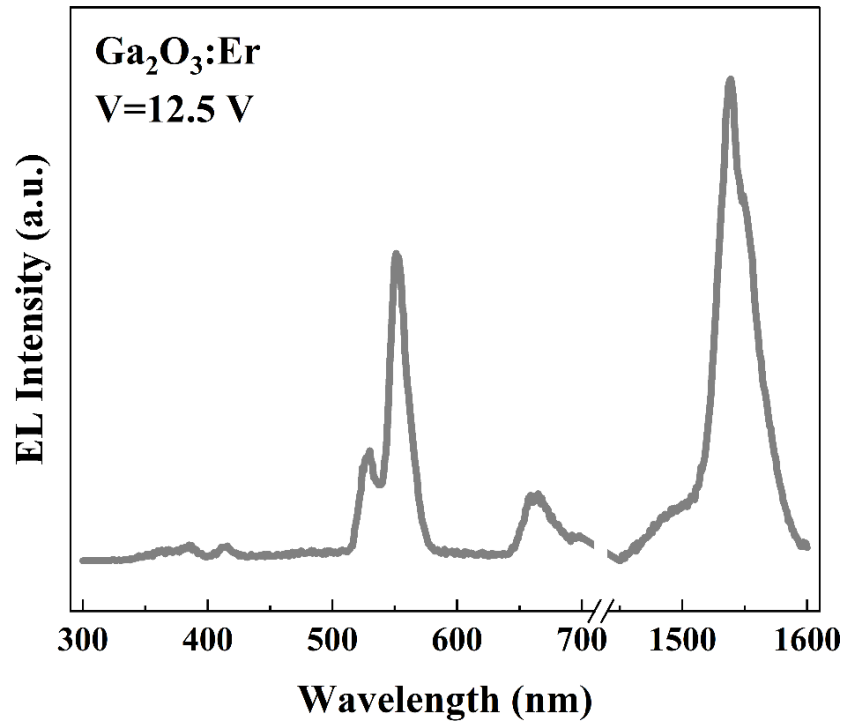


Fig. 1. Electroluminescence spectra of light-emitting devices based on $\text{Ga}_2\text{O}_3:\text{Er}$ films with the applied voltage of 12.5 V.

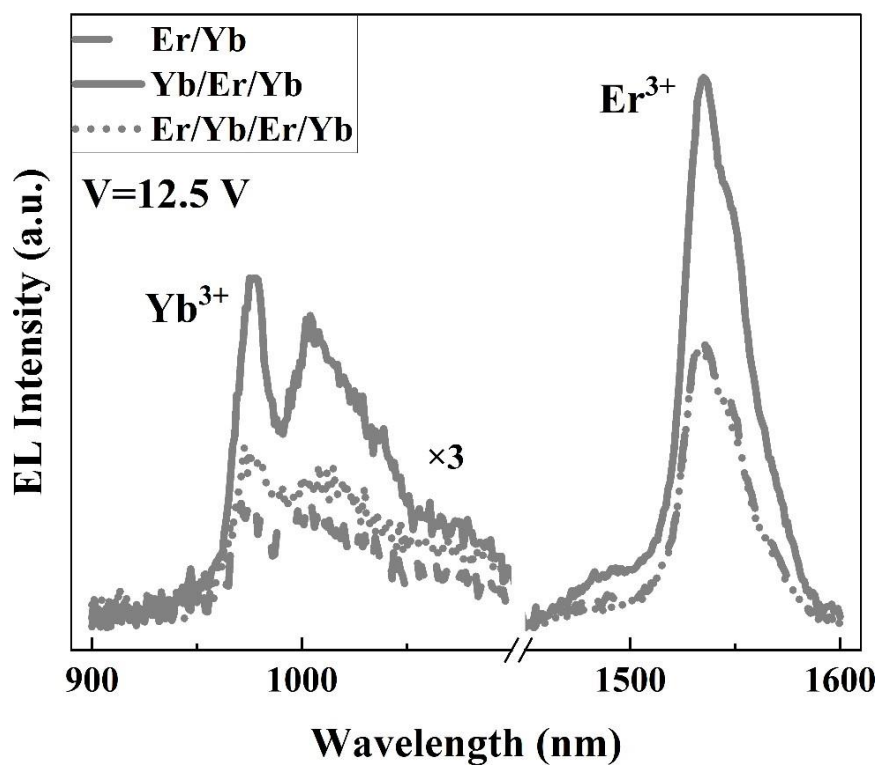


Fig. 2. Electroluminescence spectra of Er^{3+} and Yb^{3+} doped Ga_2O_3 light-emitting devices with structures of Er/Yb, Yb/Er/Yb, and Er/Yb/Er/Yb at the applied voltage of 12.5 V.

Defect Noise & Multi-Defect Leakage Paths in Amorphous PECVD SiCN

Nishant Saini^{1,2}, Davide Tierno¹, Kristof Croes¹, Valeri Afanas'ev^{1,2}, Jan Van Houdt^{1,2} ¹imec,
Kapeldreef 75, 3001, Leuven, Belgium

²KU Leuven, Department of Physics & Astronomy, Celestijnlaan 200D, 3001, Leuven, Belgium

Email: Nishant.Saini@imec.be

Introduction. Stress-induced defect generation is the core mechanism behind dielectric failures in chips, commonly studied using time-dependent dielectric breakdown (TDDB). This allows one to estimate the time-to-failure (TTF), usually following a power law $TTF \sim V^{-m}$, with voltage V and acceleration m [1]. An unresolved issue of TDDB is its temperature

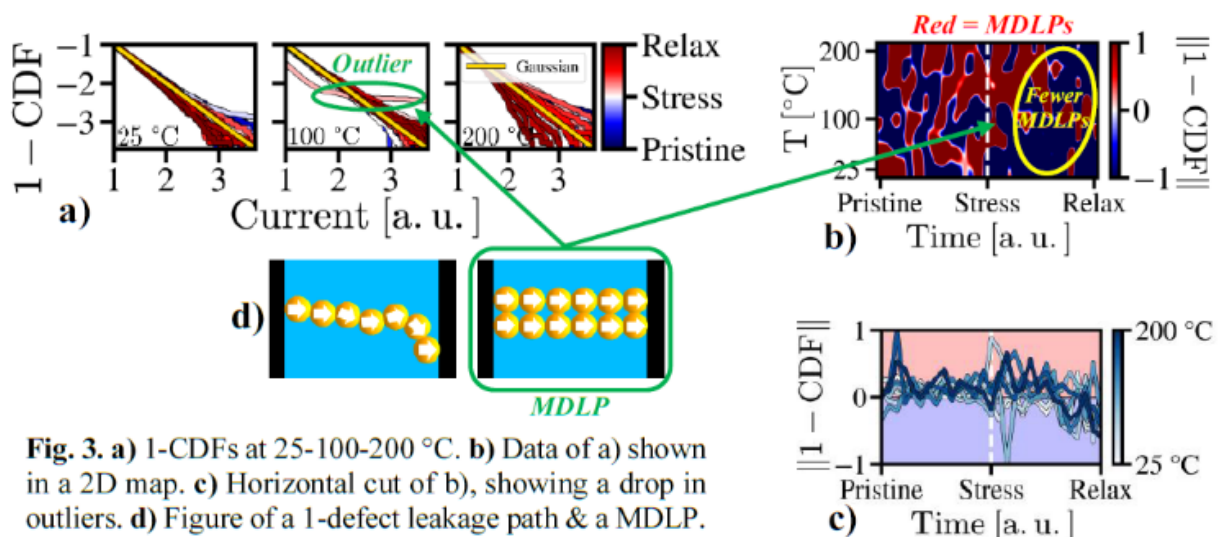
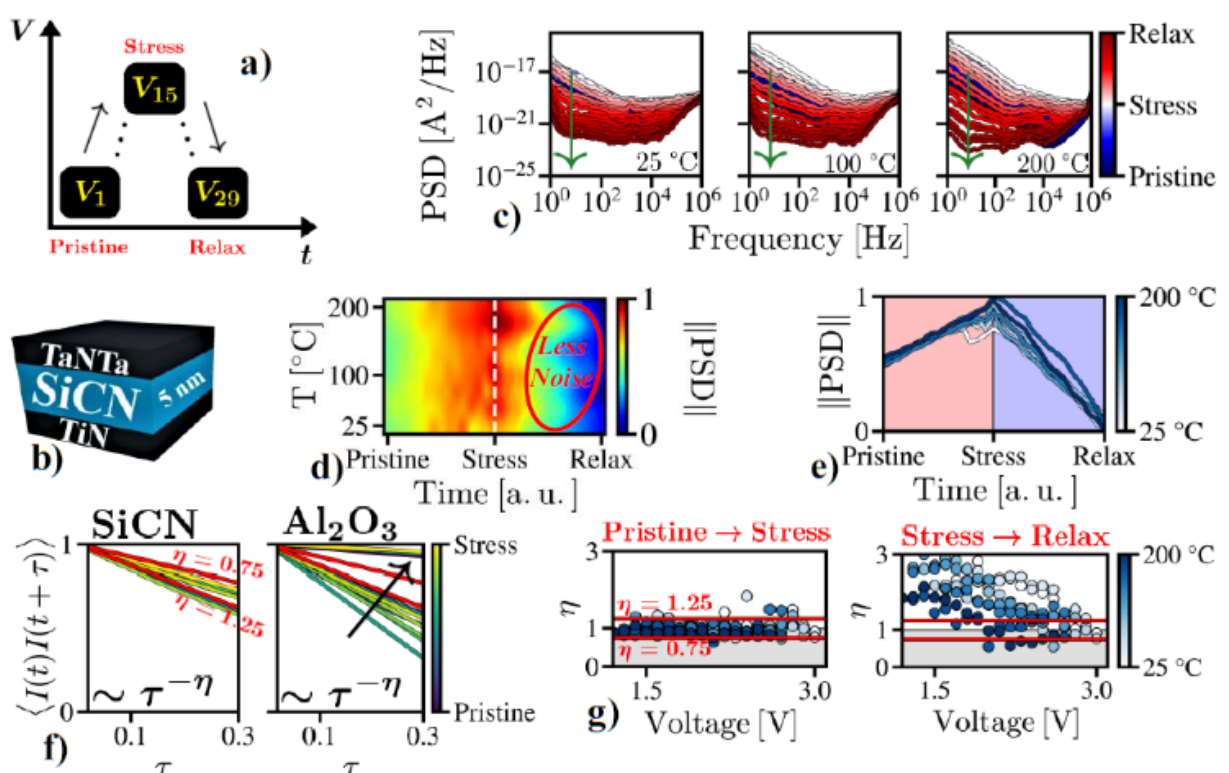
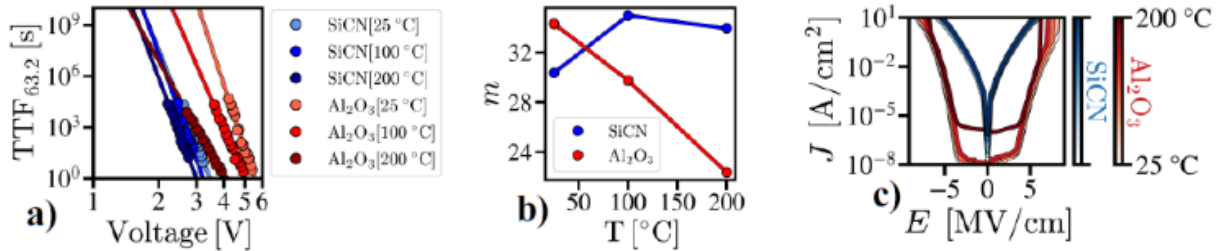
(T) dependence (Fig. 1a). For most dielectrics $m(T)$ decreases, but for some (e.g. SiCN), $m(T)$ remains constant (Fig. 1b), the reason for which is unknown [2]. Other techniques such as current-voltage (IV) allow leakage identification (Fig. 1c), but neither improve the understanding of T-induced degradation (cf. $m(T)$), nor do they explain the role of defects & leakage paths herein. Here, we study dielectric degradation in a material exhibiting a constant $m(T)$. We use 1/f noise to study electron trapping in dispersive defects, where films are progressively stressed, followed by gradual relaxation [3]. We observe the post-stress noise to be significantly lower than the pre-stress one. We show that this is linked to a decrease in long-range correlations between defects. Finally, we study the outliers in the cumulative distribution function (CDF), to estimate the density of multi-defect leakage paths (MDLPs) causing early failures [4]. We relate MDLPs to both the decrease in 1/f noise & the defect correlations, improving the understanding of T-induced degradation.

Experimental. We study a plasma-enhanced chemical vapour deposited (PECVD) 5 nm SiCN in metal-insulator-metal (MIM) stacks (100 μm x 100 μm), via a *Pristine-to-Stress-to- Relax* experiment (Fig. 2a-b), with 29 voltages, over 5400 s. At 25 °C, the voltage range is [1.6 V → 3.0 V → 1.6 V] (steps of 0.1 V), the T range is [25 °C → 200 °C] (steps of 25 °C).

Results & Discussion. *1) Raw Data.* The power spectral densities (PSDs) from the experiment of Fig. 2a, show a lower post-stress magnitude (Fig. 2c). Transforming the PSDs (at 10 Hz) to a 2D map (Fig. 2d), accentuates this decrease. Two observations follow from Fig. 2e: i) pre-stress PSDs coincide, post-stress ones tend to diverge; ii) the post-stress rate of variation is higher. Thus, the way in which defects respond to the applied voltage, and how they collectively contribute to noise production, changes. *2) Defect Correlations.* The time domain autocorrelations tend to increase with stress (Fig. 2f), whilst exhibiting power law decay ($\sim \tau^{-\eta}$). Decay exponents η with $0 < \eta < 1$ are typical for strong correlations, where defects spontaneously form leakage paths. For SiCN, we see a pre-stress $\eta \approx 1$, and a post- stress $\eta > 1$, implying quickly decaying correlations (Fig. 2g). Equivalent studies on Al2O3 (not shown here), for which $m(T)$ decreases, show no difference between pre- & post-stress PSDs, suggesting that 1/f noise & defect correlations could explain the behaviour of $m(T)$. *3) Outliers & MDLPs.* Outliers in the 1-CDFs represent MDLPs [4, 5]. In Fig. 3a, the 1- CDFs are shown (obtained from Fig. 2c). By calculating the sums of the differences between the data & a Gaussian, we construct a 2D map of the outlier density (Fig. 3b), which shows fewer outliers after stress. Stress removal inhibits the formation of MDLPs, explaining the decreasing PSDs (Figs. 2c-d-e), and the increasing autocorrelation exponents η (Fig. 2g). In Figs. 3b-c, the 1-CDFs show similar behaviour at all T, conform the 1/f noise (Figs. 2c-d-e). **Conclusions.** Less noise & weaker defect correlations are observed in SiCN. MDLPs (1-CDF outliers) are used to explain this. While often attributed to hydrogen passivation of defects, we show that less noise in SiCN is due to fewer MDLPs & weaker defect correlations. Moreover, the conclusions hold at all T, which could improve understanding of $m(T)$.

References:

- [1] T. Wong, Materials (Basel) 2012, Vol. 5(9): p. 1602-1625.
- [2] M. Hosseini et al., IEEE IITC, 2022, p. 145-147.
- [3] N. Saini et al., IEEE IITC/MAM, 2023, p. 1-3.
- [4] P. Roussel et al., IEEE TDMR, 2001, Vol. 1, No. 2., p. 120-127.
- [5] R. Degraeve et al., IEEE TED, 1998, Vol. 45, No. 4, p. 904-911.



Investigation of striations in single-crystalline silicon wafers by THz-TDS and other characterization methods

Kuei-Shen Hsu,¹ Joshua Hennig,² Christian Röder,^{1,3} Jan Beyer,¹ Franziska C. Beyer,³ Daniel Molter,² and Johannes Heitmann^{1,3}

¹ Institute of Applied Physics, Technische Universität Bergakademie Freiberg,
 Leipziger Str. 23, 09599, Freiberg, Germany

² Department for Materials Characterization and Testing, Fraunhofer Institute for Industrial Mathematics
 ITWM, Fraunhofer-Platz 1, 67663 Kaiserslautern, Germany

³ Group Spectroscopy and Test devices, Fraunhofer Institute for Integrated Systems and Device Technology
 IISB, Schottkystr. 10, 91058 Erlangen, Germany

Email: Kuei-Shen.Hsu@physik.tu-freiberg.de

The silicon wafer stands as a crucial component in modern technology, serving as a substrate for electronic devices. In the photovoltaic (PV) market, silicon wafer-based photovoltaics dominate with a market share of about 95% [1]. Silicon, being the second most abundant element on earth, has witnessed recent cost reductions, significantly enhancing its competitiveness [2]. Given these factors, silicon wafer-based technology is likely to maintain a pivotal role in the future.

Single-crystalline silicon is among the best-understood semiconductor materials, and various manufacturing methods have been established to enhance or control the crystal quality. Methods such as the Czochralski (Cz) method and the Float Zone (FZ) method are typically employed in the production of silicon single crystals.

Terahertz time-domain spectroscopy (THz-TDS) has proven as a powerful tool in materials science. It has been used to determine resistivity of semiconductors contact-less, by employing the sensitivity of THz wave reflectivity and absorption to the free charge carrier plasma [3,4,5].

In this study, we screened a wide range of resistivity from about 10^{-3} to $10^4 \Omega\text{cm}$ of commercially available n-type, p-type and intrinsic Si wafers and provide a comparative analysis of the resistivity using various mapping techniques. Moreover, we find, that the notorious striations in Si wafers due to the Czochralski (Cz) growth method are detectable with high spatial resolution and sensitivity through our THz-TDS mapping technique. These striations, commonly associated with impurities, have the potential to impact the performance of subsequently manufactured devices [6,7]. The results will be discussed and are complemented by photoluminescence (PL), Microwave Detected Photoconductivity(MDP), and other characterization methods. In particular, Four-Point-Probe measurements were performed as benchmark for the THz-TDS resistivity mapping.

This work is financially supported by the Federal Ministry of Economic Affairs and Climate Action within the ZIM project THz SEMICON under grant no. KK5247701KK1.

References:

- [1] C. Ballif, F. J. Haug, M. Boccard et al. *Nature Review Materials* **2022**, 7, 597–616.
- [2] G. Wilson, M. Al-Jassim, W. Metzger et al. *Journal of Physics D: Applied Physics* **2020**, 53, 493001.
- [3] J. Hennig, J. Klier, S. Duran et al. *arXiv physics.optics* 2401.12787
- [4] J. Neu, C. A. Schmuttenmaer, *Journal of Applied Physics* **2018**, 124, 231101
- [5] K. Muthuramalingam, W. C. Wang, *Materials Science in Semiconductor Processing* **2024**, 170, 107932
- [6] A. Donne, S. Binetti, V. Folegatti et al. *Applied Physics Letters* **2016**, 109, 033907
- [7] G. Coletti, P. Mandshanden, S. Bernardini et al. *Solar Energy Materials & Solar Cells* **2014**, 130, 647–651.

For your remarks

Nanoscale Periodic Modulation of Doping over Large Areas by Means of Block Copolymer Lithography and Ion Implantation

Michele Perego¹, Stefano Kuschlan^{1,2}, Gabriele Seguini¹, Marco De Michielis¹, Graziella Tallarida¹, Riccardo Chiarcos², Michele Laus², Jordi Llobet³, Marta Fernandez-Regulez³, Francesc Pérez-Murano³

¹ CNR-IMM, Unit of Agrate Brianza, Via C. Olivetti 2, I-20864 Agrate Brianza, Italy

² Università del Piemonte Orientale "A. Avogadro", Viale T. Michel 11, I-15121 Alessandria, Italy

³Institute of Microelectronics of Barcelona (IMB-CNM, CSIC), Bellaterra 08193, Spain

Email: michele.perego@cnr.it

Ultralow energy implantation has been widely used to synthesize nanostructures [1] and/or modify materials properties by changing the doping of thin semiconductor layers.[2] In this work, block copolymer lithography and ion implantation are combined to modulate the concentration of dopant impurities in the near-surface layer of a Si substrate.

Phosphorus ions are implanted at ultra-low energy (3keV) and high dose (5×10^{14} atoms/cm²) inducing local amorphization of the Si substrate. The low energy of the implanted ions allows using thin mesoporous polymer films as soft mask.[3,4] Phosphorus is activated by solid phase epitaxial regrowth (SPER) of the implanted region with a thermal treatment at 650°C, preventing diffusion of phosphorus atoms and preserving their spatial localization.[2,5] Surface morphology of the sample (AFM), crystallinity of the Si substrate (UV, Raman), and position of the phosphorus atoms (ToF-SIMS) are monitored.

Electrostatic potential (KPFM) and the conductivity (C-AFM) maps of the sample surface upon dopant activation are compatible with simulated I–V characteristics. Sheet resistance (R_s) and Hall measurement in van der Pauw configuration demonstrated the activation of dopants. Decreasing temperature, R_s initially decreases, consistently with the metallic nature of the degenerately doped silicon. A clear anomaly appears as a broadened step-like increase in R_s at $T < 50$ K. Additionally, an intense positive magnetoresistance is observed in the range

$-0.8 \text{ T} \leq B \leq 0.8 \text{ T}$. A comprehensive picture of these phenomena is delineated considering weak antilocalization phenomena and Kondo effect.[6,7]

These results demonstrate the possibility to locally modify the potential landscape and conductivity of the semiconductor substrate by the introduction of a periodic array of dopants. The localization of dopants in small nanovolumes paves the way to several applications like engineering of the semiconductor band structure, synthesis of artificial crystals, or formation of quantum dot arrays in a semiconductor host matrix.

References:

- [1] C. Bonafos *et al.*, *J. Appl. Phys.* **2004**, 95(10), 5696-5702.
- [2] N. Chery *et al.*, *J. Appl. Phys.* **2022**, 131, 065301.
- [3] C. Castro *et al.*, *Nanotechnology* **2013**, 24 (7), 075302.
- [4] C. Castro *et al.*, *Nanotechnology* **2017**, 28 (1), 014001.
- [5] S. Kuschlan *et al.*, *ACS Appl. Mater. Interfaces*, **2023**, 15, 57928–57940.
- [6] T.E. Park *et al.*, *Nano Lett.* **2011**, 11, 4730–4735
- [7] H. Im *et al.*, *Nature Physics* **2023**, 19, 676–681

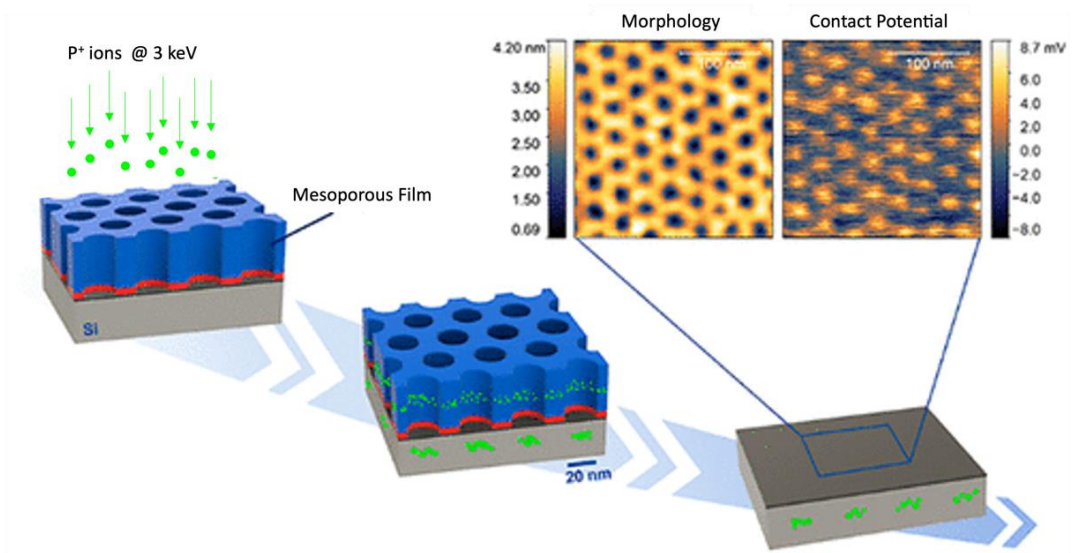


Fig. 1 Scheme of the process flow for the synthesis of the p–n nanojunctions by ion implantation of phosphorus ions at 3 keV into a silicon substrate through a mesoporous polymer film. Morphology and contact potential maps of the sample upon implantation and subsequent annealing at 650°C for phosphorus activation. There are no references to the figures in the text.

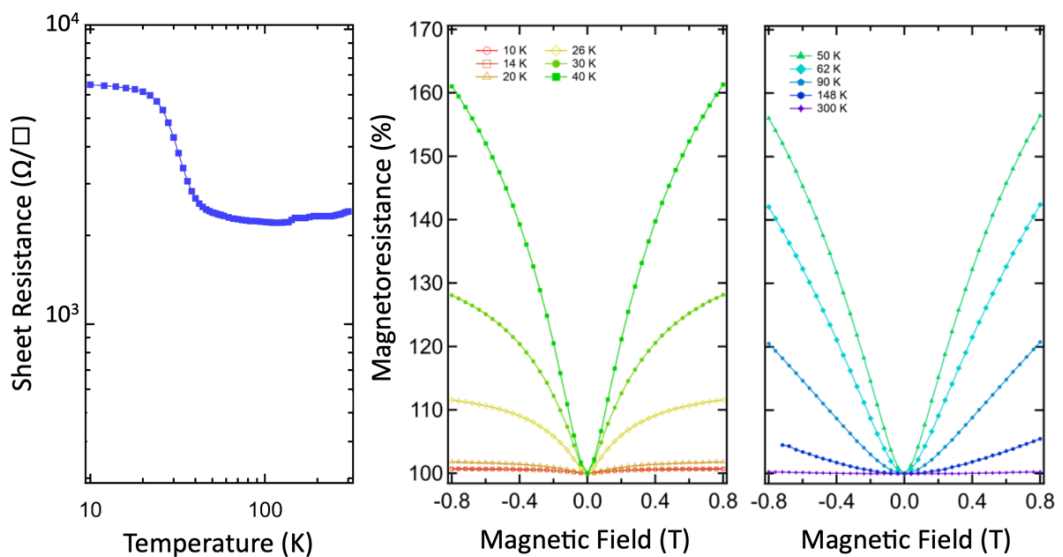


Fig. 2 Sheet resistance (left) and magnetoresistance (right) values for a sample implanted with P^+ ions at 3 keV through a mesoporous polymer film.

Direct Acceptor Modulation Doping for nano-Si: Foundations, Material Systems, Applications

D. König,¹ D. Hiller² and S. Smith¹

¹ Integrated Materials Design Lab, Australian National University, Canberra, ACT 2601, Australia

² Institute of Applied Physics, Technische Universität Bergakademie Freiberg, 09599 Freiberg, Germany

Email: solidstatedirk@gmail.com

Silicon nanovolumes (nanowells, nanowires, nanocrystals – NWells, NWires, NCs) suffer from effects that impede conventional doping due to fundamental physical principles: out-diffusion [1,2], small number statistics [3], and quantum- or dielectric confinement [2,4-8]. For III-V semiconductors, modulation doping was discovered by Störmer & Dingle in 1978 [9], paving the way for loss-free and fast carrier transport as required for ultrafast VLSI electronics and lasing, and Störmer having been awarded the 1998 Physics Nobel Price.

In 2017, *direct* modulation doping of SiO₂ with Al-induced acceptor states for introducing holes as majority carriers to adjacent Si was demonstrated in theory and experiment [10]. This approach offered a whole new vista on preventing problems in compound with impurity doping of nano-Si in VLSI, and also yielded highly conductive hole-selective contacts to Si solar cells with excellent field-effect passivation as a spin-off [10,11]. Recent work on intrinsic Si-NWires with ultrathin Al-doped SiO₂ coatings demonstrated in experiment that the conductivity of such NWires rose by nearly seven orders of magnitude to p-type [12]. In addition, the Schottky barriers of NWire to Ni contacts were reduced from

0.45 to 0.09 eV, decreasing contact resistivity to $\exp(-5) = 0.67\%$ of its nominal value [13].

Here, we will focus on the fundamentals of *direct* modulation doping of Si: its principle (Why direct? What are the consequences?) [14], its quantum-chemical requirements, control of active dopant density [14,15] (Why/how do we defeat the ‘small number statistics’ problem?), modulation acceptor candidates [14] and similarities and differences to impurity acceptors in bulk Si (Al works, B does not – why?) [14,15], the structural properties of modulation acceptors in SiO₂ [16], and its impact on the deactivation of interface trap states [17]. This fundamental part will be rendered by a glimpse on the numerous applications of direct modulation doping and corroborated with experimental data [10-13,17]. We will further discuss whether an antipolar counterpart to direct modulation acceptors in SiO₂ – that is, an Si-based solid with *direct modulation donors* for adjacent Si – could exist and how such a material system would probably look like.

References:

- [1] G.M. Dalpian et al., *Phys. Rev. Lett.*, **2006**, 96, 226802. [2] D. König et al., *Sci. Rep.*, **2015**, 5, 09702. [3] D.J. Norris et al., *Science*, **2008**, 319, 1776. [4] D. Hiller et al., *Sci. Rep.*, **2017**, 7, 863. [5] D. Hiller et al., *Sci. Rep.*, **2017**, 7, 8337. [6] D. Hiller et al., *Beilstein J. Nanotech.*, **2018**, 19, 1501. [7] D. Hiller et al., *Phys. Stat. Sol. B*, **2021**, 258, 202000623. [8] M.T. Björk et al., *Nature Nanotech.*, **2009**, 4, 103. [9] R. Dingle et al., *Appl. Phys. Lett.*, **1978**, 33, 665. [10] D. König et al., *Sci. Rep.* **2017**, 7, 46703. [11] D. Hiller et al., *Solar Energy Mater. & Solar Cells* **2020**, 215, 110654. [12] S. Nagarajan et al., *Phys. Stat. Sol. A* **2023**, 220, 2300068. [13] S. Nagarajan et al., *Adv. Mater. Interfaces* **2024**, 11, 2300600. [14] D. König et al., *Phys. Rev. Appl.* **2018**, 10, 054034. [16] D. Hiller et al., *ACS Appl. Mater. Interfaces* **2018**, 10, 30495. [15] D. Hiller et al., *J. Phys. D: Appl. Phys.* **2021**, 54, 275304. [17] D. Hiller et al., *J. Appl. Phys.* **2019**, 125, 015301.

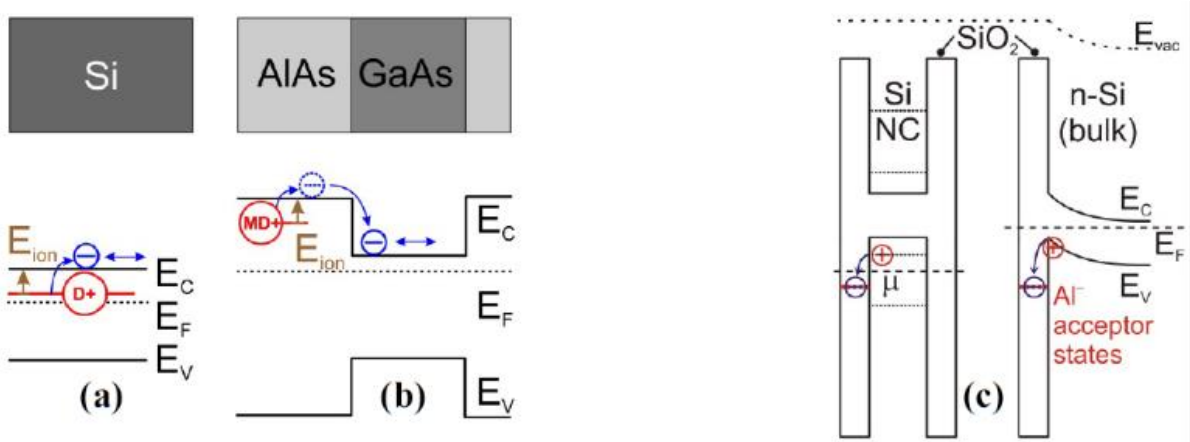


Fig. 1: Principles of (a) impurity doping, (b) modulation doping, and (c) *direct* modulation doping, illustrated with respective band diagrams.

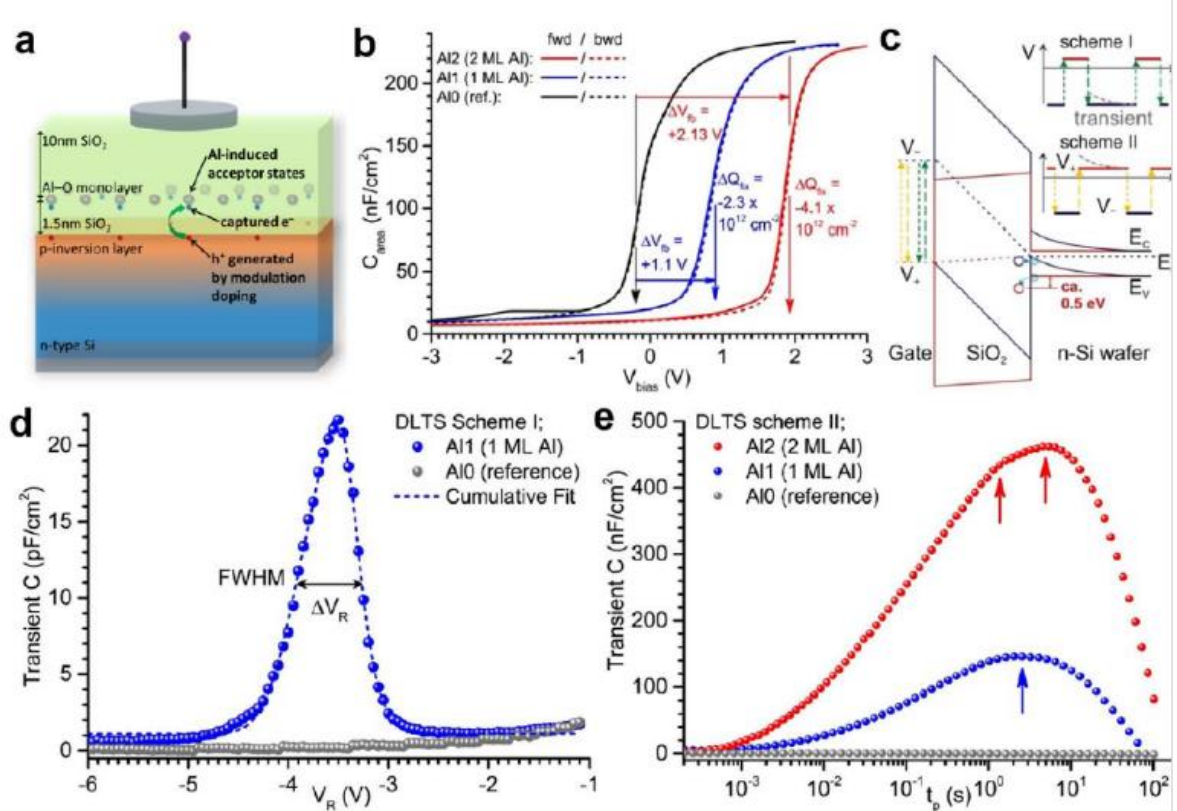


Fig. 2: (a) MOS capacitor sample structure showing Al modulation acceptors on Si sites in SiO_2 charged from Si substrate by electron tunnelling. (b) CV curves of reference sample Al0, and samples with 1ML and 2 ML Al (AL1, AL2) measured at $T = 300$ K; change in flat band voltage ΔV_{fb} and fixed charge density ΔQ_{fix} due to negatively ionized Al shown by coloured arrows. (c) Band structure scheme of charge transient measurements for electron release [scheme I] and for electron capture [scheme II] by Al in Deep Level Transient Spectroscopy (DLTS). (d) Electron release of Al in SiO_2 with pulse time $t_p = 205$ μ s, transient time $TW = 31$ ms and pulse voltage $V_p = +0.5$ V as function of reference voltage V_R measured at $T = 102$ K to freeze out inelastic scattering and trap-assisted processes for maximum energy resolution by direct electron tunnelling into Si. (e) Electron capture with transient time $TW = 3.63$ s, pulse voltage $V_p = -4$ V and reference voltage $V_R = 0$ V as function of pulse time t_p measured at $T = 502$ K to activate all transport paths (hopping, direct and trap assisted tunnelling) for maximum occupation probability of Al in SiO_2 . Arrows show sub-peaks in accord with Al-O MLs. Capacitance per area scale changes from pF/cm² in (d) to nF/cm² in (e). Further details can be found in [10].

The Effect of Aluminium-Modulation-Doped SiO₂ on the Transport Properties of Silicon

Soundarya Nagarajan,¹ Daniel Hiller,² Ingmar Ratschinski,² Dirk König,³ Thomas Mikolajick,^{1,4} and Jens Trommer¹

¹ Nanoelectronic Materials Laboratory gGmbH (NaMLab gGmbH), Dresden, Germany

² Institute of Applied Physics (IAP), TU Bergakademie Freiberg, Germany

³ Integrated Materials Design Lab (IMDL), Australian National University (ANU), Canberra, Australia

⁴ Institute of Semiconductors and Microsystems, TU Dresden, Germany

Email: jens.trommer@namlab.com

To address the challenges of doping on low nanoscale silicon, a novel approach is proposed by doping a thin layer of SiO₂ with trivalent Al impurities in a tunnelling-distance from the silicon surface. The method has its roots in the modulation doping technique familiarly known from III-V semiconductors, which intend to spatially separate the free carriers from parent dopants [1]. The incorporated trivalent impurities in the outermost SiO₂ shell form an active site for trapping electrons from the host, thereby creating hole carriers in silicon, thus bypassing the drawbacks of direct doping [2-5]. In analogy to electrostatic doping which aims to replace the donors and acceptors by gate induced free carriers in the silicon channel, this method follows a charge transfer mechanism where the electrons tunnel from silicon and relax into the lower energetic Al defect state. Furthermore, a field-effect induced by the charged defects formed in the dielectric [2,5].

Proof of concept is realized by studying the electronic transport properties on intrinsic silicon nano- and microstructures [7]. It has been demonstrated that the effect of SiO₂:Al doping is independent of silicon dimensions and contact materials (Table 1). Device test structures made using e-beam and laser lithography were patterned prior to the doping process on a 20 nm thick silicon-on-insulator. A precisely controlled thermal oxide was grown on the top of the silicon followed by atomic layer deposition (ALD) of one or few monolayers of Al₂O₃. The formation of the Al defect state is enabled by rapid thermal annealing at 850°C. The test devices were contacted with either Ni- or Pt-based silicide contacts for electrical characterization.

In principle, this approach turns the silicon highly conductive. In addition, it has shown to reduce the contact resistance at the metal-semiconductor interface, and extensively tunes the Schottky barrier height. Transport measurements performed on nanowires down to 50 nm exhibit a resistivity drop of more than two orders of magnitude when compared to the undoped, intrinsic silicon and a minimum contact resistivity forming a non-rectifying junction at the metal-semiconductor interface [6-8]. The longitudinal Hall resistivity calculated from Hall structures is also consistent with the findings of the nanowires and demonstrates high reproducibility of the approach. The area coverage of silicon with SiO₂ and Al₂O₃ layers in combination with Coulomb blockade effects between the charged acceptor states self-regulate the hole doping process (see figure 1). This correspondingly overcomes the dopant fingerprint of nanoscale MOS devices which suffers statistical fluctuations due to random number and distribution of the dopants.

References:

- [1] R. Dingle et al., *Appl. Phys. Lett.*, 1978, 33, 665.
- [2] D. König et al., *Sci. Rep.* 2017, 7, 46703.
- [3] D. Hiller et al., *ACS Appl. Mater. Interfaces* 2018, 10, 30495.
- [4] D. Hiller et al., *J. Appl. Phys.* 2019, 125, 015301.

- [5] D. Hiller et al., *J. Phys. D Appl. Phys.* 2021, **54**, 275304.
[6] I. Ratschinski et al., *Phys. Status Solidi A* 2023, **220**, 2300068.
[7] S. Nagarajan et al., *Adv. Mater. Interfaces* 2023, **2300600**.
[8] S. Nagarajan et al., *In 2023 DRC, IEEE* 2023.

Table 1. Resistivity of silicon for different device test structures with variation in the number of ALD Al_2O_3 cycles

Test device	Nominal width	Number of ALD Al_2O_3 cycles	Silicon Resistivity ($\Omega \cdot \text{cm}$)
Wafer	-	0	14.9
	50nm	2	0.19
Nanowire	50nm	6	0.04
	50nm	9	0.04
	50nm	15	0.05
Hall bar	30 μm	9	0.02

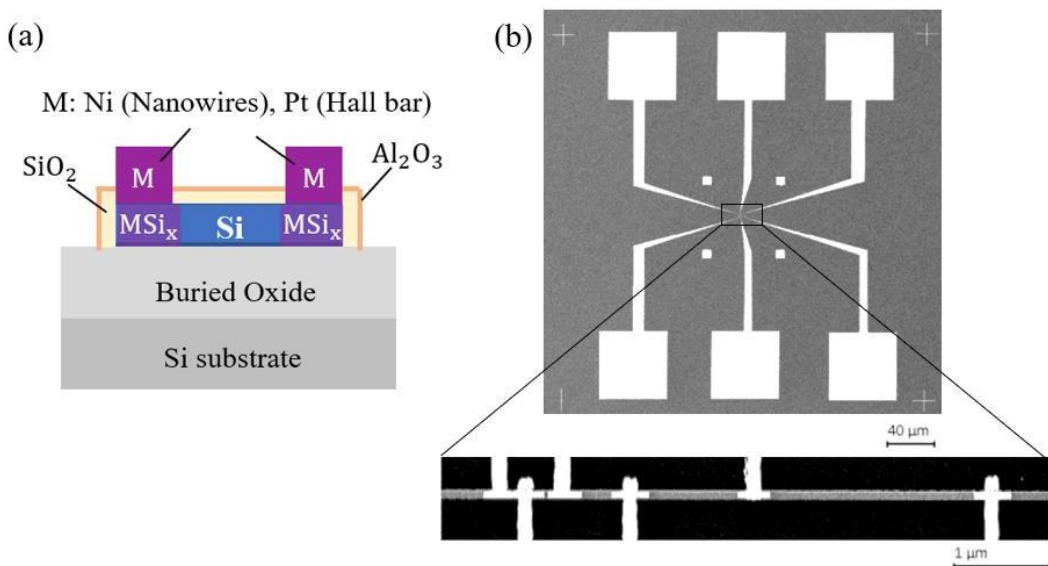


Fig. 1. (a) Schematic cross-section of test device (Nanowire/Hall bar) showing the modulation doping layers ($\text{SiO}_2/\text{Al}_2\text{O}_3$) and contacts with different metal silicides (MSi_x). (b) SEM image of test device- Nanowire with contacts for transfer length measurement (TLM) having a channel width of 50nm.

Ex-situ doping of ultra-thin silicon nanofilms: phosphorus deactivation and mobility enhancement

Andrea Pulici^{1,2}, Stefano Kuschlan^{1,3}, Gabriele Seguini¹, Marco De Michielis¹, Riccardo Chiarcos³, Michele Laus³, Marco Fanciulli^{1,2}, Michele Perego¹

¹ CNR-IMM, Unit of Agrate Brianza, Via C. Olivetti 2, I-20864 Agrate Brianza, Italy

² Università degli Studi di Milano-Bicocca, Via Roberto Cozzi 55, I-20125 Milano, Italy

³ Università del Piemonte Orientale ‘‘A. Avogadro’’, Viale T. Michel 11, I-15121 Alessandria, Italy

Email: a.pulici5@campus.unimib.it

The microelectronics industry is currently transitioning toward gate-all-around FETs exploiting stacked ultrathin Si nanofilms as channels to offer better channel control, be faster and less power-consuming. Interestingly, limited fundamental studies have been reported regarding dopant incorporation and activation in ultra-thin Si nanofilms. To overcome the limitations of conventional ex-situ doping techniques, *Perego et al.*[1] suggested a mild bottom-up alternative approach based on phosphorus-end-terminated polymers to create a source of dopants. P impurity atoms are then driven-in via high temperature annealing. In this work, different silicon-on-insulator (SOI) samples are doped confining the same amount of P impurity atoms in device layers with thickness $6 \text{ nm} \leq H_{\text{SOI}} \leq 70 \text{ nm}$. **Fig.1** shows the results of the electrical (Hall) and compositional (SIMS) analysis. When $H_{\text{SOI}} \geq 30 \text{ nm}$, the fraction of ionized P atoms (η) is compatible with the incomplete ionization model of *Altermatt et al.* for bulk Si[5]. In particular $\eta \sim 95\%$ are obtained when $H_{\text{SOI}} \sim 30 \text{ nm}$ [2] but

η values drop progressively to 5%, when reducing H_{SOI} to 6 nm. Concomitantly, carrier mobility increases achieving values significantly higher than those reported for bulk Si[3]. This mobility increase (**Fig.2a**) is compatible with data reported by *Kadotani et al.*[4], suggesting a transition to almost 2D conduction, which results in the reduction of Coulomb scattering due to the lower number of neighbor donor ions (**Fig.2b**). If $H_{\text{SOI}} < 30 \text{ nm}$ the bulk incomplete ionization model[5] needs to be corrected to account for interface and surface effects. However, even considering the effect of the depleted regions created by interface states[6] and the increased ionization energy due to the Si/SiO₂ dielectric mismatch[7], the proposed model cannot fully describe the experimental results in the case of ultra-thin SOI, suggesting that additional effects, probably related to quantum confinement, start to play a major role.

References:

- [1] M. Perego *et al.*, *ACS Nano* 12, 1 (2018) 178–186
- [2] A. Pulici *et al.*, *Mater. Sci. Semicond. Process.* 163 (2023) 107548
- [3] S. M. Sze and K. K. Ng, *Physics of Semiconductor Devices* (2006)
- [4] N. Kadotani *et al.*, *J. Appl. Phys.* 110, 3 (2011) 034502
- [5] P. P. Altermatt *et al.*, *J. Appl. Phys.* 100, 11 (2006) 113714
- [6] V. Schmidt *et al.*, *Appl. Phys. A* 86, 2 (2007) 187–191
- [7] M. T. Björk *et al.*, *Nat. Nanotechnol.* 4, 2 (2008)

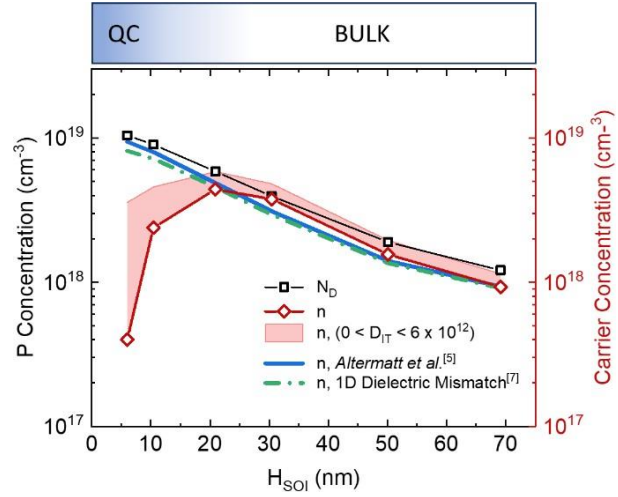


Fig.1. The average P concentration obtained by calibrated ToF-SIMS depth profiles (squares, N_D) and the carrier concentration computed by Hall measurements (diamonds, n) versus H_{SOI} upon drive-in of the dopants. Additionally reported are the electron concentration predicted by the incomplete ionization model of *Altermatt et al.* only (solid line)[5] or by taking into account the contribution of the 1D dielectric mismatch (dash-dotted line)[7], as well as the carrier concentration, corrected due to the effect of D_{IT} , which causes a reduction of the conductive channel (pattern).

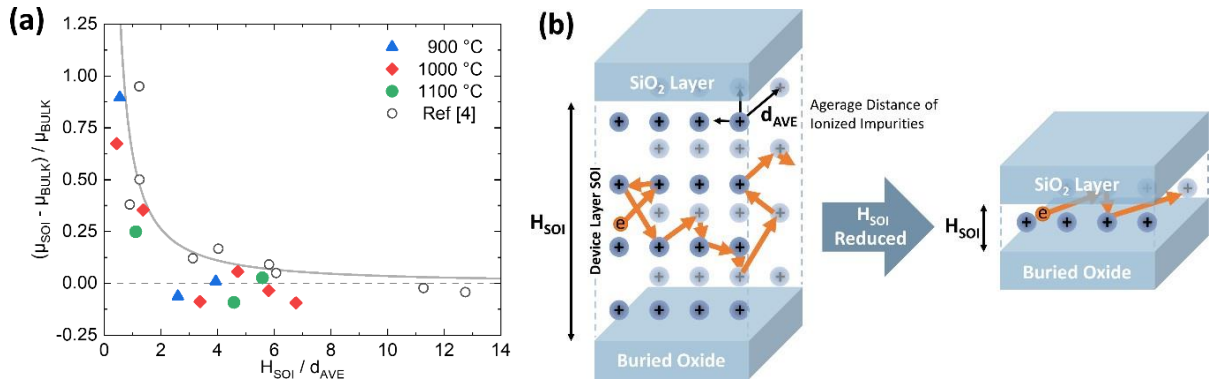


Fig.2. (a) Electron mobility increase ratio ($(\mu_{SOI} - \mu_{BULK}) / \mu_{BULK}$) versus H_{SOI} / d_{AVE} for SOI samples upon drive-in at 1100 °C (circles) 1000 °C (diamonds) and 900 °C (triangles). d_{AVE} is the average distance between ionized impurities. Experimental data are compatible with those reported in the literature by Kadotani et al.[4]. (b) Schematic representation of donor ions and the effect of impurity scattering on an electron in thick and an ultra-thin SOI, highlighting the electron can scatter with fewer neighbor ions when H_{SOI} is reduced. It is assumed that the donors are regularly distributed.

For your remarks



TUBAF
Die Ressourcenuniversität.
Seit 1765.

20th meeting
Gettering and Defect Engineering
in Semiconductor Technology

GADEST 20/24

Late abstracts

DLTS analysis of (010) β -Ga₂O₃ epilayers grown by metal organic chemical vapour deposition on native Sn-doped substrates

C. A. Dawe¹ V. P. Markevich¹, M. P. Halsall¹, I. D. Hawkins¹, A. R. Peaker¹, A. Nandi², I. Sanyal² and M. Kuball²

¹ Photon Science Institute and Department of Electrical and Electronic Engineering, The University of Manchester,
 Manchester, M13 9PL, United Kingdom

² Center for Device Thermography and Reliability, University of Bristol, Bristol, BS8 1TL, United Kingdom

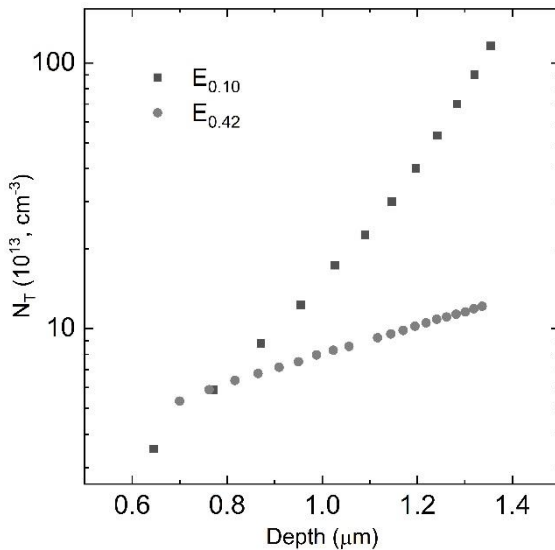
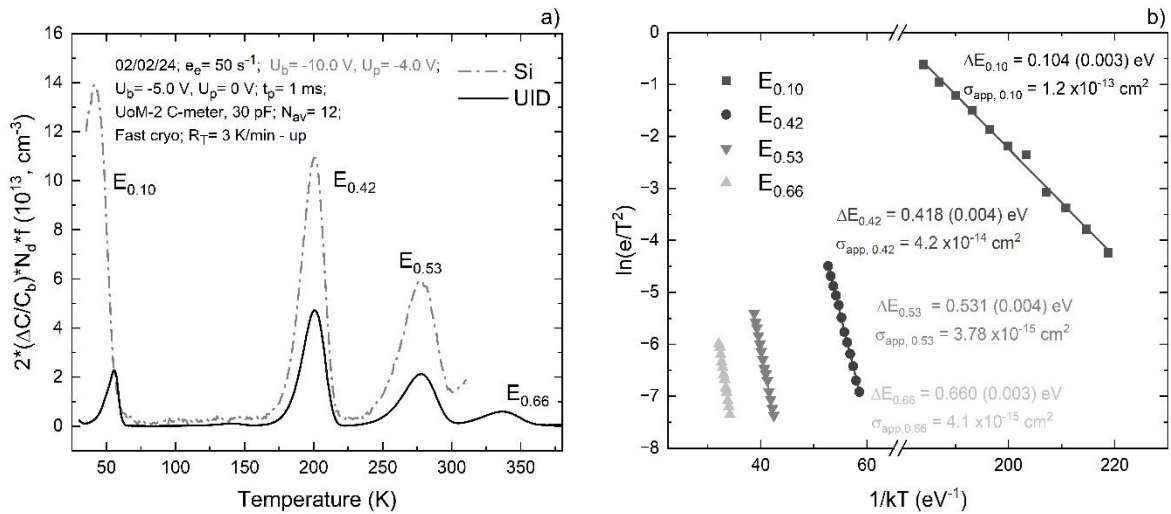
Email: christopher.dawe@postgrad.manchester.ac.uk

β -Ga₂O₃ has significant potential in power electronics due to its large breakdown fields, high Baliga figure of merit and high quality epilayers on large-area native substrates can be grown [1]. Performance of some β -Ga₂O₃-based electronic and optoelectronic devices can be affected by defects with deep energy levels in the gap. Therefore, several studies of deep-level defects in β -Ga₂O₃-based materials and devices have been reported [2]. However, a comprehensive understanding of deep-level defects in β -Ga₂O₃ is still missing. An effective method to obtain the properties of electrically active defects in β -Ga₂O₃ is deep-level transient spectroscopy (DLTS) in conjunction with high-resolution Laplace-DLTS (L-DLTS) [3].

DLTS and L-DLTS have been used to characterise deep-level traps in (010) β -Ga₂O₃ epilayers grown by MOCVD on native Sn-doped substrates. Two types of epilayers have been studied, one doped with silicon to about 1.5×10^{17} cm⁻³, the other type was unintentionally doped (UID). Four electron traps with emission activation energies of 0.10, 0.42, 0.53 and 0.66 eV have been detected in both epilayers, with the Si-doped epilayer exhibiting larger trap concentrations (N_T) for each level. Relative N_T , between both epilayers, for the E_{0.10} trap support suggestions that this trap is related to Si_{Ga(II)} [4]. Dependencies of electron emission rate (e_n) on the electric field (E) as well as concentration-depth profiles { $N_T(W)$ } have been measured and analysed for the E_{0.10} and E_{0.42} traps. The $e_n(E)$ dependence for the E_{0.10} trap is characteristic for a donor level, while that for the E_{0.42} trap indicates an acceptor level. The $N_T(W)$ dependencies show non-uniform spatial distributions of both the E_{0.10} and E_{0.42} traps in the UID samples, with the concentration of the E_{0.10} trap dropping from $\sim 1 \times 10^{15}$ cm⁻³ at 1.5 μ m from the surface to $\sim 2 \times 10^{13}$ cm⁻³ at 0.5 μ m, indicating out-diffusion from the substrate/interface into the epilayer as a likely source.

References:

- [1] A. J. Green et al. *APL Mater* **2022**, *10*, 029201.
- [2] Z. Wang, X. Chen, F. F. Ren, S. Gu and J. Ye, *J. Phys. D: Appl. Phys.* **2021**, *54*, 043002.
- [3] A. R. Peaker, V. P. Markevich and J. Coutinho, *J. Appl. Phys.* **2018**, *123*, 161559.
- [4] A. T. Neal, S. Mou, R. Lopez, J. V. Li, D. B. Thomson, K. D. Chabak, G. H. Jessen, *Sci Rep*, **2017**, *7*, 13218



Investigation of Cu Corrosion Defects Induced by Humidity Imbalance in the Cu Damascene Process of Semiconductors

Koeun Lee^{1,2}, Taesung Kim^{3,4,*}

¹*Global Manufacturing & Infra Technology, Samsung Electronics, Hwaseong, Republic of Korea*

²*Department of Semiconductor and Display Engineering, Sungkyunkwan University, Suwon, Republic of Korea*

³*School of Mechanical Engineering, Sungkyunkwan University, Suwon, Republic of Korea*

⁴*SKKU Advanced Institute of Nanotechnology, Sungkyunkwan University, Suwon, Republic of Korea*

E-mail: tkim@skku.edu

As integrated circuit design rules shrink in semiconductor, Copper (Cu) has been employed as the back end of line (BEOL) interconnect metal to enhance device performance through reduced resistivity and resistive-capacitive delay.[1] However, Cu metal lines are prone to degradation caused by Cu oxidation-induced defects, including extrusions and voids, owing to their inherent properties.[2],[3] Consequently, it becomes essential to regulate the oxidation rate during the chip fabrication process, particularly when the Cu metal line is exposed during the Damascene process. This control is crucial for ensuring long-term reliability and achieving a higher yield.[4]

From the learning of earlier technological nodes, we are aware to and already precisely controlling both process queue time and wafer surface humidity. We must exercise control over the queue time, addressing both inter-process intervals and in-process queuing. [5] This underscores the importance of managing queue time and maintaining low environmental humidity to mitigate wafer surface defects when the FOUP (Front Opening Unified Pod) is opened at the EFEM (Equipment Front End Module).[6] Those humidity and queue times related Cu corrosion defects have been mitigated by N₂ purge in FOUP and reducing the wafer quantity. However, dividing the lot, typically consisting of 25 wafers, by half or less to reduce queue times leads to an imbalance in low humidity due to N₂ purging. This occurs when the FOUP is opened in EFEM. This paper examines Cu corrosion under low humidity conditions in a FOUP with a small quantity of wafers, specifically examining the influence of queue time during N₂ purging in the EFEM. Through simulation of the interaction between the inlet air entering the EFEM and the purged N₂ gas, a vulnerable area is identified where copper oxidation takes place. In addition, we propose an arrangement to mitigate high humidity, supported by experiments conducted under real equipment conditions.

Figure 1 illustrates a chart depicting the humidity inside the FOUP under various conditions. The humid region within the FOUP when opened on the N₂ purged load port without wafers. (Fig.1a) While the extent of the humid area is contingent upon the flow rate of the N₂ purge and the intake of air through the Fan Filter Unit (FFU), the vortex of the inlet air from the cleanroom (<42% RH) is notably observed at the bottom and front side of the FOUP. Therefore, wafers stored in the lower slot of the FOUP face an increased risk of Cu corruptions when subjected to elevated humidity levels during processes like ILD etching and subsequent cleaning. Specifically, an extended queue time amplifies the probability of Cu defects occurring in this high-humidity slot compared to slots with lower humidity. We observed an unintended increase to 28.2% RH in specific configurations when reducing the quantity of wafers to minimize queue time. (Fig. 1b)

Hence, we propose an arrangement for wafers that maintains low humidity with small quantity. When placing 12 wafers in the FOUP, an arrangement with equal spacing from the first slot to the 25th slot ensures uniform N₂ flow, thereby reducing the highest humidity from 28.2% RH to 14.0% RH by half. (Fig.2a) Alternatively, positioning all wafers on the upper section is another method. (Fig.2b) Therefore, by halving the quantity of wafers and reducing the process wait time by half, and applying the optimal wafer arrangement that maintains low humidity balance even with a small number of wafers, we confirmed the absence of Cu corrosion.

References:

- [1] Y.-L. Cheng et al. Copper Metal for Semiconductor Interconnects. *Noble and Precious Metals – Properties. Nanoscale Effects and Applications* <http://dx.doi.org/10.5772/intechopen.72396> (2018)
- [2] Y. Homma et al. Control of Photocorrosion in the Copper Damascene Process. *J. Electrochem. Soc.* **147**(3), 1193–1198 (2000)
- [3] N. R. Kamat et al. A Study of Sulphur Assisted Corrosion in Technologies with Copper Interconnects. *2006 13th International Symposium on the Physical and Failure Analysis of Integrated Circuits* 183–186 (2006)
- [4] B. Li et al. Reliability challenges for copper interconnects. *Microelectron. Reliab.* **44**, 365–380 (2004)
- [5] J. Jeong et al. Control of Wafer Slot-Dependent Outgassing Defects during Semiconductor Manufacture Processes. *2019 30th Annual SEMI Advanced Semiconductor Manufacturing Conference (ASMC)* **21**, 1–4 (2019)
- [6] S. C. Hu et al. 450mm FOUP/LPU system in advanced semiconductor manufacturing processes: A study on the minimization of oxygen content inside FOUP when the door is opened. *2015 Joint e-Manufacturing and Design Collaboration Symposium (eMDC) & 2015 International Symposium on Semiconductor Manufacturing (ISSM)*, 1-4 (2015)

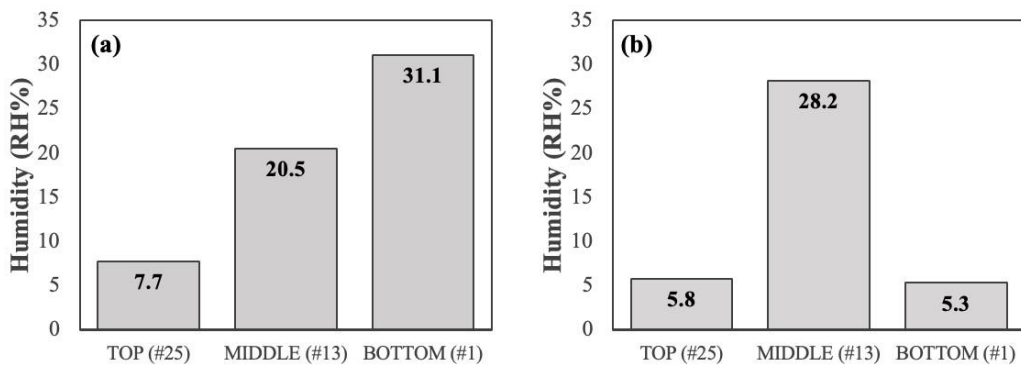


Fig. 1 The relative humidity by location according to WFs arrangement; (a) empty FOUP (b) #1~12 slots are filled with WFs .

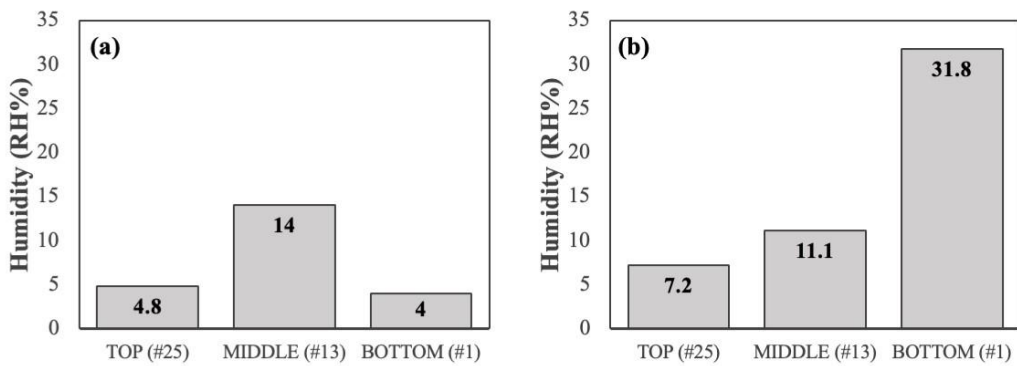


Fig. 2 The relative humidity by location according to WFs arrangement; (a) The odd-numbered slots are filled with WFs . (b) #13~25 slots are filled with WFs to avoid lower slots.

„Hopefully something goes wrong - defects in art“/ artist talk

Walter Padao

Bad Schandau, Germany

Padaos Bilder reflektieren die verschiedenen Ebenen und Dimensionen von gegenständlicher Malerei: das direkt Sichtbare, also vermeintlich „Reale“, Spuren der eigenen Geschichte, vage Erinnerungen, Vorstellungen, Träume... Alles landet im Schmelztopf der Malerei. Fundament dieser Malerei ist der Aspekt von Zeitlichkeit. Padao erforscht Möglichkeiten, Bewegung und Zeit ins „klassische Gemälde“ einfließen zu lassen. Sie enthält zudem Fehler und Brüche – Zufälle, die den Entstehungsprozeß prägen. Mit expressivem Pinselstrich und bewußter Betonung des Materiellen entstehen spannungsgeladene geheimnisvolle Bilder.

Padao's pictures reflect the different levels and dimensions of representational painting: what is directly visible, i.e. supposedly "real", traces of one's own history, vague memories, ideas, dreams... Everything ends up in the melting pot of painting. The foundation of this painting is the aspect of temporality. Padao explores ways to incorporate movement and time into "classical paintings." It also contains errors and breaks - coincidences that shape the creation process. With expressive brushstrokes and conscious emphasis on the material, exciting, mysterious images are created.



Die Pferde 2021, Acryl/ Lwd, 180x320 cm



Tag und Mond 2023, Acryl/ Lwd, 105x170cm

Sunday		08 September, 2024		9 September, 2024		10 September, 2024		11 September, 2024		12 September, 2024		13 September, 2024	
Start	End	Registration		Material processing		Defects in solar cells		Si-based Quantum devices		Material growth+characterization		Friday	
8:30	9:10	9:10	9:30	9:30	9:50	10:10	10:10	10:40	10:40	11:00	11:00	13:00	13:00
9:10	9:30	Invited: Enrico Napolitani	Invited: José Coutinho	Invited: Vladimír Voronkov	Invited: Teimuraz Mcchedlidze	Invited: Johannes Aberl	Coffee Break	09:09/TuM1, start at 08:30	10:09/TuM1, start at 08:30	11:09/WeM1, start at 08:30	12:09/ThM1, start at 08:30	13:09/FrM1, start at 08:30	Doping I
9:30	9:50	Tim Niewelt	Vladimir Voronkov	Kevin Lauer	Johannes Aberl	Katja Mustonen	Coffee Break	Invited: Shao Qi Lim	Invited: Alexander Malwin Jakob	Invited: Shuai Yuan	Invited: Jie Huang	Invited: Soundarya Nagarajan	Doping II
9:50	10:10	Damiano Ricciarelli	Clara Rittmann	Coffee Break	Coffee Break	Coffee Break	Coffee Break	Coffee Break	Coffee Break	Coffee Break	Coffee Break	Andrea Pulici	Break
10:10	10:40	Hui Jia	Coffee Break	09:09/MoM2, start at 10:40	10:09/TuM2, start at 10:40	Passivation methods	Passivation methods	Invited: Bart Macco	Invited: Mariana Bertoni	Solar Cell Degradation	Awards & closing, start at 11:00	Young scientist awards	Annoucements
10:40	11:20	11:20	11:40	11:40	12:00	12:00	12:20	Invited: Marianne E. Bathen	Invited: Nicholas Grant, John Murphy	Katharina Peh	Zhenyi Ni	Daniel Cavalcoli	Closing: Johannes Heitmann
11:20	11:40	Vladimir Markevich	Aravind Subramanian	John Murphy	Constantinos Efstatios Falidas	Lunch break	Lunch break	Lunch break	Lunch break	Lunch break	Lunch & departure	Break	Break
11:40	12:00	Martin Perrosé	Coffee Break	09:09/MoA1, start at 13:30	10:09/TuA1, start at 13:30	Group IV: alloys	Group IV: defects	Invited: Laetitia Vincent	Invited: Jörg Schulze	Excursion with light lunch	12:09/ThA1, start at 13:30	12:09/ThA2, start at 16:00	Conference dinner
12:00	12:20	12:20	13:30	13:30	14:10	14:30	14:50	Registration	Invited: Kevin Sewell	Eddy Simoen	Invited: Koji Yokoyama	Invited: Roland Weingärtner	Diner
14:10	14:30	Christoph Zechner	Christoph Wilfingseder	Felix Kipke	Dawid Kot	14:30	15:10	Opening, start at 15:30	Invited: Antonino Scandurra	Alexandra Abbadie	Invited: Viktorija Nikanova	Houwei Pang	Conference dinner
14:30	14:50	15:10	15:30	15:30	16:00	15:30	16:00	Johannes Heitmann	Invited: Laurie Dentz	Felix Murphy Armando	Invited: Nishant Saini	Kuei-Shen Hsu	Conference dinner
15:10	15:30	Klaus-Dieter Barbknecht	Coffee Break	Coffee Break	Coffee Break	15:30	16:00	16:00	Invited: Moritz Brehm	Industrial Session	09:09/UP	09:09/MOP	Poster Session 1
15:30	16:00	16:00	16:00	16:00	16:00	16:00	16:00	16:00	16:00	16:00	16:00	16:00	1 Poster Session 2 & Exhibition 26 posters
16:00	16:15	16:15	16:30	16:30	16:45	16:45	17:00	17:00	17:00	17:00	17:00	17:00	Get together & Vernissage Walter Padoa: „hopefully something goes wrong -defects in art“ artist talk
16:15	16:30	Stefan Eichler	Invited: Jonathan Veinot	Invited: Martin Kuball	Invited: Antonino Scandurra	Invited: Lijie Sun	Invited: Alexander Kinstler	Invited: Stefan Schmult	Break	Break	Break	Break	Conference dinner
16:45	17:00	08:09/SuA2, start at 17:00	Invited: Joachim Knoch	Invited: Michael Trupke	Industrial Session	Invited: Moritz Brehm	Invited: Alexander Kinstler	Invited: Stefan Schmult	Break	Break	Break	Break	Conference dinner
17:00	17:20	17:20	17:40	17:40	18:00	18:00	18:20	18:20	18:20	18:20	18:20	18:20	Get together & Vernissage Walter Padoa: „hopefully something goes wrong -defects in art“ artist talk
17:20	17:40	Break	Break	Break	Break	Break	Break	Break	Break	Break	Break	Break	Conference dinner
17:40	18:00	18:00	18:20	18:20	19:00	19:00	19:00	19:00	19:00	19:00	19:00	19:00	Get together & Vernissage Walter Padoa: „hopefully something goes wrong -defects in art“ artist talk
18:00	18:20	18:20	18:40	18:40	19:00	19:00	19:20	19:20	19:20	19:20	19:20	19:20	Get together & Vernissage Walter Padoa: „hopefully something goes wrong -defects in art“ artist talk
18:20	18:40	18:40	19:00	19:00	19:20	19:20	19:40	19:40	19:40	19:40	19:40	19:40	Get together & Vernissage Walter Padoa: „hopefully something goes wrong -defects in art“ artist talk
19:00	19:20	19:20	19:40	19:40	19:40	19:40	19:40	19:40	19:40	19:40	19:40	19:40	Get together & Vernissage Walter Padoa: „hopefully something goes wrong -defects in art“ artist talk
19:20	19:40	19:40	19:40	19:40	19:40	19:40	19:40	19:40	19:40	19:40	19:40	19:40	Get together & Vernissage Walter Padoa: „hopefully something goes wrong -defects in art“ artist talk
19:40	20:00	20:00	20:00	20:00	20:00	20:00	20:00	20:00	20:00	20:00	20:00	20:00	Get together & Vernissage Walter Padoa: „hopefully something goes wrong -defects in art“ artist talk
20:00	20:00	20:00	20:00	20:00	20:00	20:00	20:00	20:00	20:00	20:00	20:00	20:00	Get together & Vernissage Walter Padoa: „hopefully something goes wrong -defects in art“ artist talk
20:00	20:00	20:00	20:00	20:00	20:00	20:00	20:00	20:00	20:00	20:00	20:00	20:00	Get together & Vernissage Walter Padoa: „hopefully something goes wrong -defects in art“ artist talk
20:00	20:00	20:00	20:00	20:00	20:00	20:00	20:00	20:00	20:00	20:00	20:00	20:00	Get together & Vernissage Walter Padoa: „hopefully something goes wrong -defects in art“ artist talk
20:00	20:00	20:00	20:00	20:00	20:00	20:00	20:00	20:00	20:00	20:00	20:00	20:00	Get together & Vernissage Walter Padoa: „hopefully something goes wrong -defects in art“ artist talk
20:00	20:00	20:00	20:00	20:00	20:00	20:00	20:00	20:00	20:00	20:00	20:00	20:00	Get together & Vernissage Walter Padoa: „hopefully something goes wrong -defects in art“ artist talk
20:00	20:00	20:00	20:00	20:00	20:00	20:00	20:00	20:00	20:00	20:00	20:00	20:00	Get together & Vernissage Walter Padoa: „hopefully something goes wrong -defects in art“ artist talk
20:00	20:00	20:00	20:00	20:00	20:00	20:00	20:00	20:00	20:00	20:00	20:00	20:00	Get together & Vernissage Walter Padoa: „hopefully something goes wrong -defects in art“ artist talk
20:00	20:00	20:00	20:00	20:00	20:00	20:00	20:00	20:00	20:00	20:00	20:00	20:00	Get together & Vernissage Walter Padoa: „hopefully something goes wrong -defects in art“ artist talk
20:00	20:00	20:00	20:00	20:00	20:00	20:00	20:00	20:00	20:00	20:00	20:00	20:00	Get together & Vernissage Walter Padoa: „hopefully something goes wrong -defects in art“ artist talk
20:00	20:00	20:00	20:00	20:00	20:00	20:00	20:00	20:00	20:00	20:00	20:00	20:00	Get together & Vernissage Walter Padoa: „hopefully something goes wrong -defects in art“ artist talk
20:00	20:00	20:00	20:00	20:00	20:00	20:00	20:00	20:00	20:00	20:00	20:00	20:00	Get together & Vernissage Walter Padoa: „hopefully something goes wrong -defects in art“ artist talk
20:00	20:00	20:00	20:00	20:00	20:00	20:00	20:00	20:00	20:00	20:00	20:00	20:00	Get together & Vernissage Walter Padoa: „hopefully something goes wrong -defects in art“ artist talk
20:00	20:00	20:00	20:00	20:00	20:00	20:00	20:00	20:00	20:00	20:00	20:00	20:00	Get together & Vernissage Walter Padoa: „hopefully something goes wrong -defects in art“ artist talk
20:00	20:00	20:00	20:00	20:00	20:00	20:00	20:00	20:00	20:00	20:00	20:00	20:00	Get together & Vernissage Walter Padoa: „hopefully something goes wrong -defects in art“ artist talk
20:00	20:00	20:00	20:00	20:00	20:00	20:00	20:00	20:00	20:00	20:00	20:00	20:00	Get together & Vernissage Walter Padoa: „hopefully something goes wrong -defects in art“ artist talk
20:00	20:00	20:00	20:00	20:00	20:00	20:00	20:00	20:00	20:00	20:00	20:00	20:00	Get together & Vernissage Walter Padoa: „hopefully something goes wrong -defects in art“ artist talk
20:00	20:00	20:00	20:00	20:00	20:00	20:00	20:00	20:00	20:00	20:00	20:00	20:00	Get together & Vernissage Walter Padoa: „hopefully something goes wrong -defects in art“ artist talk
20:00	20:00	20:00	20:00	20:00	20:00	20:00	20:00	20:00	20:00	20:00	20:00	20:00	Get together & Vernissage Walter Padoa: „hopefully something goes wrong -defects in art“ artist talk
20:00	20:00	20:00	20:00	20:00	20:00	20:00	20:00	20:00	20:00	20:00	20:00	20:00	Get together & Vernissage Walter Padoa: „hopefully something goes wrong -defects in art“ artist talk
20:00	20:00	20:00	20:00	20:00	20:00	20:00	20:00	20:00	20:00	20:00	20:00	20:00	Get together & Vernissage Walter Padoa: „hopefully something goes wrong -defects in art“ artist talk
20:00	20:00	20:00	20:00	20:00	20:00	20:00	20:00	20:00	20:00	20:00	20:00	20:00	Get together & Vernissage Walter Padoa: „hopefully something goes wrong -defects in art“ artist talk
20:00	20:00	20:00	20:00	20:00	20:00	20:00	20:00	20:00	20:00	20:00	20:00	20:00	Get together & Vernissage Walter Padoa: „hopefully something goes wrong -defects in art“ artist talk
20:00	20:00	20:00	20:00	20:00	20:00	20:00	20:00	20:00	20:00	20:00	20:00	20:00	Get together & Vernissage Walter Padoa: „hopefully something goes wrong -defects in art“ artist talk
20:00	20:00	20:00	20:00	20:00	20:00	20:00	20:00	20:00	20:00	20:00	20:00	20:00	Get together & Vernissage Walter Padoa: „hopefully something goes wrong -defects in art“ artist talk
20:00	20:00	20:00	20:00	20:00	20:00	20:00	20:00	20:00	20:00	20:00	20:00	20:00	Get together & Vernissage Walter Padoa: „hopefully something goes wrong -defects in art“ artist talk
20:00	20:00	20:00	20:00	20:00	20:00	20:00	20:00	20:00	20:00	20:00	20:00	20:00	Get together & Vernissage Walter Padoa: „hopefully something goes wrong -defects in art“ artist talk
20:00	20:00	20:00	20:00	20:00	20:00	20:00	20:00	20:00	20:00	20:00	20:00	20:00	Get together & Vernissage Walter Padoa: „hopefully something goes wrong -defects in art“ artist talk
20:00	20:00	20:00	20:00	20:00	20:00	20:00	20:00	20:00	20:00	20:00	20:00	20:00	Get together & Vernissage Walter Padoa: „hopefully something goes wrong -defects in art“ artist talk
20:00	20:00	20:00	20:00	20:00	20:00	20:00	20:00	20:00	20:00	20:00	20:00	20:00	Get together & Vernissage Walter Padoa: „hopefully something goes wrong -defects in art“ artist talk
20:00	20:00	20:00	20:00	20:00	20:00	20:00	20:00	20:00	20:00	20:00	20:00	20:00	Get together & Vernissage Walter Padoa: „hopefully something goes wrong -defects in art“ artist talk
20:00	20:00	20:00	20:00	20:00	20:00	20:00	20:00	20:00	20:00	20:00	20:00	20:00	Get together & Vernissage Walter Padoa: „hopefully something goes wrong -defects in art“ artist talk
20:00	20:00	20:00	20:00	20:00	20:00	20:00	20:00	20:00	20:00	20:00	20:00	20:00	Get together & Vernissage Walter Padoa: „hopefully something goes wrong -defects in art“ artist talk
20:00	20:00	20:00	20:00	20:00	20:00	20:00	20:00	20:00	20:00	20:00	20:00	20:00	Get together & Vernissage Walter Padoa: „hopefully something goes wrong -defects in art“ artist talk
20:00	20:00	20:00	20:00	20:00	20:00	20:00	20:00	20:00	20:00	20:00	20:00	20:00	Get together & Vernissage Walter Padoa: „hopefully something goes wrong -defects in art“ artist talk
20:00	20:00	20:00	20:00	20:00	20:00	20:00	20:00	20:00	20:00	20:00	20:00	20:00	Get together & Vernissage Walter Padoa: „hopefully something goes wrong -defects in art“ artist talk
20:00	20:00	20:00	20:00	20:00	20:00	20:00	20:00	20:00	20:00	20:00	20:00	20:00	Get together & Vernissage Walter Padoa: „hopefully something goes wrong -defects in art“ artist talk
20:00	20:00	20:00	20:00	20:00	20:00	20:00	20:00	20:00	20:00	20:00	20:00	20:00	Get together & Vernissage Walter Padoa: „hopefully something goes wrong -defects in art“ artist talk
20:00	20:00	20:00	20:00	20:00	20:00	20:00	20:00	20:00	20:00	20:00	20:00	20:00	Get together & Vernissage Walter Padoa: „hopefully something goes wrong -defects in art“ artist talk
20:00	20:00	20:00	20:00	20:00	20:00	20:00	20:00	20:00	20:00	20:00	20:00	20:00	Get together & Vernissage Walter Padoa: „hopefully something goes wrong -defects in art“ artist talk
20:00	20:00	20:00	20:00	20:00	20:00	20:00	20:00	20:00	20:00	20:00	20:00	20:00	Get together & Vernissage Walter Padoa: „hopefully something goes wrong -defects in art“ artist talk
20:00	20:00	20:00	20:00	20:00	20:00	20:00	20:00	20:00	20:00	20:00	20:00	20:00	Get together & Vernissage Walter Padoa: „hopefully something goes wrong -defects in art“ artist talk
20:00	20:00	20:00	20:00	20:00	20:00	20:00	20:00	20:00	20:00	20:00	20:00	20:00	Get together & Vernissage Walter Padoa: „hopefully something goes wrong -defects in art“ artist talk
20:00	20:00	20:00	20:00	20:00	20:00	20:00	20:00	20:00	20:00	20:00	20:00	20:00	Get together & Vernissage Walter Padoa: „hopefully something goes wrong -defects in art“ artist talk
20:00	20:00	20:00	20:00</										